THE UNIVERSITY *of* EDINBURGH

The roles of HDACs in chromatin remodelling and response to chemotherapy in cancer

Rui Huang

THE UNIVERSITY
of EDINBURGH

Doctor of Philosophy
The University of Edinburgh
2013

Declaration

I hereby declare that the thesis has been composed by myself. The work was performed by me, except where expressly indicated, and has not been submitted for any other degree or professional qualification. All sources of information have been acknowledged. The experiments described were designed in collaboration with my supervisors Prof. David J. Harrison and Dr. Dana Faratian.

Rui Huang

Acknowledgement

First I would like to make a grateful acknowledgement to my supervisors, Prof. David Harrison and Dr. Dana Faratian, for all their kind support, assistance, and guidance over the past 4 years. I would also like to thank Dr. Simon Langdon for all his kind and great help and advice throughout the years.

I appreciate help from all members in our Breakthrough Unit past and present for their expertise and enthusiasm in scientific research, particularly Peter Mullen, Charlene Kay, Huizhong Hu for their help throughout the research, Danielle Marlow, In Hwa Um for their assistance in IHC/IF experiments, Helen Caldwell for her experience in immunofluorescence experiments, Kenneth Macleod and Sylvie Dubois-Marshall for their suggestion on PCR. I am grateful for the precious lab experiences from Carol Ward, Alexey Larionov, Colette Meyer, Jyoti Nanda and Elad Katz, and persistent generous help from Ying Zhou, Elaine Mclay, and Kate Britton. I also thank Elisabeth Freyer, Matthew Pearson, and Paul Perry in MRC Human Genetics Unit for their kind assistance with data collecting from Flow Cytometry and microscopy. The summer project student Matthew Tse also helped a lot with collecting the data for nuclear texture analysis. Moreover, I am truly grateful for support and encouragement from my friends Romina Briffa, Mengmeng Liu, Wei Gong, Arran Turnbull, Ghassan Tashkandi, Kyle Francis, Peter Caie, Carlos Martinez Perez and so on, whose friendship means a lot to me during the PhD study and even more in the future.

Finally, I am indebted to my family, my Mother and my Father, for their unwavering support and patience during my study. And I also appreciate financial support from the University of Edinburgh/China Scholarship Council joint Scholarship.

Abstract

Background: The higher-order structure of chromatin changes in response to extracellular and environmental signals. We observed nuclear morphological changes in biopsied cancer tissue after chemotherapy. Since chromatin structure dictates gene expression, and therefore function, further investigation of this phenomenon may increase our understanding of therapeutic responses. I hypothesised that nuclear morphological changes in cancer in response to DNA-damage by chemotherapy are mediated by histone deacetylases (de Ruijter, van Gennip et al.). Methods: Ovarian cancer cell lines PEO1/PEO4 (platinum sensitive/resistant) were selected as *in vitro* models, and primary ovarian cancer xenografts OV1002 and HOX424 as *in vivo* models. Expression levels of HDACs, heterochromatin protein 1 (HP1), and DNA damage response (DDR) proteins were profiled by Western blot analysis after treatment with cisplatin. Immunofluorescence imaging was undertaken using confocal microscopy, and nuclear texture and γH2AX foci were measured in Image J. Cell cycle and apoptosis were detected by flow cytometry. Thirty eight different ovarian cancer biopsies and 175 xenograft samples were assessed for HDAC and HP1 expression in response to chemotherapy by quantitative immunofluorescence. HDAC2 expression was modulated by interfering RNAs (siRNA). Results: I demonstrated nuclear morphological changes in clinical tumours, xenografts, and cell lines in response to platinum chemotherapy by robust measurement of nuclear texture. Expression of HDAC2 increased in PEO1 cells treated with cisplatin at 24h, and this was accompanied by high expression of HP1s. Expression of components of both HDACs and DDR pathways (pBRCA1, γH2AX,

pATM, pATR) showed time dependent changes after cisplatin treatment. Knockdown of HDAC2 reduced the expression of HP1, induced DNA double strand breaks (DSB) measured by γH2AX, and interfered with the activation of DDR induced by cisplatin. Furthermore, HDAC2 depletion affected γH2AX foci formation, cell cycle distribution, and apoptosis triggered by cisplatin, and was additive to the inhibitory effect of cisplatin in cell lines. By inhibiting expression of HDAC2, I observed reversible alteration of chromatin patterns during cisplatin treatment to some degree. In clinical ovarian cancer specimens, expression of HDAC4, HDAC8 and HP1γ significantly increased after chemotherapy in sensitive patients, with enhanced heterogeneity in chromatin pattern. HDAC2, HDAC8, and HP1 expression were also increased after carboplatin treatment in carboplatin-sensitive xenografts. Conclusion: These results demonstrate alterations in nuclear morphology after chemotherapy, and implicate HDACs in having a role in higher order chromatin changes and in cellular DNA damage responses in ovarian cancer both *in vitro* and *in vivo*.

Abbreviations

ADP	adenosine diphosphate
APC	adenomatous polyposis coli
APL	acute promyelocytic leukaemia
AQUA	automated quantitative analysis
ATM	ataxia telangiectasia mutated
ATP	adenosine triphosphate
ATR	ataxia telangiectasia and Rad3-related
BCA	bicinchoninic acid
BER	base-excision repair
BRCA1	breast cancer 1
CHK1	checkpoint kinase 1
CTCL	cutaneous T-cell lymphoma
DAB	diaminobenzidine
DAPI	4,6-diamidino-2-phenylindole
DDR	DNA damage response
DMEM	dulbecco's minimal essential media
DNA	deoxyribonucleic acid
DNA-PK	DNA-dependent serine/threonine protein kinase
DSBs	double strand breaks
EDTA	ethylenediaminetetraacetic acid
ERCC1	excision repair cross-complementation group 1
FANCM	Fanconi anemia complementation group M
FCS	fetal calf serum
HATs	histone acetyltransferases
HDACs	histone deacetylases
HP1	heterochromatin protein 1
HR	homologous recombination
ICLs	interstrand crosslinks
IF	immunofluorescence
IHC	immunohistochemistry
IR	ionising radiation
IVCs	individually ventilated cages
JAK2	Janus Kinase 2
JNK	c-Jun N-terminal kinase
MEK1	mitogen-activated protein kinase 1
NER	nucleotide-excision repair
NHEJ	non-homologous end joining
NSCLC	non-small cell lung cancer
p38MARP	p38 mitogenactivated protein kinase
PAR	poly-ADP-ribose
PARPs	poly-ADP-ribose polymerases

PBS	phosphate buffered saline
PCR	polymerase chain reaction
PI3K	phosphatidylinositol 3-kinase
PLZF	promyelocytic leukaemia zinc finger
PML	promyelocyte
RAR	retinoid acid receptor
Rb	retinoblastoma
RNAi	RNA interference
RPA	replication protein A
RT	reverse transcription
SDS-PAGE	sodium dodecyl sulphate polyacrylamide gel electrophoresis
SIRTs	silent information regulators
TMA	tissue microarray
TSA	trichostatin A
VHL	von hippel–lindau
XPA	xeroderma pigmentosum complementation group A

List of Figures

List of Tables

Contents

1 Introduction

1.1 Epigenetic regulation in cancers and cancer therapy

From DNA, nucleosome, 30nm fibre, to higher order chromatin structure, human genomic DNA is extensively compacted. Appropriate organisation of DNA allows specificity of gene replication and expression. Recent studies have shown that chromatin is dynamic, with changes occurring within its structure and histone modifications during development and in response to extracellular signals (Ho and Crabtree 2010). Epigenetic change is defined as the modification of genome function without changes in DNA sequence, and has been extensively studied over the past few years, particularly in cancer research.

There are at least four processes which contribute to changes in chromatin conformation (Figure1.1-1): DNA methylation, histone-tail acetylation, poly-ADP-ribosylation, and ATP-dependent chromatin-remodelling mechanisms (Lafon-Hughes, Di Tomaso et al. 2008). Different sets of modifications result in distinct readouts of genetic information (Margueron, Trojer et al. 2005; Santos-Rosa and Caldas 2005). As epigenetic changes are known to be mitotically heritable, their contribution to the development in cancer is undeniable (Akhtar and Cavalli 2005; Jones and Baylin 2007). Along with histone acetylation/deacetylation, discussed below in more detail, other modifications have been proposed to contribute to the connection between environmental factors and changes in gene expression in cancer.

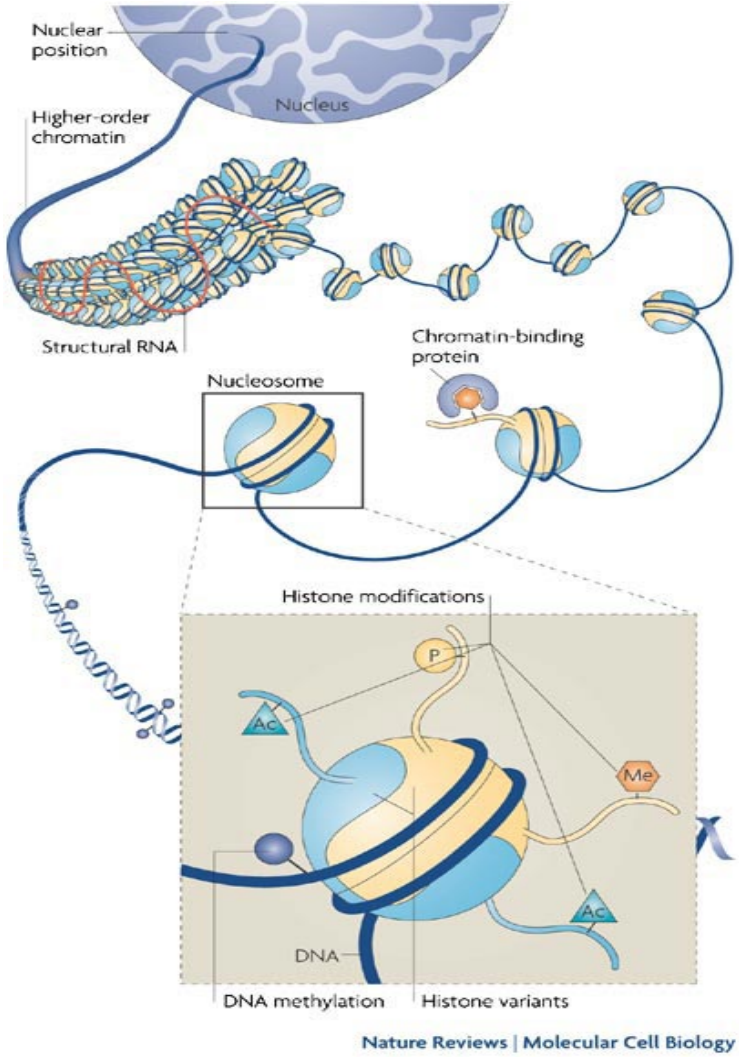

Figure 1.1-1 Chromatin organisation and candidate players for epigenetic inheritance. (Probst, Dunleavy et al. 2009)

DNA methylation acts as a heritable silencing mechanism through addition of methyl groups to cytosines. These are found at dinucleotide CpG sequences, particularly in human tissues (Ehrlich, Gama-Sosa et al. 1982). Methylation occurs in about 60-90% spread CpG sequences, while those regions with a high CG content (CpG island) demonstrate a low level of methylation during development and in different tissues (Lafon-Hughes, Di Tomaso et al. 2008). This dynamic transcriptional silence varies between tissues and is critical for the expression of tissue-specific genes, X

chromosome inactivation, genomic imprinting, and differentiation (Robertson 2005; Meissner 2010). Apart from its physiological role, alteration of genomic DNA methylation can act as an important contributor to several pathological processes, such as immune diseases and cancer (Portela and Esteller 2010; Taberlay and Jones 2011). As a well-identified chromatin modification mechanism, there is strong evidence that DNA methylation can act as an initial event in carcinogenesis. Hypomethylation of disperse CpG sequences and hypermethylation of CpG islands have been recognised as a hallmark in tumorigenesis with respect to epigenetic disruption in cancer (Sharma, Kelly et al. 2010). Identifying critical tumour suppressor genes silenced by DNA methylation in tumour induction and progression provides the basis for the development of targeted epigenetic therapies (Kelly, De Carvalho et al. 2010). For instance, BRCAl can be hypermethylated in breast cancer, while promoters of the genes VHL, APC, and Rb are silenced through hypermethylation of CpG islands in renal cancers, colon cancers and retinoblastomas, respectively (Robertson and Jones 2000; Ting, McGarvey et al. 2006).

By using the energy released from ATP hydrolysis, ATP-dependent chromatin-remodelling complexes can alter the location of nucleosomes and regulate the gene transcription. This form of epigenetic remodelling has also been recognised as another contributory mechanism in oncogenesis (Jones and Baylin 2007). For instance, mutations in hSnf5, one of the remodelling complex members, have been found in paediatric choroid carcinomas and primary neuroectodermal tumours (Gibbons 2005; Vries, Bezrookove et al. 2005; Jones and Baylin 2007). Another study identified mutations in the BRG1 ATPase coding sequence, which is part of

one of the ATP-dependent remodelling complexes SWI/SNF, in non-small cell lung cancer (NSCLC) (Medina, Romero et al. 2008).

Poly-ADP-ribosylation (PARlation) can produce poly-ADP-ribose (PAR), which consists of a homopolymer of ADP-ribose units under the activity of poly-ADP-ribose polymerases (PARPs). The main function of PARlation in chromatin remodeling is proposed to be involvement in histone modification and DNA methylation (Klenova and Ohlsson 2005), and it therefore acts as an important mechanism in chromatin structural regulation and gene expression in both normal tissues and cancers. Supporting this, there is evidence demonstrating that PARP (poly (ADP-ribose) polymerase) activity is elevated in adenomatous colon polyps and oral cancers (Das 1993; Shimizu, Nomura et al. 2004; Ratnam and Low 2007).

It is now widely accepted that these chromatin modelling mechanisms do not function in isolation, but as part of a network, and crosstalk between different chromatin-remodelling mechanisms has been reported. It was observed that both chromatin acetylation and DNA methylation status corresponds to gene expression (Fischle, Wang et al. 2003). ATPases, the largest family of enzymes in the ATP-dependent chromatin-remodelling mechanisms, have been described to interact with methyl DNA-binding proteins (Fitzgerald, DeLuca et al. 2004) and histone deacetylases (Saha, Wittmeyer et al. 2005).

The importance of these epigenetic regulators during carcinogenesis and cancer progression provides novel therapeutic targets for cancer treatment. Various DNA methylation inhibitors and histone deacetylation inhibitors have been investigated in clinical trials (Olsen, Kim et al. 2007; Fenaux, Mufti et al. 2009). The reversibility

of epigenetic chromatin remodelling also makes these targeted epigenetic therapies an exciting field to investigate with the hope of re-establishing a normal epigenome as part of effective cancer treatment.

1.2 Histone acetylation/deacetylation modification and cancer

One of the important chromatin modifications is the regulation of histone tails, which alters the accessibility of DNA to regulating enzymes by converting the chromatin to either a loose or tight structure (Figure1.2-1). By adding acetyl groups to the amino-terminal tails of core histones, the acetylation of histones is the most common frequent post-translational histone modification (Davie 2003). Chromatin becomes decondensed and DNA accessibility is increased after acetylation of histone lysine residues, which reduces the force between the nucleosome core and negatively charged DNA (Lafon-Hughes, Di Tomaso et al. 2008). The acetylation status is determined by the balance between activity of histone acetyltransferases (HATs) and histone deacetylases (HDACs) (Kornberg and Lorch 1999). Alteration of histone acetylation is known to be involved in differentiation, mitosis and meiosis, DNA transcriptional regulation, DNA damage, DNA replication and circadian rhythms (Margueron, Trojer et al. 2005) (Jeppesen 1997; Hassa and Hottiger 2005; Williams, Azuara et al. 2006).

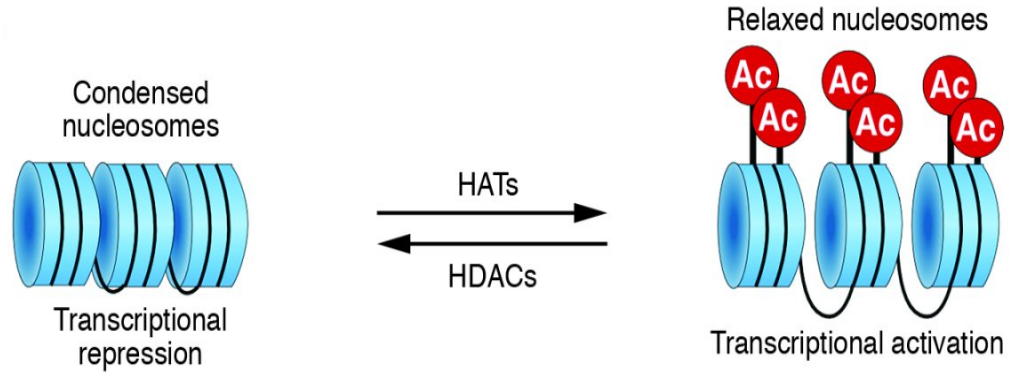

Figure 1.2-1 Process of histone tail acetylation and deacetylation during alteration of chromatin structure (McKinsey and Olson 2005).

HATs are mainly classified into three groups due to their sequence similarity: GNA, MYST and p300/CBP (Yang 2004; Santos-Rosa and Caldas 2005; Verdone, Agricola et al. 2006), and 18 characterized mammalian HDACs are separated into four classes (Table 1.2-1) based on the structural homologies, enzymatic activities and cellular localisation (Gibbons 2005; Fog, Jensen et al. 2007; Gronbaek, Hother et al. 2007; Senese, Zaragoza et al. 2007). Class I HDACs are mainly located in the nucleus in a variety of tissues, and interact with both histones and other proteins (Acharya, Sparreboom et al. 2005; Santos-Rosa and Caldas 2005). Class II HDACs are expressed in a tissue dependent manner and can be detected in both nucleus and cytoplasm (Acharya, Sparreboom et al. 2005). Both Class I and Class II HDACs can be inhibited by the majority of HDAC inhibitors (Vannini, Volpari et al. 2004; Acharya, Sparreboom et al. 2005). Class III HDACs, namely sirtuins (SIRTs, silent information regulators), have no response to most inhibitors and work in the presence of the cofactor NAD+. Finally, the Class IV HDAC, which includes HDAC11 alone, is expressed in the nucleus and has homology with both class I and class II HDACs (Vannini, Volpari et al. 2004; Gronbaek, Hother et al. 2007).

Classifation	HDAC members
I	HDAC1, HDAC2, HDAC3, HDAC8
II	IIa: HDAC4, HDAC5, HDAC7, HDAC9 IIb: HDAC6, HDAC10
III	SIRT1, SIRT2, SIRT3, SIRT4, SIRT5, SIRT6, SIRT7
IV	HDAC11

Table 1-1 Classfication of HDACs.

HATs and HDACs activity can be altered by means of mutation, over-expression or translocation, disrupting the balance between acetylation/deacetylation, and consequently participating in the initiation and progression of some cancers. This has been demonstrated in leukaemia, prostate cancer, breast cancer, colorectal cancer, and ovarian cancer (Mahlknecht and Hoelzer 2000; Acharya, Sparreboom et al. 2005). Three possible mechanisms are proposed in terms of deregulation of acetylation in carcinogenesis. Some tumour suppressor genes promoter regions, such as for p21, are silenced by histone hypoacetylation because of either HAT dysfunction or enhanced HDAC activity (Johnstone and Licht 2003; Gui, Ngo et al. 2004). Conversely, increased HAT activity or reduced/absent HDAC function, resulting in histone hyperacetylation, could activate some repressed genes, causing abnormal expression of proteins and perhaps contributing to cancer initiation and progression. A third mechanism is suggested by which abnormal recruitment of HATs or HDACs could contribute to carcinogenesis (Acharya, Sparreboom et al. 2005). Typical examples regarding the aberrant recruitment of HDACs are their roles during development of haematological malignancies. Fusion proteins composed of RAR (retinoid acid receptor), and its fusion partners PML and PLZF (coded by

promyelocyte gene and promyelocytic leukaemia zinc finger genes, respectively) due to chromosomal translocation are a conspicuous feature of acute promyelocytic leukaemia (APL). HDAC mechanistically plays an essential role by being recruited by those fusion proteins to form constitutive transcriptional repression of genes regulating normal differentiation and proliferation of myeloid cells, resulting in neoplasia by deregulating chromatin structure (Lin, Sternsdorf et al. 2001).

The expression and role of HDACs in cancer have been reviewed and investigated in detail over the past few years. For a summary of these data, see Table 1.2-2. HDAC2, which has been intensively investigated in this study, enhanced expression has been shown to be associated with poor prognosis in pancreatic carcinoma (Miyake, Yoshizumi et al. 2008), and also in association with outcome in prostate, colorectal, and ovarian cancer (Weichert, Roske et al. 2008) (Jin, Pak et al. 2008; Weichert, Roske et al. 2008). Depletion of HDAC2 induced $P21^{Cip1/WAF1}$-dependent apoptosis in cervical cancer cells (Huang, Laban et al. 2005), inhibited growth of breast cancer cells through senescence (Harms and Chen 2007), and also repressed proliferation of colon cancers cells (Weichert, Roske et al. 2008).

HDACs in cancer: expression and functional studies

	HDAC family member	Expression in tumor tissues	Function in cancer cells
class I	HDAC1	*gastric cancer*: elevated expression, associated with nodal spread and poor prognosis; *pancreatic cancer:* expression associated with de-differentiation, enhanced proliferation and poor prognosis; *colorectal cancer*: increased expression associated with poor prognosis; *prostate cancer*: increased in high grade, hormone refractory cancers; *hepatocellular carcinoma*: high expression associated with portal vein invasion, poor differentiation, advanced TNM stage	*cervical cancer cells*: HDAC1 knockdown results in inhibition of proliferation and induction of autophagy; *osteosarcoma and breast cancer cells*: knockdown causes cell cycle arrest, growth inhibition, apoptosis; *colon cancer cells*: knockdown suppresses growth; *prostate cancer:* overexpression increases proliferation and de-differentiation; *neuroblastoma cells:* knockdown sensitizes for chemotherapy; *CLL cells*: knockdown sensitizes for TRAIL-apoptosis
	HDAC2	*colorectal cancer*: upregulation in polyps, associated with poor prognosis; *cervical carcinoma*: high expression in dysplasia; *gastric and prostate cancer*: increased expression associated with advanced stage and poor prognosis	*cervical cancer cells:* HDAC2 knockdown results in differentiation, apoptosis and p53 independent p21 expression; *breast cancer cells:* increased p53 activity, inhibition of proliferation, induction of senescence, induction of apoptosis; *colon cancer cells:* knockdown causes growth arrest; *neuroblastoma cells*: knockdown induces apoptosis; genetic HDAC2 mutation reduces intestinal tumor development in APC mice in vivo; *CLL cells*: knockdown sensitizes for TRAIL-apoptosis
	HDAC3	*gastric, prostate, colorectal cancers*: high expression associated with poor prognosis (together with HDAC1 and 2)	APL cells: HDAC3 associated with PML-RARa fusion protein, knockdown induces differentiation genes; *AML:* AML-1-ETO binds HDAC3 (and HDACs 1, 2), disrupts cell cycle
	HDAC8	childhood *neuroblastoma:* high HDAC8 expression significantly correlates with advanced stage disease, clinical and genetic risk factors and poor long term survival	*neuroblastoma cells*: HDAC8 knockdown induces differentiation, cell cycle arrest and inhibits clonogenic growth; *lung, colon, cervical cancer cells*: knockdown of HDAC8 reduces proliferation
class II A	HDAC4	*breast cancer:* upregulation compared with renal, bladder, colorectal cancer	*APL cells*: HDAC4 interacts with PLZF-RARa fusion protein, represses differentiation genes; renal carcinoma cells: knockdown inhibits expression and functional activity of HIF-1a
	HDAC5	*colorectal cancer:* upregulation compared with renal, bladder, breats cancer	*erythroleukemia*: HDAC5 shuttles from nucleus to cytoplasm upon differentiation, interacts with GATA-1
	HDAC7	*colorectal cancer*: high expression compared with bladder, renal, breast cancer tissues	*endothelial cells:* HDAC7 silencing alters morphology, migration and tube-forming capacity
	HDAC9	nd	nd
class II B	HDAC6	*oral squamous cell cancer*: high expression, increased in advanced stage; *breast cancer*: high expression correlates with response to endocrine treatment, inverse correlation of expression with survival and tumor size	Targeted inhibition of HDAC6 leads to acetylation of HSP90 and disruption of its chaperone function, resulting in depletion of pro-growth and pro-survival client proteins including the Bcr-Abl oncoprotein in *K562 leukemic* cells; HDAC6 targeting blocks EGF induced nuclear translocation of ß-catenin and c-myc expression in *colon carcinoma* cells; knockdown of HDAC6 causes donwregulation of HIF-1a, VEGFR1/2; HDAC6 invovled in TGFb induced epithelial-mesenchymal transition of *lung carcinoma* cells
	HDAC10	nd	Knockdown of HDAC10 downregulates VEGFR
class IV	HDAC11	nd	nd

Abbreviations: CLL, chronic lymphatic leukemia; APL, acute promyelocytic leukemia; AML, acute myeloid leukemia; RARa, retinoic acid receptor alpha; CML, chronic myeloid leukemia; nd, no data

Table 1-2 Recent studies about the expression and function of HDAC families in cancers (Witt, Deubzer et al. 2009).

Meanwhile, HDAC inhibitors are intensively studied modulators of transcription and chromatin structure, and some inhibitors demonstrate efficacy in certain cancer therapies, making it an exciting strategy for cancer treatment. Those inhibitors are grouped into at least four classes: (1) hydroxamic acids, (2) aliphatic acids (Corbett, Blimkie et al.), (Corbett, Blimkie et al.) benzamides and (4) cyclic tetrapeptides (Kim and Bae 2011). The widely used inhibitor trichostatin A (TSA) is included in the hydroxamic acids class and was the first compound discovered to inhibit HDACs (Yoshida, Kijima et al. 1990). Another member of the first class, vorinostat (suberoylanilide hydroxamic acid, SAHA), was first utilised in the clinic for the treatment of refractory cutaneous T-cell lymphoma (CTCL) and was approved by the FDA (Duvic, Talpur et al. 2007). Other HDAC inbitors, such as entinostat, panobinostat, and abexinostat, are also in active clinical trials, as summarised in Table 1.2-3 (Stiborova, Eckschlager et al. 2012).

Chemistry	Compound	Clinical status
Hydroxymate	SAHA (vorinostat)	Approved (CTCL) phase II, III
	PXD101 (belinostat)	Phase I, II
	LBH589 (panobinostat)	Phase II, III
	ITF2357 (givinostat)	Phase I, II
	PCI-24781 (CRA-024781)	Phase I
	JNJ-26481585	Phase I
	4SC-201 (resminostat)	Phase I, II
Benzamide	MS-275 (entinostat)	Phase II
	MGCD0103 (mocetinostat)	Phase II
Cyclic tetrapeptide	Depsipeptide/FK228 (romidepsin)	Approved (CTCL) phase I, II
Aliphatic acids	Valproic acid	Phase I, II, III
	Butyrate	Phase II
	Pivanex (AN-9)	Phase I, II

Table 1-3 HDAC inhibitor development and usage in clinical trials. Abbreviations: CTCL, cutaneous T-cell lymphoma; SAHA, suberoylanilide hydroxamic acid (Khan and La Thangue 2012).

Various effects of HDAC inhibitors have been observed in tumour cells, including cell-cycle arrest, induction of apoptosis, and cell signalling pathway modulation. Several studies have suggested inhibition of HDACs may induce increased expression of the p21 gene (Richon, Sandhoff et al. 2000; Sandor, Senderowicz et al. 2000; Gius, Cui et al. 2004; Ocker and Schneider-Stock 2007), and also repress transcription of genes encoding cyclin D and cyclin A (Qiu, Burgess et al. 2000; Sandor, Senderowicz et al. 2000) to trigger cell cycle arrest. The apoptotic effect of

HDAC inhibition generally results from the increased regulation of pro-apoptotic genes (e.g. FAS and TNF-α) and decreased regulation of anti-apoptotic genes (e.g. BCL-2), which are involved in both the extrinsic and intrinsic apoptotic pathways (Stiborova, Eckschlager et al. 2012). Another essential property of HDAC inhibition is the regulation of some cellular pathways, such as the phosphatidylinositol 3-kinase (PI-3K)/Janus Kinase 2 (JAL2)/MEK-1 pathway (Bassa, Roh et al. 1999; Cieslik, Abrams et al. 2001) and Wnt signaling (Blaheta and Cinatl 2002) pathway.

Although studies about HDACs and their role in epigenetic regulation have exploded since last ten years in cancer research, many problems remained unsolved. There is considerable evidence on the abnormal expression of HDACs in a variety of cancers, and even association with patient survival and treatment outcomes. However, the detailed mechanisms of how those HDACs are involved in progression and outcome still remain unclear. Questions are also raised about the therapeutic potential of either pan-specific HDAC inhibitors or class-specific HDAC inhibitors, and some observed side effects including diarrhoea, myelosuppression, and cardiac QT persistence are another challenge in applying HDAC inhibitors clinically (Ververis, Hiong et al. 2013). Despite their antitumor activity, several HDAC inhibitors, including vorinostat and depsipeptide, show disappointing results in clinical trials of solid tumours as a single treatment, compared with its proven clinical advantage in hematological cancer therapy (Kim and Bae 2011). For example, vorinostat induced significant toxicities when treating patients with metastatic castration-resistant prostate cancer in a phase 2 trial (Bradley, Rathkopf et al. 2009). With continued investigation, improved knowledge of their modulatory roles on gene expression, cell

cycle progress, and proliferation will be better understood, and this will facilitate better application of HDAC inhibitors in the clinic, particularly as cancer therapies.

1.3 The DNA damage response in chemotherapy

1.3.1 DNA damage responses

DNA damage is an extremely common event occurring in cells threatened by both endogenous or exogenous factors. Endogenous sources of damage mainly come from reactive oxygen products from cellular metabolic reactions, and also from errors during DNA replication. On the other hand, exogenous damage can be caused by factors such as ultraviolet radiation, ionising radiation, toxins, and compounds which interact with DNA. Those agents can induce a variety of different types of DNA damage, as illustrated in Figure1.3-1, which then are repaired by specific DNA repair mechanisms to preserve genome stability.

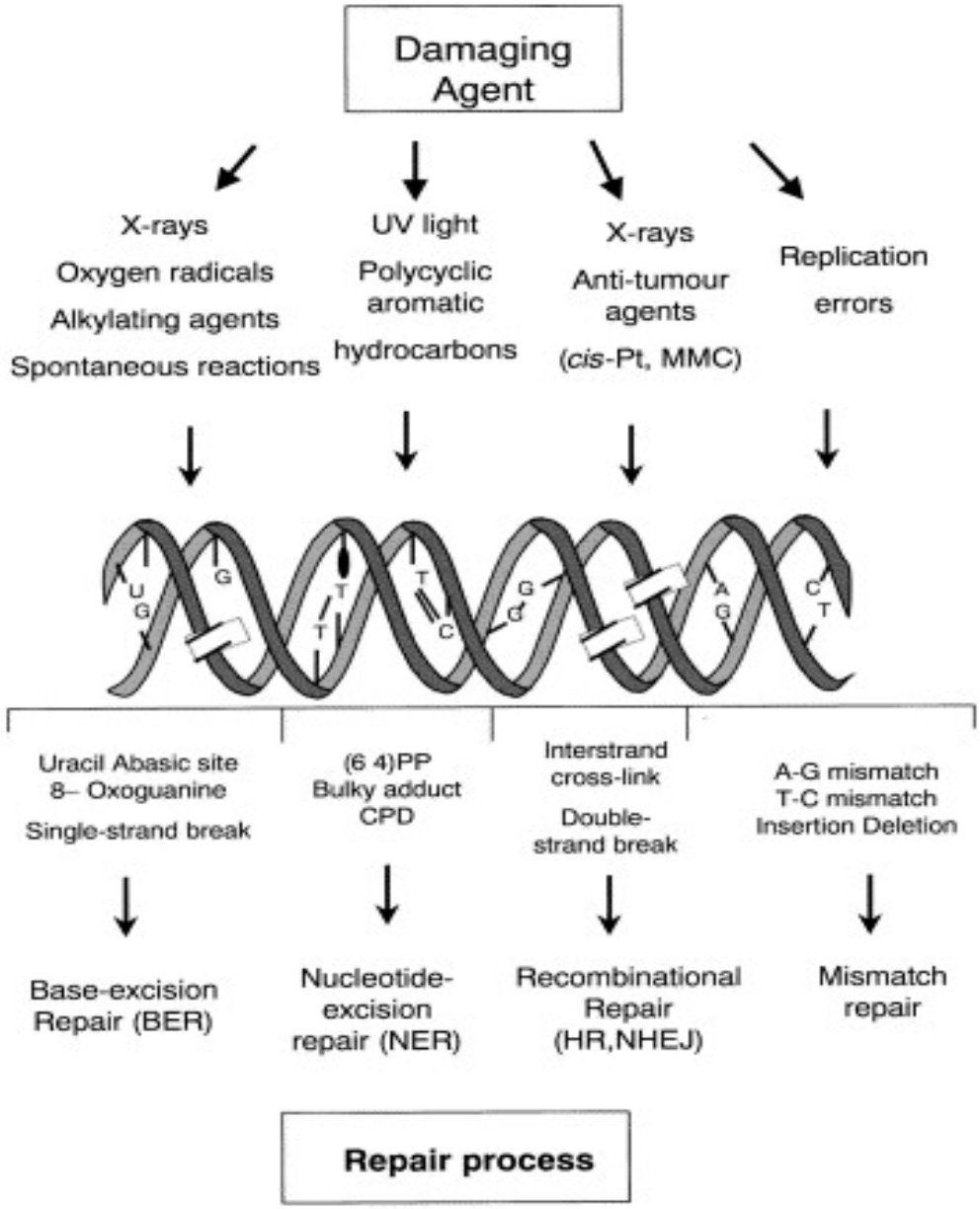

Figure 1.3-1 Types of DNA damage and the associated repair mechanisms. Both endogenous and exogenous agents can induce several types of DNA damage,lesion, and corresponding repair process can be involved based on the different damage type. Abbreviations: *cis*-Pt, cisplatin; MMC, Mitomycin C; (6 4)PP, 6-4 photoproduct; CPD, cyclobutane pyrimidine dimer; BER, base-excision repair; NER, nucleotide-excision repair; HR homologous recombination; NHEJ non-homologous end joining (Martin 2001).

There are four main types of DNA repair processes. These are base-excision repair (BER), nucleotide-excision repair (NER), homologous recombination (HR), non-homologous end joining (NHEJ), and mismatch repair. BER is mainly involved in

the repair of endogenous damage from base changes, in order to to prevent miscoding mutations,. NER repairs damage in helix-distorting lesions which particularly impede transcription and replication. These two mechanisms are both associated with single strand damage, and lesions can be repaired by replacing the damaged sequence with the correct sequence based on the complementary strand in a 'cut and patch' manner (Hoeijmakers 2001).

In contrast, the repair processes of homologous recombination (HR) or non-homologous end joining (NHEJ) are involved in the repair of severe damage which involves both DNA strands (Martin 2001). They have been intensively studied over several decades (Figure1.3-2). NHEJ functions through direct ligation of the double strand break (DSB) ends with the assistance of double-stranded DNA end-binding protein complex Ku70/80, although this simple re-ligation is error-prone and can lead to the addition of small nucleotides or deleted sequence at the damaged site (Lieber 2010). On the other hand, HR is considered error free repair. After resection of the damaged site, the recombinase filament on the resection-induced single-strand tails facilitate the use of the homologous sequence as a template in a conservative or non-conservative manner (San Filippo, Sung et al. 2008). Because of the nature of these two repair methods, NHEJ can occur throughout the cell cycle, but it is suggested that it occurs more frequently during G1 phase. HR occurs typically after normal DNA replication when the non-damaged homologous sister chromatid serves as a template for repair synthesis (Chapman, Taylor et al. 2012).

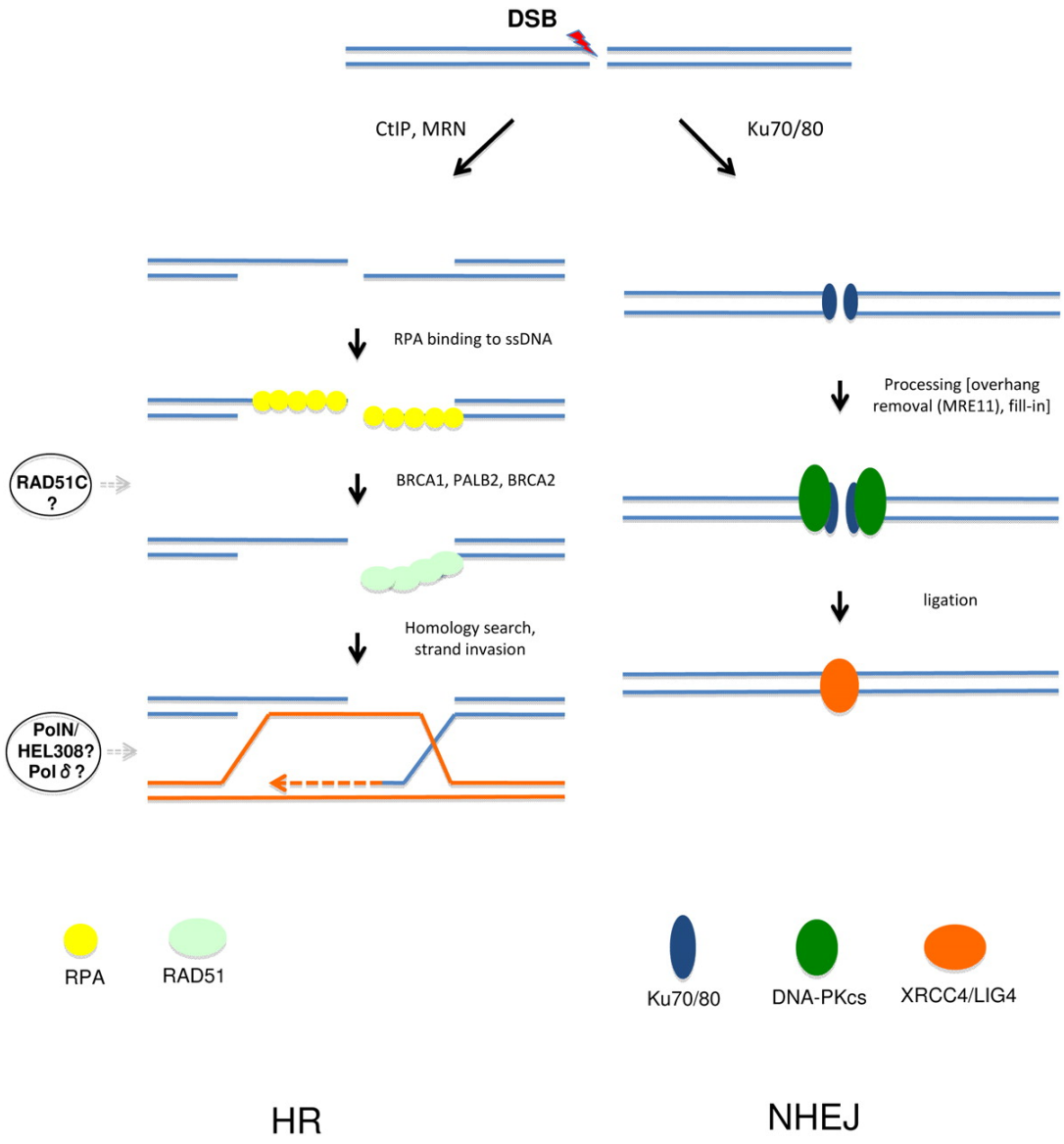

Figure 1.3-2 Process of DNA double strand break repair by homologous recombination (HR) or non-homologous end joining (NHEJ) (Kee and D'Andrea 2010).

With continued, advanced biochemical studies of DNA damage over the past 15 years, the knowledge of the DNA damage response (DDR) has expanded in concept and range. The notion of DDR now includes the sensors which detect the damage, mediators which function as both recruiters and scaffolds at damaged sites, effectors controlling the direction of response, and interconnections with a variety of pathways

such as cell cycle and chromatin remodeling. In addition there have been important advances with respect to chromatin regulation and ubiquitin during DDR, as summarized in Figure1.3-3 (Harper and Elledge 2007).

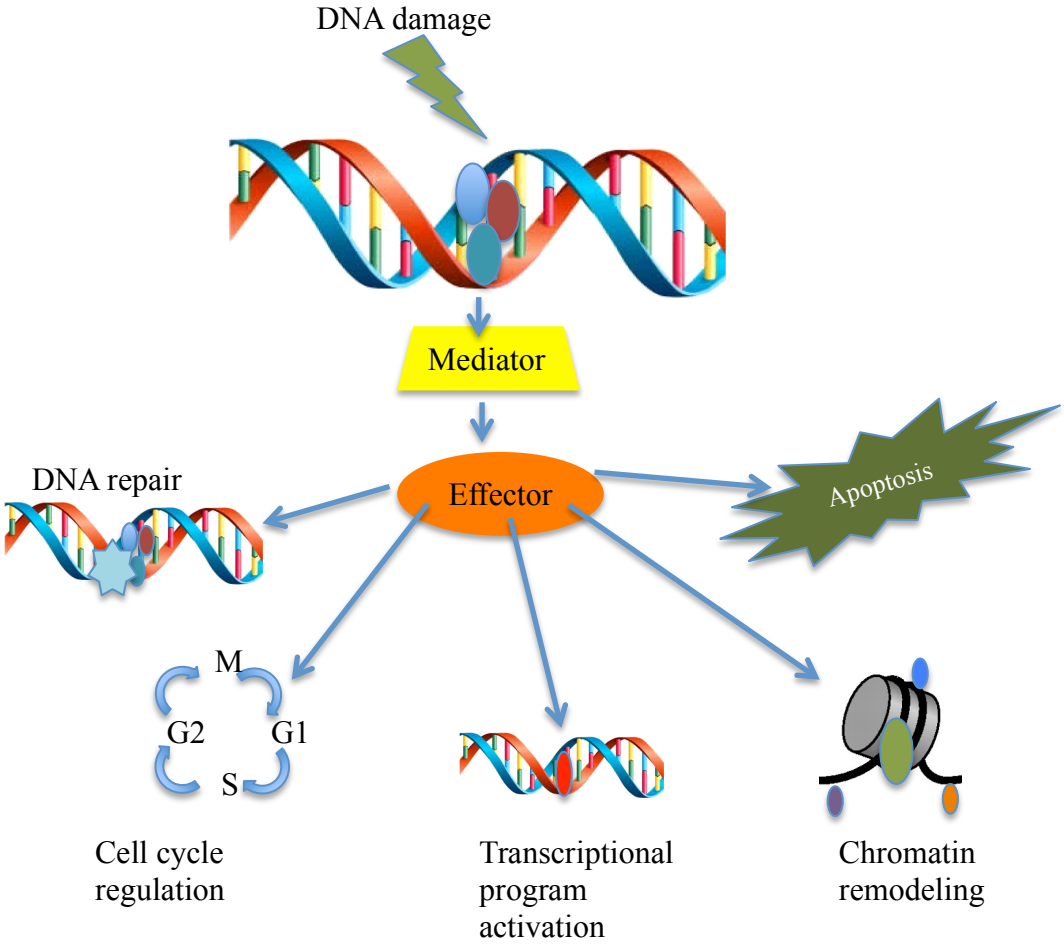

Figure 1.3-3 Cellular DNA damage process.

1.3.2 Mechanisms of cisplatin-induced DNA damage response

Platinum-based drugs are used as cancer therapy for a wide variety of solid tumours. The *cis*-diammine-dichloroplatinum(Akahira, Sugihashi et al.) is one of the most widely used platinum drugs, and is also known as cisplatin or CDDP. It has been used in the clinic as chemotherapy for several cancers, including testicular, bladder, ovarian, colorectal, lung, and head and neck neoplasms (Galluzzi, Senovilla et al. 2012). Carboplatin and oxaliplatin are analogues to cisplatin, and are also used as cancer treatments. However, either intrinsic or acquired resistance to cisplatin still remains as a critical problem for anticancer therapy.

The success of cisplatin as an anti-tumour drug is associated with its interaction with DNA, where it forms platinum-DNA adducts, which are known as cisplatin-induced DNA damage. The drug mainly reacts with N7 site of purine bases in DNA, and forms intrastrand crosslinks and a low ratio of interstrand crosslinks (ICLs), as is shown in Figure1.3-4. The intrastrand crosslink with G residues is considered to be more damaging (Basu and Krishnamurthy 2010). The distorted DNA structure interferes with normal replication and activates cell cycle checkpoints which result in cell death (Comess, Burstyn et al. 1992; O'Brien and Brown 2006; Basu and Krishnamurthy 2010).

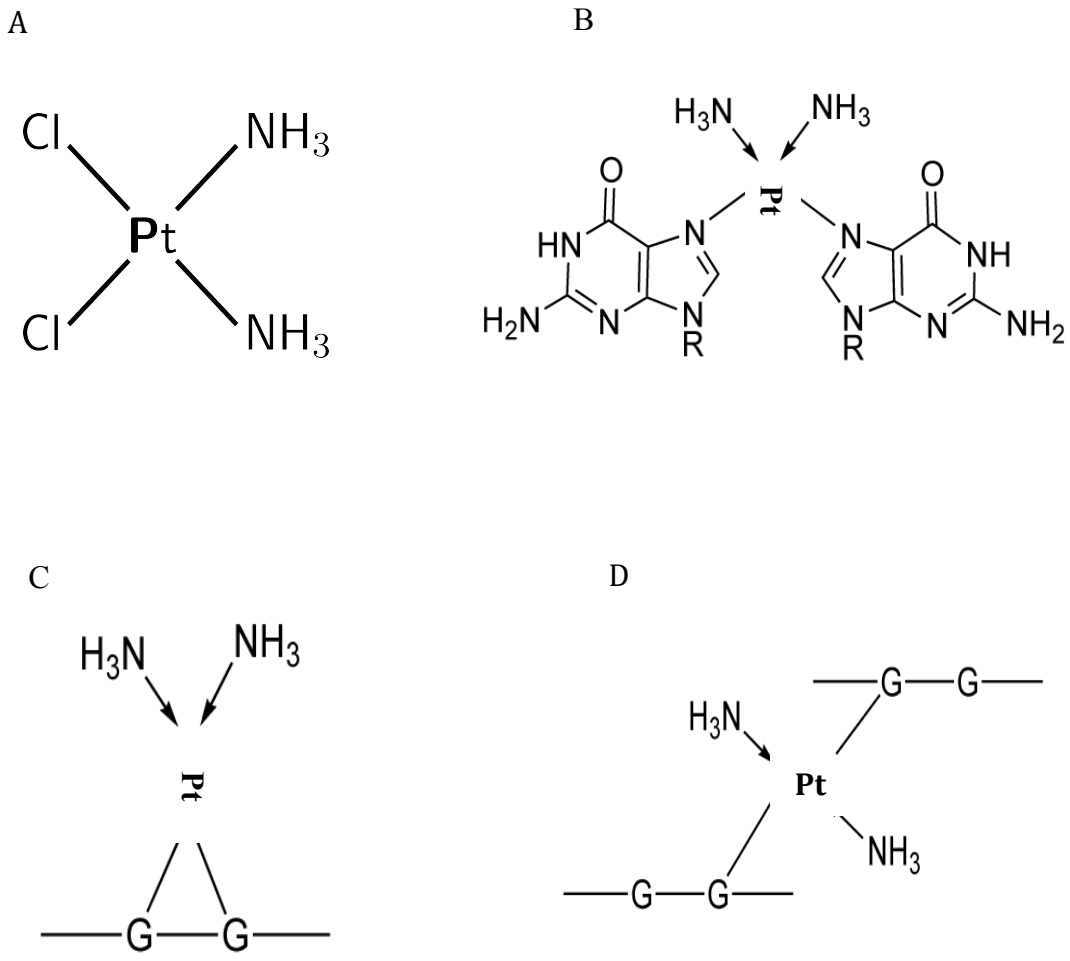

Figure 1.3-4 Cisplatin-induced DNA crosslinks. A. The structure of cisplatin. B. Reaction between cisplatin and guanine bases. C. Intrastrand crosslinks induced by cisplatin. D. Interstrand crosslinks formed by cisplatin.

The DNA intrastrand crosslinks caused by cisplatin can be repaired via nucleotide excision repair (NER). Two components in this pathway, Xeroderma Pigmentosum complementation group A (XPA) and excision repair cross-complementation group I (ERCCI), are believed play essential roles for this repair process, and increased expression of ERCC1 and XPA proteins have been implicated in cisplatin resistance (Wu, Fan et al. 2003). Although there is low ratio of ICLs (5%) induced by cisplatin (Groocock, Prudden et al. 2012), they are highly toxic to DNA and prevent DNA

separation, obstructing replication. Recognition of ICLs relies on the Fanconi anemia, complementation group M (FANCM) complex to send signals of damage to downstream effectors and recruit cell cycle checkpoint proteins and repair components. The replication protein A (RPA)-ataxia telangiectasia and Rad3-related (Kothandapani, Dangeti et al.)-CHK1 signaling is typically responsible for cell cycle regulation in response to this type of damage. BRCA1 and BRCA2 complexes trigger the activation of HR repair for these double strand breaks (Deans and West 2011). H2AX can be immediately phosphorylated on the C-terminal Ser^{139}, namely γH2AX, which accumulates at damaged sites. Therefore γH2AX has been widely used as a biomarker of DSBs. It also plays a principle role in the recruitment and activation of a range of downstream DNA damage response proteins, such as ataxia telangiectasia mutated (Miyake, Yoshizumi et al.), ATR, BRCA1, and DNA-PK (Hartlerode and Scully 2009). In addition to these pathways, other signaling pathways controlling cell growth, cell cycle arrest, apoptosis, differentiation and cellular stress responses have also been elucidated to participate in the process of DDR induced by cisplatin. These include proteins such as p53, p73, JUN amino-terminal kinase (JNK) and p38 mitogenactivated protein kinase (p38MARP) (Siddik 2003; Kelland 2007).

The cellular DDR induced by cisplatin is a well understood process with various steps and pathways involving an orchestrated and tightly regulated network; however, there are still gaps in our understanding of the mechanisms of this response. One of the crucial unresolved issues is: how and why does cisplatin resistance occur in cancer treatment? It has been pointed out that the success of chemotherapy is dependent not only on its capacity to cause DNA damage, but also on a cell's

susceptibility to sense and respond to the damage (Kerr, Winterford et al. 1994; Basu and Krishnamurthy 2010). However, the toxic effects of chemotherapeutics are a common issue that compromises cancer treatment for patients. Toxicity effects include immunosuppression and myelosuppression, secondary neoplasm, infertility, neurological adverse effects, and organ damage, so the balance between applying an adequate dose to damage cancer cells and maintaining minimal and acceptable side effects becomes an essential goal during chemotherapy (Felici, Verweij et al. 2002; Liu, Chen et al. 2011). In this case, combination treatments of cisplatin with drugs targeting those pathways which sense and respond to damage are urgently required to improve chemotherapy efficacy and overcome resistance. Detailed investigation about the mechanisms involved in the cellular responses to cisplatin are likely to provide novel targets for therapy and development of better strategies for effective anticancer therapy.

1.4 Chromatin remodeling in DNA damage responses

Over the past twenty years, chromatin remodelling has become one of the most essential fields contributing to our understanding of DDR, due to the intimate association between chromatin conformation and the ability of cells to repair damage. A wide range of research has implicated chromatin remodelling in the DDR process.

1.4.1 Crosstalk between chromatin modification and the DNA damage response

Unsurprisingly, how chromatin is packaged can definitely influence the response of a cell to DNA-damaging agents. Initial investigations established that depletion of histones induced sensitivity to extracellular ionising radiation, compared with condensed chromatin where transcription is silenced (Elia and Bradley 1992). Several studies have revealed the impact of chromatin structure on DDR process at the sites of DNA damage. Increased DDR signalling was detected when condensed chromatin was pharmacologically perturbed by expressing a galactose-inducible HO endonuclease, and H2AX phosphorylation mainly remained within areas in accessible chromatin (Kim, Kruhlak et al. 2007; Di Micco, Sulli et al. 2011). Moreover, the DSBs triggered by ionising radiation were prolonged within compact chromatin (Cowell, Sunter et al. 2007). However, the concept that an accessible chromatin environment facilitates DDR has recently been challenged. The spread of γH2AX was impeded within open chromatin regions where RNA polymerase II was recruited, and gene transcription was regulated within γH2AX domains (Iacovoni, Caron et al. 2010). In particular, there have been recent investigations into the effect of chromatin context on DNA damage repair. It has been shown that repair of DSBs near or within condensed chromatin is inefficient (Sulli, Di Micco et al. 2012). On the other hand, it has been demonstrated that homologous recombination-mediated DNA repair could be assisted by recruiting an important component of constitutive heterochromatin, namely heterochromatin protein a (HP1) (Baldeyron, Soria et al. 2011). A recently proposed dynamic model may explain these conflicting findings: noticeable DNA damage in compacted chromatin might only occur very early after

damage, and DSBs then progress outside the heterochromatic region to complete DNA repair (Chiolo, Minoda et al. 2011; Sulli, Di Micco et al. 2012). The exact mechanism by which the pre-existing and dynamic chromatin environment contributes to DDR has not been clearly identified.

More recently is has also been proposed that the chromatin alterations induced by DDR activation differ both at the site of the DNA damage lesion, and throughout the whole genome. Dynamic expansion of condensed chromatin was observed in response to ionising radiation (IR) in Drosophila cells, and chromatin with DSBs experienced a local expansion after DNA damage to a more open structure of chromatin fibers in a H2AX and ATM independent manner (Kruhlak, Celeste et al. 2006; Chiolo, Minoda et al. 2011). It has also been shown that DSBs cause an ATP-dependent chromatin de-condensation, and chromatin modification results in the initial events of DDR signalling activation, including ATM phosphorylation at serine1981 (Bakkenist and Kastan 2003). Meanwhile, DNA breaks release heterochromatin protein 1 (HP1)-beta to induce chromatin structure alterations and promote H2AX phosphorylation in mammalian cells, and this mobilization of HP1-beta relies on HP1-beta phosphorylation on Thr51 (Ayoub, Jeyasekharan et al. 2008). In addition, dynamic changes in the undamaged homologous chromosome were also observed to facilitate DDR signalling, dependent on activation of Rad51 recombinase. This provides evidence that DNA damage-induced chromatin modulation occurs globally in the genome other as well as at damaged sites (Mine-Hattab and Rothstein 2012).

Although the fact that chromatin relaxation induced by DDR facilitates downstream response signaling has been proven in several studies, there are also remarkable

evidence demonstrating the existence of compact chromatin following DNA damage. Luijsterburg and colleagues observed the recruitment of components of condensed chromatin, HP1 proteins, to the DSBs sites induced by ultraviolet radiation in human cells, which was suggested to be essential for DNA repair and chromatin reorganization in cellular DDR (Luijsterburg, Dinant et al. 2009). HP1 recruitment has been identified within damaged regions in both heterochromatin and euchromatin immediately after DNA damage (Zarebski, Wiernasz et al. 2009). In another study, chromatin decondensation which was dependent on RNA polymerase II elongation was repressed during DNA damage, which was inhibited by ATM (Shanbhag, Rafalska-Metcalf et al. 2010). Furthermore, as a silent marker within compacted chromatin, hypermethylated CpG islands were also observed in DSB DNA to suppress the transcription of genes near damaged sites, which suggested an important role for hypermethylated CpG islands in the maintainance of a stable alteration of damage ie so that there is no propagation of damage (O'Hagan, Mohammad et al. 2008; Lee, Kim et al. 2010). In this scenario, by compacting chromatin within the damaged sites, the cell protects itself from further potential injury from exogenous damage and transcription with DSBs by constructing an isolated region where repair and other DDR downstream signalling may progress.

It can be argued that the conflicting observations about chromatin structural alterations in response to DNA damage might be due to differing experimental conditions and the models applied in those studies. However, they also provide evidence which highlights the comprehensive network of chromatin reorganisation induced by DNA damage and its role in the DDR pathways. Although there are evidence showing the importance of genome stability for a cell to respond effectively

to DNA damage, and studies proving nuclear changes are triggered by DNA damage, their relationship and underlying mechanisms are incompletely understood and still deserve to be investigated.

1.4.2 Histone acetylation and DDR signalling

As discussed above, chromatin remodelling and DNA damage response pathways interact with each other in an extremely complex network. The conflicting observations about chromatin decondensation and condensation after DNA damage can be acceptably explained by a study suggesting biphasic chromatin modification after the induction of DNA damage. The authors propose that rapid histone hypoacetylation occurs after DSBs to generate a compressed chromatin condition which facilitate NHEJ. This is followed by histone acetylation to create accessible chromatin architecture which promotes HR (Miller, Tjeertes et al. 2010).

Initial investigations into the role of histone acetylation indicate the requirement of acetylation of lys56 on histones (H3H3k56Ac) for nucleosome reorganisation after damage, and participation in DNA repair (Masumoto, Hawke et al. 2005; Chen, Carson et al. 2008). In contrast, it has recently been shown that level of H3K56Ac decreased rapidly after DNA damage, and is associated with localisation of HDAC1 and HDAC2 to the damaged sites (Tjeertes, Miller et al. 2009; Miller, Tjeertes et al. 2010). HDAC1 was also found to play an important role in the DNA damage response by cooperating with the ATR checkpoint in DSBs, initiating autophagy (Robert, Vanoli et al. 2011). HDAC inhibition causes relaxation of condensed chromatin and enhanced DDR signalling and apoptosis (Di Micco, Sulli et al. 2011).

After treatment with the HDAC inhibitor PCI-24781, colon cancer cells demonstrate a significantly reduced ability for HR, with decreased transcription of HR-related genes, including Rad51, and increased sensitivity to radiation treatment as shown by decreased colony formation *in vitro* (Adimoolam, Sirisawad et al. 2007). Another line of evidence is that depletion of both HDAC1 and HDAC2 supress DSB repair with a slightly decrease in homologous recombination and abundant reduction in NHEJ (Miller, Tjeertes et al. 2010). This is consistent with the finding of overexpression of HDAC1 and HDAC2 in many tumours, especially malignant ones, possibly with the reason that they are required to modify histones and facilitate effective DNA repair during DNA damage (Fraga, Ballestar et al. 2005). Another study showed that depletion of HDAC5 sensitised sells to DNA-targeted agents and induced more apoptosis, and elucidated involvement of HDAC for the maintenance of heterochromatin structure (Peixoto, Castronovo et al. 2012). In addition, HDAC inhibitors enhanced sensitivity to DNA-damaging reagents in six human ovarian cancer cell lines with different cisplatin sensitivities, induced accumulation of γH2AX, and enhanced cell death with the combination treatment with DNA-damaging drugs (Ozaki, Kishikawa et al. 2008).

HDAC inhibitors show potential effectiveness in cancer treatment, but knowledge of how these inhibitors work is still unclear. By understanding the complex interplay between HDAC and DNA damage-induced responses in cancer therapy we can develop more effective strategies for the combination treatment of tumours with HDAC inhibitors and DNA-damaging reagents.

1.5 Heterochromatin and heterochromatin proteins

Heterochromatin is cytologically defined as nuclear regions where DNA is highly compacted (Figure 1.5-1), and it constitutes about 15-25% of mammalian DNA (Murray, Stiff et al. 2012). Heterochromatin plays an important role in the silencing of gene expression and to guard to genome integrity. The formation of heterochromatin required methylation of histone H3 at lysine 9 (H3K9me) and heterochromatin protein 1, HP1 (Piacentini, Fanti et al. 2003; Vakoc, Mandat et al. 2005). Studies have also demonstrated that heterochromatin proteins play a role in the recruitment of mediators which recruit RNA polymerase II (Pol II) to heterochromatin regions (Zofall and Grewal 2006).

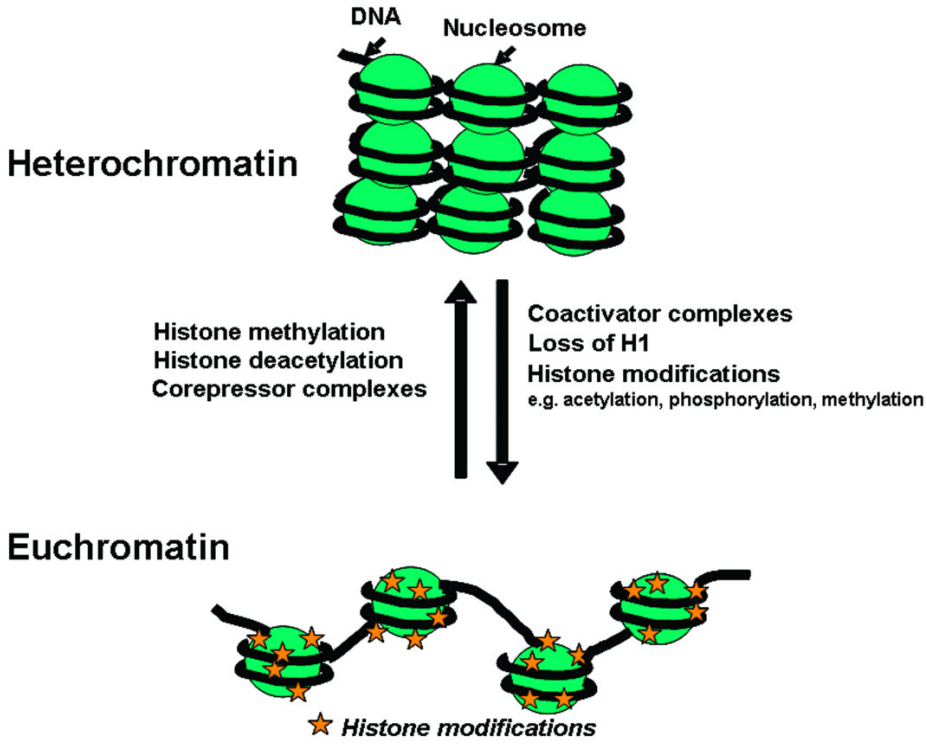

Figure 1.5-1 Compaction of heterochromatin (Adcock, Ford et al. 2006).

Heterochromatin protein 1 (HP1) is one of the essential components constituting heterochromatin and it plays various roles in establishing and maintaining heterochromatin structure, which leads to repressed transcription (Cheutin, McNairn et al. 2003). It has been reported that HP1 overexpression could cause global gene repression and /or chromatin condensation (Popova, Claxton et al. 2006; Dialynas, Vitalini et al. 2008). There are three HP1 proteins identified in human genome: HP1 alpha (HP1α), HP1 beta (HP1β), and HP1 gamma (HP1γ), and they share some functions and localise to chromatin with incomplete overlapping (Minc, Allory et al. 2001). These proteins demonstrate different localszation to centric heterochromatin, telomeres and specific sites within euchromatin (James, Eissenberg et al. 1989). Alterations in protein expression of HP proteins have been identified in some cancers in several studies, including ovarian cancer (Maloney, Clarke et al. 2007), breast cancer (Kirschmann, Lininger et al. 2000), and colorectal cancer (Ruginis, Taglia et al. 2006). Thus, along with their roles in chromatin remodelling during DDR, HP1 proteins are used in these studies as a marker for heterochromatin and the level of condensation of chromatin. We hypothesise that if HDAC protein(s) is/are involved in this 'protective' response in cells by which gene silencing occurs in order to assist cells to survive via a chromatin remodelling mechanism, then there will be alteration of HP1 protein expression and/or distribution within nuclei.

1.6 Nuclear morphology studies during cancer treatment

Cellular morphological studies (ie cytology and histopathology) are essential and useful in the evaluation of stem cell differentiation, and diagnosis of haematological and solid organ malignancies. These techniques are also used to examine responses to therapies, especially in cancer treatment; however, there is only limited research on the cellular and nuclear morphological responses caused by treatment. Early studies demonstrated alteration of cellular morphology with loss of polarity and fragmentation of nuclei into micronuclei after taxol treatment (Tishler, Schiff et al. 1992). Nuclear abnormalities, in the form of enlarged nuclei and polyploidy, have also been in the livers of perinatal embryos with ERCC-1 deficiency (McWhir, Selfridge et al. 1993). A detailed description was made in a study, stating that chemotherapy-responding ovarian tumours showed low nuclear:cytoplasmic ratio and irregular nuclear outlines with clumped chromatin after chemotherapy, and remarkable stromal changes were also noticed (McCluggage, Lyness et al. 2002). In another study, cellular morphological alterations were seen after treatment with the HDAC inhibitor, SAHA. Cell size was enlarged and they became flattened after treatment, and nuclei also exhibited distinct borders and less visible nucleoli (Munster, Troso-Sandoval et al. 2001).

With only limited descriptions about cellular morphological alterations during or in response to cancer treatment, our knowledge about these pathological responses are still in their infancy. Further investigation is deserved to establish the biological meaning of these observation and link these visible changes to fundamental cellular mechanisms during anti-cancer therapy.

1.7 Observations and preliminary studies

1.7.1 Nuclear pathological changes were observed in damaged cells

Examining the histopathological characteristics of tissues is gold-standard for disease diagnosis, especially in cancer. This also provides opportunity to observe any visible morphological changes within cells, for example changes in nuclei. Under the microscope, quite similar pathological changes of chromatin pattern and condensity are observed in the nuclei in ovarian tumours after chemotherapy (Figure 1.7-1A), breast tumours after chemotherapy (Figure 1.7-1B), and colorectal tumours post-radiotherapy (Figure 1.7-1C).

	Before treatment	After treatment
A. Ovarian tumour **Platinum** **H&E**	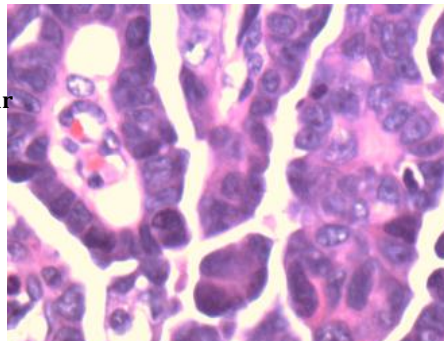	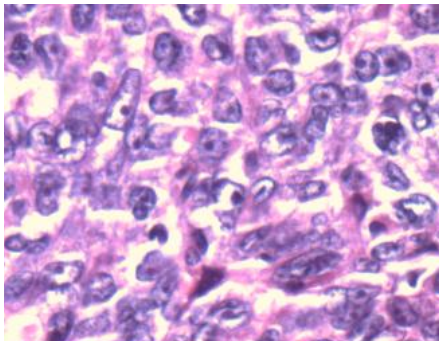
B. Breast tumour **Neoadjuvant Therapy** **H&E**	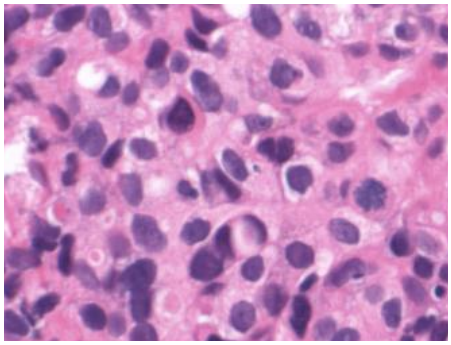	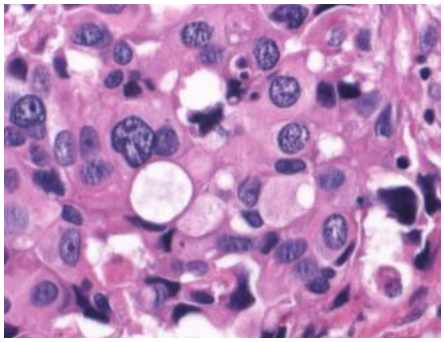
C. Colorectal Tumour **Radiotherapy** **H&E**	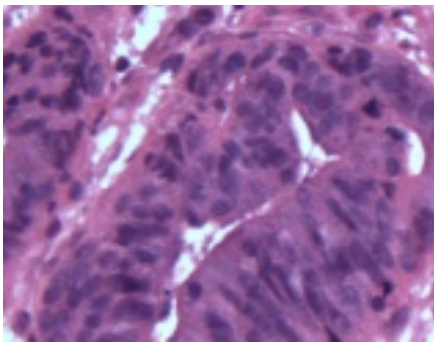	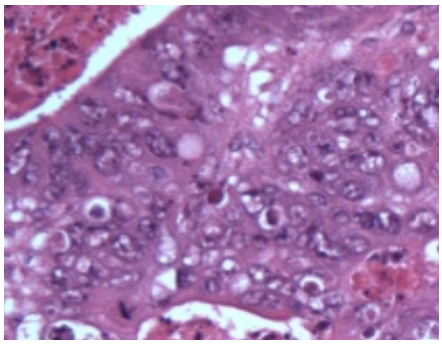

(Continued)

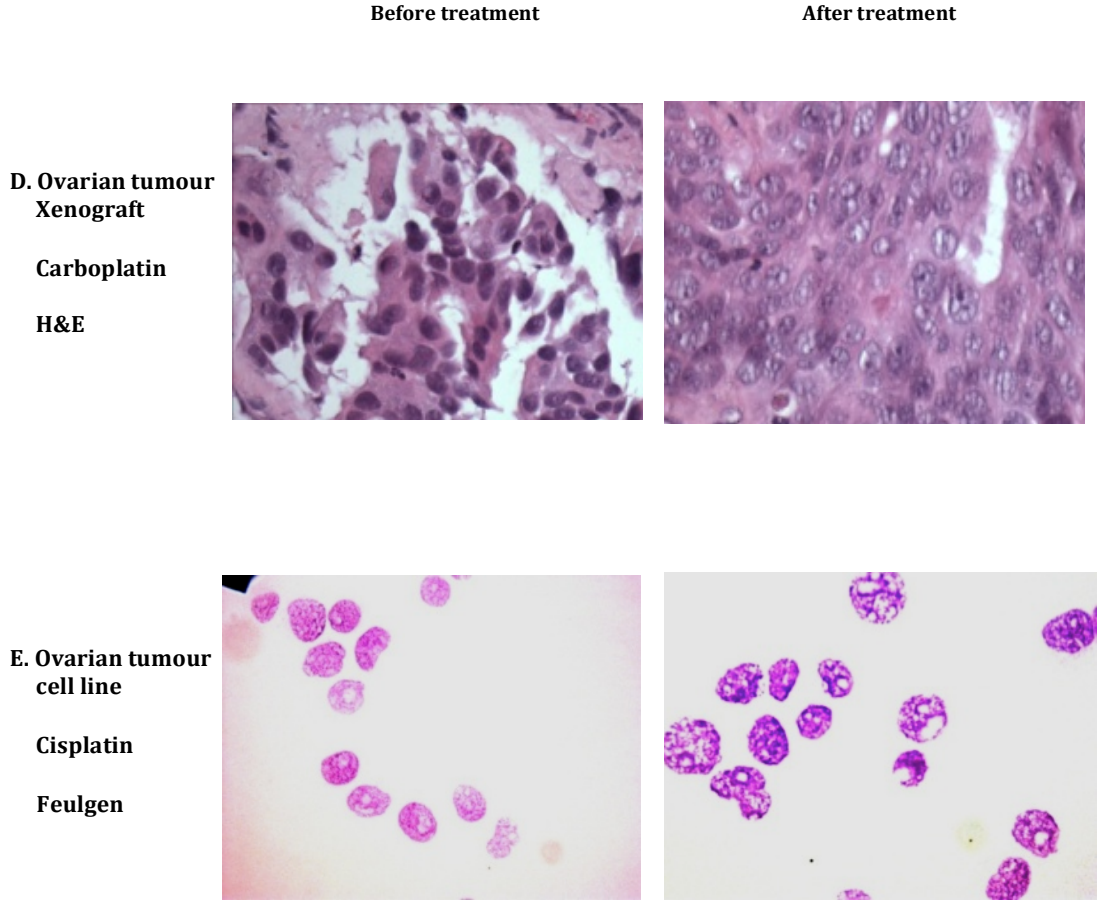

Figure 1.7-1 Similar nuclear texture changes occur in A. ovarian tumours after chemotherapy, B. breast tumours after neoadjuvant therapy, and C. colorectal tumours after radiotherapy, D. ovarian tumour xenografts, and E. ovarian cancer cell line PEO1 after cisplatin treatment under microscope. A-D are formalin-fixed, paraffin embedded sections cut from tumour samples, and stained by H&E. E are cytospinned PEO1 cells from cell culture using Feulgen stain to indicate nuclear region in each cell.

The nucleus (purple areas in H&E-stained samples and pink areas in Feulgen-stained samples) tends to be much more heterogeneous either after radiotherapy or chemotherapy, which may be regarded in a general sense as cellular injury. Tissue damage or changes occur after exposure to ionising radiation from radiotherapy or receiving chemical drugs due to their cytotoxity in chemotherapy, as described above. In addition, similar changes occurred in ovarian tumour xenografts (Figure1.7-1D) during carboplatin treatment and the ovarian cancer cell line PEO1 (Figure1.7-1E) treated with cisplatin. Thus this phenomenon about nuclear change appears to be quite general.

1.7.2 A histone deacetylase is potentially associated with response to chemotherapy in ovarian cancers

As discussed above, chromatin change may manifest itself as peripheralisation, which is known to be associated with methylation/acetylation of histones and gene repression, after chemotherapy or radiotherapy injury. This peripheralisation has also been reported in cells containing double strand breaks (DSBs) after DNA damage (Oza, Jaspersen et al. 2009).

Initially, a V250 antibody microarray was used to investigate differential phosphoprotein expression of 125 selected signalling proteins related to cancer among a range of ovarian cancer cell lines in our lab (unpublished data, D. Faratian). The V250 proteomic data (Figure 1.7-2) showed that phosphorylation of histone deacetylase, particularly HDAC8 (indicated by ‘deacetylation’ in the heatmap), was the top discriminator between clusters in an unsupervised analysis of ovarian cancer cell lines (p=0.001, t-test). These clusters (cluster A and cluster B) appeared to be

associated with exposure to therapy/platinum resistance (see table 1.7-1 for the information about cell lines). Thus this indicated a possible association of HDAC proteins with response to chemotherapy in ovarian cancer, and we speculated that HDAC might be a factor that mediates resistance to, or might be a therapeutic target for use during, DNA damage-inducing therapies.

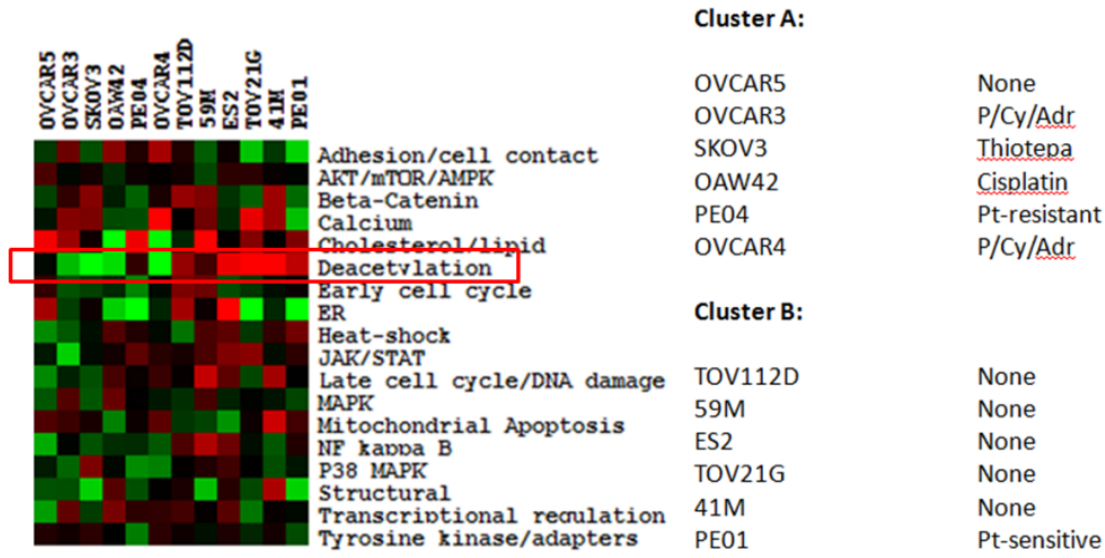

Figure 1.7-2 V250 proteomic data in an unsupervised analysis of ovarian cancer cell lines. Heatmap was generated from averaged values of normalised phospho:non-phospho ratio of 125 selected proteins summed as ontological groups to give a global overview of pathway changes (indicated on the right side of the heatmap). 12 ovarian cell lines are classified into two groups, as shown in the right panel. The full list of proteins included and grouped in different pathways in the study are shown in Table S7. Deacetylation refers to phospho:non-phospho ratio of HDAC8.

Cell line	Histotype	Source	Treatment/resistance
PEO1	Poorly differentiated serous adenocarcinoma	Ascites	Platinum treated and sensitive
PEO4	Poorly differentiated serous adenocarcinoma	Ascites	Platinum resistant
OVCAR3	Poorly differentiated papillary adenocarcinoma	Ascites	Cisplatin/ cyclophosphamide/ adriamycin treated
OVCAR4	Adenocarcinoma	Ascites	Cisplatin/ cyclophosphamide/ adriamycin treated
OVCAR5	Adenocarcinoma	Ascites	None-treated
SKOV-3	Adenocarcinoma	Ascites	Thiotepa treated
OAW42	Serous adenocarcinoma	Ascites	Cisplatin treated
41M	Adenocarcinoma	Ascites	None-treated
59M	Endometrium adenocarcinoma	Ascites	None-treated
ES2	Clear cell carcinoma	Primary tumour	None-treated
TOV112D	Endometrioid carcinoma	Primary tumour	None-treated
TOV21G	Clear cell carcinoma	Primary tumour	None-treated

Table 1-4 Properties of Ovarian cell lines used in V250 study.

1.8 Hypothesis and aims

As cancer drug resistance, especially acquired resistance, becomes a more pressing clinical concern for doctors treating patients with recurrent disease, mechanistic research into responses to treatment are of increasing importance. Dynamic structural remodelling of chromatin has a potential role during DNA damage-inducing

therapies, but large part of how they work together remains unknown. Our preliminary studies demonstrate quite general observations about global nuclear changes in morphology, and histone acetylation may be involved in the response to chemotherapy. As one of the important chromatin modifiers, we speculate that HDACs may play a causative role in these damage-induced nuclear changes. We therefore hypothesise that nuclear morphological changes in cancer in response to DNA-damage by chemotherapy are mediated by histone deacetylases (HDACs). To further understand in more detail the molecular processes behind these morphological alterations and identify novel mechanisms of ovarian cancer resistance, there are several issues which will be addressed using various techniques:

1: Do nuclear changes occur in response to injury and what is the cellular effect (+/- HDAC as key mediator)?

- Establishing tractable cell line models
- Establishing robust quantification of nuclear changes with image analysis and/or other markers
- Detecting nuclear phenotype alteration after therapy (platinum), with/without inhibition of HDAC
- Analysing nuclear morphological changes in clinical ovarian samples pre- and post-treatment and in *in vivo* models
- Measuring other markers of heterochromatin (e.g. HP1 proteins)
- Quantifying apoptosis, cell cycle, DNA-damage in cells exhibiting the phenomenon

- Detecting the reversibility with withdrawal of stimulus

2: Is HDAC a resistance factor to DNA-damaging therapy and how does it mediate its effect?

- HDAC expression with chemotherapy confirmed in cell lines by WB or PCR
- Quantifying HDAC and HP1 expression pattern *in vivo* (using ovarian xenografts)
- Inducing sensitivity with HDAC depletion
- Reversing sensitivity in cancer cells to establish functions of HDAC proteins in cellular DNA damage response induced by platinum
- Evaluation the cellular effect of DDR after HDAC depletion such as cell cycle distribution and apoptosis induction

2 Materials and Methods

2.1 Cell culture

Cells were always grown in a humidified atmosphere of 5% CO_2 at temperature of 37°C.

2.1.1 Routine cell line culture conditions

For cell culture, these cells were grown as monolayer cultures in RPMI supplemented with 10% heat-inactivated fetal calf serum (FCS) and penicillin / streptomycin (100IU/mL).

2.1.2 Subculturing of cells

For continuing growth, cells were passaged when cell number achieved 80-90% confluence. Media was removed and cells were washed with warmed PBS once. After incubation with trypsin for a few minutes in the incubator, media was added to neutralise the trypsin and cells were spun down at 285 x g for 4 minutes. The pellets were re-suspended in normal culture media and transferred into flasks at an appropriate dilution.

2.1.3 Cell culture for drug treatment

All the experiments in terms of drug treatment utilised this protocol unless otherwise stated. Cells were harvested in RPMI supplemented with 10% heat-inactivated FCS and penicillin / streptomycin (100IU/mL) for 72h before drug treatment.

2.1.4 Cryopreservation and cell recovery from liquid nitrogen

Cells were grown to 80-90% confluence in a 175cm^2 flask, trypsinised, and centrigued at 285 x g for 4 minutes. Cell pellet were then resuspended in about 5ml of Freeze Mixture-heat-inactivated FCS/10% DMSO, and aliquoted into cryopreservation vials. All the cells were frozen and stored in the liquid nitrogen

storage room of Breakthrough Breast Cancer Unit (Western General Hospital, Edinburgh) until needed.

To recover cells from liquid nitrogen, cell samples were thawed and transferred into a 25ml universal container, and warm normal culture media was added to make up a volume of 25ml. After centrifugation at 285 x g for 4 minutes, cell pellets were resuspended in fresh media and transferred into a suitable flask for routine culture.

2.2 Knockdown of HDAC2 in PEO1 and PEO4 cells with RNAi

The knockdown work for HDAC2 by transfecting RNAi to cells was conducted in 60mm cell culture dishes, and the reverse transfection method was performed as the manufacture's instruction.

Briefly, the RNAi duplex-LipofectamineTM RNAiMAX complexes were prepared as follows.

a. 10-100pmol RNAi duplex was diluted in 500µl Opti-MEM® I Medium without serum in each cell culture dish and mixed gently.

b. Lipofectamine^{TM} RNAiMAX was mix gently, 0.8 µl of which were added to each dishes containing the diluted RNAi molecules. The mixture was incubated for 20 minutes at room temperature.

After the incubation, cells were diluted in complete growth medium without antibiotics with the concentration of 700,000 – 800,000 cells/ 5mL so that cell density would be 30-50% confluent 24hours after seeding. To each well with RNAi

duplex-LipofectamineTM RNAiMAX complexes, 5mL of the cell mixture was added, and also mixed gently by rocking the plate back and forth.

Several control groups were also included in experiments to detect the efficiency of knockdown: untransfected control group without any of transfection agents, mock group only with Lipofectamine^{TM} RNAiMAX mixture, and negative control group with the random RNAi duplex containing similar range of GC content to siHDAC2.

The cells and the complexes were incubated for 24-120h at 37^{o}C in full serum without antibiotics. For drug treatment, cisplatin was added after 48 hours of transfection, and cells were collected after several time points as indicated.

2.3 Xenograft models

Two systematic mice models were established in our lab model OV1002 and model HOX242. Female adult CD-1 nude mice housed in IVCs (individually ventilated cages) were treatment with Carboplatin (50 mg/kg i.p.) on Day 0, and tumour samples were collected on Day0, 1, 4, 7, and 14 after treatment. Model OV1002 showed much more sensitive to carboplatin treatment compared with HOX242.

2.4 Cell proliferation analysis by Sulforhodamine B assay

Cells were harvested in log phase, then split by trypsin, counted using a haemocytometer and optimal initial numbers of cells in an aliquot of 200 uL per well were seeded into 96 well cell culture plates in a humidified atmosphere of 5% CO_2 at 37°C for 72h. Cells were then treated with reagents specified in result section. After incubation for 0-6 days with testing materials, cells were fixed by 25% cold

trichloroacetic acid (50uL/well), and incubated for 1h at 4°C. Plates then were washed with running tap water by ten times and air-dried in a warm oven (50°C), after which cells were stained with sulforhodamine B dye (0.4 % solution in 1 % acetic acid, 50 μl/well) for 30 min. After washed with 1% acetic acid by 4 times, plates were dried in the oven again. 100uL Tris buffer (10mM, pH 10.5) were added into each well 1h prior being read and were shaken gently during the incubation. The optical density (OD) was recorded using Biohit BP800 Microplate reader at 540 nm.

2.5 Protein extraction from mammalian cell lines

Cells were harvested in log phase, plated into 60mm petri dishes and incubated for 72hr or specified period after treatment. After the incubation, cells were washed in cold PBS, and lysed with scraping in ice-cold isotonic lysis buffer [50mM Tris-HCl (pH7.5), 5mM EGTA (pH 8.5), 150mM NaCl, 1% Triton X-100] supplemented with aprotinin (10 μg/mL) and a 'Complete' Protease Inhibitor Cocktail Tablet (Roche, 11836153001) for 30min on ice. Lysates were then centrifuged for 6min at 13,000 × g. The supernatant was recovered as cleared cell lysate and sorted at -70°C.

2.6 Protein quantification

This assay is carried out in 12 x 75mm borosilicate glass tubes (Fisher; 14-961-26). A 1mg/mL protein standard in 0.15M Sodium Chloride (Sigma; P0914-5AMP) was used to create an 8-point standard curve. Protein concentrations were determined using the Bicinchoninic Acid (BCA) assay (Sigma, BCA-1). In brief, 1 part of a protein was mixed with 20 parts of the BCA Working Reagent and then incubated for 15min at 60°C. Absorbance of the sample solution was measured at 562 nm using

Microplate reader (Biohit BP800). Protein concentration was then calculated using the standard curve generated from known standards.

2.7 SDS polyacrylamide gel electrophoresis

The separation of proteins on the basis of their electrophoretic mobility was achieved by denaturing sodium dodecyl sulphate polyacrylamide gel electrophoresis (SDS-PAGE), using the vertical electrophoresis system (Bio-Rad, Mini-PROTEAN® 3). Concentrations of polyacrylamide gels were 10%. First, the resolving gel (8-12% Acrylamide, 390mM Tris-HCl pH8.8, 0.1% SDS, 0.1% APS, polymerisation was initiated by adding 0.08% TEMED) was set up in a gel caster and was overlaid with isopropanol or distilled water in order to remove air bubbles. After the resolving gel was polymerised at room temperature, the isopropanol was removed followed by setting up of the stacking gel (5% Acrylamide, 123mM Tris-HCl pH6.8, 0.1% SDS, 0.1% APS, 0.1% TEMED). 25ug of each protein lysate sample was prepared in SDS-PAGE sample buffer and was heated at 60°C for 60min, and then loaded on to the gel and electrophoretically resolved with protein ladder (Prestained Protein Marker, Broad Range, 7-175 kDa, New England Biolabs) in the running buffer (192mM Glycine, 25mM Tris, 0.1% (w/v) SDS) at 80V for the stacking gel and 140V for the resolving gel.

Since their large molecular weight, AMT, pATM, ATR, and pATR were analyzed by using 3-8% Tris acetate gels and Tris acetate running buffer from NOVEX® under manufacturer's instruction.

2.8 Western blotting

After the SDS-PAGE, the resolved proteins were electrophoretically transferred onto a nitrocellulose membrane at 30V, 4°C overnight. After transfer, membranes were rinsed in PBST and then blocked with Li-Cor Odyssey Blocking Buffer (diluted 50:50 in PBS) for 1h at room temperature before probing overnight at 4°C with the appropriate primary antibody made up in Li-Cor Odyssey Blocking Buffer (diluted 50:50 in PBS) using 1:1000 dilution. Primary antibodies used for western blotting were listed in Table 2.2-1. The membranes were then washed by PBS-Tween20 (1mL Tween20 /1L PBS) before incubated with fluorescently-labelled secondary antibodies diluted with Odyssey Blocking Buffer (diluted 50:50 in PBST) at dilution 1:10,000. Mouse-derived primary antibodies were detected using an anti-mouse fluorescently-labelled secondary antibody (680nm wavelength) whilst rabbit-derived primary antibodies were detected using an anti-rabbit fluorescently-labelled secondary antibody (800nm wavelength). By combining a mouse primary and a rabbit primary along with their respective secondary antibodies (one of 680nm and the other of 800nm), dual-labelled Westerns were obtained. Secondary antibody incubation lasted 45min at room temperature in the dark with gentle shaking. The membranes were then scanned on the Li-Cor Odyssey scanner, and the fluorescence value (integrated intensity, I.I.) corresponded with the detected protein expression levels. A-tubulin (Mouse derived, Abcam, ab7291) was selected as loading control.

Primary antibody	Working Dilution	Source	Supplier/Catalogue No.
Anti-HP1 alpha	1:1000	Rabbit	Cell Signaling/2623
Anti-HP1 beta	1:1000	Rabbit	Abcam/ab10478
Anti-HP1 gamma	1:1000	Rabbit	Cell Signaling/2619
Anti-HDAC1	1:1000	Mouse	Cell Signaling/5356
Anti-HDAC2	1:1000	Rabbit	Cell Signaling/2540
Anti-HDAC3	1:1000	Rabbit	Abcam/ab32369
Anti-HDAC4	1:1000	Rabbit	Abcam/ab32534
Anti-HDAC8	1:1000	Rabbit	Abcam/ab39664
Anti-AMT	1:750	Mouse	Abcam
Anti-pATM (Ser1981)	1:1000	Rabbit	Cell signalling/4526
Anti-ATR	1:1000	Rabbit	Abcam/ab2905
Anti-pATR(Ser428)	1:1000	Rabbit	Cell Signaling/2853
Anti-pBRCA1(Ser1524)	1:1000	Rabbit	Cell Signaling/9009
Anti-γH2AX	1:1000	Rabbit	Cell Signaling/2577
Anti-Rad51 (H-92)	1:1000	Rabbit	Santa Cruz/sc-8349
Anti-α-tubulin	1:6000	Mouse	Abcam/ab7291
Anti-β-tubulin	1:6000	Rabbit	Abcam/ab6046
Anti-GAPDH	1:8000	Mouse	Abcam/ab8245

Table 2-1 Primary antibodies used for Western blot analysis.

2.9 Preparation of RNA

Total RNA was extracted from cultured cells using Qiagen Mini RNeasy Kit. Cell culture medium was completely aspirated before the cell lysis. Cells (no more than 1 x 10^7 cells) were directly lysed by adding 350µl Buffer RLT to the cell-culture dish. After that, the lysate was collected by a rubber policeman, pipetted into a microcentrifuge tube, and then vortexed to remove cell clumps. 1 volume of 70% ethanol was applied to the homogenized lysate. Immediately after pipetting, the sample which included any precipitate that might have formed was transferred into an RNeasy Mini spin column in a 2ml collection tube, centrifuge at 8000 x g for 15s at room temperature. Flow-through was discarded and this step was repeated till the entire sample was done. The RNA sample in the column was washed by Buffer RPE with centrifugation for 15s at 8000 x g. After washing, the RNeasy Mini spin column was transferred to a new 1.5ml collection tube. The total RNA was eluted in 30ul RNase-free water by centrifuging for 1 min at 8000 x g. The concentration and quality of RNA was assessed by NanoDrop.

2.10 Real time Polymerase chain reaction (PCR)

1µg of total RNA from each individual sample was reverse transcribed by using the QuantiTect Reverse Transcription kit (Qiagen) following the manufacturers' protocol. The contaminating genomic DNA was effectively removed by incubating with gDNA Wipeout Buffer (comes with the kit) at 42°C for 2min. After genomic DNA elimination the reverse transcription was carried out by adding a master mix prepared from Quantiscript Reverse Transcriptase, Quantiscript RT Buffer and RT Primer Mix

to the RNA sample. The entire reaction was incubated at 42°C for 15 min and then inactivated at 95°C for 3 min. 20μL of cDNA was yielded from 1μg total RNA following the reverse transcription.

cDNA was quantified using Rotorgene (Corbett Research, San Francisco, CA) and the QuantiTect SYBR Green system (Qiagen) following the manufacturers' instructions. For PCR reaction, a 13-fold dilution of the above cDNA mixture (10-fold dilution for standard curve) and a 10-fold dilution of primers HDAC8, β-actin (ordered from Qiagen) were used. A 15ul mixture of 7.5μl 2xQuantiTect SYBR Green iMaster Mix, 1.5 μL primer mix (0.3 μM), 2.5mM of $MgCl_2$, 1.5 μL cDNA was prepared in RNase-free water for the PCR reactions. The standard PCR protocol used was as follows: initial activation at 95°C for 15min; 45 cycles of denaturation at 94°C for 15s; annealing at 56°C for 30s; extension at 72°C for 30s and a final extension at 72°C for 5min followed by a melt step from 55°C to 95°C at 0.2°C/s.

2.11 Human sample study population

Ovarian cancer samples were collected before and after chemotherapy respectively. There were 38 pairs remaining for statistical analysis after TMA construction, immunostaining, AQUAsition and AQUAnalysis. TMAs were constructed in biological triplicates (patient information shown in Table 2.2-2 and full data are provided in Table S8).

Classification	sub-classification	patient number	% total
Regimen	Carboplatin/Paclitaxel	11	29
	Cisplatin	7	18
	Carboplatin	17	45
	Cisplatin/Topotecan	3	8
Sensitivity	responsive	19	50
	resistant/refractory	19	50
FIGO stage	2A	2	5
	2B	2	5
	2C	2	5
	3(pre FIGO)	4	11
	3A	2	5
	3C	16	42
	4	6	16
Grade	2	10	26
	3	27	71
Histology	Endometrioid	14	37
	Mucinous	3	8
	Serous papillary	15	39
	mixed Serous/endometrioid	1	3
	Clear cell	2	5
	Mixed endometrioid/clear cell	2	5
	Undifferentiated carcinoma	1	3

Table 2-2 Ovarian cancer Patient information in the TMA used in this study.

2.12 Tissue Microarray (TMA) construction

TMAs consist of paraffin blocks in which as many as up to 1000 tissue cores of samples to be tested are assembled in array fashion to allow simultaneous histological analysis. A hollow needle is used to sample tissue cores from regions of interest in paraffin embedded tissues, which includes clinical biopsies or tumour samples. The extracted tissues are then embedded into a recipient paraffin block in a precisely spaced array pattern for further analysis.

For this thesis, the TMAs (constructed by In Hwa Um; University of Edinburgh) were made according to protocols established in our lab. In brief, 0.6 mm tissue cores were removed from each 'donor' paraffin-embedded tumour block and then precisely mounted into new 'recipient' paraffin blocks (Figure2.2-1) to form the TMAs in certain orientation, after which 4μm of formalin-fixed, paraffin embedded sections were cut from each TMA block on to microscope slides.

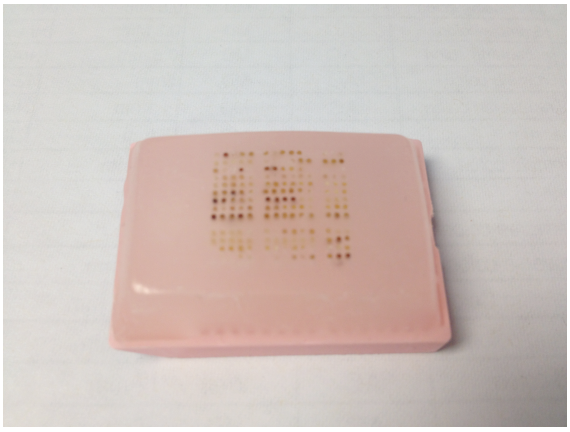

Figure 2.12-1 Representative picture for a TMA block. The spot on paraffin block were from each 'donor' paraffin-embedded tumour block. The TMAs were constructed in certain orientation so that every core will be easily distinguished to link to relative tumour information.

2.13 Immunohistochemistry (IHC)

This assay was performed for antibody optimization. 4μm of formalin-fixed, paraffin embedded sections cut from each TMA block were deparaffinised in xylene for 5min and rehydrated in 99%, 99%, 80% and 50% ethanol for 2min, respectively. Antigen retrieval was then achieved by treating slides with microwave pressure cooking in 0.15mM Sodium Citrate, pH6.0 buffer or Tris-EDTA, pH9.0 for 5min. After the antigen retrieval, slides were left at room temperature for at least 20min to cool down. Cooled slides were rinsed in 0.05% phosphate buffered saline (PBS, OXOID, #BR0014G)-Tween (Tween20, BIO-RAD, #170-6531) (PBS-T) twice for 5min followed by blocking in 3% hydrogen peroxide (in order to block endogenous peroxidase activity) and serum free protein block (Dako, #X0909) for 10min each in staining trays. After rinsing in PBS-T 2 x 5min, the blocking slides were then incubated with primary antibody diluted using Dako antibody diluent (Dako, #S0809). The optimal dilution factor of each antibody was determined by our own laboratory. Table 2.2-3 lists information of all primary antibodies used in this assay. Target primary antibodies were incubated for either 1 h at room temperature or overnight at 4°C according to the antibody optimization and validation data and then rinsed again with PBS-T. In order to stain sections the Dako REAL EnvisonTM Detection system (Dako, #K5007), which consists of Envision™/HRP solution, diaminobenzidine (DAB chromogen) and substrate buffer containing hydrogen peroxide, was applied to the primary antibody-treated samples. In brief, sections were incubated at room temperature with Dako Envision Envision™/HRP solution which comprised of a dextran backbone coupled to multiple peroxidase (HRP) molecules and a mixture of secondary mouse antibody molecules for 30min, rinsed

with PBS-T, and then incubated with DAB substrate in DAB buffer diluted 1:50 for 10min to visualise the colour develops. Following the staining step, sections were counterstained in haematoxylin for 30s and then rinsed with Scott's tap substitute. After that, sections were dehydrated by going through graded alcohols to xylene. As described before sections were treated for 2min in each alcohol solution and 5min in each xylene. Finally dehydrated sections were mounted with glass coverslip using DPX mountant. By using negative controls, different antigen retrieval methods, and different antibody concentration and incubation methods, optimum conditions for each antibody and each tissue were evaluated on the following aspects: intensity of positive staining (with scoring ranging from 3 points for maximum intensity positive staining to 0 points for no positive staining), lack of non-specific background (with scoring ranging from 3 points for no background staining to 0 points for intense widespread background staining), and signal to noise ratio (with scoring ranging from 3 points with no non-specific staining, to 0 points for no positivity but strong widespread non-specific staining).

Primary antibody	Tissue tested	Dilution tested	Source	Type	Supplier details	Final silution
HP1 alpha	Breast	1:50, 1:150, 1:300	Rabbit	IgG	Cell Signaling	1:50
HP1 alpha	Ovary	1:50, 1:100	Rabbit	IgG	Cell Signaling	1:100
HP1 beta	Breast	1:50, 1:150, 1:300	Rabbit	IgG	Abcam	1:100
HP1 beta	Ovary	1:100, 1:150	Rabbit	IgG	Abcam	1:150
HP1 gamma	Breast	1:100, 1:250, 1:500	Rabbit	IgG	Cell Signaling	1:250
HP1 gamma	Ovary	1:250, 1:400	Rabbit	IgG	Cell Signaling	1:400
HDAC1	Ovary	1:100, 1:200, 1:400	Mouse	IgG	Cell Signaling	1:200
HDAC2	Ovary	1:25, 1:50, 1:100, 1:200	Mouse	IgG	Cell Signaling	1:25

Table 2-3 Primary antibodies used for antibody optimization in immunohistochemistry.

2.14 Immunofluorescence (IF) on TMAs

This assay was performed with the optimized condition for each target protein as listed in Table 2.2-4. 4µm of sample sections were deparaffinised in xylene for 5min and rehydrated in 99%, 80% and 50% ethanol for 2min, respectively. For antigen retrieval, sections were treated with 0.15mM Sodium Citrate, pH6.0 buffer or Tris EDTA, pH9.0 using a microwave pressure cooker for 5min. Sections were then left at the room temperature for at least 20min followed by rinsing in 0.05% PBST, blocking in 3% hydrogen peroxide and serum free protein block (Dako, #X0909), 10min each. After blocking slides were then incubated with primary antibodies diluted with optimal dilution in second primary antibody (Mouse anti- cytokeratin, Invitrogen, #18-0132) diluted in Dako antibody diluents with 1:25 dilution either for

1h at room temperature or overnight at 4°C. Sections were then rinsed in 0.05% PBST 3 times 5min each followed by incubation with secondary antibodies for 1h at room temperature, which included a 1:25 dilution of the goat anti-mouse Alexa 555 antibody (Invitrogen, #A21422). After rinsing in 0.05% PBST 3 × 5min, sections were transferred from the sequenza to the humidity chamber and incubated with target signal amplification diluents and the Cy5 Tyramide at 1:50 concentration in the dark for 10min at room temperature to allow the visualisation of target protein. Slides were rinsed again in 0.05% PBST 3 × 5min, dehydrated in 80% ethanol for 1min and air dried in the dark. For counterstaining and coverslipping, 45ul of Prolong Gold anti-fade reagent with DAPI (Invitrogen, P36931), nuclear visualisation media was applied to the 20 × 26mm coverslip, which was then placed over the tissue. Mounted slides were left in the dark overnight in order to dry, secured with nail polish to ensure long term preservation and kept in a 4°C refrigerator. The antibodies used for IHC and IF were validated by western blotting. Blots were required to show a single band at the correct molecular weight. These validation experiments were performed either by myself or other individuals working with the same antibodies in the laboratory.

Primary Antibody	Tissue tested	Dilution	Antigen retrieval method	Antigen retrieval buffer	Primary antibody incubation	Supplier details
HP1 alpha	Breast	1:50	Microwave + pressure cooking	Sodium Citrate	Over night at 4°C	Cell Signaling
HP1 alpha	Ovary	1:100	Microwave + pressure cooking	Sodium Citrate	Over night at 4°C	Cell Signaling
HP1 beta	Breast	1:100	Microwave + pressure cooking	Sodium Citrate	One hour at room temperature	Abcam
HP1 beta	Ovary	1:150	Microwave + pressure cooking	Sodium Citrate	One hour at room temperature	Abcam
HP1 gamma	Breast	1:250	Microwave + pressure cooking	Sodium citrate	Over night at 4°C	Cell Signaling
HP1 gamma	Ovary	1:400	Microwave + pressure cooking	Sodium citrate	Over night at 4°C	Cell Signaling
HDAC8	Breast	1:100	Microwave + pressure cooking	TE Tris	One hour at room temperature	Abcam
HDAC8	Ovary	1:100	Microwave + pressure cooking	TE Tris	One hour at room temperature	Abcam
HDAC1	Ovary	1:200	Microwave + pressure cooking	Sodium citrate	One hour at room temperature	Cell Signaling
HDAC1	Ovary	1:25	Microwave + pressure cooking	Sodium citrate	Over night at 4°C	Cell Signaling
Aurora A	Ovary	1:25	Microwave + pressure cooking	Sodium citrate	Over night at 4°C	Cell Signaling
Aurora A	Ovary	1:400	Microwave + pressure cooking	Sodium citrate	One hour at room temperature	Abcam
Geminin	Ovary	1:800	Microwave + pressure cooking	Sodium citrate	One hour at room temperature	Abcam

Table 2-4| Antibodies used in immunofluorescence.

2.15 Automated Quantitative Analysis (AQUA) of protein expression

The IF result was analysed using the automated quantitative analysis (AQUA) system. After the counterstaining and cover-slipping steps, the slides were imaged on the HistoRx PM- 2000™ instrument (Camp, Chung et al. 2002) by an automated spot capturing system (Figure 2.2-2).

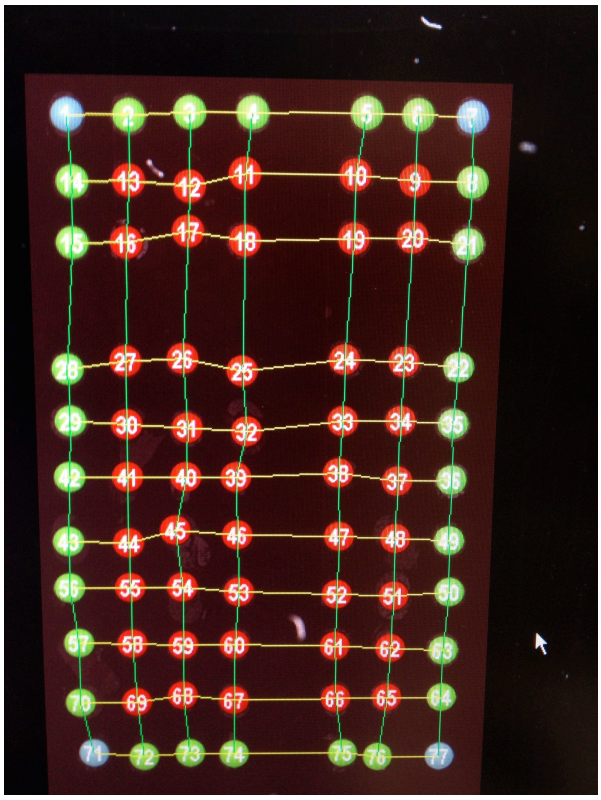

Figure 2.15-1 TMA Spot finding (Red spot-inner spots, Green-outer line spots, Blue-four corner spots).

Images were visualised by using AQUAsition software at 20 x magnifications via DAPI, CY3 and CY5 channels (Figure2.2-3). Afterwards, high-resolution images obtained were analysed using the AQUA® technology platform. For each immunofluorescence image, AQUAnalysis software evaluated the quantity (in

AQUA units=Au) of target protein expression (through Cy-5-thymide) within the cytoplasm (identified by cytokeratin) and nuclei (4,6-Diamidino-2-phenylindole, DAPI counterstaining).

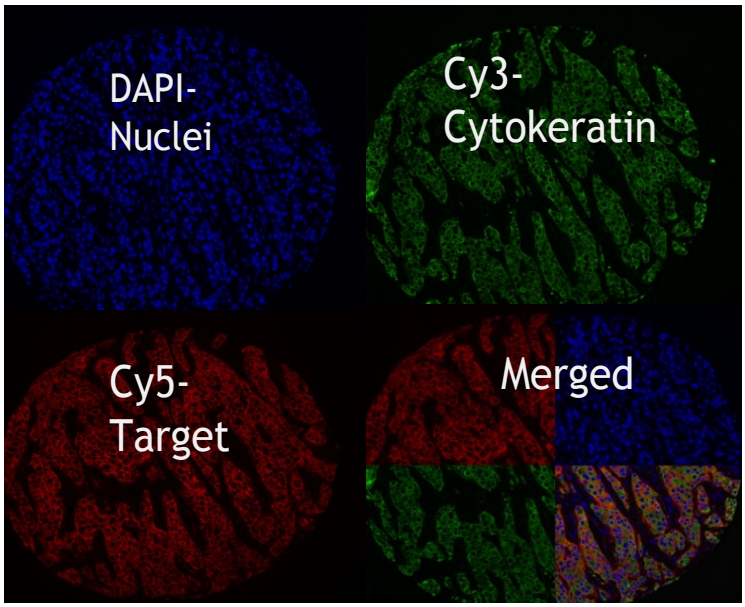

Figure 2.15-2 The process of compartmentalisation in AQUA analysis. DAPI counterstaining in blue was used to identify nuclear (top left), cytokeratin staining in green was to separate tumour cells and normal epithelial cells (top right), Cy-5-thymide in red detects target protein (bottom left) and compartmentalised analysis of tissue sections (bottom right).

Before obtaining the final AQUA scores, each image was examined to exclude imaging faults and normal tissue, thus target protein expression was scored only in invasive cancers. In addition, cores containing epithelium <5% of their total area were automatically excluded by the software to make sure that tumours were appropriately represented for AQUA scoring (Camp *et al.*, 2002). An in-house quality control slide was used for control to ensure the proper staining each time (Figure 2.2-4). The final normalised AQUA score detecting the fluorescence correlates with the expression level of target protein.

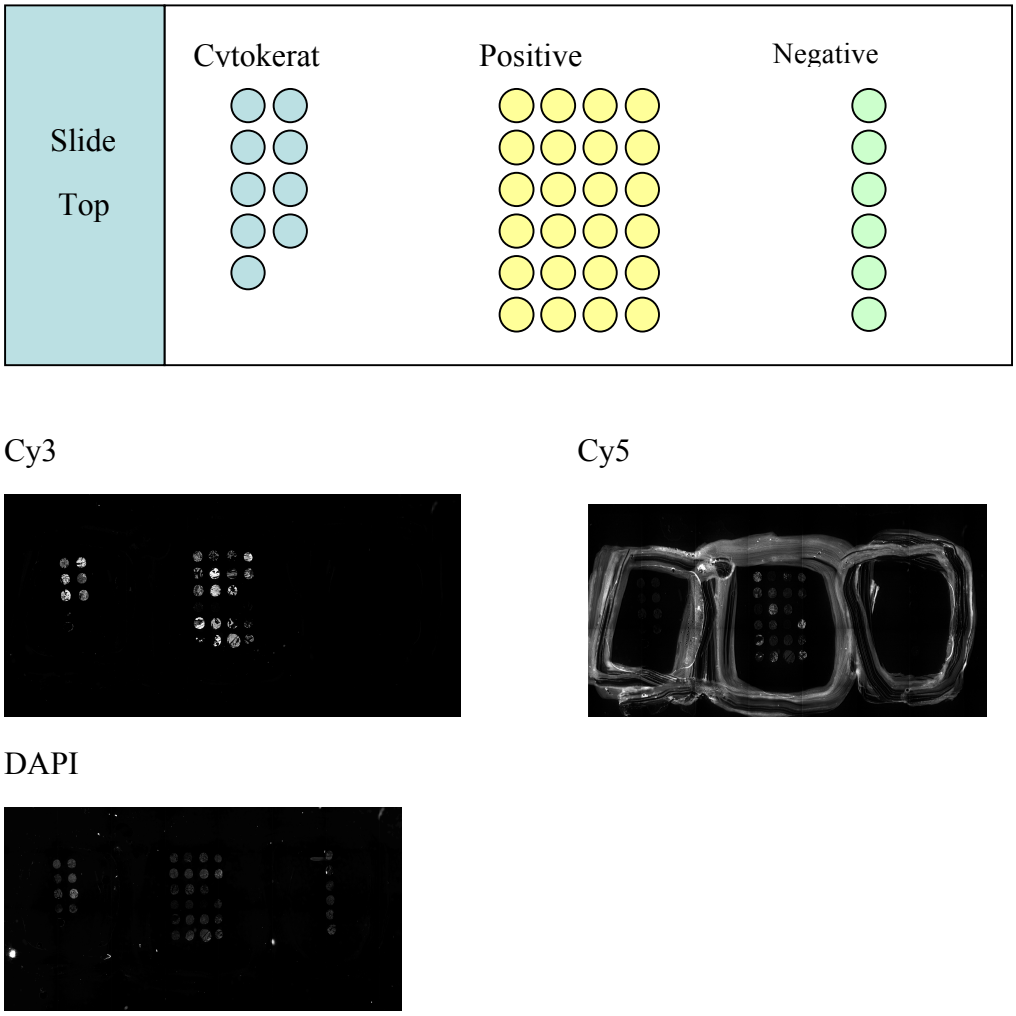

Figure 2.15-3 An example of our in-house quality control slide and the process of validation of staining for each control. There are three different groups of tissue cores on the control slide (top figure), and a PAP Pen was used to separate groups to provide a hydrophobic barrier for different antibody probing. Cytokeratin TMA visualised in the Cy3 channel was used to check the quality of the tumour mask staining, while a positive control TMA was used to ensure the quality of each antibody used. Finally, the negative control TMA, without any primary antibody added, was used to show any non-specific binding as a result of unsuccessful blocking.

2.16 Cell cycle analysis

Cells were harvested and plated as described for western blotting. At each time point, cells were trypsinised and then transferred to 5 mL BD Falcon tubes (BD Biosciences). Citrate buffer (Trisodium Citrate (301287F, BDH Laboratory Supplies), 121mg Tris Base (T1378, Sigma), 1044mg Spermine Tetrahydrochloride (S2876,

Sigma) and 2mL Nonidet NP40 (N3516, Sigma) in 2000mL distilled water, pH7.6) was added as the stock solution after centrifuge. Then the following solutions were added incubating in sequence before running: 450uL solution A (0.003% Trypsin Type IX-S (T0303, Sigma) in Citrate buffer pH7.6) for 2 minutes, solution B (0.05% Trypsin Inhibitor (T9253, Sigma) and 0.01% RNAse A (R4875, Sigma) in Citrate buffer pH7.6) for 10 minutes, and solution C (0.0416% Propidium Iodide (81845, Sigma) and 0.1% Spermine Tetrahydrochloride (S2876, Sigma) in 500mL Citrate buffer pH7.6) for 10 minutes in the dark. Flow cytometric analysis for samples was then performed using a BD FACSAriaII SORP (Becton Dickinson). The 488nm laser was used for measuring forward scatter, side scatter, and PI fluorescence (685/35 bandpass filter). BD FACSDiva software (Becton Dickinson, Version 6.1.2) was used for instrument control and Flowjo software (Version 7.6.5) for Data analysis.

2.17 Detection of apoptosis by annexin-V assay

Cells were harvested in log phase and plated into 60mm petri dishes and incubated for 72h with or without siRNA transfection. After treatment with drug, cell apoptosis was detected at 24h by using the TACS Annexin V-FITC Kits (R &D Systems) according to the manufacturer's protocol. Cells were collected and washed with ice-cold PBS once, and then 100uL Annexin V Incubation reagent (10uL 10x Binding Buffer, 10uL Propidium Iodide (PI), 1uL Annexin V- FITC, and 79uL Distilled water) was added into each sample. 400uL 1x Binding Buffer was then applied to each sample after 15 min incubation in the dark. Negative stained, PI stained only, Annexin V- FITC stained only were prepared as controls. The apoptotic cells were

detected by BD FACSAriaII SORP (Becton Dickinson). BD FACSDiva software (Becton Dickinson, Version 6.1.2) was used for instrument control and Data analysis were performed by Flowjo 7.6.5.

2.18 V250 Proteomic analysis

This proteomic microarray was performed by Eurogentec. Briefly, 120 signalling proteins and their phosphorylated (activated) forms were selected to detect their expression level change among 12 ovarian cell lines (OVCAR3, OVCAR4, OVCAR5, SKOV3, OAW42, PE01, PE04, TOV112D, TOV21G, 41M, 59M, and ES2). Each array was constructed by one cell line; every six spots were six replicates for one protein detection. Fluorescence of the second antibody detected was associated with the expression level of relative protein.

2.19 Immunofluorescence assay on cell lines

Cells were grown with or without treatment on autoclaved coverglasses (thickness No.1, VWR, 631-0149) and fixed by 4% paraformaldehyde for 15 minutes. After washing with PBS-0.05% TWEEN20 for 10 minutes and blocked in DAKO serum-free blocking buffer (X0909), slides or cover glasses are incubated with primary antibodies for one hour at room temperature. Secondary Goat anti Rabbit Alexa 488 (1:400) or anti Mouse Alexa 654 (1:400) and Gold anti-fade reagent with DAPI (Invitrogen, P36931) were used to detect the target proteins and nuclear compartment respectively.

2.20 Nuclear texture analysis

Confocal images were obtained using a Nikon A1R Confocal Microscope and images were obtained via NIS viewer software. Cells were grown in chambered slides for specific period and fixed by 4% formalin in PBS for 10 minutes. After washing with PBS-0.05% TWEEN20 three times, slides were counterstained with anti-fade reagent with DAPI (Invitrogen, P36931). The nuclear texture was then analysed with Image J software. Briefly, after 8-bit images were input, any unclear or non-tumour areas were cropped and clearly focused areas with tumour cells were selected. Proper thresholds for nuclear size were set up and individual nuclear was then selected within region of interest (ROI) (Figure 2.2-2). Nucleus counters and GLCM (Gray-Level Co-Occurrence) manager plugins were performed for each image, and 5 parameters associated with texture: correlation, contrast, angular second moment, inverse different moment, and entropy were obtained (Table 2.2-5).

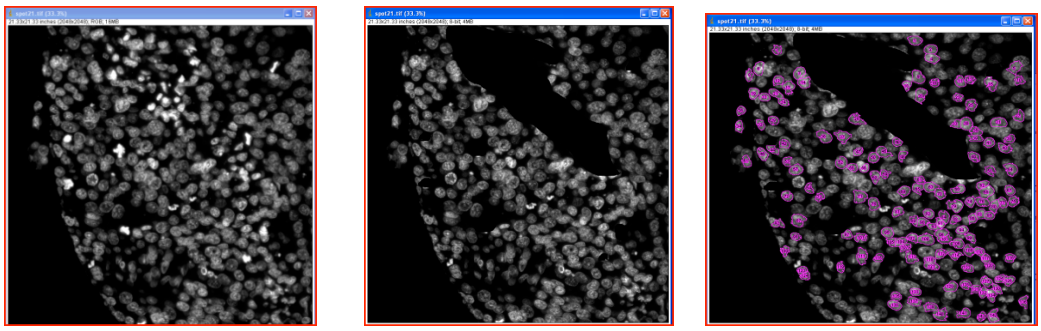

Figure 2.20-1 Selection of region of interest (ROI) in Image J software.

heterogeneity of chromatin patterns	homogeneity of chromatin patterns	contrast of chromatin patterns
Correlation (+)	angular second moment (+)	difference entropy
sum variance	Entropy (-)	difference variance
variance	sum entropy	inverse difference moment (-)
	run percentage	Contrast (+)

Table 2-5 Common morphometric parameters in nuclear texture study. The ones in red are from output in Image J, and +/- indicated their positive or negative correlation with each related kind of chromatin pattern (heterogeneity, homogeneity, or contrast).

2.21 Quantitative analysis of γH2AX foci formation in cells

Cells were grown and stained as described in 2.2.19, and the primary antibody anti-phosphohistone H2AX (ser139, γH2AX) was from Millipore (cat. 05-636). After slides were mounted with DAPI and air-dried, the cells were visualised by BriteMAC or MacRd microscope in the Imaging Suite of MRC Human Genetics Unit in Western General Hospital. The nuclear images were taken by IPLab software under single filters for each channel with the same exposure setting for each set of experiment. For each slide, more that 100 nuclei were counted for the foci formation analysis.

After immunofluorescence images were acquired, the number of γH2AX foci in each nucleus was counted by the PZ Foci EZ plugin in ImageJ software using the instructions on the website (available at www.pz**foci**ez.com). For short, a nuclear mask, which defined the regions of interest (ROI, i.e. nuclear outlines), was made

first for each channel, and then the foci number was counted automatically in the proper channel within the ROI defined. Several background threshold and noise tolerance may be tried to get the optimum result.

2.22 Statistical analysis

To be able to compare our results to that of the V250 arrays, we calculated the ratio of non-phospho form over phospho form of each antibody. Student's t-test was used in comparison of two independent samples. One-way ANOVA followed by Tukey HSD post HOC test was used to conduct multiple comparisons of groups with equal variance. Pearson correlation analysis was performed in the association detection for IF result. Wilcoxon signed-rank test is used to compare target protein expression differences between the pre- and post-treatment samples from patients Man-whitney test was performed to compare xenograft data.

3 Results

3.1 Quantifiable changes in nuclear structure during chemotherapy in ovarian cancer cells

In order to robustly measure the nuclear morphological changes described, nuclear texture was first analysed using microscopy and ImageJ image analysis software. The condensation and distribution of chromatin in the nucleus has been demonstrated by nuclear texture changes in image cytometric studies (Yatouji, El-Khoury et al. 2007). The higher-order chromatin structure was quantified through nuclear texture analysis using digital images to get computational analysis even for subtle differences to the naked eyes.

3.1.1 Study method development for texture analysis

As described in the Materials and Methods, cells grown on coverslips were treated with cisplatin or ionising radiation at different doses, and incubated for 0h, 6h, 12h, and 24h. After DAPI staining and imaging, cellular nuclear texture was quantitatively analysed using the widely available computational image analysis software ImageJ (Figure 3.1-1).

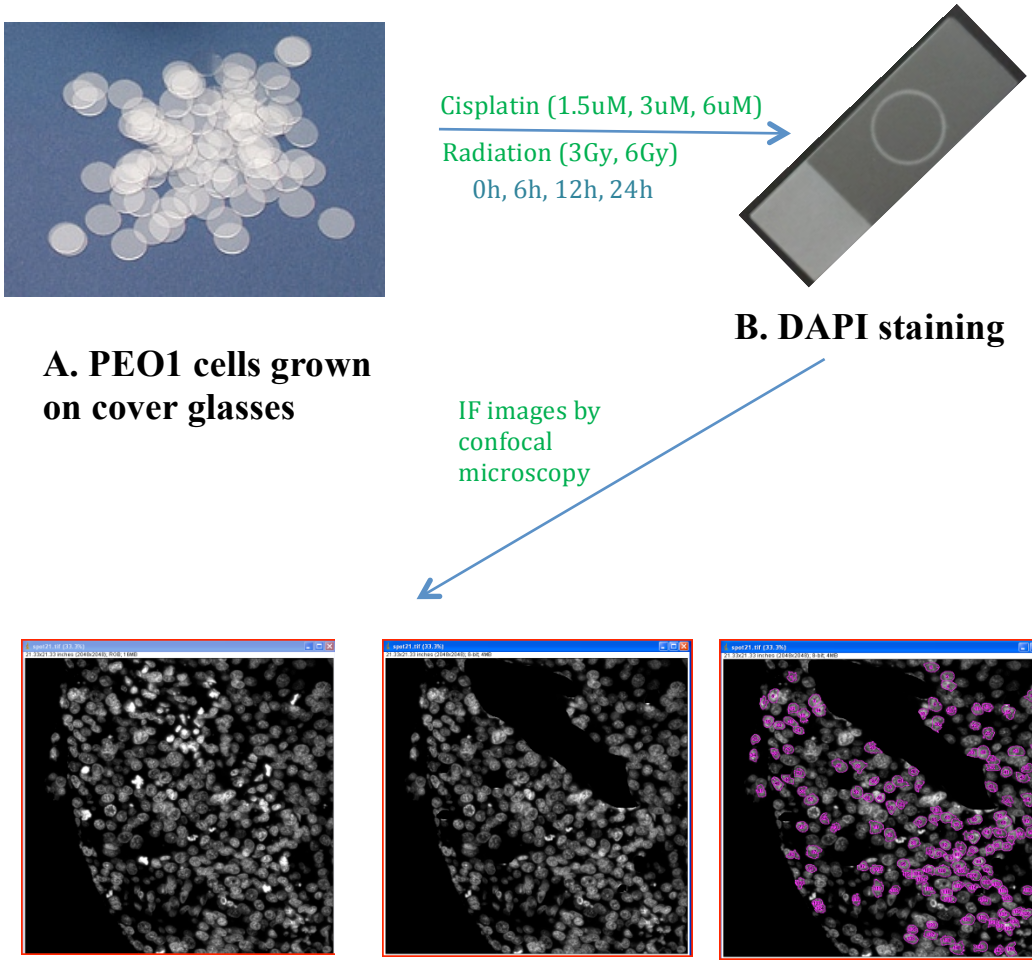

Figure 3.1-1 Microscope image acquisition procedures for the study of nuclear texture. For detailed methodology, refer to Material and Methods.

The texture of an image can be evaluated using mathematical formulae based on the 'grey level co-occurrence matrix' (GLCM) (Alvarenga, Pereira et al. 2007). Haralick et al. described in detail how to turn the pixel data from greyscale images into matrices to represent an image's texture. This represents a second order texture calculation that considers the distance and angle relationship between groups of two pixels in the original greyscale image under the same intensity of grey pixels within a defined area. Since the reporting of the formulae, texture analysis has been applied in

a range of studies including analysis of nuclear texture for a number of purposes, such as differentiating between benign and malignant cancers (Murata, Mochizuki et al. 2002), and examining apoptotic cells (Pantic et al., 2012). After images were imported into ImageJ, five texture parameters were generated from the GLCM manager plugins for each selected nucleus within the images, namely correlation, angular second moment (ASM), entropy, inverse different moment (IDM), and contrast.

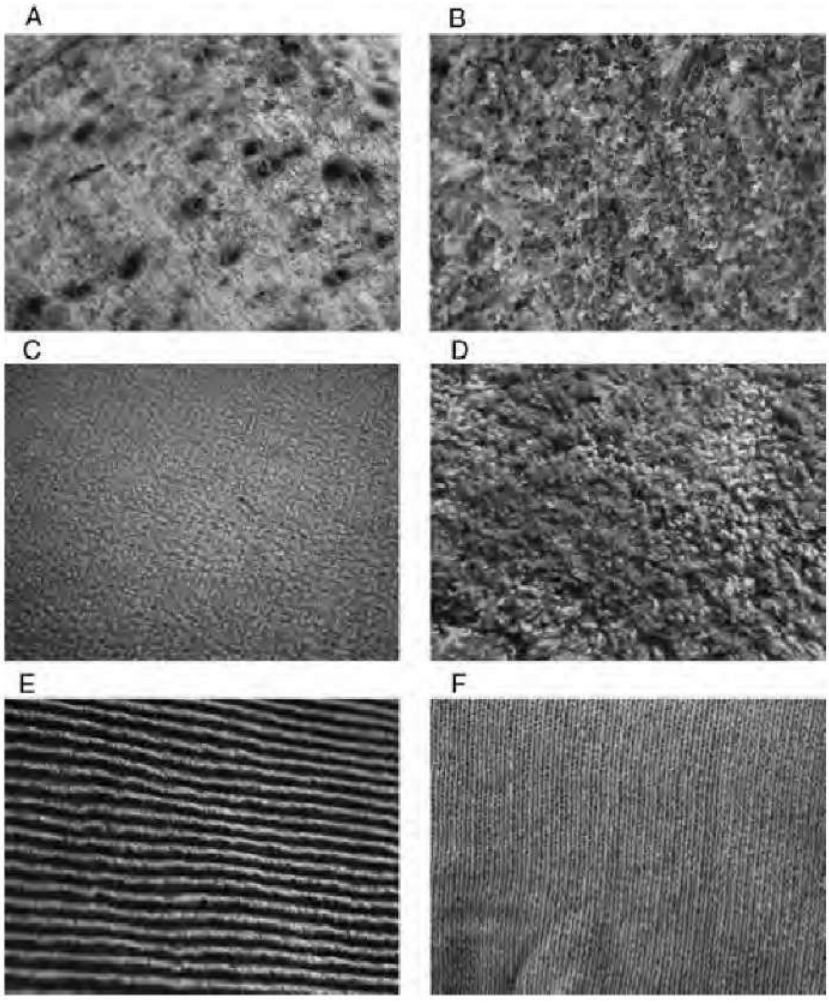

Figure 3.1-2 Examples of some common textures: tree bark (A), polished granite (B), glass (C), carpet (D), corduroy (E), and knit (F). The textures of these images are becoming more regular, namely more homogenous and less entropy. Pictures were acquired from the online source: http://what-when-how.com/biomedical-image-analysis/texture-analysis-biomedical-image-analysis/.

The five measured parameters are essential in order to fully describe the texture within a defined region. As explained in the literature (Murata, Mochizuki et al. 2002; Sacile, Montaldo et al. 2003), the texture features can be either positively or negatively correlated with several chromatin patterns (homogeneity, heterogeneity, and contrast) as a description of the arrangement of the surface of nuclei (Table 3.1-1):

- ASM provides a strong measurement of uniformity or smoothness of an image and positively correlates with overall homogeneity of chromatin patterns.
- Entropy, which effectively measures the overall disorder of patterns, correlates negatively with overall homogeneity.
- IDM measures the local homogeneity of an ROI and is affected by the homogeneity of the image. Non-homogeneous areas normally result in low IDM values. Thus it is described as 'contrast' of chromatin patterns.
- Contrast measures the local variability of patterns, local intensity variation, and will favour contributions from pixels away from the diagonal.
- Correlation calculates the grey-level linear dependency of the image, and correlates negatively with the heterogeneity of chromatin patterns.

Heterogeneity of chromatin patterns	Homogeneity of chromatin patterns	Contrast of chromatin patterns
Correlation (-)	Angular second moment (+) Entropy (-)	Inverse difference moment (-) Contrast (+)

Table 3-1 The parameters generated by the GLCM manager plugins in ImageJ and their association with different chromatin patterns: heterogeneity, homogeneity, and contrast. The (-) and (+) in red indicates the positive and negative correlation with each related kind of chromatin pattern, respectively.

A. 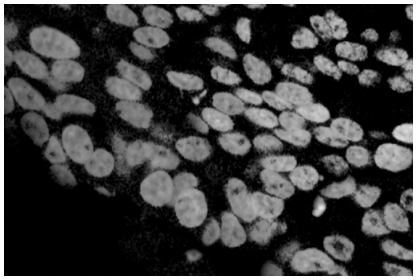 B. 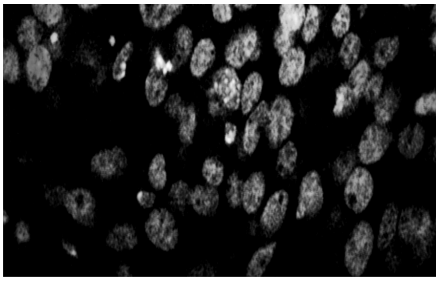

	Angular Second Moment	Contrast	Correlation	Inverse Difference Moment	Entropy
A	0.0104	97.6683	0.000525	0.2086	6.8727
B	0.0044	143.1648	0.000552	0.1959	7.1211

Figure 3.1-3 Example of nuclear texture analysis and parameter acquirement. Image and data are from ovarian cancer xenografts without (A) or with (B) carboplatin treatment, and samples were stained with DAPI.

Illustrations are shown in Figure 3.1-2 to demonstrate the texture variation among different original images, and an example is displayed in Figure 3.1-3 showing how those parameters can reflect the chromatin conformation seen under microscope.

3.1.2 Nuclear texture analysis in DNA damage-based therapies *in vivo* and *in vitro*

Having defined a robust method of measurement for nuclear texture features, I applied the method to detect nuclear texture changes in both the PEO1 ovarian cancer cell line and the xenograft model after treatment with DNA damage-based therapies (cisplatin, radiation, or carboplatin).

3.1.2.1 Measurement of nuclear texture changes in vitro upon cisplatin/radiation treatment

After 24h treatment with 6μM cisplatin or 6Gy radiation, (similar to several previous studies) (Petru, Sevin et al. 1997; Arafa el, Zhu et al. 2009; Cooke, Ng et al. 2010; Liang, Kong et al. 2012), the image texture parameters all changed in a positive or negative direction compared with the untreated group. As shown in Figure 3.1-2, similar results were observed after cells were treated with either cisplatin or radiation. ASM, correlation, and IDM all decreased after treatment of cisplatin/radiation by 20%/23%, 25%/49%, and15%/11% respectively, while entropy and contrast increased by 6%/8% and 15%/11%, indicating the texture of those nuclear images altered to a certain degree.

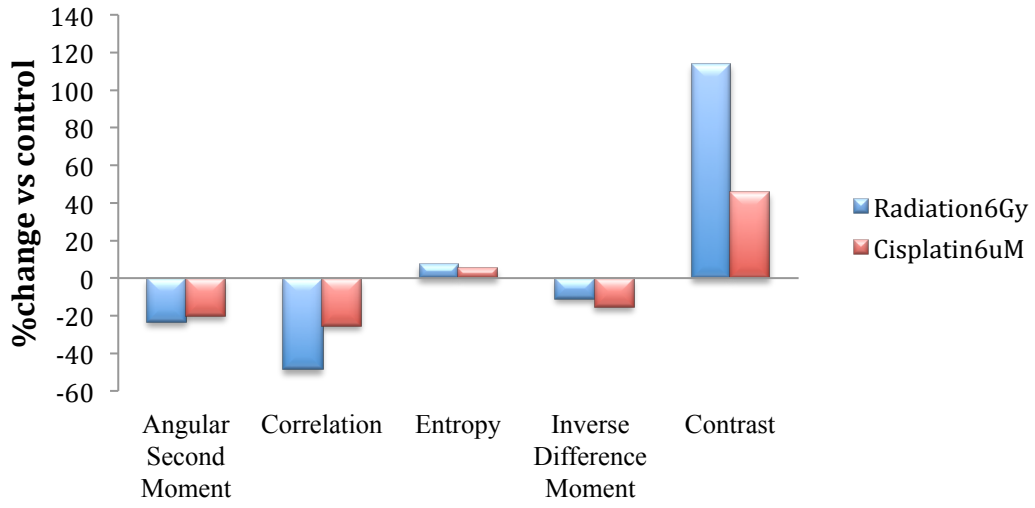

Figure 3.1-4 Changes in features describing nuclear texture in PEO1 cells after radiation or cisplatin treatment. PEO1 cells were grown on coverslips and treated with ionising radiation (6Gy) or cisplatin (6uM) for 24h, and nuclei were stained with DAPI for visualisation using a fluorescence microscope. At least 100 nuclei were included for each experiment. Nuclear texture was analysed by measuring five texture parameters (angular second moment, correlation, entropy, inverse different moment, and contrast) in the ImageJ software. Data are presented as the average change (%) in the treated group for each parameter over the control group.

Using the method described previously, the changes in parameters were described in terms of nuclear texture (Table 3.1-2). A decreased correlation indicated a more heterogeneous chromatin pattern; in contrast, decreased ASM and increased entropy suggested less homogeneity in the chromatin pattern The opposite changes in IDM and contrast demonstrated increased contrast in nuclear texture.

	Heterogeneity of chromatin patterns	Homogeneity of chromatin patterns	Contrast of chromatin patterns
Texture parameters	Correlation (-)	Angular second moment (+) Entropy (-)	Inverse difference moment (-) Contrast (+)
Cisplatin 6mM/ Radiation 6Gy	↑	↓	↑

Table 3-2 Changes in chromatin patterns in PEO1 cells after cisplatin (6uM) or radiation (6Gy) treatment for 24h, measured by parameters describing nuclear texture using ImageJ. The (+) and (-) represent positive and negative correlations with each type of chromatin pattern, respectively, and the arrows indicate the direction of change for each pattern.

By quantitatively measuring the chromatin patterns based on nuclear texture, we demonstrated an increase in heterogeneity and contrast of chromatin, and decreased homogeneity in the nuclei of these cells after DNA damage-induced treatment, such as cisplatin and radiation, which is consistent with the observations viewed using light microscopy.

3.1.2.2 Measurement of nuclear texture changes in response to carboplatin in vivo

As the results of the *in vitro* study demonstrated the existence of changes in higher order chromatin organization in ovarian cancer cells after either cisplatin or radiation treatment, we sought to identify whether similar changes in nuclear texture exist *in vivo*.

As described in the Materials and Methods, the ovarian tumour tissue samples from the OV1002 xenograft model, already developed in our laboratory, were analysed. After treatment with carboplatin, ovarian tumours were collected on day 0, 1, 2, 4, 7, and 14 after a single dose treatment. Samples were then cut and spotted on a tissue microarray slide for further study.

In order to obtain an overall qualitative view of the nuclear organization in these tumour samples, an H&E stained TMA slide was first assessed. As shown in Figure 3.1-3, the nuclear morphology in most untreated tumours was strongly stained and homogeneous (Figure 3.1-3 A-F), while lighter staining and greater heterogeneity was observed in the nuclei of samples after carboplatin treatment (Figure 3.1-3 G-M). This observation argues against the features seen in clinical specimens being purely artefactual, since the fresh staining is performed on samples treated for a short term period (0-14 days) and collected at the same time for untreated and treated groups on each day.

A.

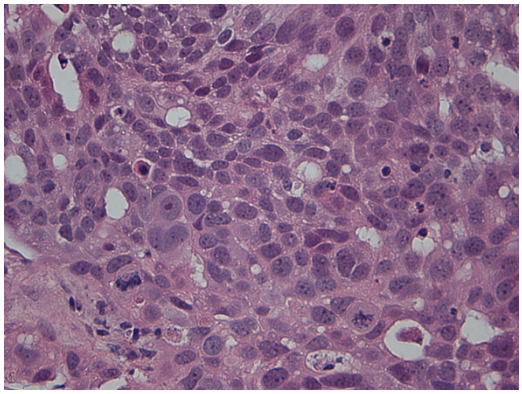

B.

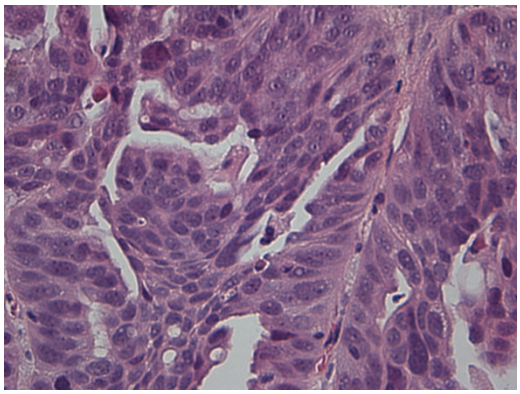

C.

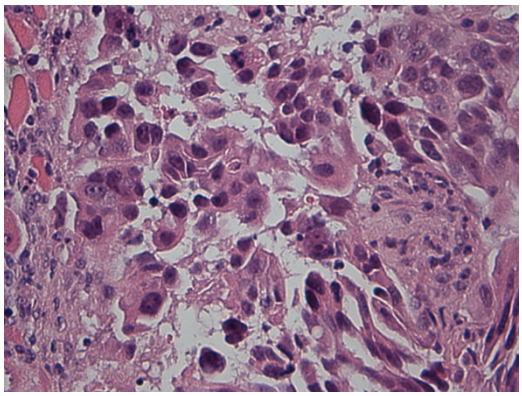

D.

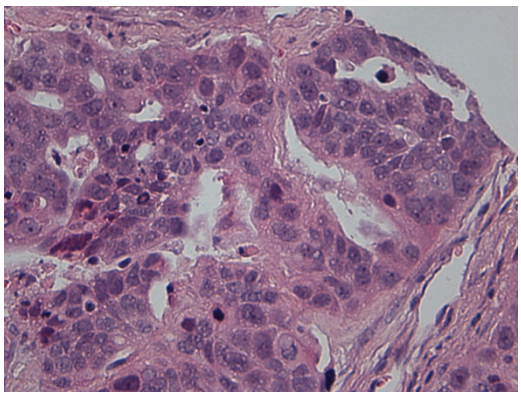

E.

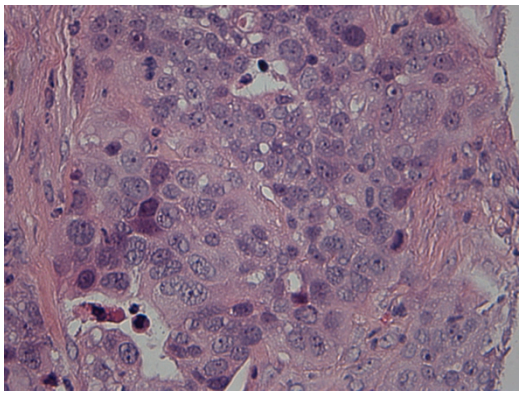

F.

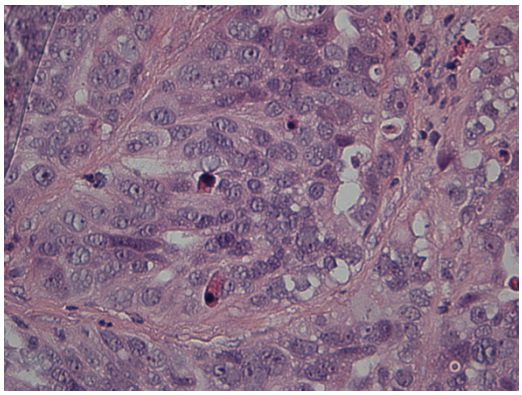

(continued)

G.

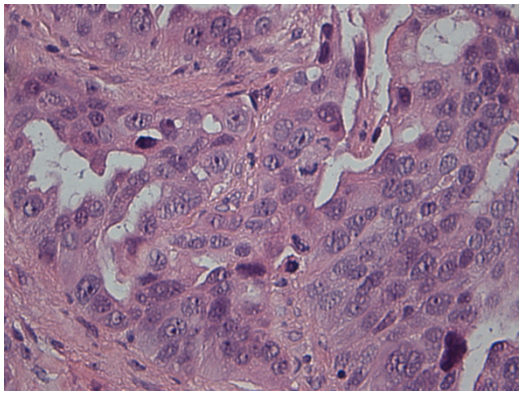

H.

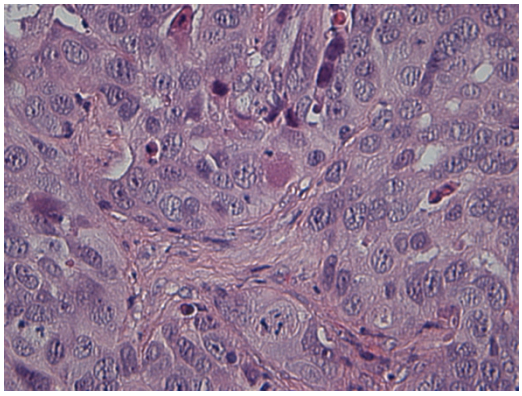

I.

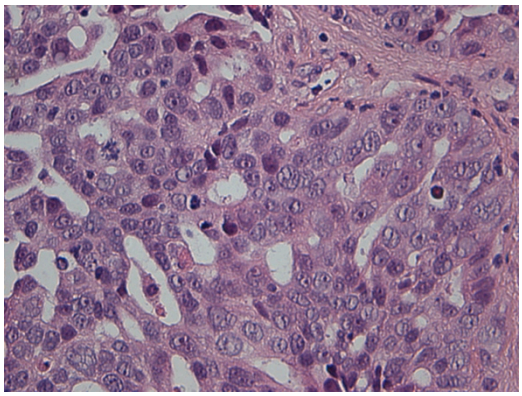

J.

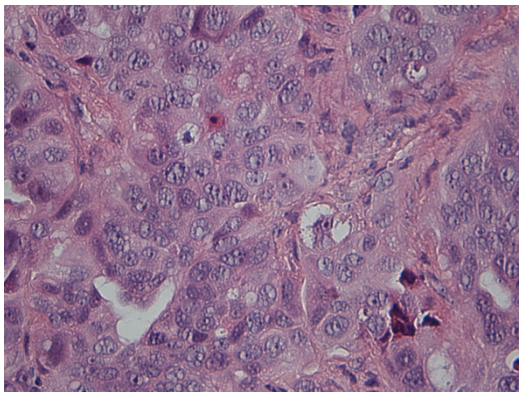

K.

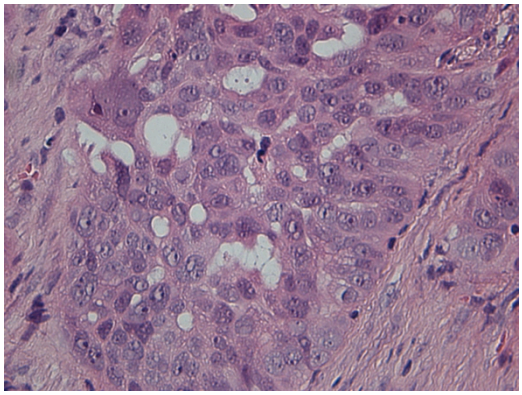

L.

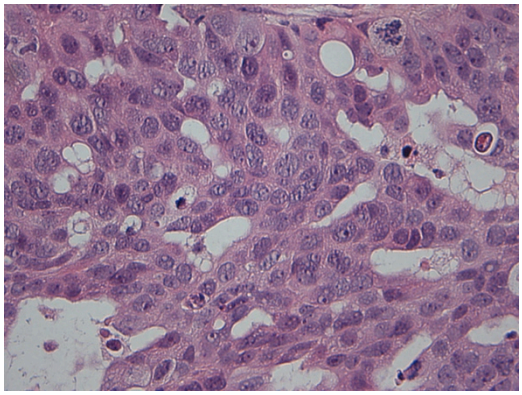

(continued)

M.

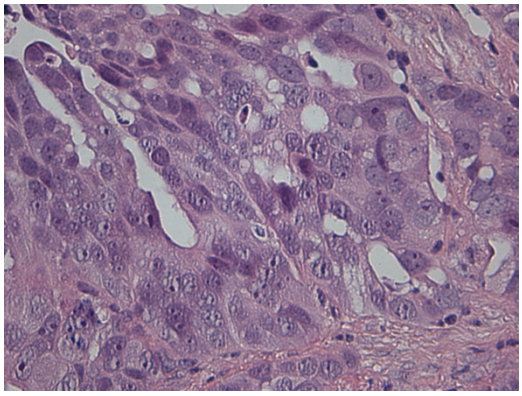

Figure 3.1-5 Representative images from H&E stained OV1002 ovarian tumour samples before (A-F) and after (G-M) carboplatin treatment *in vivo*. Female adult CD-1 nude mice housed in IVCs (individually ventilated cages) were treated with Carboplatin (50 mg/kg i.p.) on Day 0, and tumour samples were collected on Day 0, 1, 2, 4, 7, and 14 after treatment. H&E staining was performed on TMA slides, and the images were acquired using a camera mounted on a light microscope under 40X magnification.

Similar to the *in vitro* study, we analyzed the nuclear texture using ImageJ to quantitate the changes in chromatin pattern. The number of nuclei analysed per sample ranged from 16 to 213 (average 103), and the number of mean values per group ranged from 13 to 21 (average 16). See Table S1 in the Supplement for a summary of these statistics.

As is shown in Figure 3.1-4, the distribution of the texture parameters in samples after carboplatin treatment was altered compared to control groups, while the most significant effects of single dose carboplatin on xenografts were typically seen two days after treatment, with two parameters (entropy and IDM) showing statistically significant difference ($p=0.034$ and 0.008, respectively; Figure3.1-4), indicating that changes in chromatin patterns occurred after platinum treatment *in vivo* as well *in vitro*.

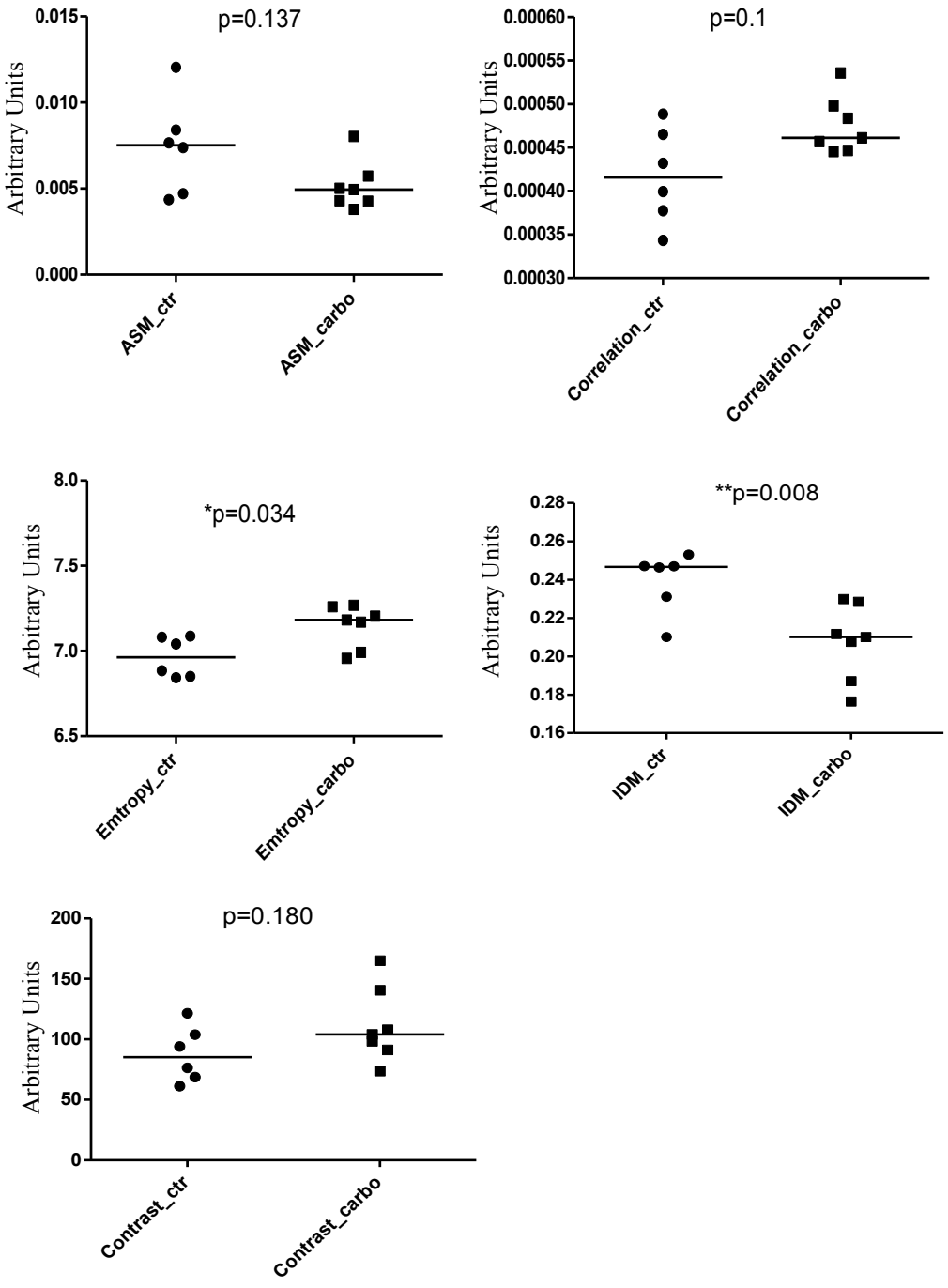

Figure 3.1-6 Nuclear texture parameter analysis in xenografts with and without carboplatin treatment on Day 2. Data for each spot represents the average value of each single sample from triplicate TMAs, and the number of nuclei analysed per sample ranged from 16 to 213 (average 103). Mann-Whitney U test (2-tailed); *P<0.05, **P<0.01

The observed changes in the parameters were very similar to the changes seen *in vitro*. As shown in Table 3.1-3, the homogeneity of the chromatin patterns decreased, as shown by a significant increase in entropy after treatment (0.034), compared to control. The contrast of the chromatin patterns increased with inverse difference moment reaching significance when comparing treated samples to untreated ones (p=0.008).

	Heterogeneity of chromatin patterns	**Homogeneity of chromatin patterns**	**Contrast of chromatin patterns**
Texture Parameters	Correlation (-)	Angular second moment (+) Entropy (-)	Inverse difference moment (-) Contrast (+)
Carboplatin (Day2)	-	↓	↑

Table 3-3 Changes in chromatin patterns in xenograft samples after carboplatin treatment on day 2, measured by parameters representing nuclear texture using ImageJ. The (+) and (-) represent positive and negative correlation with each type of chromatin pattern, respectively. Arrows indicate the direction of alteration for each pattern.

The quantitative measurements support the qualitative observation in changes in nuclear morphology using H&E. Only two parameters were statistically significant; this might be due to the small sample size (six or seven samples each group), or due to heterogeneity of the tumour tissue since only a proportion of the tissue is sampled using TMA cores. As shown in Figure 3.1-3 E and F, some nuclei in tumors without

treatment showed condensed structure similar to those after treatment, although the majority demonstrated a more homogenous morphology.

		Heterogeneity of chromatin	Homogeneity of chromatin	Contrast of chromatin
Texture parameters		Correlation (-)	Angular second moment (+) Entropy (-)	Inverse difference moment (-) Contrast (+)
In vitro	**Cisplatin 6μM/**	↑	↓	↑
In vivo	**Carboplatin (Day2)**	-	↓	↑

Table 3-4 Summary of changes in chromatin patterns *in vitro* and *in vivo* after DNA damage-based therapy, measured by parameters representing nuclear texture using ImageJ. The (+) and (-) represent positive and negative correlation with each type of chromatin pattern, respectively. The arrows indicate the direction of alteration for each pattern.

In summary, the trend in alterations for each chromatin pattern was comparable both *in vitro* and *in vivo*, and the chromatin tended to be more condensed after those treatments. Thus these data strongly support our hypothesis that nuclear morphological changes occur after certain cellular damage.

3.2 Molecular effect of cisplatin treatment on chromatin patterns and HDAC expression in ovarian cancer cells

Since morphological changes were observed and could be quantified during DNA damage-based therapy, this raised questions about the biological cause of these changes and the cellular events occurring in the surviving cells during treatment. To better understand the processes occurring in the nuclei associated with the chromatin pattern changes during treatment, the well-studied ovarian cancer cell lines PEO1 and PEO4 cells were chosen for further *in vitro* studies.

3.2.1 Characterization of the cell line models, including cisplatin responsiveness

As described in the original report describing the original ovarian adenocarcinoma cell lines (Langdon, Lawrie et al. 1988), PEO1 and PEO4 cells were derived from peritoneal ascites obtained from the same patient with poorly differentiated serous adenocarcinoma at different stages of therapy. PEO1 cells were collected after *cis*-platinum (CDDP), 5-fluorouracil (5-FU), and chlorambucil treatment and showed responsiveness to treatment after 22 months (Ng, Cooke et al. 2012). However, PEO4 cells were established when clinical resistance was exhibited to those agents ten months later. The study also detailed other characteristics of these cell lines, including growth characteristics, modal chromosome numbers, and antigen expression. The different cisplatin sensitivity between the cell lines has also been

studied and suggested to be due to a BRCA2 deficiency in PEO1 cells and a secondary mutation to restore BRCA2 proficiency in PEO4 cells (Sakai, Swisher et al. 2009).

3.2.1.1 Morphological characteristics of PEO1 and PEO4 cells

The morphology of these two cell lines was first examined in cells grown in monolayers after settling in dishes, and subtle differences were visible by light microscopy. Although both cell lines tended to grow as islands of uniform polygonal cells, PEO4 cells formed smaller clusters when compared to PEO1 cells. Furthermore, the growth rate of PEO4 cells was much slower.

A. PEO1 B. PEO4

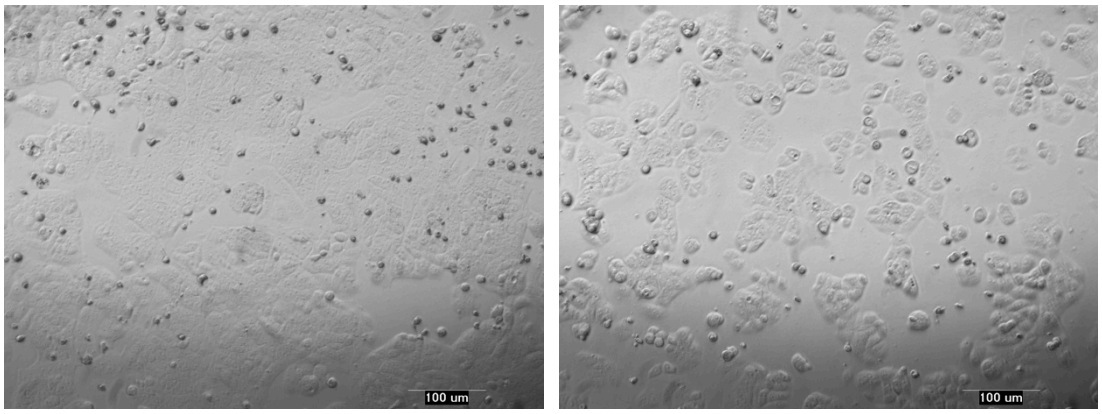

Figure 3.2-1 Images of live PEO1 and PEO4 cells under the light microscope. PEO1 and PEO4 cells were seeded and grown on plastic cell culture dishes for 24-72h; typical images were taken using the light microscope to compare their morphological characteristics.

3.2.1.2 Cisplatin sensitivity of PEO1 and PEO4 cells

To address the sensitivity to cisplatin treatment and demonstrate the PEO1/PEO4 cell line pair as an appropriate model to investigate resistance during chemotherapy, SRB assays were performed to confirm the growth characteristics of these two cell lines with cisplatin treatment. Four concentrations of cisplatin from a serial dilution were applied to the cells, and cell density was detected on each day after treatment from 0 to 5 days. As shown in Figure 3.2-2, cell number was reduced in both PEO1 (Figure 3.2-2A) and PEO4 cell lines (Figure 3.2-2B) after cisplatin treatment compared to the control group. At 12uM of cisplatin on day 5, the cell number in the treated group was only 10% of control group in PEO1 cells, and 29% in PEO4 cells. With treatment using different concentrations of cisplatin and periods of incubation, it was clearly demonstrated that this inhibitory effect of cisplatin was both time- and dose-dependent.

The sensitivity to cisplatin was compared between these two cell lines on day five (Figure 3.2-2C). The greatest differential inhibition was at a concentration of 6uM ($p<0.001$), indicating the relative resistance of PEO4 cells in response to cisplatin.

A.

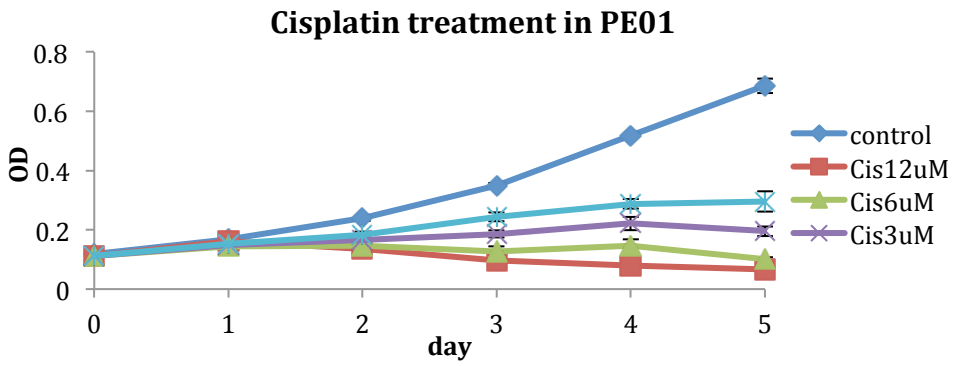

B.

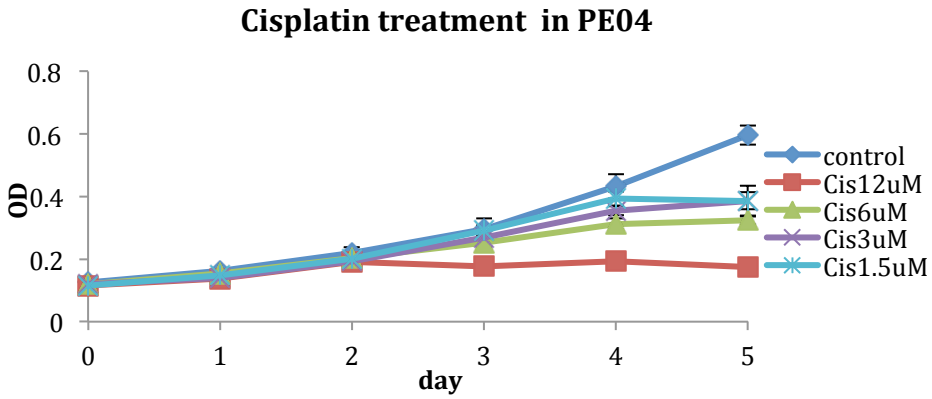

C.

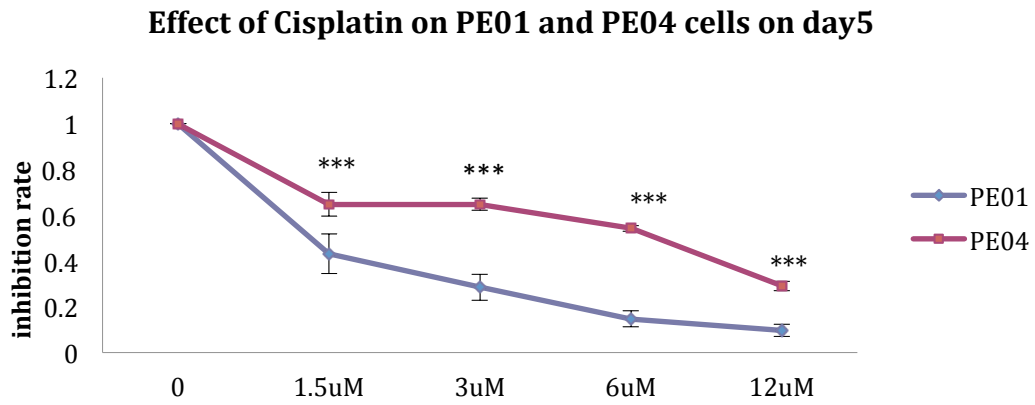

Figure 3.2-2 The effect of Cisplatin treatment on cell number in PEO1 (A) and PEO4 (B) cell lines using the SRB assay. PEO4 cells were less sensitive to cisplatin treatment compared to PEO1 cells (C). Cells were seeded and treated as described previously. O.D. values were measured on days 0 to 5. Data were plotted as a mean of O.D values +/- SD from three repeated experiments, and each experiment was carried out using six replicate samples. SD was calculated from averaged O.D values for each biological replicate (n=3). Statistical significance noted for inhibition rate of PEO4 cells compared with that of PEO1 cells were ***P<0.001 (Student's t-test).

3.2.2 Effect of the HDAC inhibitor TSA on cell growth of PEO1 and PEO4 cells

We speculated that the changes in higher order chromatin structure were associated with histone deacetylation, and HDACs are suggested to contribute to the mechanism of ovarian cancer resistance and its development. To further understand the effects that HDACs have on ovarian cancer cell growth, the SRB assay was performed using an HDAC inhibitor, Trichostatin A (TSA), which inhibits the class I and II mammalian histone deacetylase (HDAC) families of enzymes. TSA is one of the hydroxamic acid-derived compounds and is regarded as a classical HDAC inhibitor, which has been reported to produce growth inhibition and induce apoptosis *in vitro (Chen, Chen et al. 2004)*.

3.2.2.1 Cell growth inhibition with TSA treatment alone in PEO1 and PEO4 cell lines

This assay was used to obtain a quantitative measure of cell number after treatment with TSA. A two-fold dilution series of TSA from 320nM to 20nM was applied to PEO1 and PEO4 cells, and the cell density of both cell lines detected on each day from day 0 to day 5 after treatment. Similar to the result shown for cisplatin, this HDAC inhibitor also showed an inhibitory effect on cell number in both sensitive (PEO1) and relatively resistant (PEO4) cells in a time and dose dependent manner (Figure 3.2-3A and Figure 3.2-3B). Furthermore, by comparing PEO1 and PEO4 data, the inhibitory effect was significantly greater in PEO1 cells compared with PEO4 cells (Figure 3.2-3C). This indicated HDAC proteins might be involved in cell growth and resistance to chemotherapy.

A.

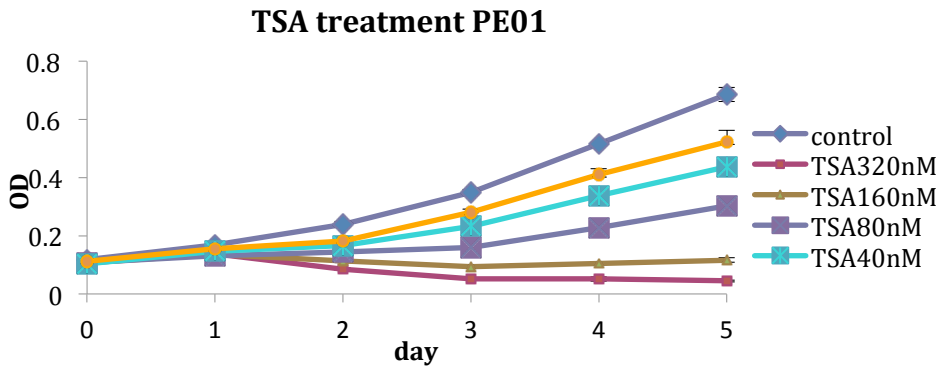

B.

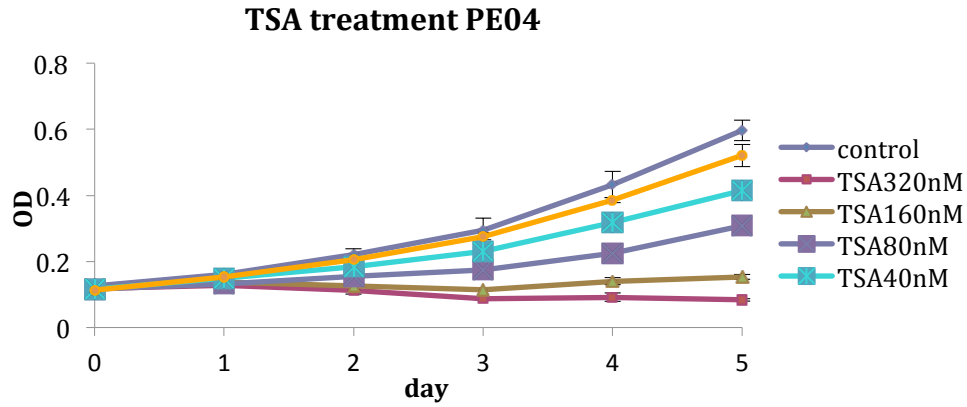

C.

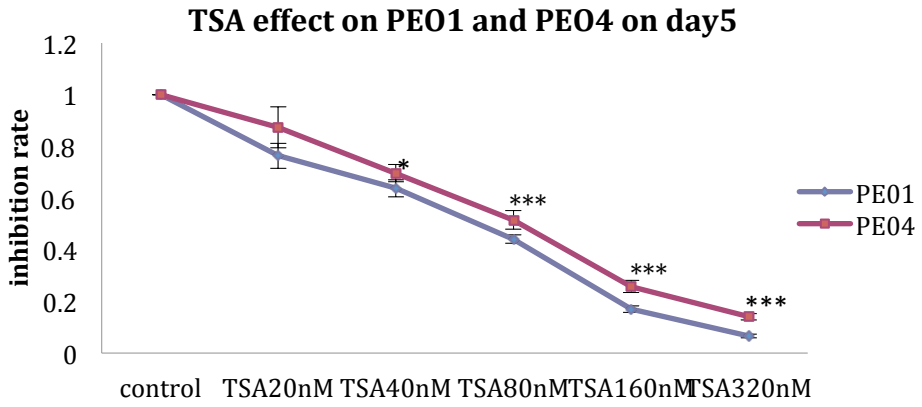

Figure 3.2-3 The effect of the HDAC protein inhibitor TSA on the growth rate of (A) PEO1 cells, and (B) PEO4 cells. All cells were incubated for 72h after seeding, and treated with or without TSA from 20nM to 320nM in a two-fold dilution series. O.D. values were measured on days 0, 1, 2, 3, 4, 5, and 6. The TSA inhibition rate between the two cell lines was plotted from the data on day 5 compared to control group. Data were plotted as a mean of O.D values +/- SD from three repeated experiments, and each experiment was carried out using six replicate samples. SD was calculated from averaged O.D values for each biological replicate (n=3). *P<0.05, ***P<0.001 (Student's t-test).

3.2.2.2 Effect of combination treatment with TSA and cisplatin on cell number in PEO1 and PEO4 cells

Since both cisplatin and TSA were inhibitory to PEO1 and PEO4 cells, we next investigated whether there were additive effects when cells were treated with a combination of both drugs. Unsurprisingly, after being treated with both cisplatin and TSA, cell numbers in both PEO1 (Figure3.2-4A) and PEO4 (Figure3.2-4B) cell lines were additionally reduced compared with each individual treatment alone. These further reductions were obvious after three (PEO1) or four (PEO4) days of treatment, and remained at the lowest OD level during the time course treatment. Parallel to the analysis performed on TSA-only treatment, we compared the inhibitory effect of each group on day five (Figure3.2-4C). Cell numbers in both cell lines were significantly inhibited with the combination treatment of cisplatin and TSA ($p<0.001$). This result shows that the inhibitory effects of TSA and cisplatin on cell number occur in both sensitive and resistant cell lines, suggesting that HDAC proteins have role on tumor cell growth and an impact on modulating a cancer cell's susceptibility to DNA damage-based therapy. Notably, although TSA showed statistically significant inhibitory effect on PEO1 cells, the effect of TSA during this experiment set indicate a possible opposite result that PEO4 seems more sensitive to TSA inhibition. There are several considerations: firstly, the previous TSA experiment apparently demonstrated a statistically significant difference, but the absolute difference is actually very small, possibly suggesting minor different effects of TSA on between PEO1 and PEO4 cells. Secondly, to make the expected low cell density detectable after combined TSA and cisplatin treatment, the initial cell number plated was enhanced, indicated by a higher O.D. value in Figure 3.2-4,

which implies PEO1 and PEO4 might response dynamically to TSA during their different stage of growth status.

A.

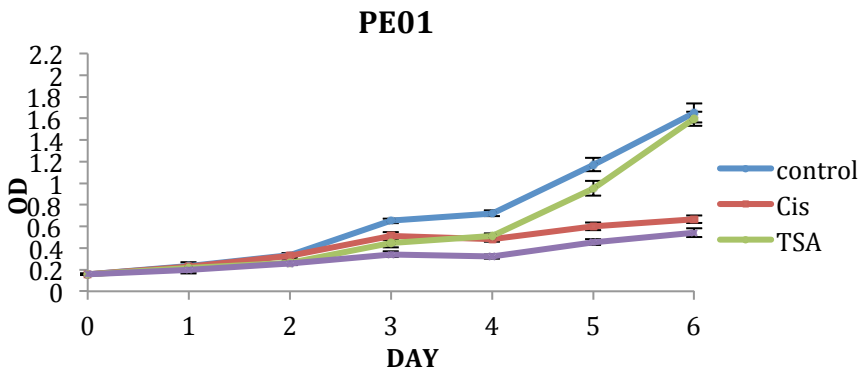

B.

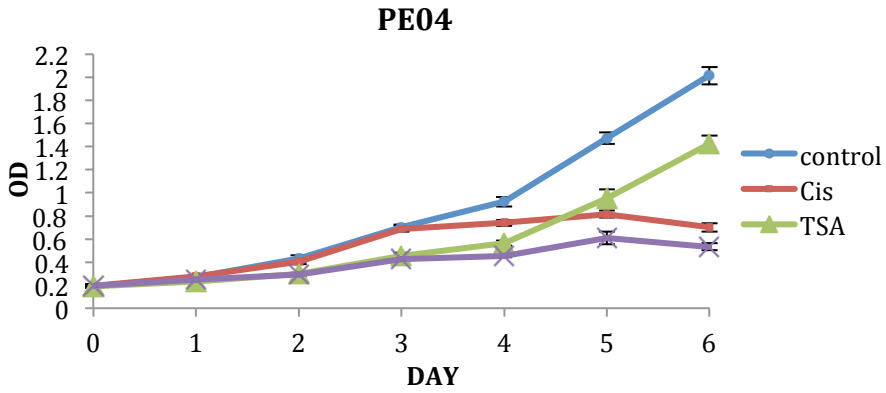

C.

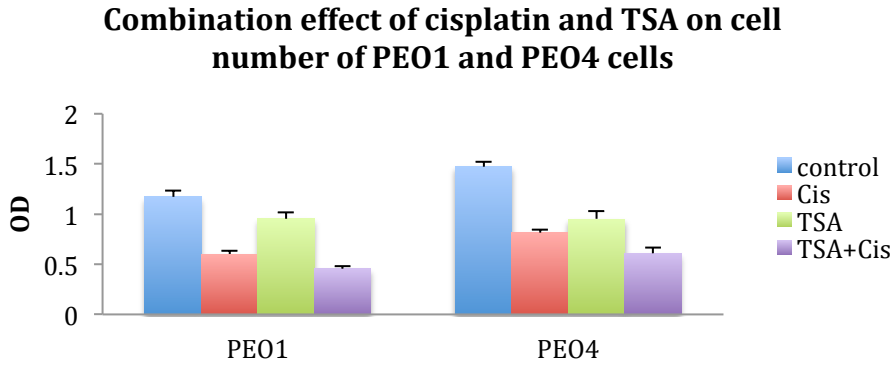

Figure 3.2-4 The effect of combination treatment of cisplatin and the HDAC protein inhibitor TSA on the growth rate of PEO1 cells (A), and PEO4 cells (B). All cells were incubated for 72h after seeding, and treated with TSA (100nM), cisplatin (6μM) to 320nM by two-fold dilution. O.D values were measured on days 0, 1, 2, 3, 4, 5, and 6. The cell lines were compared using the data on day 5 (c). Data were plotted as a mean of O.D values +/- SD from three repeated experiments, and each experiment was carried out using six replicate samples. SD was calculated from averaged O.D values for each biological replicate (n=3). One-way ANOVA followed by Tukey HSD Post Hoc test was performed between groups for statistical analysis (Table S2 for full analysis data).

These data indicate that HDACs have a role in cancer cell growth, and also support the current view that HDACs are potential targets during chemotherapy in cancer. By linking to their roles in chromatin structure formation discussed previously, these results provide some evidence for further investigation of the roles of HDACs in nuclear morphological change during DNA damage-based treatment in cancers.

3.2.3 Expression induction of HDAC and HP1 after cisplatin treatment in cells

We next evaluated the effect of cisplatin treatment on the expression of HDAC proteins in PEO1 and PEO4 cells. Since some studies have demonstrated a role for HDACs in mediating condensed or open chromatin structure, we also evaluated chromatin formation during this process by using the HP1 heterochromatin markers. Thus we examined the expression of HDAC and HP1 using several complementary methodologies, namely protein expression level, cellular immunostaining, and mRNA levels.

3.2.3.1 Protein expression of HDAC and HP1 after 24h of cisplatin treatment

Our preliminary data using the V250 proteomics array indicated a possible role for HDAC proteins in ovarian cancer in terms of response to chemotherapy. These data suggested that HDAC1, HDAC2, HDAC3, and HDAC4 are associated with chemotherapy resistance and poor prognosis in cancers (de Ruijter, van Gennip et al. 2003; Witt, Deubzer et al. 2009; Hayashi, Horiuchi et al. 2010; Stronach, Alfraidi et al. 2011). To further investigate in detail whether other HDAC members are involved in DNA damage-based treatment, we detected protein expression levels of HDAC Class I members (HDAC1, 2, 3, and 8) and IIA (HDAC4) in PEO1 and PEO4 cells after cisplatin treatment. As performed in a number of similar studies (Kao, McKenna et al. 2003; Yeung, Hoberg et al. 2004; Chinnaiyan, Varambally et al. 2006; Solomon, Pasupuleti et al. 2006), tubulin was applied as a protein loading control in this study.

From the nuclear texture results, we observed a change in nuclear texture after 24h of cisplatin treatment, thus we supposed that chromatin structure regulators such as HDACs would demonstrate changes at this time point. After incubating with cisplatin for 24 hours, total protein was collected from PEO1 and PEO4 cells and specific protein expression levels detected using antibodies against HDAC1, HDAC2, HDAC3, HDAC4, HDAC8, HP1α, HP1β, and HP1γ.

Among these HDAC family members, the expression level of HDAC2 was enhanced approximately 1.5 times compared to the control group after 24 hours cisplatin exposure in PEO1 cells, while other protein expression were similar after cisplatin treatment (Figure 3.2-5). In PEO4 cells, all of these targets showed little change in protein level after cisplatin treatment. This suggests that the class IA member HDAC2 might work as a response marker to cisplatin treatment *in vitro*, and also indicates its possible role in chromatin remodelling in DNA damage treatment in ovarian cancers, especially in sensitive ones.

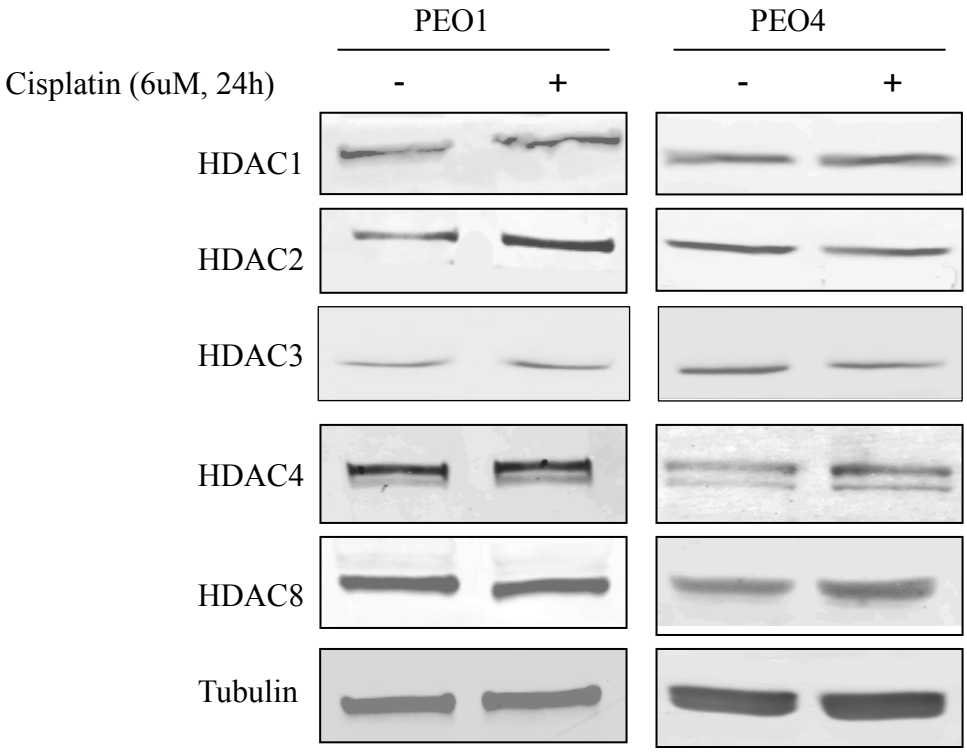

Figure 3.2-5 Expression of HDAC family members after cisplatin incubation. Western blot for expression of HDAC1, HDAC2, HDAC3, HDAC4, and HDAC8 in PEO1 and PEO4 cells with/without cisplatin treatment (6μM, 24h). Membranes were probed with the indicated antibodies, and tubulin was used as a loading control. Densitometry measurement is shown in Figure S3.

In parallel, by detecting the expression of the HP1 heterochromatin markers, which are essential participants during the formation of condensed heterochromatin, we also compared the chromatin patterns or the conformation of chromatin in these cell lines during cisplatin treatment (Figure3.2-6). Protein expression level of two HP1 isoforms (HP1α and HP1β) increased by about 30% and 70%, respectively, but only in PEO1 cells after 24h treatment of cisplatin, HP1γ protein remained unchanged. Compared with PEO1 cells, these heterochromatin proteins in PEO4 cells changed little as assessed by the results of western blotting.

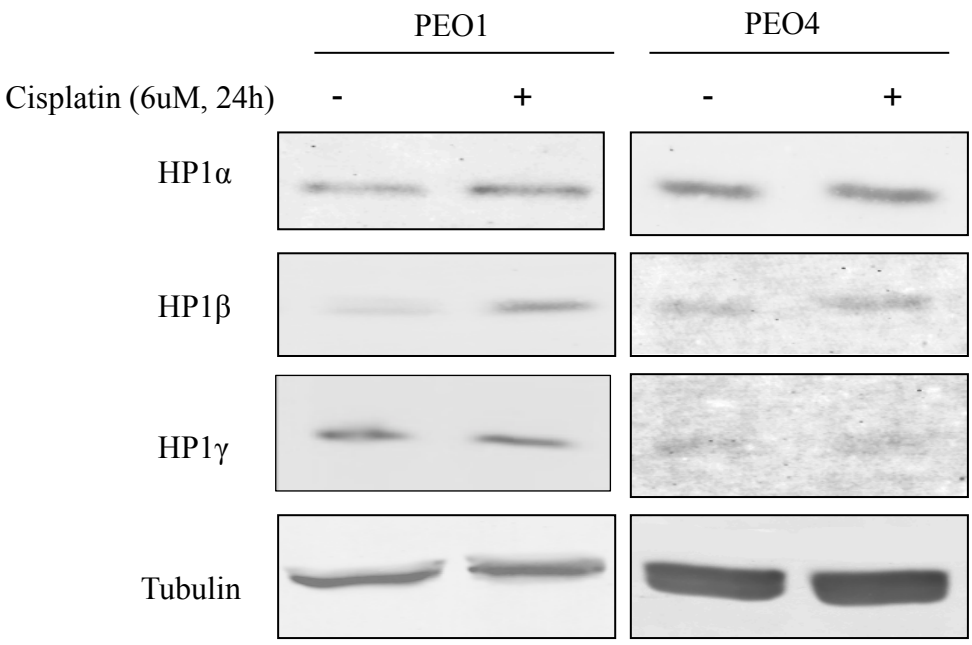

Figure 3.2-6 Expression of heterochromatin proteins after cisplatin incubation. Western blot for expression of HP1α, HP1β, and HP1γ in PEO1 and PEO4 cells with/without cisplatin treatment (6uM, 24h). Membranes were probed with the indicated antibodies, and tubulin was used as a loading control. Densitometry measurement is shown in Figure S3.

The measurement of HP1 protein is another evaluation of chromatin patterns at the molecular level, and the consistent expression pattern observed between HDACs and HP1s also indicate the involvement of HDAC family members in chromatin reorganization during cisplatin or DNA damage-based treatment in cancer.

3.2.3.2 mRNA Expression of HDAC and HP1 after 24h of cisplatin treatment

Since the protein expression of HDAC2 and HP1s showed pronounced change after cisplatin treatment in PEO1 cells, we next measured their mRNA expression levels to see if this DNA damage-based treatment could also induce similar changes in transcription in both cell lines. Cells were treated with or without cisplatin for 24

hours, and mRNA for each target was detected by a two-step real time PCR. As illustrated in Figure 3.2-7, mRNA levels of HDAC2, HP1α, HP1β, and HP1γ were all significantly elevated by cisplatin treatment ($p<0.05$) after 24h incubation in PEO1 cells (Figure 3.2-7A); however, the mRNA levels remained unchanged in PEO4 cells after the same treatment (Figure 3.2-7B). The elevated mRNA level of HDAC2 could explain the increase in HDAC2 protein expression after cisplatin treatment in PEO1 cells, and also the similar change in HP1 expression suggests that heterochromatin increases after treatment.

A.

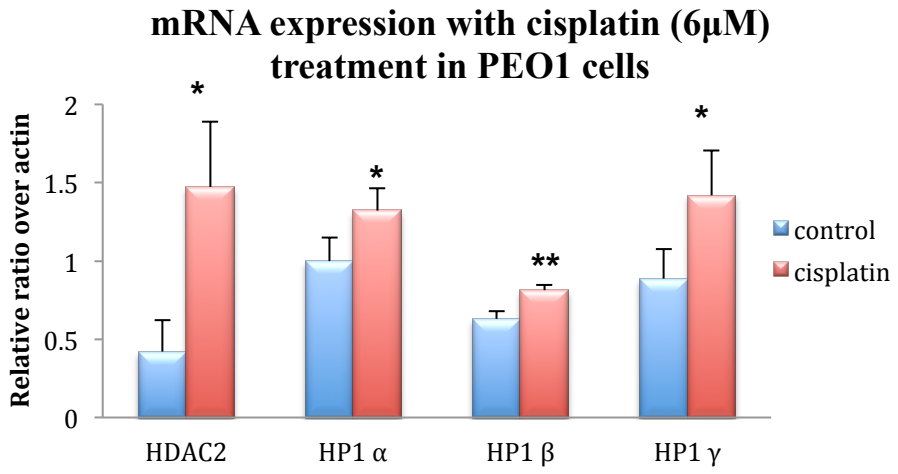

B.

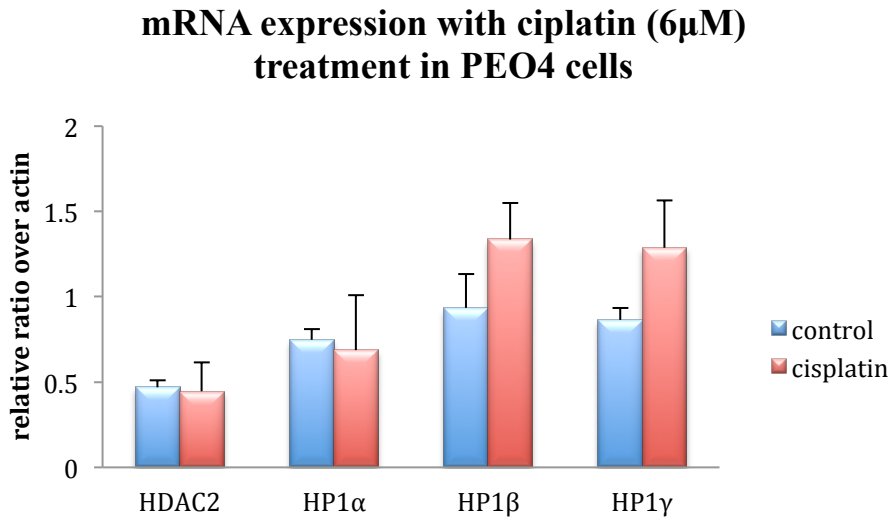

Figure 3.2-7 Expression of HDAC2, HP1α, HP1β, and HP1γ mRNA in PEO1 (A) and PEO4 (B) cells by two-step real time PCR. Total RNA was extracted from cells. The cDNA was synthesised by reverse transcription, and real time PCR was performed as described in the Materials and Methods. Relative expressions of the target gene was calculated as the average ΔCt and normalized to that of the housekeeping gene β-actin. The corresponding genes to HP1α, HP1β, and HP1γ are *CBX5*, *CBX1*, and *CBX3*, respectively. Results are as presented as mean ±SD from biological triplicates. *p<0.05, **p<0.01 (student's t-test).

This mRNA result is consistent with the changes observed for protein expression apart from HP1γ, which showed there was only increased expression of mRNA but

not protein. There may be several explanations for this: firstly, it is possible that only HP1α and HP1β are effected by cisplatin treatment, since HP1γ has been found not only in heterochromatin but also in euchromatin (Dinant and Luijsterburg 2009), except for its essential role of being a component of constitutive heterochromatin; secondly, the increased expression of HP1γ mRNA at 24h treatment might also induce more protein product at a later time point which was not included in the study here.

3.2.3.3 Cellular localisation and expression of HDAC2 and HP1s with cisplatin treatment

In order to visualize and confirm these alterations in expression, immunofluorescence (IF) was performed on PEO1 and PEO4 cells with or without cisplatin treatment by probing with antibodies against HDAC2, HP1α, HP1β, and HP1γ with DAPI to highlight the nucleus. Images were taken after 6 hours and 24 hours by confocal microscopy to establish whether there were any time-dependent expression changes in the expression of these proteins (Figure 3.2-8).

As expected, expression of HDAC2 increased at 24 hours after cisplatin incubation, and HP1 proteins showed gradual increases over 0h, 6h, and 24h after cisplatin treatment in PEO1 cells (Figure 3.2-8A). In contrast, neither HDAC2 nor HP1 proteins showed differences in expression during treatment up to 24h in PEO4 cells (Figure 3.2-8B). Additionally, the immunofluorescence images showed that all the target proteins were stained within nuclei where DAPI was present, which not only suggested that the antibody staining was specific, but also demonstrated that the

increased expression of these proteins was nuclear and therefore more likely to be associated with chromatin structure reorganization.

A.

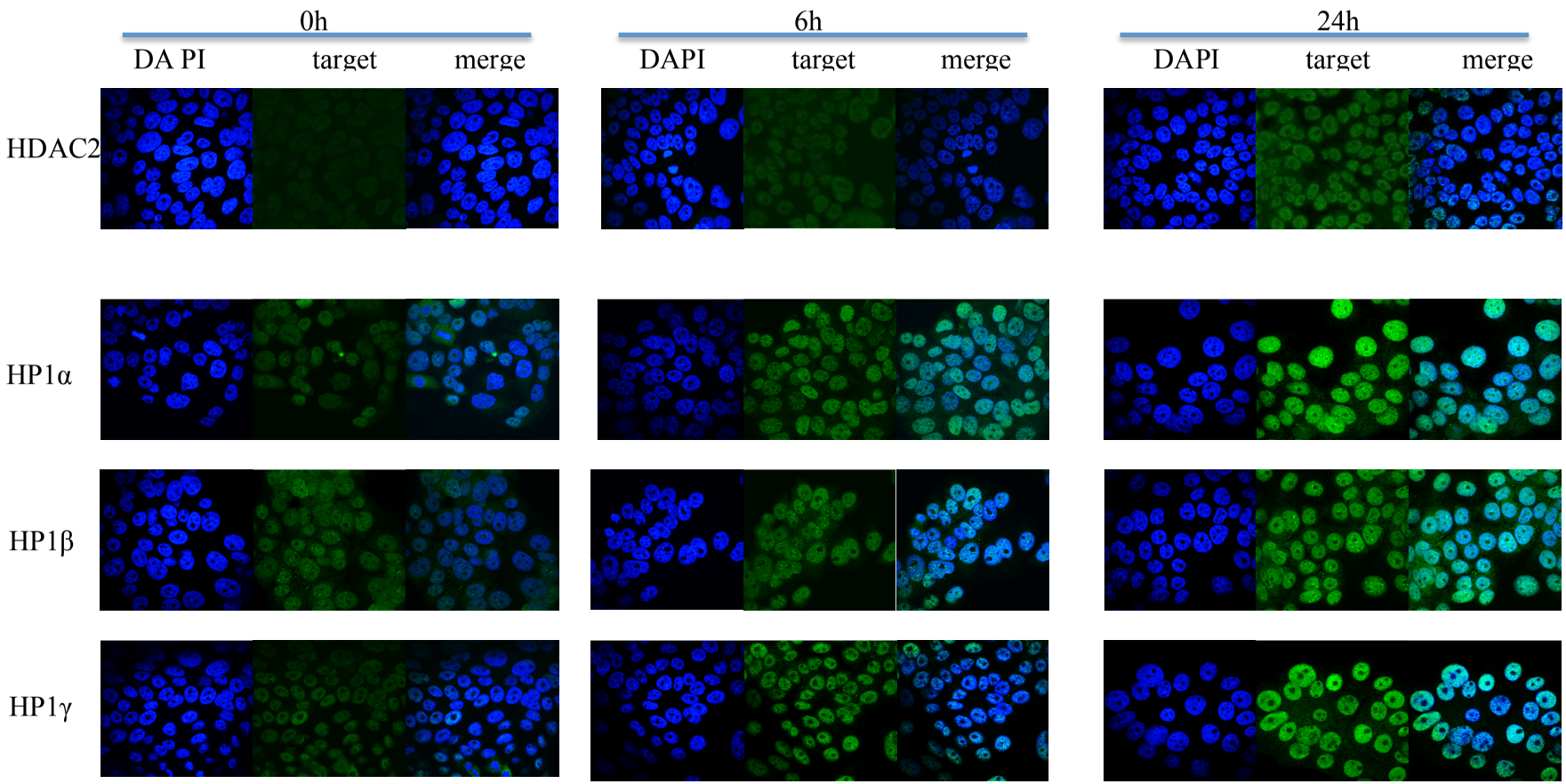
0h
6h
24h
DA PI
target
merge
DAPI
target
merge
DAPI
target
merge
HDAC2
HP1α
HP1β
HP1γ

(Continued)

B.

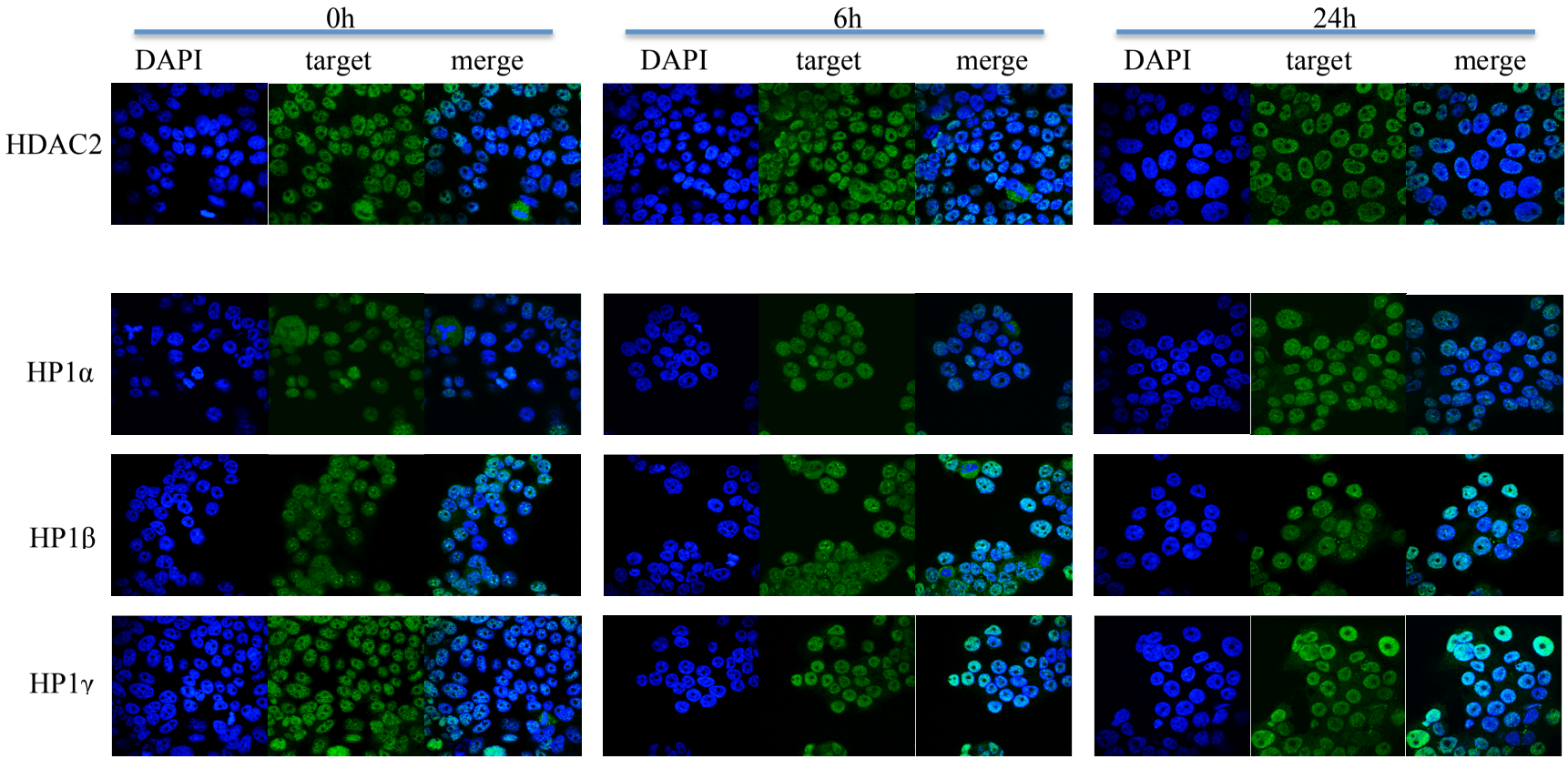

Figure 3.2-8 HDAC2 and HP1 protein expression detected by immunofluorescence. Cells were seeded on cover slips and fixed as described in the Materials and Methods in PEO1 (A) and PEO4 (B) cells after cisplatin treatment for 6h and 24h. Alexa488 (green channel) and DAPI (blue channel) were used to stain target proteins and the nuclei, respectively. Pictures were taken using a confocal microscope.

This result strongly supports the findings above, and is direct evidence that HDAC2 and heterochromatin accumulate after cisplatin treatment, which is consistent with results from western blotting and PCR. In summary, we demonstrate the increased expression of HDAC2, HP1α, and HP1β at both protein and mRNA level, and HP1γ at mRNA level, supporting the hypothesis that HDAC2 and chromatin reorganization are involved with the cellular response to cisplatin treatment, and provide important clues to associate HDACs with chromatin remodelling in chemotherapy in cancer.

3.3 Role of HDAC2 in DNA damage responses during chemotherapy

From the above results, HDAC2 turned out to be the most significantly changed HDAC member in response to cisplatin treatment *in vitro*, especially in the sensitive cell line PEO1, and may have a possible role in chromatin remodelling. Therefore, I next explored the detailed role of HDAC2 in the cellular DNA damage response (DDR) to DNA damage-based therapy, such as cisplatin treatment, by using a range of assays in PEO1 cells, and also expanded some work on PEO4 cells.

3.3.1 Time-dependent HDAC expression and the cellular DNA damage response induced by chemotherapy in ovarian cancer

Cisplatin has been widely studied for its effect on cellular DNA damage response as discussed in the Introduction. The results above also suggest that HDAC2 is a possible response marker after cisplatin treatment in PEO1 cells I therefore next asked whether there was any association between HDAC2 and the cellular DNA damage response events induced by cisplatin. As one of the most widely used chemotherapeutics in a variety of cancers, cisplatin mainly works by forming intrastrand and interstrand crosslinks in DNA (Fuertes, Alonso et al. 2003). The intrastrand crosslinks are primarily removed via nucleotide excision repair (Kartalou and Essigmann 2001). DSB repair pathways, such as HR, also contribute to the removal of interstrand crosslinks, which are considered to be crucial cytoxic damage to cells (McHugh, Spanswick et al. 2001; Kothandapani, Dangeti et al. 2011). There is also evidence showing the possible involvement of HDAC1 and HDAC2 in NHEJ (Miller, Tjeertes et al. 2010), but the knowledge about its roles in HR are not fully elucidated. The formation of nuclear DSBs triggers phosphorylation of H2AX at

Ser139; phosphorylated H2AX is named gamma H2AX (γH2AX). It is believed that histone H2AX phosphorylation is required to concentrate essential DNA repair proteins at the site of damaged chromatin (Podhorecka 2009). DNA double-strand break repair by HR (Schmidt and Schreiber) was shown to be mediated by BRCA1 phosphorylation at Ser1524, and BRCA1 is required to maintain genome integrity (Zhang, Willers et al. 2004). ATM, ATR, and their phosphorylated versions are also involved in this DNA damage response pathway. To examine how HDACs associate with DNA damage responses induced by cisplatin, we initially evaluated the expression of HDAC2 and other HDAC family members in PEO1 cells for a longer period of cisplatin treatment (0-96h), together with several DDR pathway players (γH2AX, pBRCA1, ATM, pATM, ATR, and pATR) by western blotting.

Among those HDAC family members, HDAC2 was up-regulated after cisplatin treatment at 24h as is stated previously, while expression of other members remained at a similar level between treated and untreated groups at early time point (0-48h). Meanwhile, expression of HDAC2, HDAC3, and HDAC4 all showed a time-dependent reduction after cisplatin treatment at the late time points (72h and 96h, Figure 3.3-1), and expression of other proteins remained at a similar level throughout the time course.

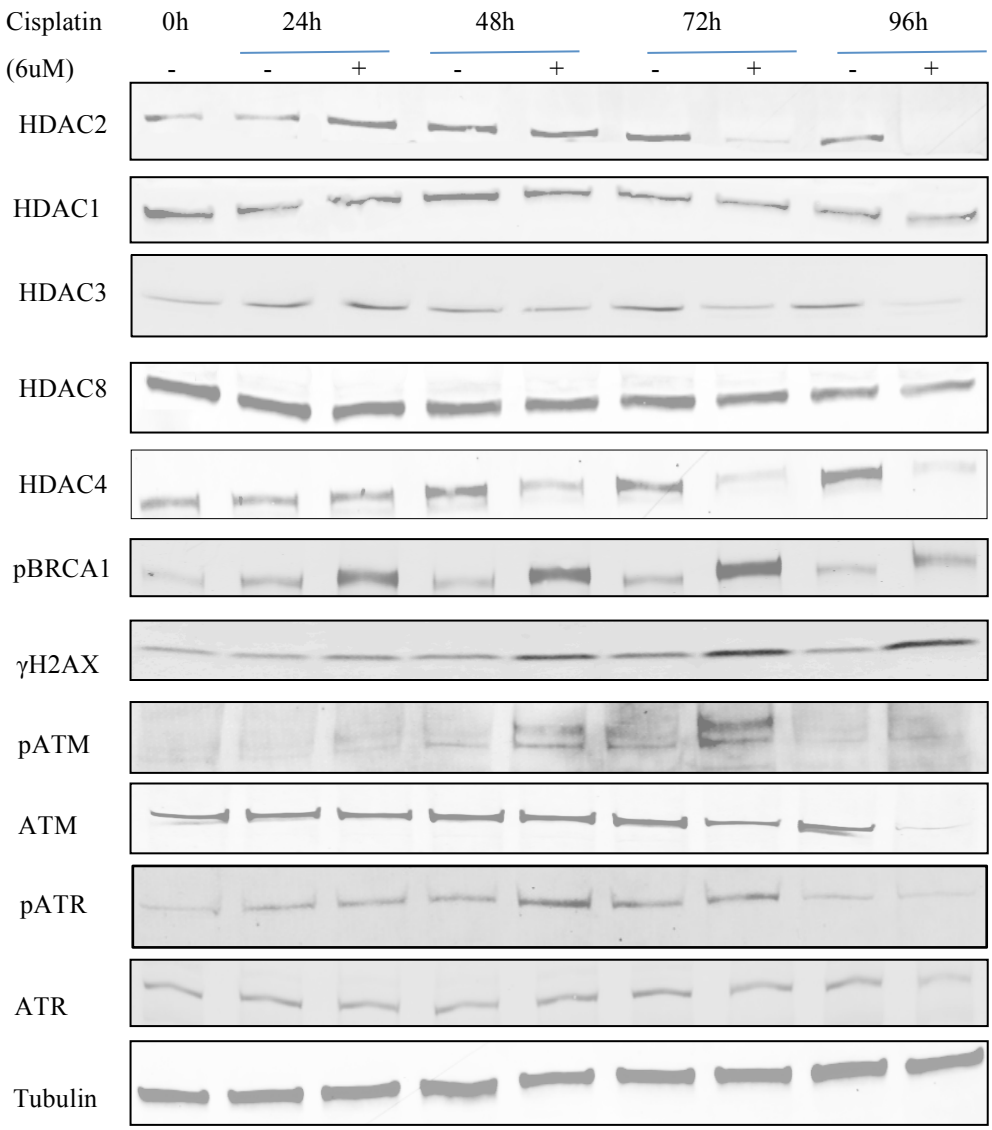

Figure 3.3-1 Time dependent expression of HDAC-family members and DNA damage response proteins in PEO1 cells. Cells were seeded and treated with or without cisplatin (6μM), and protein lysates were collected every 24h after treatment from 0h to 96h. Western blotting was performed to detect expression of HDAC1, HDAC2, HDAC3, HDAC4, HDAC8, pBRCA1, γH2AX, pATM, ATM, pATR, and ATR. Membranes were probed with the indicated antibodies, and tubulin was used as a loading control. Experiments were performed at least three times acquiring similar results. Blots from one representative experiment are shown.

Within the same lysates used in the western blotting assay, not surprisingly, the DDR proteins pBRCA1, rH2AX, pATM, and pATR participated in the response to

cisplatin, and showed up-regulation of expression after treatment. Expression levels of pBRCA1 were increased after 24h of cisplatin treatment in PEO1 cells, and this enhancement remained until 96h after therapy. Notably, the level of treated group dropped at 96h compared with the treated group at 24h, 48h, and 72h. On the other hand, expression of γH2AX, pATM, and pATR also increased after cisplatin treatment, and this occurred at late time points from 48h after treatment. Finally, total ATM and ATR protein levels remained stable except for a reduction of ATM at the late time point of 96h.

The results above showed time-dependent expression of pBRCA1, γH2AX, pATM, and pATR in PEO1 cells after cisplatin treatment, and the expression patterns varied from one protein to another. Meanwhile, expression of HDAC2, HDAC3, HDAC4, and HDAC8 also showed a relative time-dependent expression after cisplatin treatment, with only increased expression of HDAC2 at 24h. As a marker of double strand breaks, elevated γH2AX expression indicated the existence of a DNA damage response through the DSB repair pathway during cisplatin treatment in PEO1 cells; there is evidence to show that the tumour suppressor function of BRCA1 occurs through heterochromatin silencing with increased levels of both heterochromatin and BRCA1 after DNA damage treatment (Zhu, Pao et al.). Our results are consistent with these findings, and suggest that chromatin remodelling by HDACs might be involved in the cellular response to DNA damage therapy, such as double strand break and DNA repair. We speculate that HDAC members might act together with those pathway players in cellular DNA damage response via heterochromatin silencing.

3.3.2 Cellular effect of HDAC2 knockdown by siRNA transfection

The above results implicate HDAC-family members, especially HDAC2, in the response to chemotherapy, and demonstrate a possible link between nuclear structural changes and cellular DNA damage response. In order to further investigate more detailed functions of HDAC2 during cellular DDR, I explored a variety of cellular effects by knocking down HDAC2 using siRNA transfection.

3.3.2.1 Validation of HDAC2 knockdown efficiency

Gene silencing by RNA interference (RNAi) is nowadays widely used to knock down gene expression in order to investigate protein function in a variety of cell types. RNAi can be used as a process to moderate the activity of specific genes, and there are primarily two types of essential RNAi: micro RNA (miRNA) and small interfering RNA (siRNA). siRNA is a group of double-stranded RNA (dsRNA) molecules with 20-25 base pairs that works mainly through interfering with the expression of specific genes with complementary nucleotide sequences. The stealth RNAi we delivered into cells in this study is a 25bp long dsRNA with modification on the sense strand, using synthetic methods to ensure that only the anti-sense strand is functional to target genes to exclude any off-target effect from the sense strand. It is essential to ensure effective knockdown of a targeted gene, thus we evaluated the efficiency of our transfection through several approaches together with proper controls: 1. non-transfected control was included to judge the baseline level of cell viability, phenotype, and target gene level. 2. a negative control not homologous to anything in the vertebrate transcriptome was added to determine any sequence-independent silencing following siRNA delivery in cells. 3. a mock-treated control with all the transfection reagents in the absence of siRNA indicated any possible

cytotoxicity or other non-specific effects from the transfection procedure. Furthermore, time course experiments are also required to find the point of optimal knockdown and to ensure the occurrence of acceptable knockdown throughout the duration of the experiment.

3.3.2.1.1 Evaluation of HDAC2 knockdown at the RNA level

Since the gene silencing from siRNA functions at the mRNA level, I initially measured the expression of HDAC2 mRNA directly after transfection using two step real-time PCR. PEO1 cells were transfected with high or low concentrations of siRNA targeting HDAC2, and the total mRNA was collected from each sample after 48h, 72h, 96, and 120h of transfection. As is illustrated in Figure 3.3-2, about 40% of HDAC2 was knocked down after low concentrations of siRNA (10pmol in 6mL) were delivered into PEO1 cells for 48h ($p>0.05$), and the remaining expression of HDAC2 continued decreasing to 15-10% after 72-120h transfection compared with the control groups ($p<0.05$). When a high concentration of siRNA (100pmol in 6mL) was transfected, HDAC2 expression was supressed to 11% at the early time point of 48h ($p<=0.001$), and remained to 13-15% of control groups throughout the period of transfection ($p<0.05$). Comparison between the control groups indicated that mRNA expression levels of HDAC2 changed little, which suggested that the transfection method we used here was reliable without detectable sequence-independent silencing or non-specific effects on target genes from transfection reagents. Furthermore, the pronouncing reduction in HDAC expression indicated that transfection occurred at high efficiency.

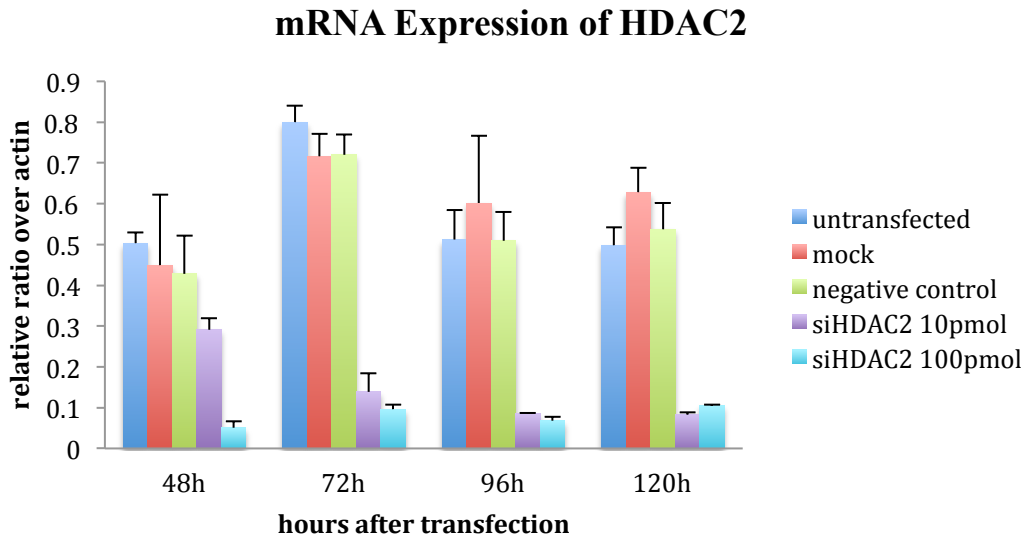

Figure 3.3-2 Expression of HDAC2 in PEO1 cells by two step real-time PCR. Cells were reverse transfected (as described previously in the methods) with siRNA (10pmol or 100pmol in 6mL) targeting HDAC2, and untransfected group, mock group, and negative control were included as controls. Total RNA was extracted from cells at 48h, 72h, 96h, and 120h after transfection. The cDNA was synthesised by reverse transcription, and real time PCR was performed as described in the Materials and Methods. Relative expression of HDAC2 was calculated as the average ΔCt and normalized to that of the housekeeping gene β-actin. Results are as presented as mean ±SD from triplicate samples. One-way ANOVA followed by Tukey HSD post hoc test was performed between groups for statistical analysis (Table S3 for full analysis data).

3.3.2.1.2 Evaluation of HDAC2 knockdown at protein level

Since the protein is more essential in terms of function during cellular events, it was also important to assess the expression of HDAC2 at the protein level after siRNA transfection. As a well-optimised method in this study, we primarily observed protein expression of HDAC2 in PEO1 cells by using the HDAC2 antibody in an immunofluorescence assay. Corresponding to the method we applied above, the three controls were also included to evaluate transfection efficiency, and the IF result is illustrated in Figure 3.3-3A.

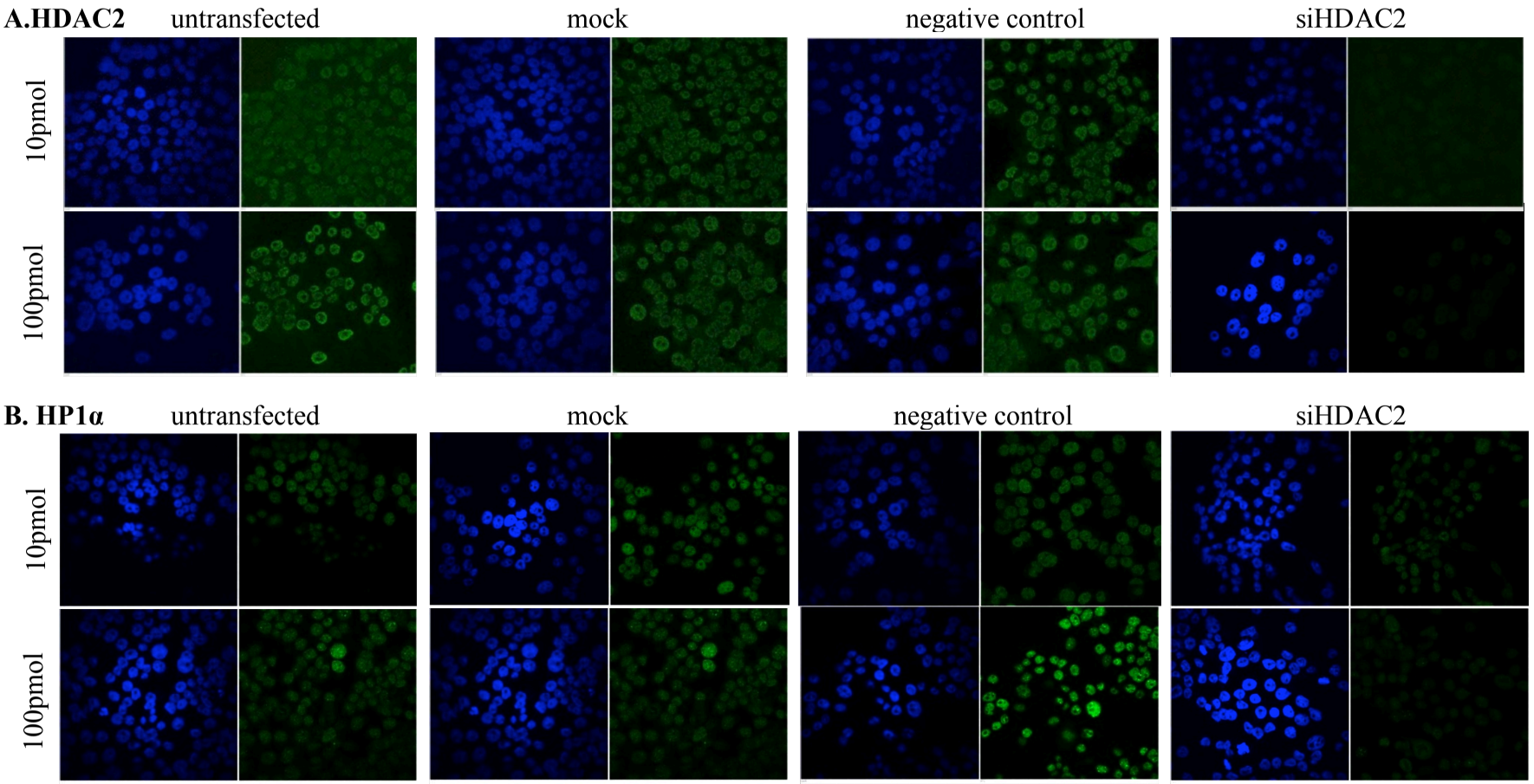

Figure 3.3-3 Representative images for HDAC2 (A) and HP1α (B) expression detected by immunofluorescence. PEO1 cells were seeded on cover glasses and fixed as described in Materials and Methods after siRNA transfection (low and high concentration) for 72h, and untransfected, mock, and negative control were used as control groups. Alexa488 (green channel) and DAPI (blue channel) were used to stain target proteins and nuclei, respectively. Pictures were taken using a confocal microscope.

The protein expression of HDAC2 was considerably reduced, as shown in the green channel with either low or high concentrations of delivered siRNA duplex, compared to control groups. Similar to the RNA expression result, protein levels of HDAC2 varied little among the three controls; meanwhile, the knockdown of HDAC2 expression was highly effective with a very low application of transfection reagents. We also detected the expression of HP1α in PEO1 cells with HDAC2 knockdown. As was expected, there was minor fluorescence detected (green channel in Figure 3.3-3B) in the transfected group, which indicated that the amount of HP1α protein in the nucleus was abundantly reduced in cells after siRNA transfection. These chromatin pattern changes as measured by HP1 protein expression directly supports the role of HDAC2 in chromatin organization.

To achieve more accurate and specific measurement of HDAC2 expression, western blotting was performed to investigate the target protein level after gene knockdown. The same time course experiment to that used for RNA detection above was carried out to detect protein expression from 48h to 120h after gene knockdown (Figure 3.3-4). The decreased expression of HDAC2 occurred as early as 48h with about 70% reduction in protein expression under both concentrations of siRNA duplex, and the knockdown effect also remained at around 70% suppression of protein expression from 72-120h.

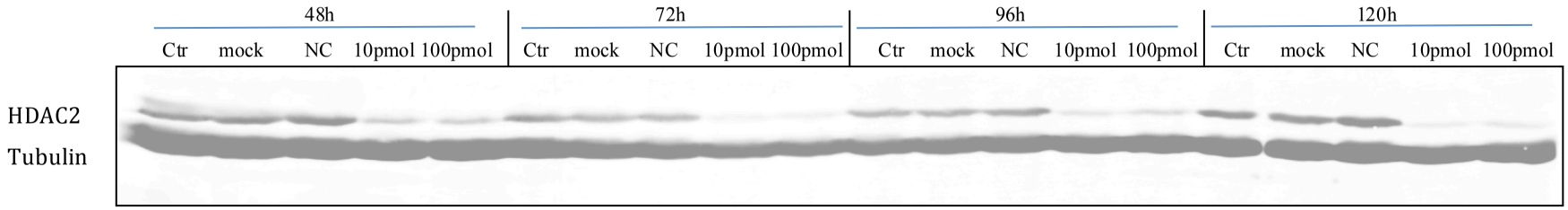

Figure 3.3-4 Assessment of HDAC2 protein expression by western blotting after HDAC2-targeted siRNA transfection in PEO1 cells. Cells were reverse transfected (as described previously in the methods) with siRNA (10pmol or 100pmol in 6mL) targeting HDAC2, and untransfected group (Ctr), mock group, and negative control (Joseph, Baum et al.) were included as controls. Total protein was extracted from the cells at 48h, 72h, 96h, and 120h after transfection. Western blotting was performed to detect expression of HDAC2. Membranes were probed with the indicated antibodies, and tubulin was used as a loading control. Figure S5 shows the densitometry measurement of expression levels.

These measurements established that the RNAi method we applied here successfully silenced HDAC2 with high efficiency at both mRNA and protein level even at lower concentrations of RNAi, and the undetected sequence-independent silencing and non-specific effect from transfection reagents provided acceptable confidence in this RNAi as a reliable method for future studies on the functions of HDAC2.

3.3.2.2 Effect of HDAC2 knockdown on cell morphology and growth in PEO1 cells

The morphology of PEO1 cells was observed after 72 hours incubation with siRNA transfection under the light microscope, and comparisons were made between the knocked-down samples and the controls (non-transfection, mock, and negative siRNA control). Figure 3.3-5 shows representative pictures from the study of the cellular morphology of PEO1 cells after HDAC2 expression was knocked down. Cells settled in the dishes as a monolayer with either normal medium or transfection reagents. After 72h treatment, the shape and appearance of those cell adherent to dishes remained similar, while noticeably there was a large number of round-shaped cells floating in the medium with the siHDAC2 duplex, leaving less cells attached to the dishes. This result indicated that HDAC2 might have an effect on cell growth or viability and colony formation in PEO1 cells, and the reduction of attached cell number was possibly due to cell death induced by HDAC2 depletion.

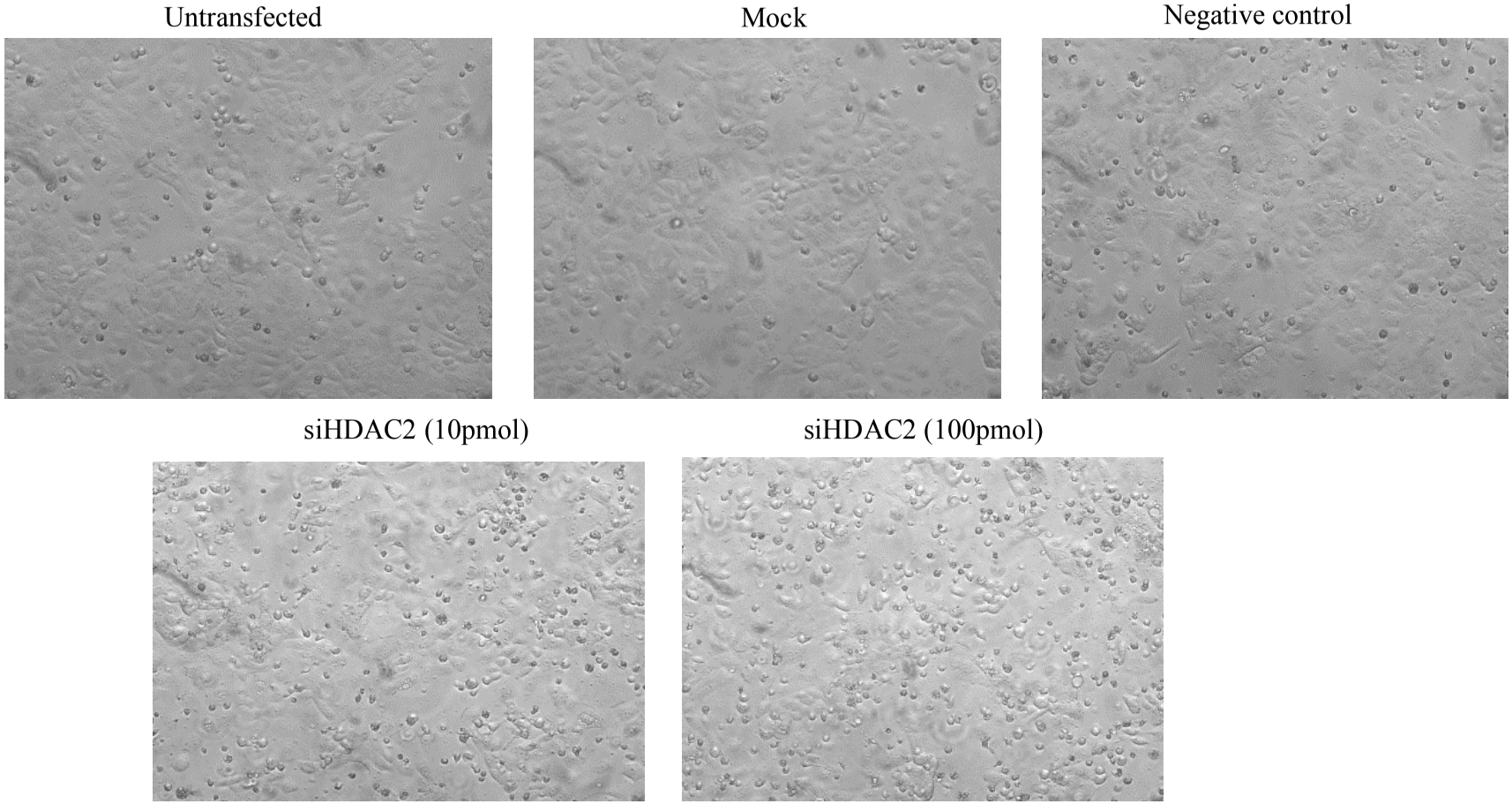

Figure 3.3-5 Cellular morphology, density, and growth after HDAC2 was knocked down in PEO1 cells. Light microscope pictures were taken after 72h using reverse siRNA transfection. Non-transfection, transfection delivery reagents, and negative siRNA duplexes were applied as untransfected control, mock control, and negative control, respectively.

3.3.2.3 Expression profiling of other HDAC family members, heterochromatin proteins, and DNA damage response proteins under HDAC2 suppression

After the RNAi methodology was validated, I next examined the effect of HDAC2 depletion on the expression of other HDAC family members, and target proteins by western blotting (Figure 3.3-5, panel 1-5). Apart from the effective depletion of HDAC2 expression even at the lower concentration of siRNA (10pmol), protein levels of HDAC3, HDAC4, and HDAC8 were not significantly affected by knockdown of HDAC2, which showed a fairly specific suppression of HDAC2 using RNAi without off-target effect on these HDAC members. Interestingly, HDAC1 expression was mildly up-regulated after HDAC2 knockdown, which indicated a possible compensatory effect between HDAC1 and HDAC2 in PEO1 cells. This compensatory mechanism between HDAC1 and HDAC2 has previously been reported in several studies (Wilting, Yanover et al. 2010; Yamaguchi, Cubizolles et al. 2010; Jurkin, Zupkovitz et al. 2011).

Since HDAC2 was implicated in heterochromatin formation as indicated by HP1 expression measured by IF above, we further assessed the expression of all three heterochromatin protein isoforms after siRNA transfection (Figure 3.3-5, panel 6-8) by western blotting. HP1 proteins exhibited a little alteration, with mild down-regulation (20%) of HP1α expression after siHDAC2 was transfected. The down-regulation of HP1α from both IF and western blotting suggests HDAC2 participates in the nuclear chromatin organisation to some degree; nevertheless we would speculate that considerable alteration of chromatin organization might result from the

cooperative effect from several HDAC family members, in terms of the relatively stable observed expression of HP1β and HP1γ.

To decipher whether those DDR proteins mentioned previously were affected in HDAC2 knockdown cells, we examined their expression. After 72h depletion of HDAC2, there was a dramatically significant up-regulation of γH2AX and reduction of pBRCA1 (Figure 3.3-6, panel 9-10). In contrast, the stability of other DDR proteins (pATM, ATM, pATR, ATR, and Rad51 in Figure3.3-6, panel 11-15) was not obviously affected. This result implies accumulation of double strand breaks and possible reduced DNA repair induced by suppression of HDAC2 expression, although the up-regulation of γH2AX might also indicate that the cells are undergoing apoptosis (Tanaka, Kurose et al. 2006).

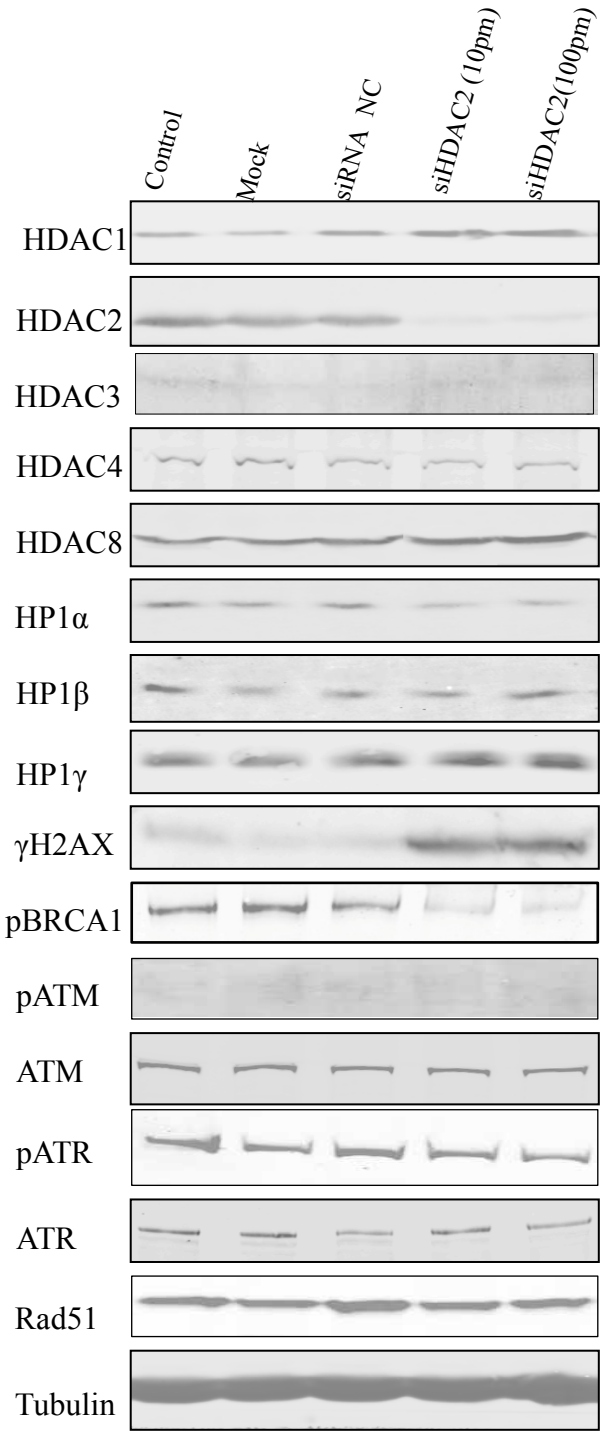

Figure 3.3-6 The effect of siHDAC2 on expression of other HDAC family members (panel 1-5), HP1s (panel 6-8), and DNA damage response proteins (panel 9-15) by western blot in PEO1 cells. Protein was lysed after HDAC2 was knocked down after 72h using reverse transfection. Non-transfection (control), mock, and siRNA negative control. were used as controls. Membranes were probed with the indicated antibodies, and tubulin was used as a loading control (panel 16). Experiments were performed at least three time acquiring similar results. Blots from one representative experiment are shown.

3.3.2.4 Characterisation of cellular responses to cisplatin treatment in ovarian cancer cells when HDAC2 is potently inhibited

Since these data implied an association between HDAC2 and the DNA damage response to cisplatin, I next explored the roles by which HDAC2 contributed to the DNA damage response induced by cisplatin. Here I broadened the detection of DDR proteins with HDAC2 siRNA transfection and cisplatin treatment in both PEO1 and PEO4 cells. After cells were transfected with HDAC2 siRNA for 72 hours (low concentration of 10pmol/6mL applied for acceptable transfection efficiency), I treated them with cisplatin and collected cellular protein after 6-96h of incubation with cisplatin.

Western blotting results from PEO1 cells are shown in Figure 3.3-7. Consistently, HDAC2 showed early up-regulation at 24h and late down-regulation during cisplatin treatment in those control groups without HDAC2 knockdown. Not surprisingly, the induction of DSBs indicated by γH2AX occurred as early as 6h, while interestingly we discovered an accumulation of γH2AX expression after 24 hours of cisplatin treatment in cells with HDAC2 depletion, compared with either the cisplatin treated group or HDAC2 knockdown-only groups. This accumulation effect from both siHDAC and cisplatin seemed to be gradually lost during the incubation time until 72h. In Figure 3.3-1, the up-regulation of several DNA damage response proteins was noted during cisplatin treatment; I therefore examined their expression in response to cisplatin treatment after HDAC2 was depleted, and also included another major player in DSBs repair, particularly in homologous recombination (Baumann and West 1998). As expected, pBRCA1, pATM, pATR, and Rad51 participated in DDR triggered by cisplatin at certain time points (6h, 24h, 48h, and 24h respectively)

with increased expression compared with untreated controls. By contrast, cisplatin caused dramatically reduced expression of those proteins in cells with HDAC2 knockdown, which was demonstrated apparently in the last lane at various time points from 24h to 72h in Figure 3.3-7.

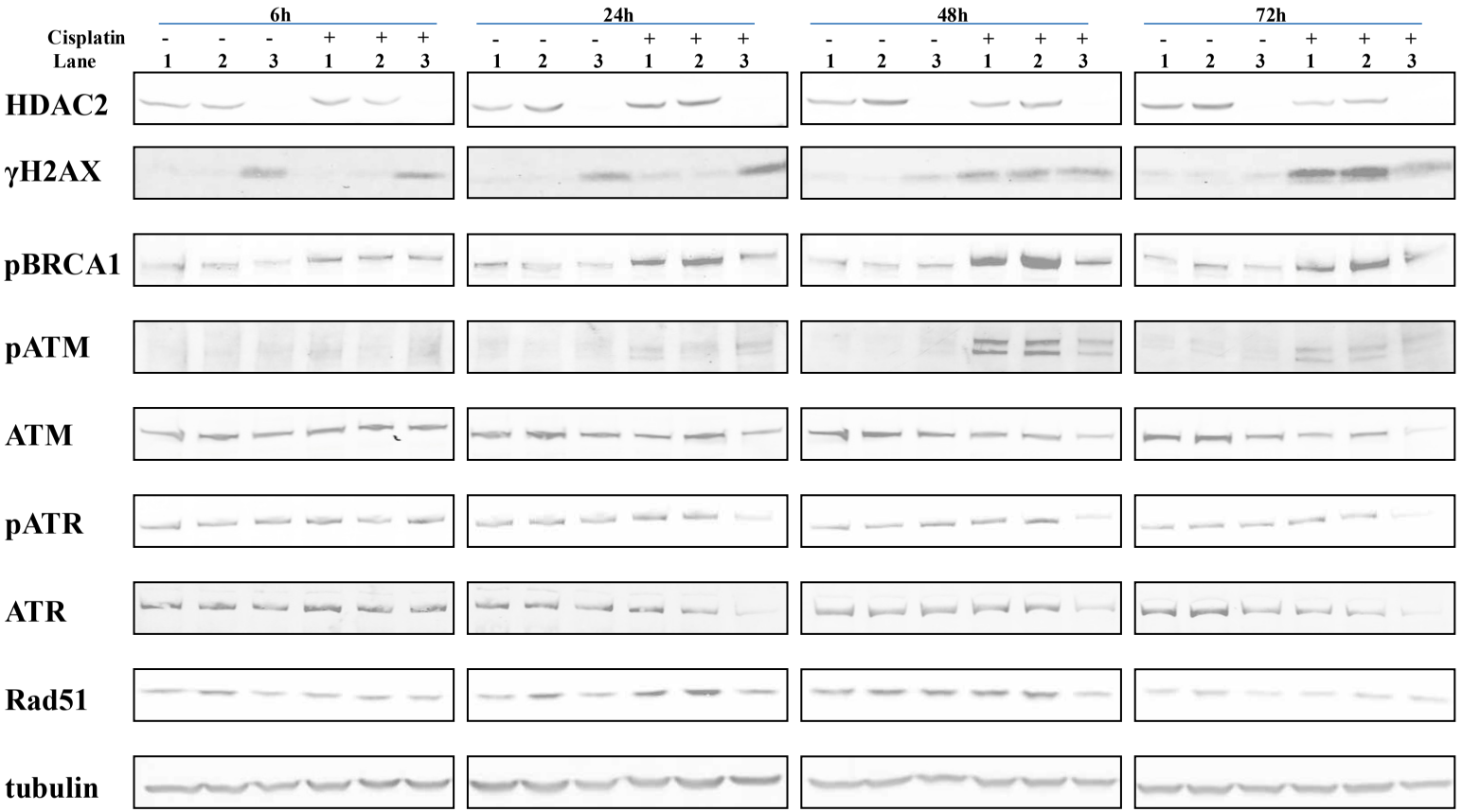

Figure 3.3-7 Effect of HDAC2 knockdown on the expression DNA damage response proteins after cisplatin treatment in PEO1 cells. Cells were treated with cisplatin (6μM) after 72h incubation with mock (lane 1), siRNA negative control (lane 2), or HDAC2 siRNA duplexes (10pmol in 6mL, lane 3). Protein lysates were collected at 6h, 24h, 48h, and 72h after cisplatin treatment and analysed by western blotting of DNA damage response proteins; tubulin was used as a loading control as before. Experiments were performed at least three time acquiring similar results. Blots from one representative experiment are shown.

To clarify further the involvement of HDAC2 during cellular DDR by cisplatin, the same assessment was performed in the cisplatin-resistant PEO4 cell line (Figure 3.3-8). HDAC2 in PEO4 cell exhibited little alteration during cisplatin treatment except for decreased expression at relatively late time point of 72h; however, the siRNA also successfully silenced the expression of HDAC2 in PEO4 cells. Differing from PEO1 cells, cumulative effect from both HDAC2 depletion and cisplatin on γH2AX was not observed in PEO4 cells, although there was induction of DSBs from 24h by cisplatin when we compared the cisplatin-treated groups with those without drug incubation. Additionally, expression of pBRCA1, pATM, and RAD51 were elevated by cisplatin treatment only, indicating the activated DNA damage response pathway via these proteins. Similarly, suppression of this activation by HDAC2 depletion was displayed through decreased levels of pBRCA1, ATM, pATR, and RAD51, though the pattern of DDR interruption from siHDAC2 was distinct between PEO1 and PEO4 cells, which was different over time.

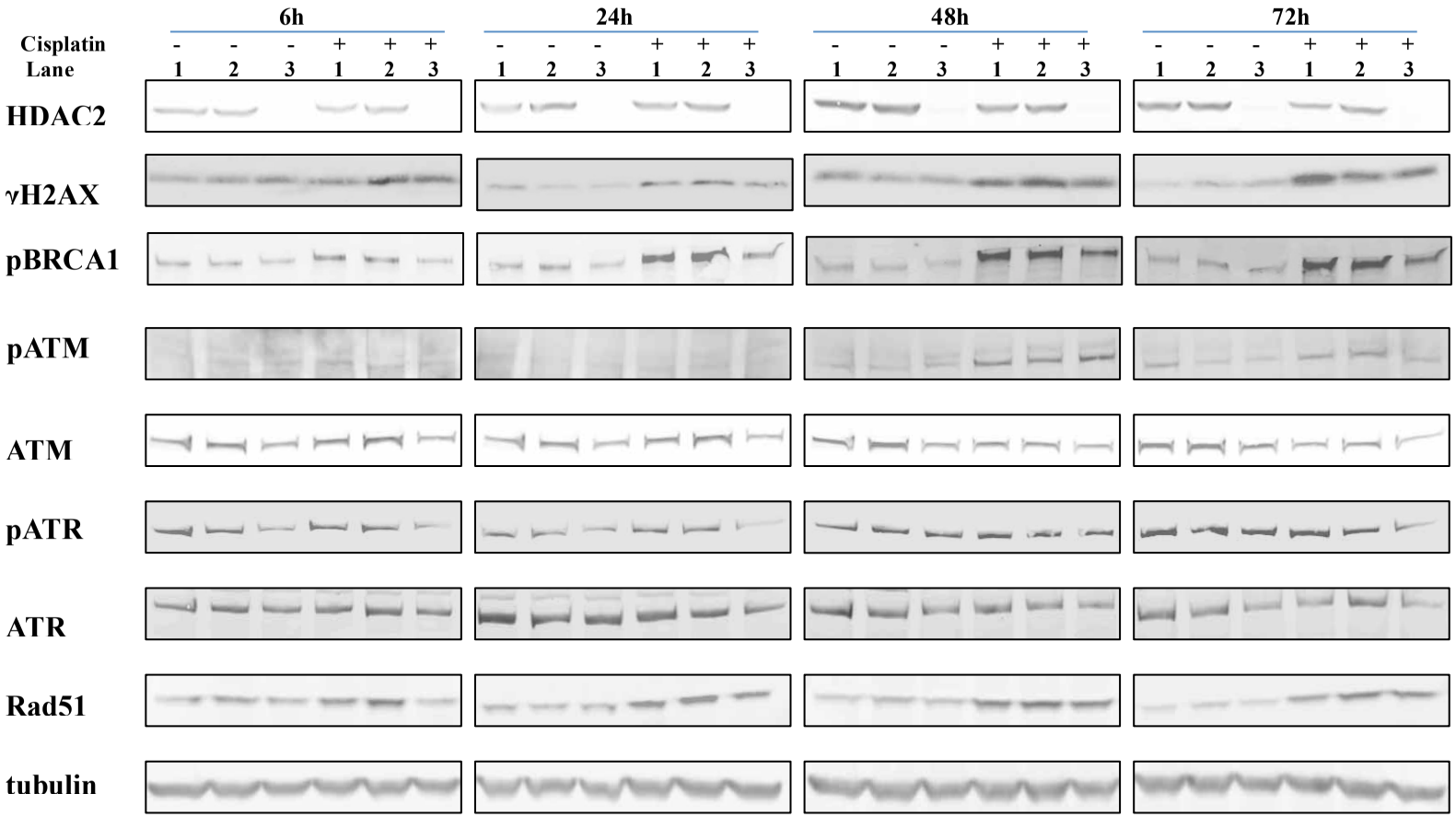

Figure 3.3-8 Effect of HDAC2 knockdown on expression of DNA damage response proteins after cisplatin treatment in PEO4 cells. Cells were treated with cisplatin (6μM) after 72h incubation with mock (lane 1), siRNA negative control (lane 2), or HDAC2 siRNA duplexes (10pmol in 6mL, lane 3). Protein lysates were collected at 6h, 24h, 48h, and 72h after cisplatin treatment for analysis by western blotting of DNA damage response proteins, and tubulin was used as a loading control as before. Experiments were performed at least three time acquiring similar results. Blots from one representative experiment are shown.

To summarise the results from the PEO1 and PEO4 cell lines, I demonstrated the participation of multiple DDR proteins (γH2AX, pBRCA1, pATM, ATM, pATR, ATR, and RAD51) and induction of DSBs by cisplatin in both PEO1 and PEO4 cells. Moreover, suppression of DDR activation occurred after HDAC2 knockdown by RNAi, which strongly suggested the involvement of HDAC2 in the cellular response to the DNA damage-based treatment. The differences between PEO1 and PEO4 cells in the manner of DSB accumulation and time point of pathway activation or suppression might be due to the nature of the two cell lines in terms of their cisplatin sensitivity. The two major pathways for DSB repair, NHEJ and HR, have compensatory effects to each other (Jeggo, Geuting et al. 2011). The balance between them might be disrupted by the distinct status of BRCA2 in PEO1 and PEO4 cells, which might influence the dominant repair mechanism in the two cell lines and cause the functional activity of those DNA damage response proteins at different stages after cisplatin treatment. Furthermore, HDAC2 also showed a different pattern of involvement during DDR induced by cisplatin between sensitive and resistant cells.

3.3.2.5 Role of HDAC2 in γH2AX foci formation during cisplatin treatment

As a marker for DSB, one of the histone variants of H2AX is phosphorylated at ser139 after being exposed to DNA damage factors, namely γH2AX (Rogakou, Pilch et al. 1998). It has been demonstrated that γH2AX could locally form foci at the DNA damaged domains, and has been suggested to be a profoundly sensitive marker of interstrand crosslinking DNA damage induced by cisplatin (Clingen, Wu et al. 2008). Additionally, γH2AX foci play an essential role in the process of recruitment of a range of DNA damage response factors, such as the checkpoint protein 53BP1 (Ward, Minn et al. 2003), and is vitally responsible for the cellular DNA damage response with co-localization with various DDR components including ATM, BRCA1, and RAD51. (Fernandez-Capetillo, Celeste et al. 2003). The detection of immunofluorescently-stained γH2AX foci has been widely applied to evaluate the degree of DSB damage. From the above results, HDAC2 has been shown to be important during cellular DDR, which prompted me to further define its role in DSBs in terms of γH2AX foci formation in cells with HDAC2 depletion. PEO1 and PEO4 cells were grown on coverslips as usual, and nuclei and γH2AX were stained as described before. The γH2AX foci were recognized and visualised using immunofluorescence microscopy.

After treating cell with cisplatin for 24h, I noticed γH2AX foci formation in both PEO1 (Figrure3.3-9A) and PE04 (Figure3.3-9B) cells without siRNA (NC+cisplatin group). This is not surprising and consistent with the previous observation showing the remarkable accumulation of γH2AX foci after cisplatin treatment in cells (Huang, Okafuji et al. 2004). Within cells transfected with HDAC2 siRNA, there was also

production of γH2AX foci in both cell lines (siRNA group in Figure 3.3-9 A and B), and immunofluorescent signal from γH2AX antibody exhibited similar intensity to that in cisplatin treated groups. It is also noteworthy to point out that the γH2AX staining in PEO4 cells with HDAC2 knockdown displayed more heterogeneity with high intensity for the foci in a few cells and near background staining in other cells. Furthermore, by investigating the foci formation in cells treated with cisplatin after HDAC2 knockdown, a remarkable increased production of γH2AX foci was recognized in PEO1 cells (siRNA+cisplatin group in Figure3.3-9A) with both enhanced number and intensity of foci compared with other groups. In PEO4 cells, this accumulative effect from both siRNA and cisplatin was not as obvious as PEO1 cells, with a similar signal to that in cells treated with cisplatin alone (siRNA+cisplatin group in Figure 3.3-9B).

A.

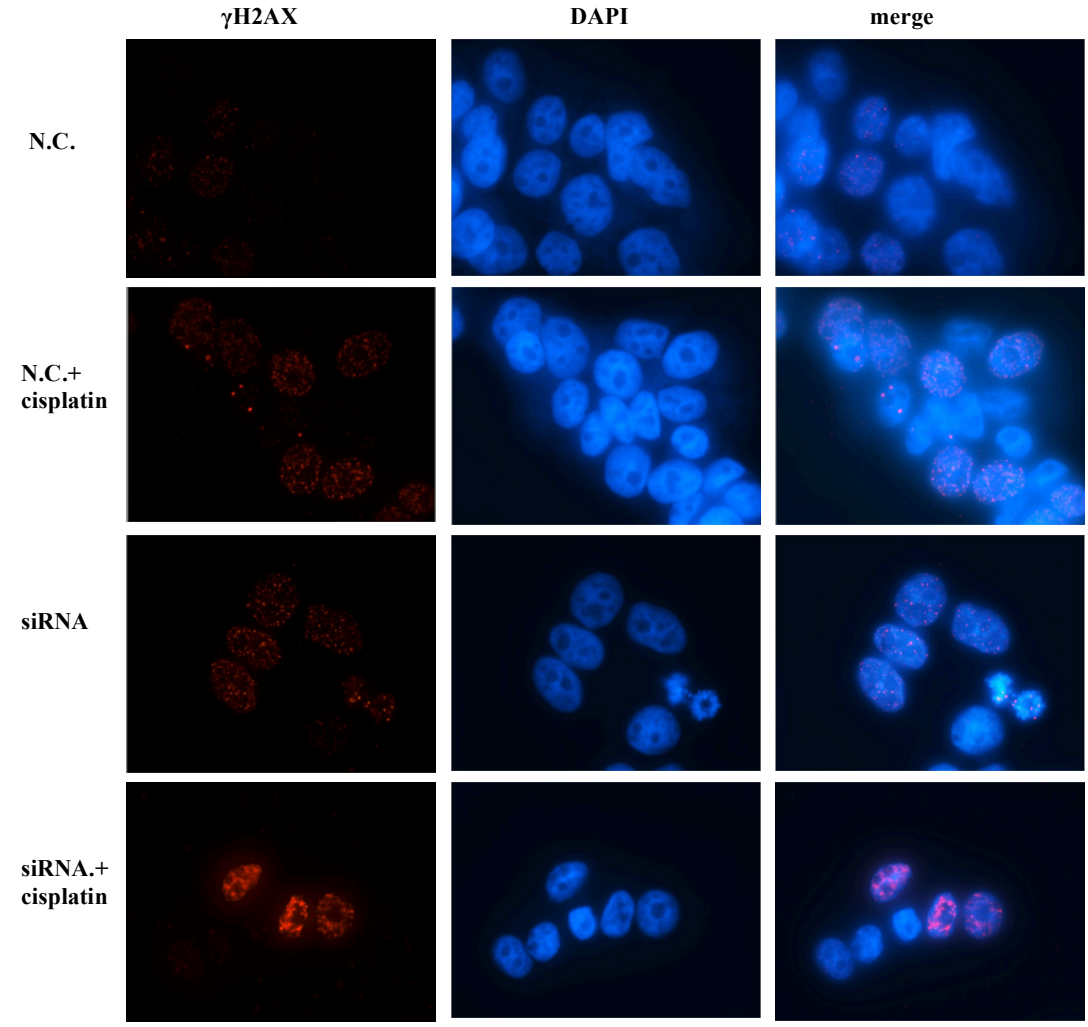

(Continued)

B.

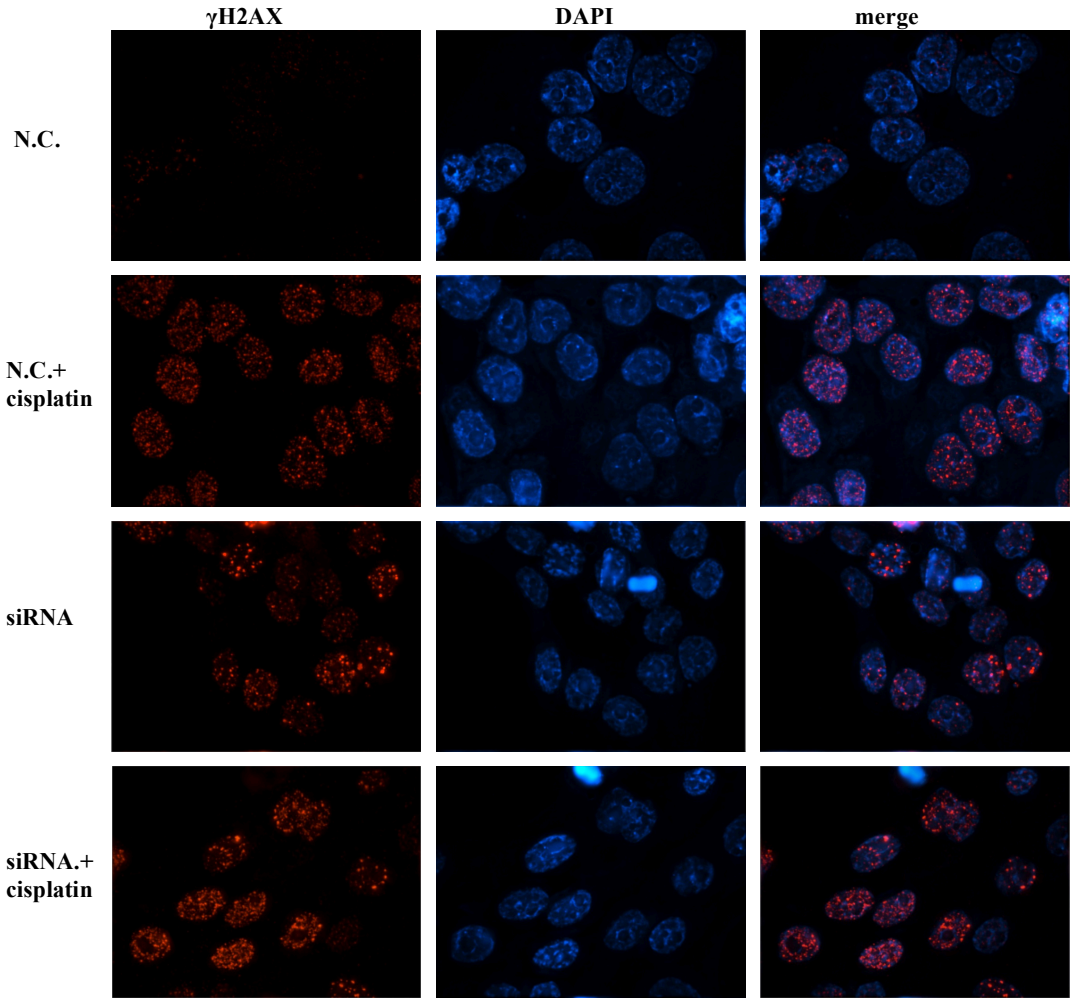

Figure 3.3-9 Immunofluorescent staining for γH2AX foci in PEO1 (A) and PEO4 (B) cells. Cells were grown and treated as described before, and images were taken after 24-hour treatment of cisplatin in cells with or without HDAC2 siRNA. Antibodies against H2AX phosphorylation at Ser 139 were used to probe cellular γH2AX foci (red channel), and DAPI was applied for nuclear staining (blue channel). Representative images from one experiment were shown. More that 100 cells in each group were included for one experiment, and three independent experiments were performed.

To quantitatively analyse γH2AX foci in my experiments, I counted the number of foci in each cell using the PZ Foci EZ plugin in ImageJ software as described in Materials and Methods, and more than 100 nuclei were included in each single experiment. Less than 5 clustered γH2AX foci were detected in the majority of the cell population in the control groups in PEO1 (Figure 3.3-10A) and POE4 (Figure 3.3-10B) cells from the distribution figures, indicating the background level. The main population distribution switched to the side with more foci per cell after either cisplatin or siRNA plus cisplatin treatment (6-15 and 16-30 foci per cell, Figure 3.3-10A) in PEO1 cells. In contrast, only cisplatin treatment caused an obvious alteration of foci number distribution in PEO4 cells with 16-30 foci per cell in most of the cells within the group, and the combined treatment with siRNA and cisplatin might affect the cell distribution with excess numbers of cells with large numbers of foci (>=16) compared with controls (Figure 3.3-10B).

A.

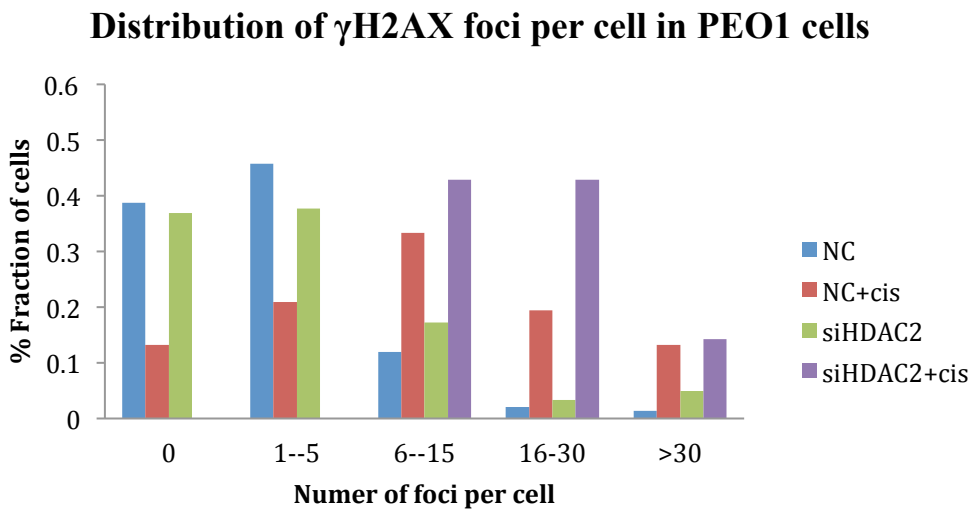

B.

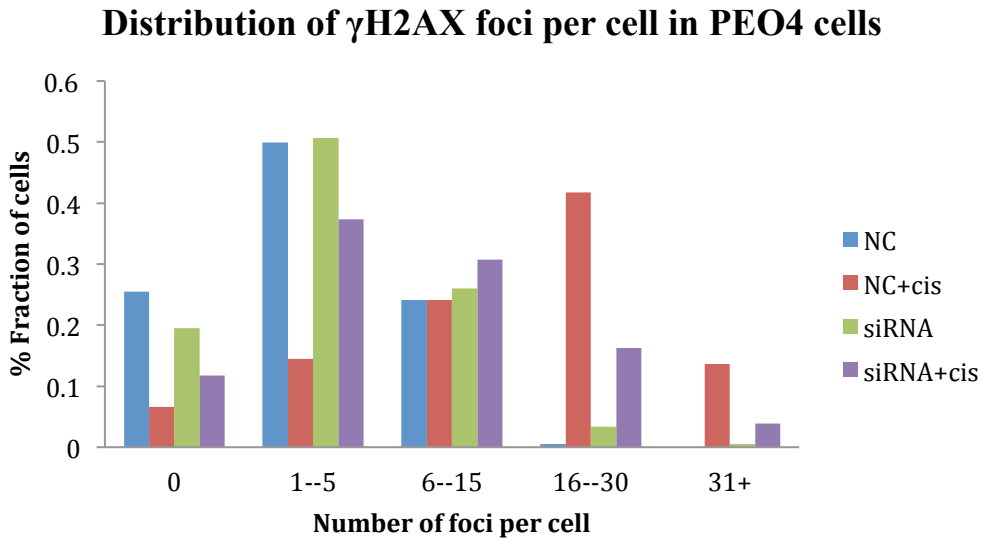

Figure 3.3-10 Distribution of γH2AX foci per cell at 24h after cisplatin treatment with or without HDAC2 knockdown in PEO1 (A) and PEO4 (B) cells. The percentage of targeted cells with different γH2AX foci numbers (0, 1-5, 6-15, 16-30, >30) is given. One representative experiment is shown where more than 100 were counted per group.

As a result, we set the 5 foci per cell as threshold for background level, and cells with 5 or less foci were defined as negative and more than 5 as positive. To acquire a statistical analysis for γH2AX foci formation, the percentage of cells with positive staining was calculated in each group, and the number was compared with negative controls in each cell line (Figure 3.3-11). In parallel with observations from IF staining, the number of PEO1 cells with positive foci significantly increased after either cisplatin treatment or HDAC2 knockdown, and additional foci were induced by cisplatin treatment in cells with HDAC2 depletion ($p<0.05$ and 0.01 compared with cisplatin-treated and siRNA transfected groups, respectively, Figure 3.3-11). The most significant effect on foci formation in PEO4 cells was generated by cisplatin treatment ($p<0.001$), while HDAC2 knockdown alone changed little the cell percentage with positive foci number compared with background levels. Among the groups, knockdown of HDAC2 also significantly increased the cell number with positive γH2AX foci ($p=0.032$), although this depletion showed minor restoration for the foci accumulation from cisplatin.

A.

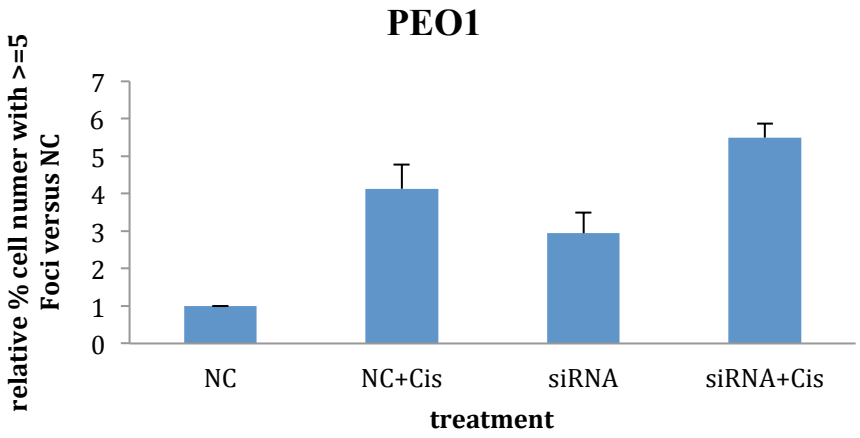

B.

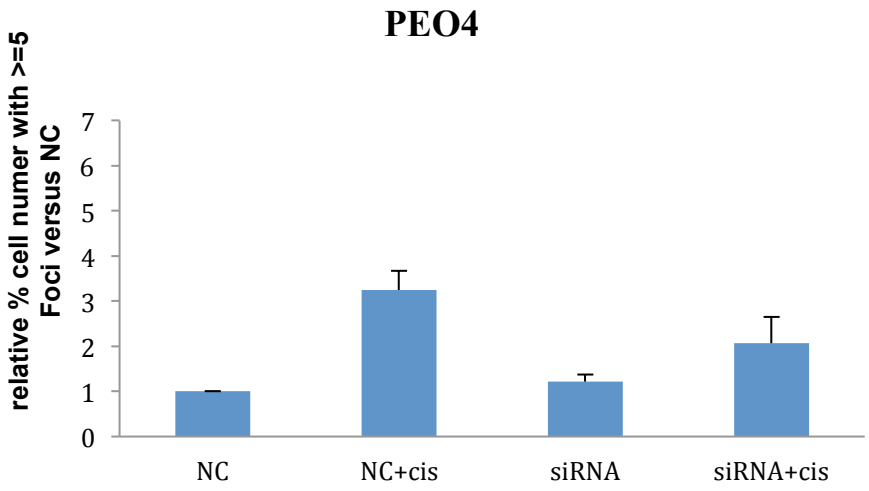

Figure 3.3-11 Relative cell number percentage with positive γH2AX foci (more that 5 foci per cell) calculated compared to background levels (negative control group, NC). Each column represents the average data from 3 independent experiments, and error bars represent the SD of average foci per cell. One-way ANOVA followed by the HSD post hoc test was performed between groups for statistical analysis (Table S4 for full analysis date).

This result is consistent with our previous data from western blotting showing the cumulative effect of HDAC2 knockdown on protein expression of γH2AX after cisplatin treatment, which was not observed in PEO4 cells but opposite with minor reductions in γH2AX level (Figure 3.3-7 and Figure 3.3-8). The enhanced number of γH2AX foci caused by HDAC2 knockdown during cisplatin treatment in PEO1 cells indicated either compromised repair during DNA damage or persistent production by cisplatin (Burdak-Rothkamm, Short et al. 2007), and this could be further examined by prolonged incubation in drug-free medium to monitor repair ability. The data here supported our hypothesis, and therefore emphasized the important roles of HDAC2 in cellular DDR, especially during DSB indicated by H2AX foci induced by cisplatin, by participating in the DDR pathways, but also suggested a possible different manner between sensitive and resistant cells in DDR.

3.3.2.6 Cell fate determination by HDAC2 knockdown during cisplatin treatment

As shown in section 3.2, the pan-HDAC inhibitor for class I and II mammalian HDACs, TSA, showed suppressive effects on cell number in both PEO1 and PEO4 cells, and also further inhibited cell number when combined with cisplatin treatment. Since HDAC2 appeared to be involved in cisplatin-induced cellular DNA damage response events, we further explored the effect of specific HDAC2 knockdown on cell fate by measuring cell growth number, cell cycle distribution, and apoptosis.

3.3.2.6.1 Cell morphology study after cisplatin treatment in PEO1 and PEO4 cells with HDAC2 knockdown

Firstly, the morphology of the cell lines with HDAC2 depletion was observed after 5 days treatment with cisplatin. As is shown in Figure 3.3-12, PEO1 (A) and PEO4 (B) cells were settled as a monolayer, and the cell number obviously decreased in the HDAC2 knockdown only group compared with control groups, which has been already indicated when we studied the effect of HDAC2 depletion on cell morphology in PEO1 cells (Figure 3.3-5). Here we also observed a similar phenomenon in PEO4 cells, and cell number was even significantly reduced with cisplatin treatment in HDAC2 knockdown groups compared with siHDAC2, cisplatin treated, or control groups in both cell lines. The floating cells also indicated possible cell death induced by cisplatin and HDAC2 knockdown. The cell growth inhibited by HDAC2 in both cisplatin sensitive and resistant cells suggested the possible role of HDAC2 to affect the cell's susceptibility to DNA damage-based therapy, such as cisplatin.

A.

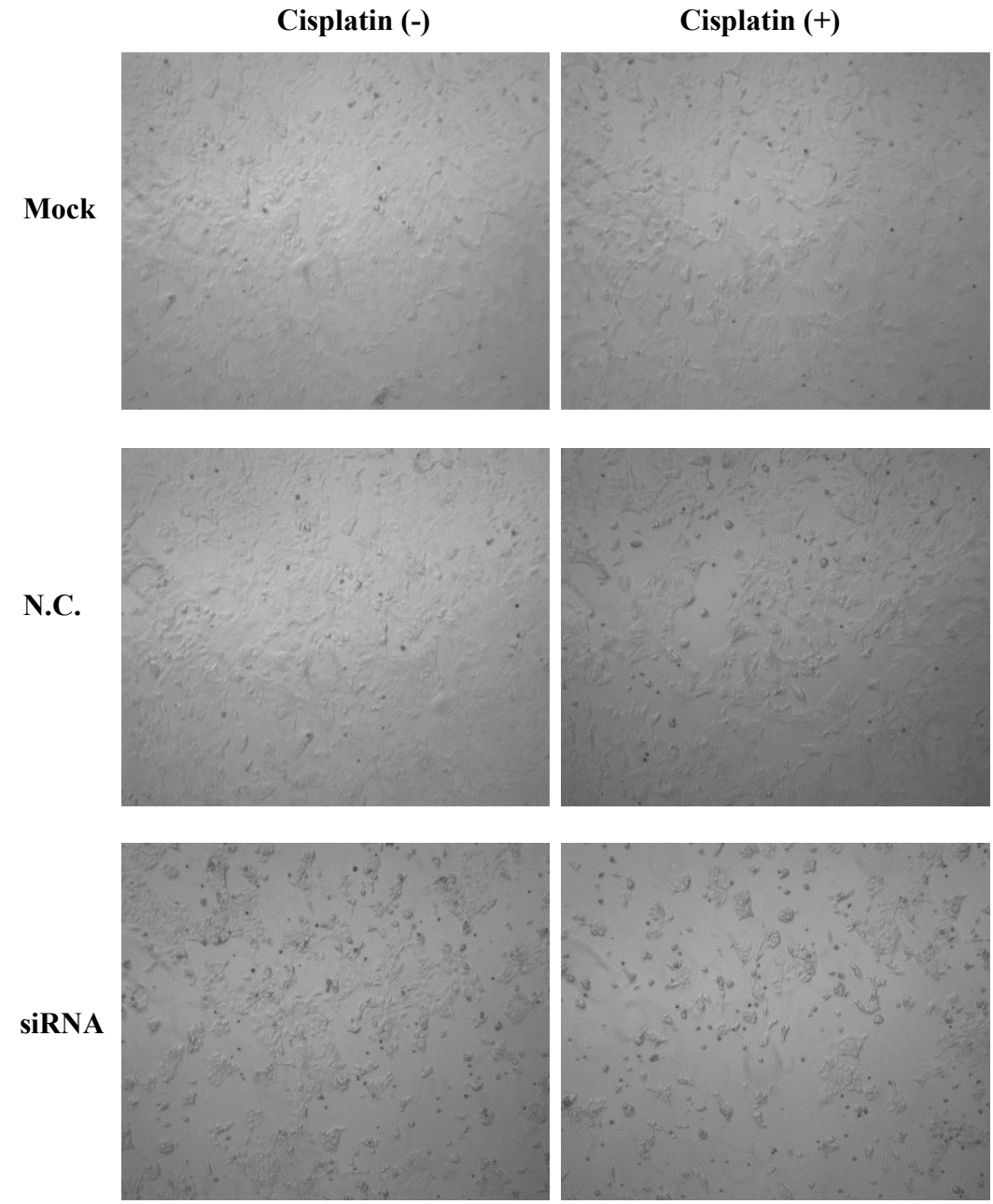

(Continued)

B.

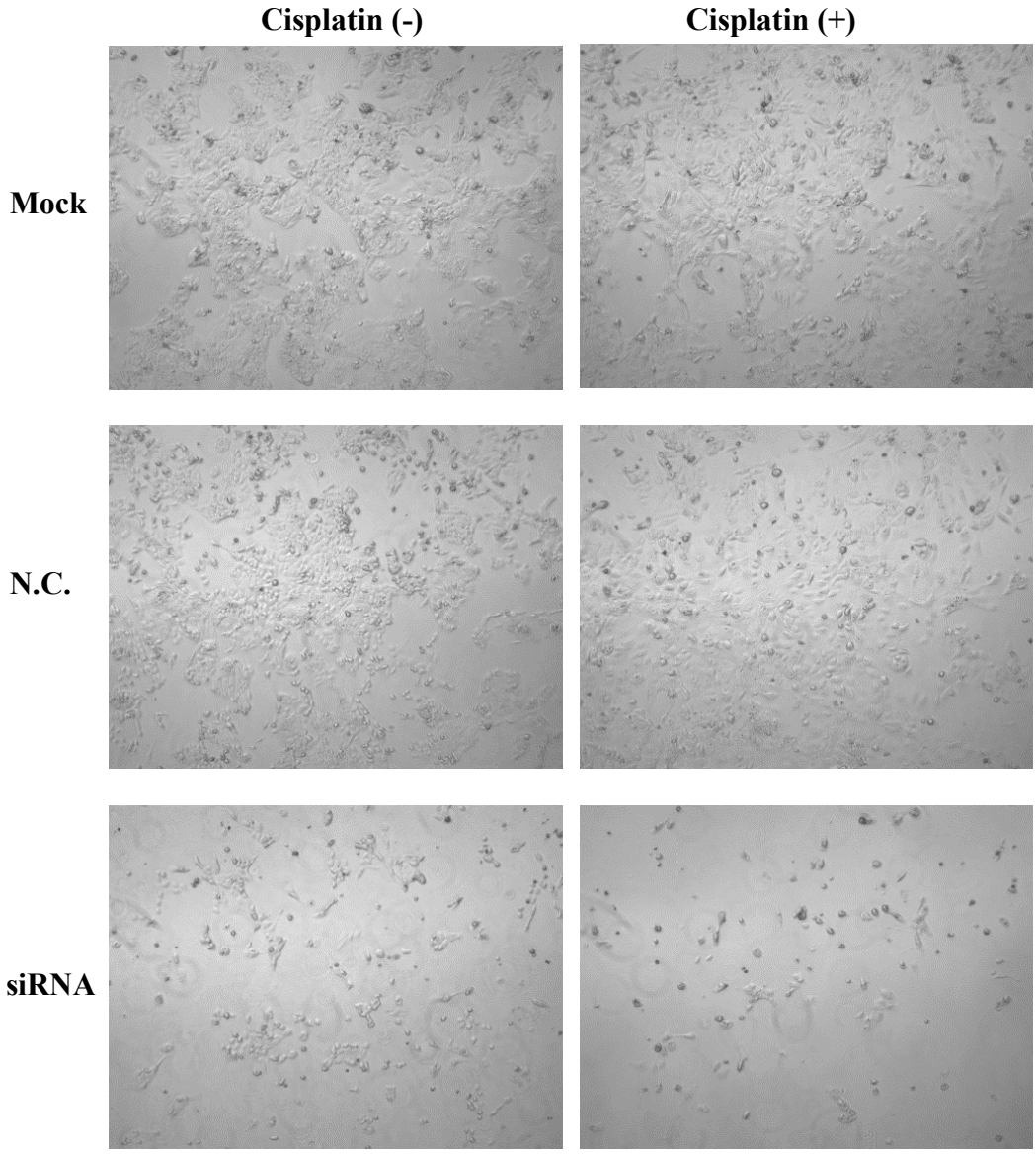

Figure 3.3-12 The effect of HDAC2 knockdown on cellular morphology of PEO1 (A) and PEO4 (B) cells after cisplatin treatment. PEO1 (A) and PEO4 (B) cells were grown on dishes and reverse transfected with HDAC2 siRNA for 72h, followed by treatment with cisplatin (6μM) for 5 days. Images were taken by light microscope, and mock and negative control siRNA were applied as controls.

3.3.2.6.2 Effect of HDAC2 knockdown on cell growth during cisplatin treatment

To quantitatively assess the inhibitory effect of HDAC2 knockdown during cisplatin treatment on cell growth, the SRB assay was utilized to measure the cell number in each group. After being transfected with HDAC2 siRNA, cells were treated with 7 concentrations of cisplatin by a titration from 0.1μM to 15μM. The SRB assay was performed on day 5 to detect the remaining cell number after treatment.

The concentration-survival curve in Figure 3.3-13 shows that cisplatin treatment (blue line) caused cell growth inhibition in a dose-dependent manner in both the control group and the HDAC2 knockdown group in both PEO1 (Figure 3.3-13A) and PEO4 (Figure3.3-13B) cells. Here the curves with or without HDAC2 depletion show similar pattern in both cell lines, which implies that the inhibitory effect from HDAC2 knockdown is be likely additive.

A.

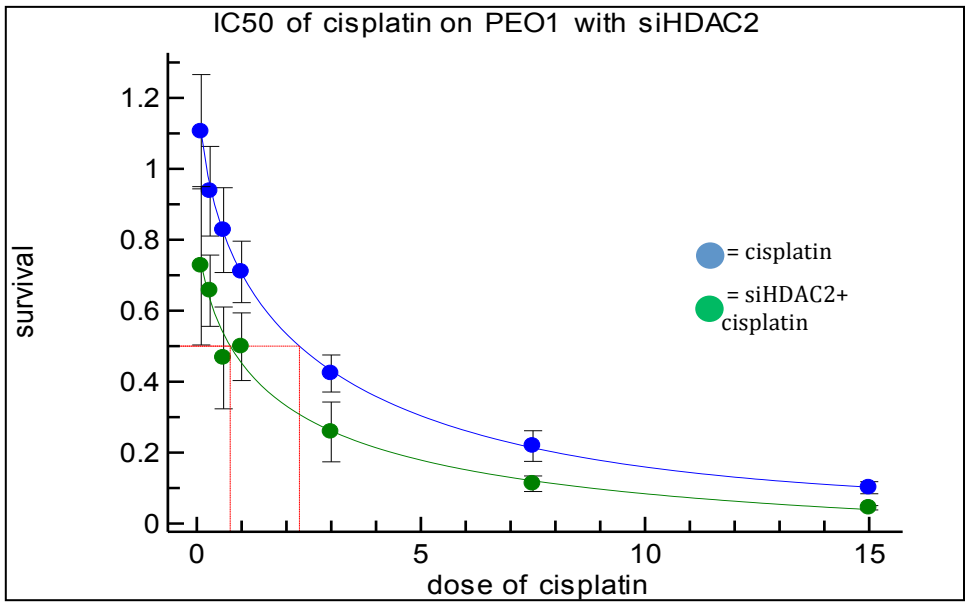

B.

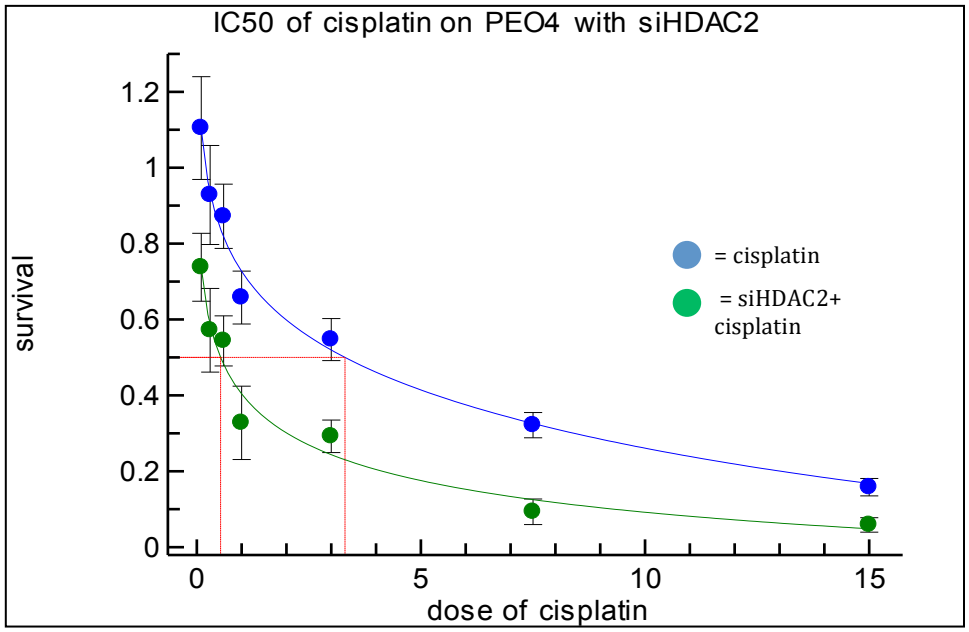

Figure 3.3-13 sulforhodamine B assay profile for inhibitory 50% concentration (IC_{50}) of cisplatin on PEO1 (A) and PEO4 (B) cells with (green line) and without (blue line) HDAC2 knockdown.

	PEO1	PEO4
siRNA-	2.29	3.31
siRNA+	0.75	0.53
Inhibitory ratio (%)	67.4	83.9

Table 3-5 Summary data for cisplatin inhibitory ratio of PEO1 and PEO4. Data are from the SRB assay above, and sensitization ratios were calculated by comparing IC_{50} in cells with siRNA to that without siRNA.

The concentration that caused an inhibition of cell growth in 50% of the treated cells (IC_{50}) was calculated for each group as listed in Table 3.3-1. Growth of both cell lines was further inhibited by cisplatin after HDAC2 knockdown, with extra 67.4% inhibitory ratio in PEO1 cells and 83.9% in PEO4 cells, and this data suggests an additive effect of growth inhibition between HDAC2 depletion and cisplatin.

3.3.2.6.3 Alteration of cell cycle progression during cisplatin treatment with HDAC2 knockdown

The cell cycle alterations triggered by cisplatin have been intensively investigated, and several studies have identified cellular S or G2 phase arrest after cisplatin treatment (Sorenson, Barry et al. 1990; Lee, Brown et al. 1999). Moreover, a large number of proteins in cellular DDR are essential for cell cycle arrest after DNA damage-based therapies, such as ATM, ATR, and BRCA1 (Deng 2006; Santra, Wajapeyee et al. 2009). Following the inhibitory effects of HDAC2 knockdown on cell growth, it raised the question as to the mechanism during this suppression. One explanation for this might be that knockdown of HDAC2 was involved in the cell cycle progression induced by cisplatin. Therefore I examined the cell cycle distribution change in both PEO1 and PEO4 cells with HDAC2 depletion during cisplatin treatment.

Cells were transfected with HDAC2-targeted siRNA, followed by treatment with cisplatin. Cell cycle distribution analysis was performed after 72h, and multiple control groups were included as before (untransfected, mock, and negative control siRNA). Figure 3.3-14 showed the cell cycle distribution for G0/1, S, and G2/M for each group in PEO1 (A) and PEO4 (B) cells. Not surprisingly, cisplatin treatment induced significant S phase arrest in both PEO1 (+160%, $P<0.001$) and PEO4 cells (+180%, $P<0.001$) compared to control groups, and decreased cell number in G1 phase (-30% and -40%, in PEO1 and PEO4 respectively, $P<0.05$). Knockdown of HDAC2 only altered the cell cycle distribution in PEO1 cells by increasing the S phase population (+120%, $P<0.05$). As expected, treatment with cisplatin in cells with HDAC2 depletion altered cell cycle distribution in both PEO1 and PEO4 cells

compared with cisplatin treated cells without transfection, but in different manners. Knockdown of HDAC2 further caused S phase arrest induced by cisplatin in PEO1 cell (+120%, $P<0.05$), and additional reduction of G1 phase (-20%, $P<0.001$). In contrast, depletion of HDAC2 seemed to reverse the cell cycle arrest caused by cisplatin by reducing S phase accumulation (-20%, $P<0.001$) and increasing G1 phase population (+140%, $P<0.05$) based on the measurement for cisplatin treated cells without transfection.

A.

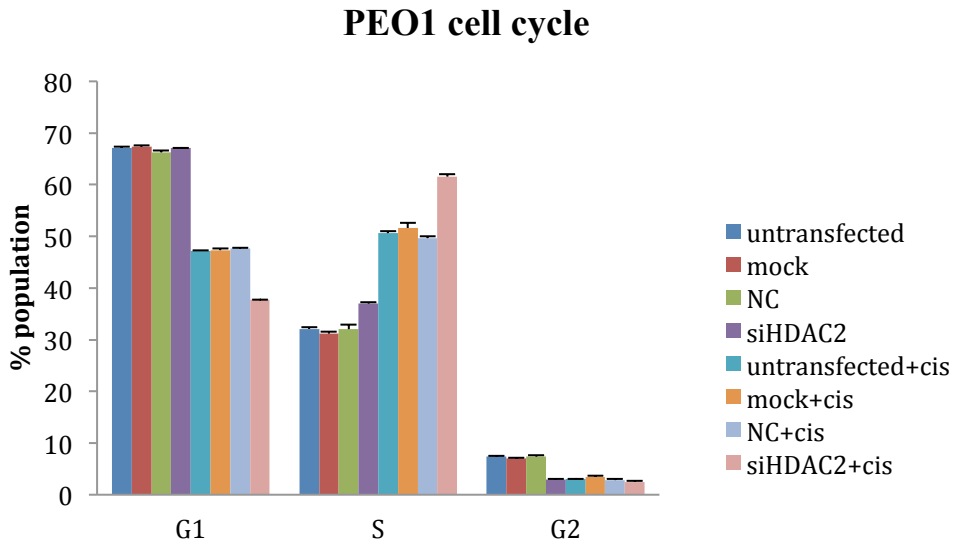

B.

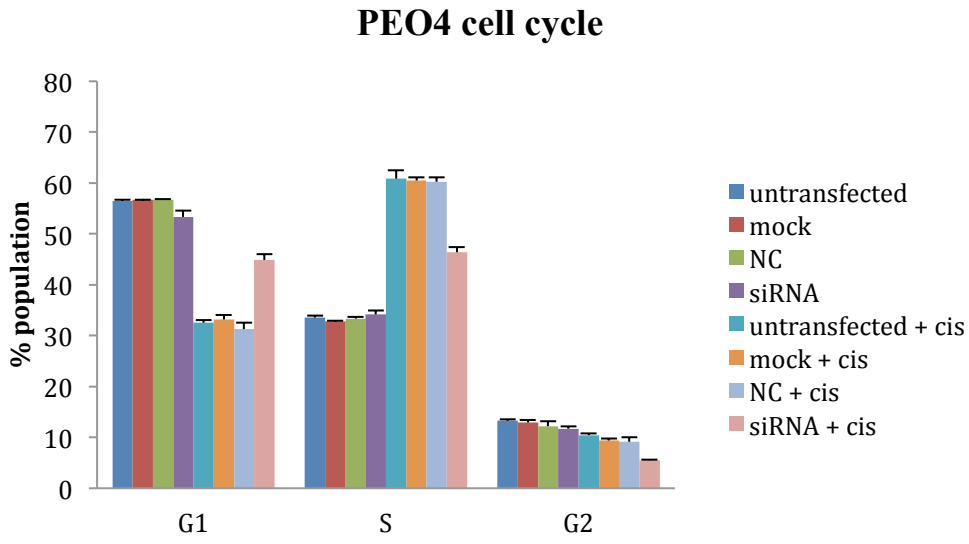

Figure 3.3-14 The effect of HDAC2 knockdown on cell cycle distribution of PEO1 (A) and PEO4 (B) cells. Cells were reverse transfected with HDAC2 siRNA, followed by treatment with cisplatin for 72 hours. Three controls were included as described before. Cell number percentages of the populations selected in G0/1, S, G2/M phases of the cell cycle were detected by flow cytometry. Columns represent the mean percentage of triplicate independent samples. Error bars represent SD. Brown-Forsythe test followed by Games-Howell pot HOC test were performed to compare groups for each phase (Table S5 for full analysis data).

These cell-cycle parameter alterations strongly suggest involvement of HDAC2 in the cellular response to cisplatin in terms of cell cycle distribution. Additionally, the cumulative effect in PEO1 cells and restorative effect in PEO4 cells indicated HDAC2 might function through different pathways to participate in the cellular response to cisplatin treatment, which is parallel with the above findings about the distinctive cellular effects of HDAC2 on PEO1 and PEO4 cells and also imply that there is a possible association with platinum sensitivity in ovarian cancers.

3.3.2.6.4 Cellular apoptosis induction by HDAC2 knockdown during cisplatin treatment

To further detect the cellular effects of HDAC2 knockdown during cisplatin treatment, I investigated the apoptotic events in PEO1 and PEO4 cells. Cell were grown and treated using the same procedure as above, and apoptotic cell numbers with positive annexin V staining were calculated by flow cytometry after 72h treatment of cisplatin. Because of its property to bind to the translocated membrane phospholipid phosphatidylserine (Hirning, Zuna et al.) during the initial process of apoptosis, the annexin V assay can identify apoptosis at earlier stage, and the cells undergoing late apoptosis can be detected by both Aneexin V and propidium iodide (PI) positivity, which only occurs in dead and membrane damaged cells.

Firgure 3.3-15 showed the apoptosis analysis in PEO1 (A) and PEO4 (B) cells after cisplatin treatment in cells with or without HDAC2 knockdown. Only Cisplatin induced early apoptosis in PEO1 cells ($P<0.001$), but not late apoptosis in PEO1 cells or PEO4 cells. This was consistent with the resistance of the PEO4 cell line to cisplatin treatment compared with PEO1 cells. Additionally, knockdown of HDAC2 remarkably caused cellular apoptosis in both early and late stage in PEO1 cells and only an early apoptosis event in PEO4 cells, compared with controls and cisplatin only groups ($P<0.001$). Furthermore, HDAC2 depletion induced significant accumulation of apoptotic cells after cisplatin treatment in both cell lines, especially at the early stage ($P<0.001$).

A.

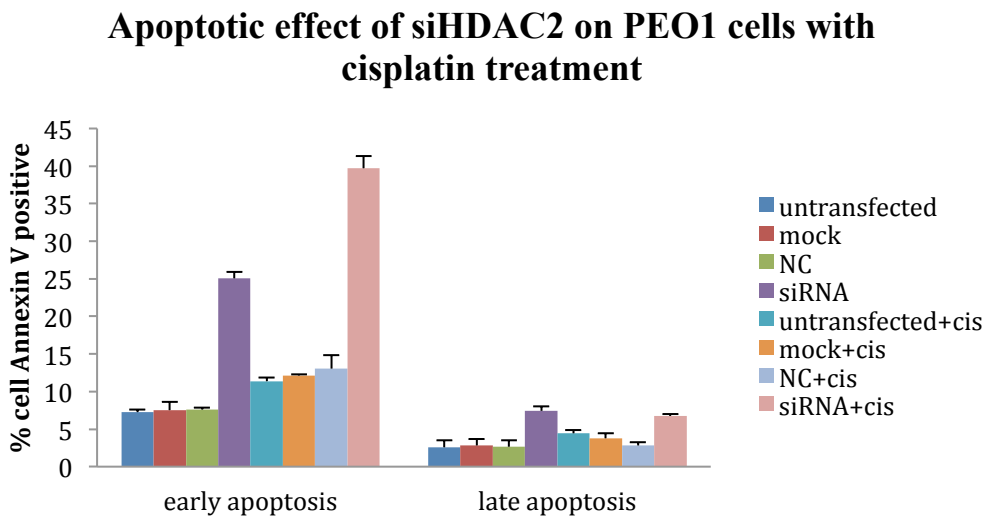

B.

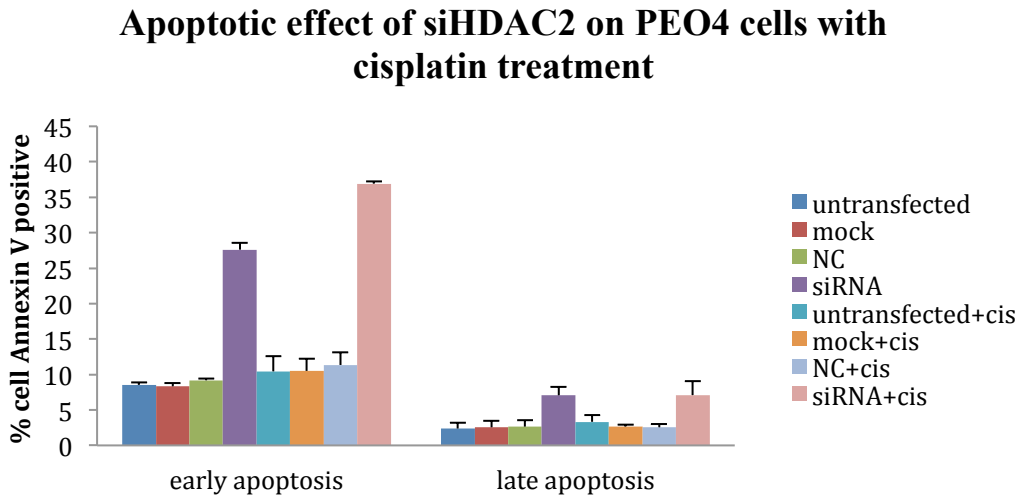

Figure 3.3-15 The effect of HDAC2 knockdown on apoptosis in PEO1 (A) and PEO4 (B) cells using the Annexin V assay. Cells were reverse transfected with HDAC2 siRNA, followed by treatment with cisplatin for 72 hours. Three controls were included as described before. Cell number percentages of the population selected with positive Annexin V staining were detected by flow cytometry after cisplatin treatment for 72h, and data are separated into early and late apoptosis based on Propidium Iodide (PI) signal. Columns represent the mean percentage of triplicate independent samples. Error bars represent SD. One-way ANOVA analysis was performed to compare data among groups, and the Tukey HSD pot HOC test was used to compare groups (Table S6 for full analysis data).

By knocking down HDAC2, I observed a greater apoptotic cell population with cisplatin treatment in both PEO1 and PEO4 cells, suggesting the cell growth inhibition from HDAC2 depletion during cisplatin treatment might be generated by apoptosis induction, and the detailed minor differences in PEO1 and PEO4 also indicated diverse roles HDAC2 might play in cells in terms of platinum sensitivity.

3.4 Reversibility of HDAC inhibition on nuclear morphological changes during cisplatin treatment

The results above demonstrate the involvement of HDAC2 during cellular DDR induced by cisplatin, and also demonstrate the nuclear morphological changes during DNA damage-based therapies in ovarian cancer cell lines. To test if this nuclear structure change was causally mediated by HDAC, or specifically HDAC2, we investigated the reversibility of nuclear morphology by applying either HDAC inhibitor or HDAC2 siRNA in PEO1 cells.

We initially examined the nuclear structure in PEO1 cells after treatment with HDAC inhibitor TSA. Similar to the method we used before, nuclear texture was measured in ImageJ after cells were treated with TSA for 24h. As expected, the five texture parameters were altered after TSA treatment: angular second moment, correlation, and inverse difference moment were elevated, while entropy and contrast were decreased after HDAC inhibition (Figure 3.4-1). By relating those parameters with certain chromatin patterns as described previously, we identified decreased heterogeneity and contrast of chromatin structure, and increased homogeneity (see below summary in Table 3.4-1) after treating cells with TSA. This is consistent with the current knowledge about the roles of HDAC in forming tight chromatin structure, and suggested that this condensed construction is reversible by using an HDAC inhibitor.

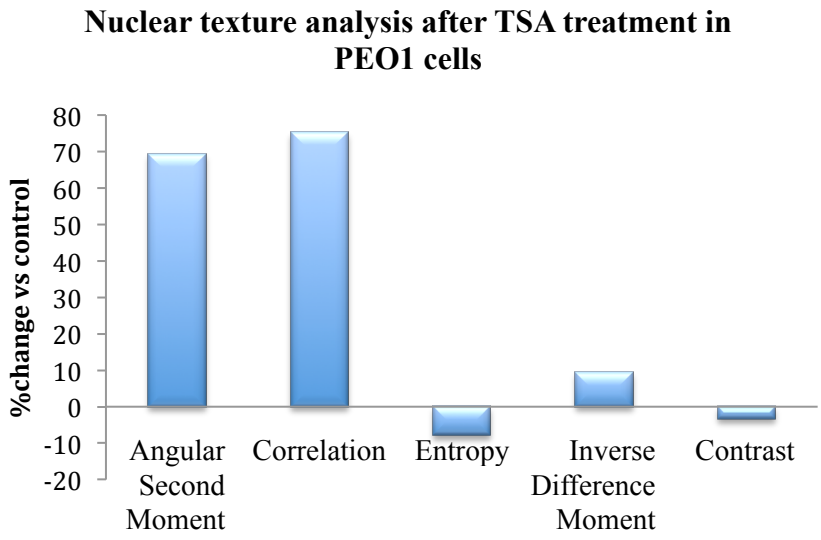

Figure 3.4-1 Changes of nuclear texture features in PEO1 cells after TSA treatment. PEO1 cells were grown on coverslips and treated with TSA (250nM) for 24h, and nuclei were stained with DAPI for visualisation using a fluorescence microscope. At least 100 nuclei were included in one experiment. Nuclear texture was analysed by measuring five texture parameters (angular second moment, correlation, entropy, inverse different moment, and contrast) in ImageJ software. Data are presented as the average change (%) in TSA treated group for each parameter over control group.

To further explore the reversibility of nuclear morphology, we applied the specific HDAC2 siRNA to evaluate the changes of chromatin pattern during cisplatin treatment (Figure 3.4-2), since HDAC2 showed potential in the response to cisplatin in our study. Cisplatin treatment here consistently altered those parameters, which caused similar effects on nuclear texture with the results shown earlier with enhanced heterogeneity and reduced homogeneity. When comparing the outcome between the HDAC2 knockdown group and cisplatin treated group, we noticed the completely opposite direction in the parameter changes caused by the two treatments, indicating the ability of specific HDAC2 silencing in altering chromatin patterns (Table 3.4-1). This suggests HDAC2 is involved in mediating certain chromatin structures.

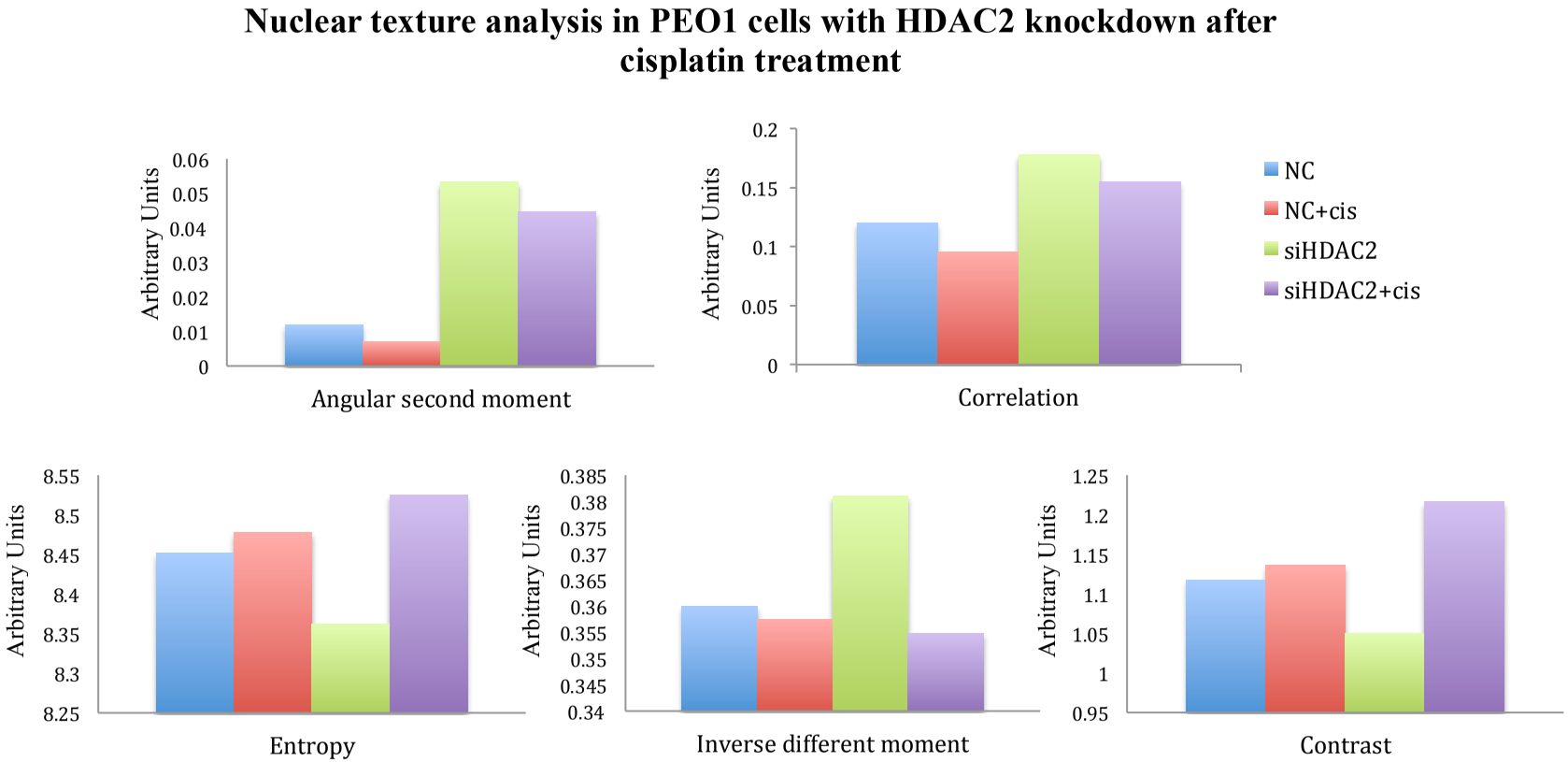

Figure 3.4-2 Changes of nuclear texture features in PEO1 cells transfected with the HDAC2 siRNA after cisplatin treatment. PEO1 cells were grown on coverslips, transfected with HDAC2 siRNA for 72h, and treated with cisplatin (6μM) for a further 24h. Nuclei were stained with DAPI for visualisation using fluorescence microscopy. At least 100 nuclei were included in each group in one experiment. Nuclear texture was analysed by measuring five texture parameters (angular second moment, correlation, entropy, inverse different moment, and contrast) using ImageJ.

The nuclear texture changes caused by both cisplatin and siHDAC2 resulted in a complicated set of changes. Changes of two parameters (angular second moment and correlation) induced by cisplatin were reversed by HDAC2 knockdown. On the other hand, alterations of the other parameters (entropy, inverse difference moment, and contrast) in cells treated with both cisplatin and siHDAC2 were enhanced from the levels changed by cisplatin.

		Heterogeneity of chromatin patterns	Homogeneity of chromatin patterns	Contrast of chromatin patterns
		Correlation (-)	Angular second moment (+) Entropy (-)	Inverse difference moment (-) Contrast (+)
1	**TSA**	↓	↑	↓
2	**siHDAC2**	↓	↑	↓
3	**cisplatin**	↑	↓	↑
4	**siHDAC2+cis**	↓	–	↑

Table 3-6 Summary of nuclear texture analysis.

To summarize the result of nuclear texture analysis, we demonstrated nuclear morphological changes induced by DNA damage-based therapies, including cisplatin, in terms of homogeneity and heterogeneity. We also identified that suppression of HDAC, especially HDAC2, could alter the nuclear structure, indicating the roles of HDAC participating in mediating certain chromatin conformations. HDAC2 silencing reversed the nuclear texture alteration caused by cisplatin to some degree, but not completely. There are several considerations for this: firstly, the desired

reversibility might occur quite early, since we suppose HDAC2 is an early mediator of DNA damage response which occurs only minutes after cellular response (Trainor, Butterworth et al. 2012); furthermore, the compensatory effect of HDAC1 from HDAC2 depletion might also interfere with the nuclear structure and cause a comprehensive consequence; additionally, the balance between HDAC and other chromatin structure regulators might be interrupted by HDAC2 knockdown, which may lead to possible negative feedback to affect chromatin patterns.

3.5 Profiling expression of HDAC and HP1 proteins in the ovarian cancer xenograft model

To investigate in detail the mechanisms mediating response in ovarian cancer, two human ovarian cancer xenograft models were established in our lab, OV1002 and HOX424. Female adult CD-1 nude mice housed in IVCs (individually ventilated cages) were treated with carboplatin (50 mg/kg i.p.) on day 0, and tumour samples were collected on day 0, 1, 4, 7, and 14 after treatment. The OV1002 model showed much more sensitivity to carboplatin treatment compared to the HOX424 model.

All xenograft tumour samples were spotted on TMA slides and expression of HDAC members (HDAC1, 2, 3, 4, and 8) and HP1 isoforms (HP1α, HP1β, and HP1γ) were detected by immunofluorescence as described in the Materials and Methods. The results of IF were scored and analysed by automated quantitative analysis (AQUA) system. After the image of each TMA slides was acquired, the normalized immunofluorescence intensities (AQUA scores) of targets were obtained from triplicate cores of each sample.

Interestingly, HDAC2, HDAC8 and all three HP1 proteins showed statistically significantly increased expression in the sensitive model (OV1002) after carboplatin treatment, and the most significant changes ($p<0.05$) were observed on day 7 (Figure 3.5-1). Expression of these proteins remained similar between control and treated groups in the HOX424 model on the same day after treatment.

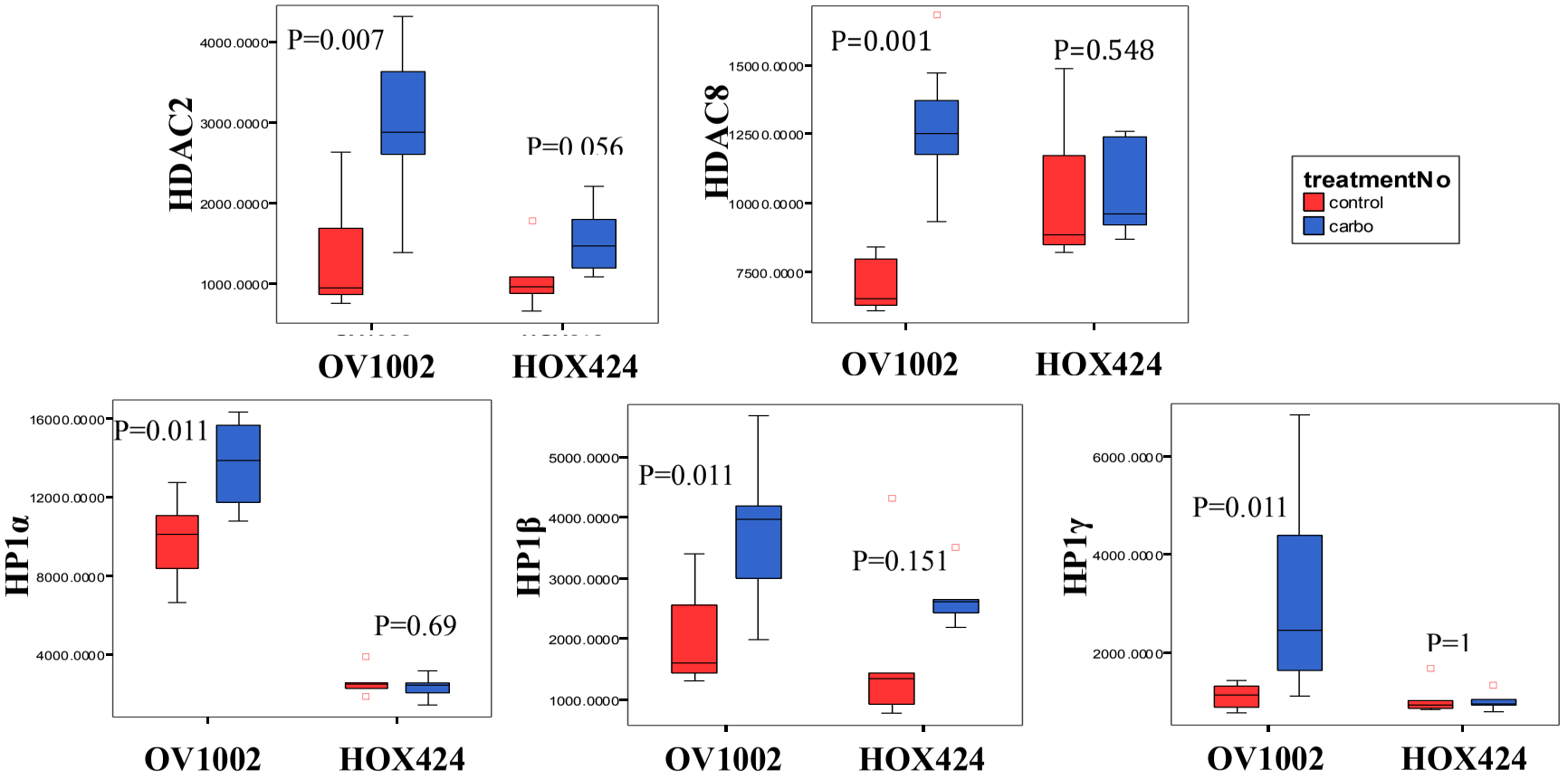

Figure 3.5-1 Expression of HDAC2, HDAC8, HP1α, HP1β and HP1γ in ovarian xenograft tumours samples on day 7. The sample TMA was probed with the indicated antibodies and expression levels were quantified by AQUA analysis. Boxplots depict AQUA scores representing the expression of proteins. The edges of the box are the upper and lower quartiles, and the band inside the box is the median value. Ends of the whiskers indicated the maximum and minimum data. Data was compared between control group (red bar) and carboplatin-treated group (blue bar) within the platinum sensitive model (OV1002) and resistant model (HOX424), respectively. Man-Whitney analysis was performed and P values were indicated.

Representative immunofluorescence images for expression of these HDAC and HP1 proteins in the xenograft model OV1002 are also shown in Figure 3.5-2. The proteins were located in the nuclear compartment, and were obviously highly expressed in tumours after chemotherapy compared with the expression in control group (red channel in Figure 3.5-2).

A. HDAC2

Control:

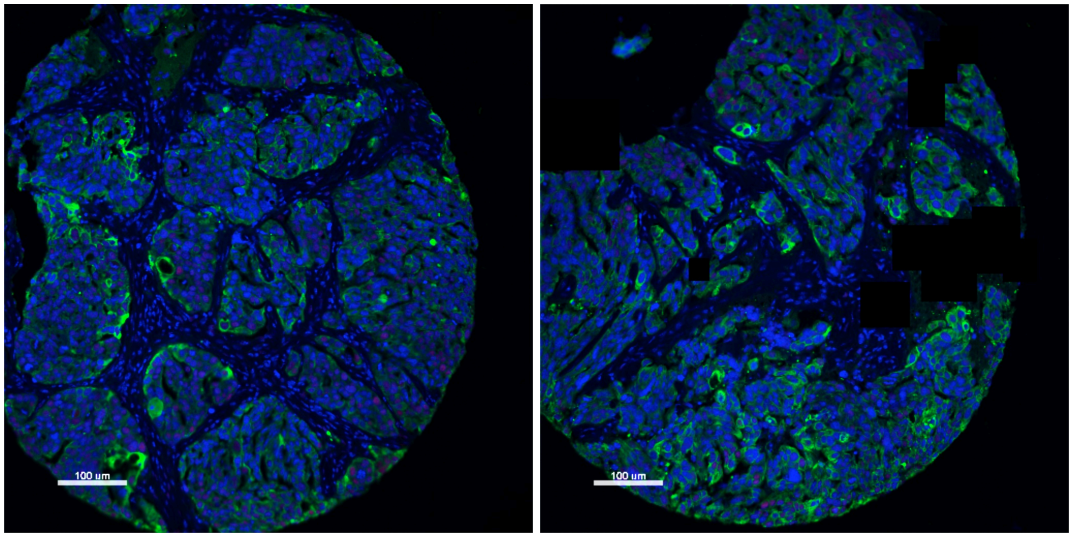

Carboplatin:

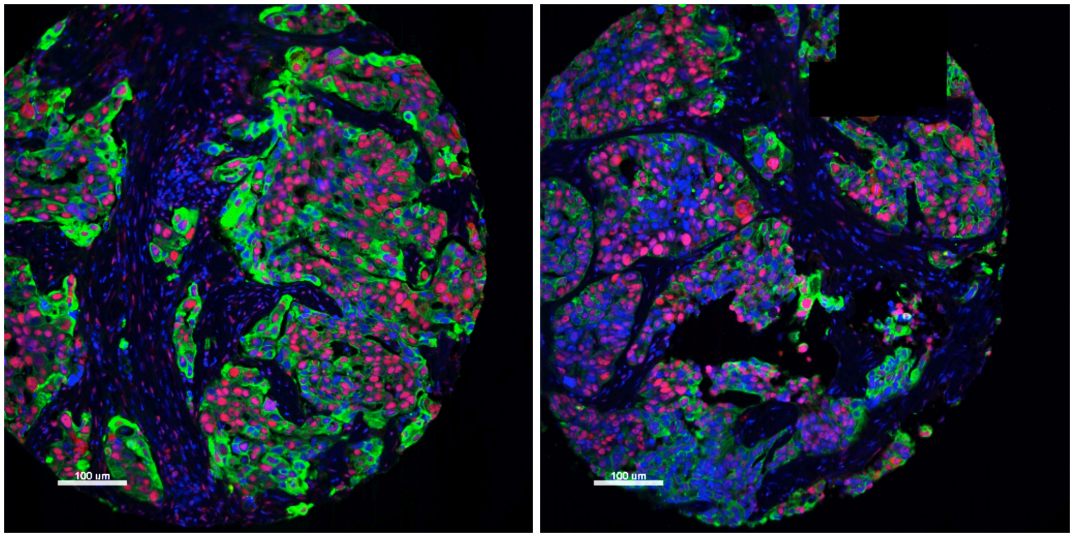

(Continued)

B. HDAC8

Control:

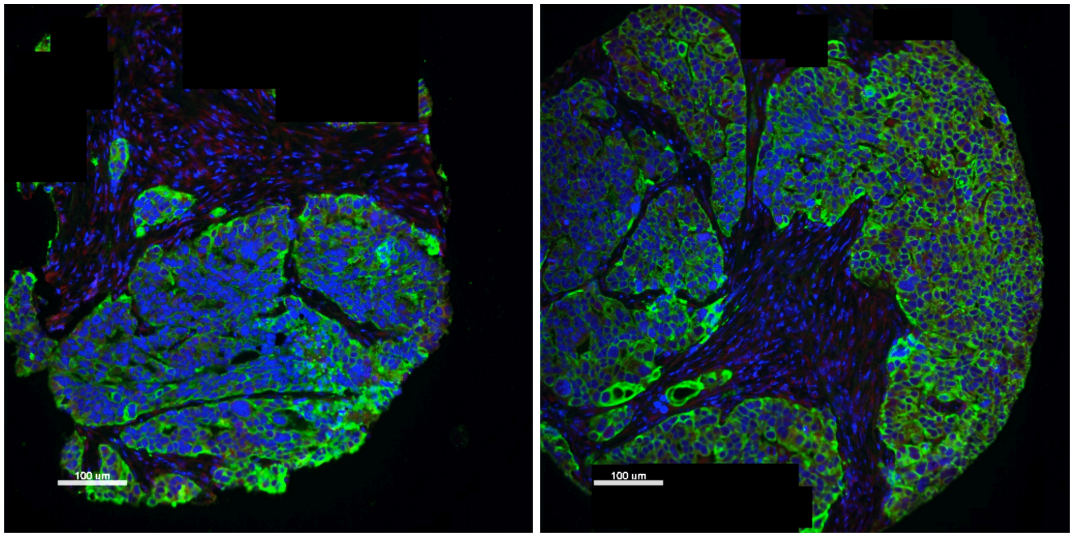

Carboplatin:

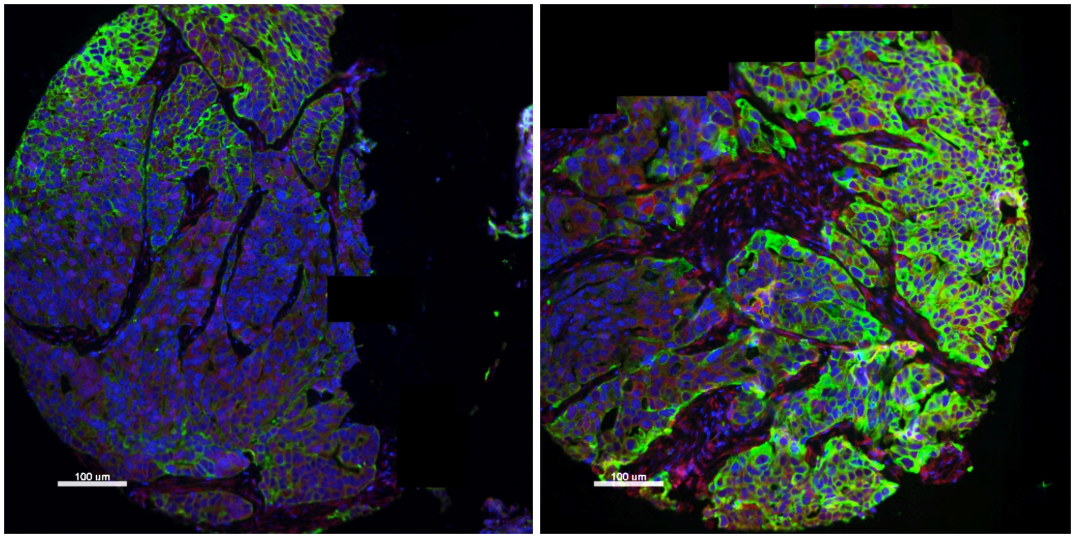

(Continued)

C. HP1α

Control:

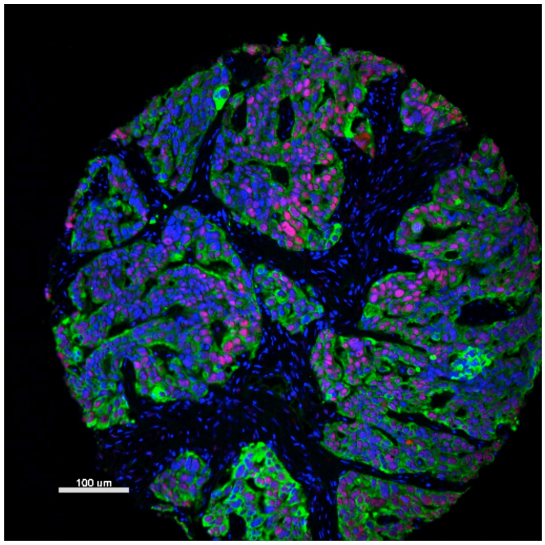

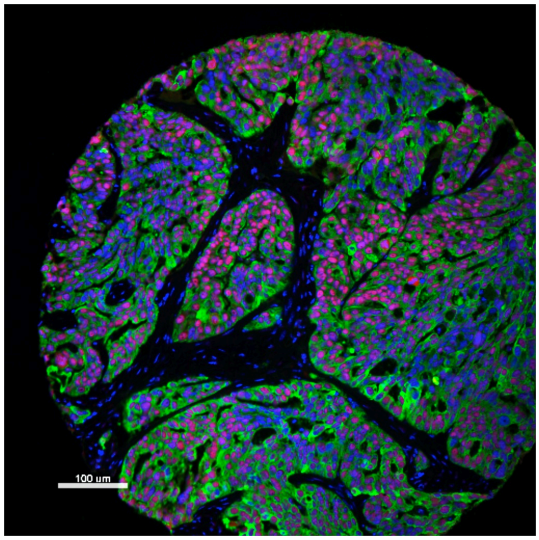

Carboplatin:

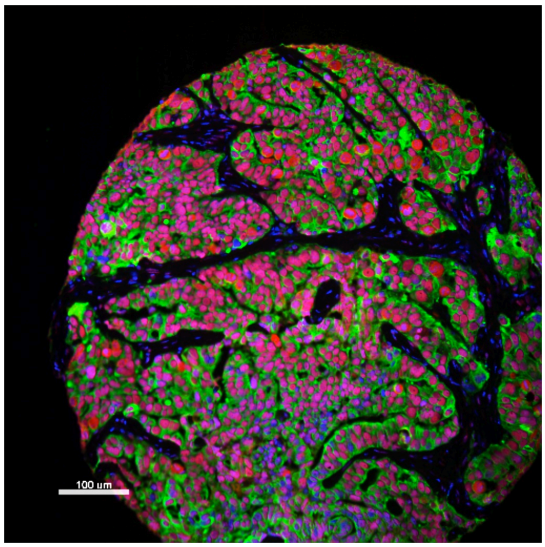

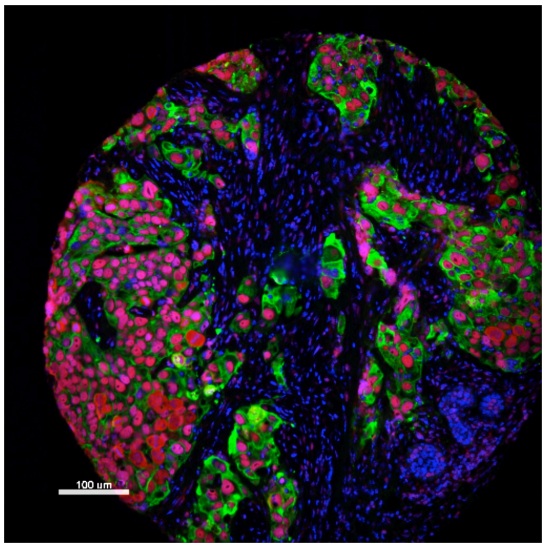

(Continued)

D. HP1β

Control:

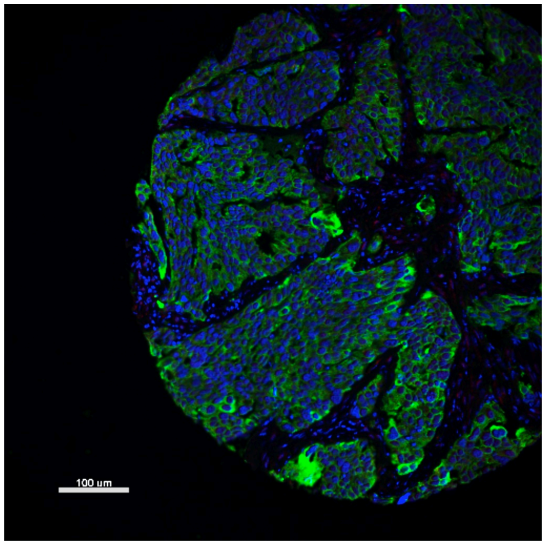

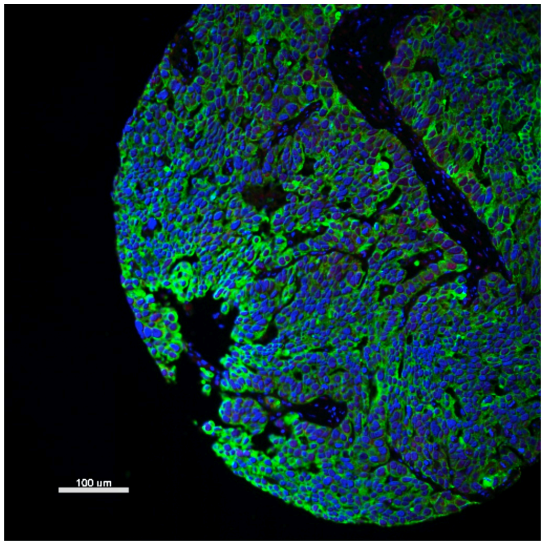

Carboplatin:

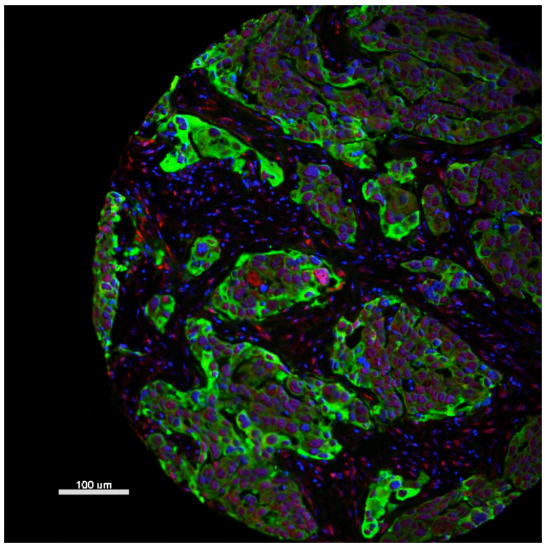

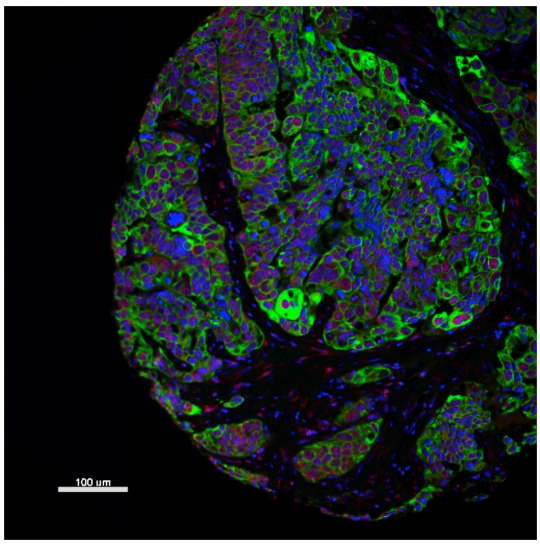

(Continued)

E. HP1γ

Control:

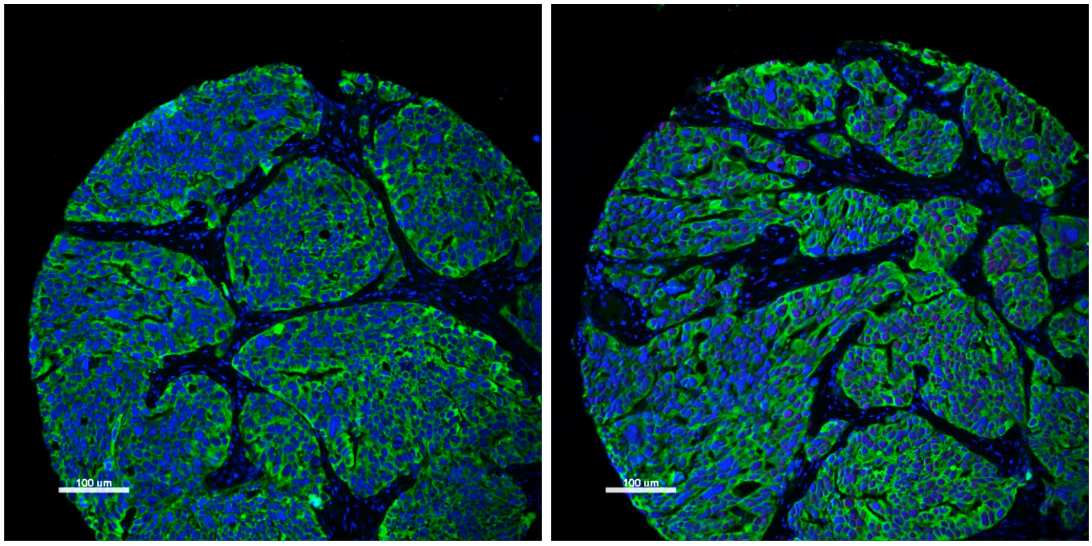

Carboplatin:

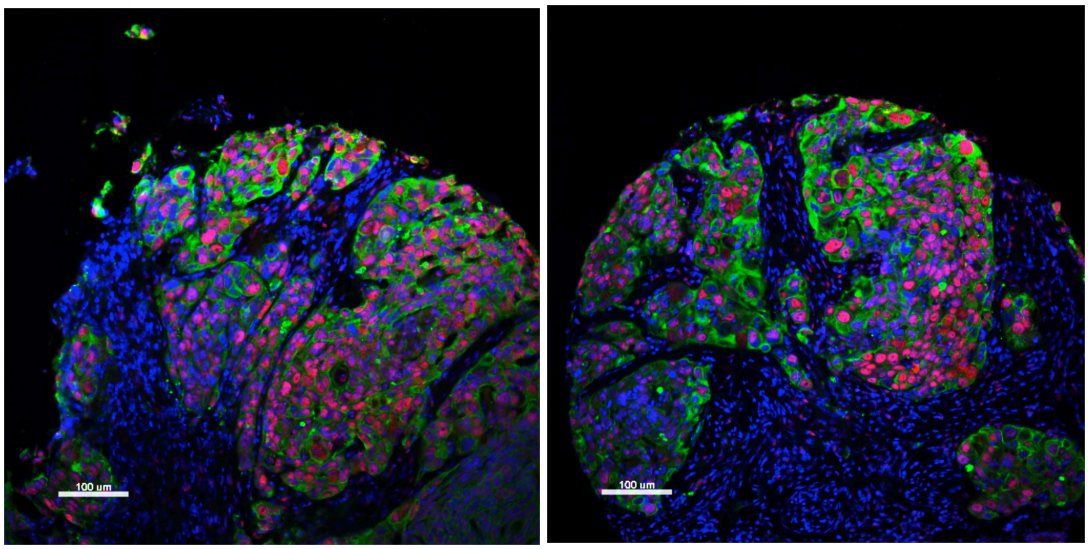

Figure 3.5-2 Representative images for detection of HDAC members and HP1 isoforms in ovarian tumour xenografts in the non-treated group and carboplatin-treated group. Sample TMAs were probed using the indicated primary antibodies and immunofluorescence images were visualised by using AQUAsition software at 20x magnification via DAPI, CY3, and CY5 channels. Blue = DAPI nuclear counterstain, green = cytokeratin tumour mask and red = target protein.

This result showed increased expression of HDAC members (HDAC2 and HDAC8) *in vivo* in response to platinum treatment, as well as enhanced heterogeneity of chromatin indicated by the expression of HP1s, providing strong evidence to support our hypothesis, and suggested that HDACs have a role in mediating chromatin remodelling during DNA damage therapy in ovarian cancer. The result here is much more significant compared to the observations *in vitro* above. One explanation might be that HDACs and HP1s function in a tissue-dependent manner, with specific roles in different tissue or growing environments (human, xenograft, and cell line). Another theory would be the differences during 2D and 3D culture, since this has been suggested in the literature about the interrelation between cell morphology and cellular event based on chromatin organization (Storch, Eke et al.).

3.6 Exploring expression of HDAC members, HP1 isoforms, and chromatin patterns in human ovarian cancer samples

The next stage of our study focused on the investigation in clinical tumour samples of HDAC expression and chromatin patterns. 38 patients, 76-paired samples were included in this final study, and these samples were acquired from patients pre-treatment and post-treatment during chemotherapy, 20 cases of which showed sensitivity to chemotherapy while the other 18 patients were resistant or refractory based on the overall disease response categories (RECIST) in response to first-line chemotherapy (see Table S8 for full sample information).

3.6.1 Differential expression of HDAC and HP1 proteins in clinical ovarian tumours

I explored HDAC1, HDAC2, HDAC3, HDAC4, HDAC8, and three HP1 isoform expression in the ovarian tumour samples. The results of IF were scored and analysed by the automated quantitative analysis (AQUA) system. After the image of each TMA slides was acquired, the normalized immunofluorescence intensities (AQUA scores) of these targets were obtained from triplicate cores of each sample as described in the Materials and Methods.

After analysing the AQUA scores, only HDAC4 ($p=0.026$) and HP1γ ($P=0.04$) showed a significant increase in patients after chemotherapy compared to the expression level before chemotherapy (Figure 3.6-1A and C), with HDAC8 reaching borderline significance ($p=0.05$, Figure 3.6-1B). By separating patients into sensitive and resistant groups, this increased expression seems to be contributed mainly by patients sensitive to chemotherapy; here we didn't observed such differences in HDAC1, HDAC2, HDAC3, HP1α or HP1β expression as in the cell line results

(Figure S1 in supplement), This might be due to the heterogeneity of cancer tissues, differences between cell line model and human samples, or the relatively low sample size employed here.

A. HDAC4

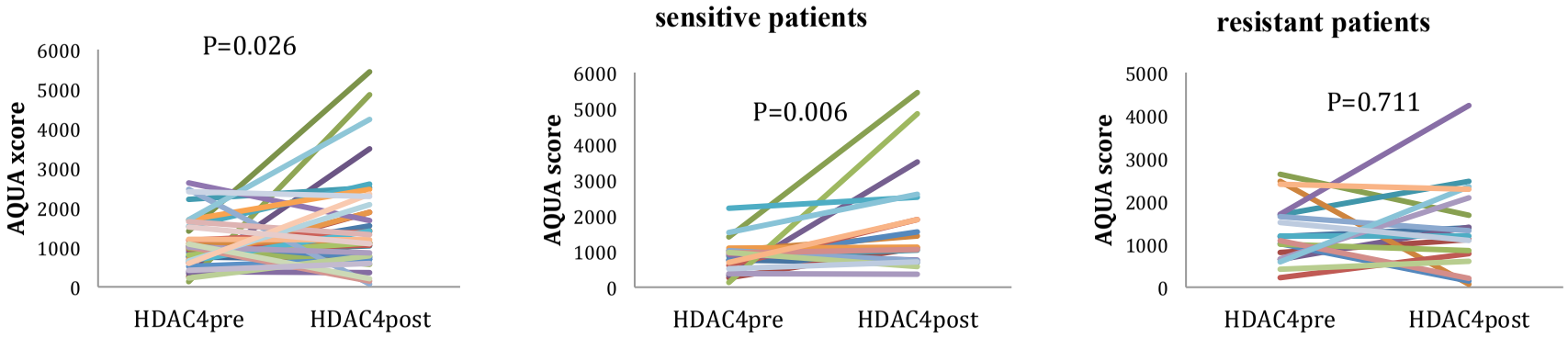

B. HDAC8

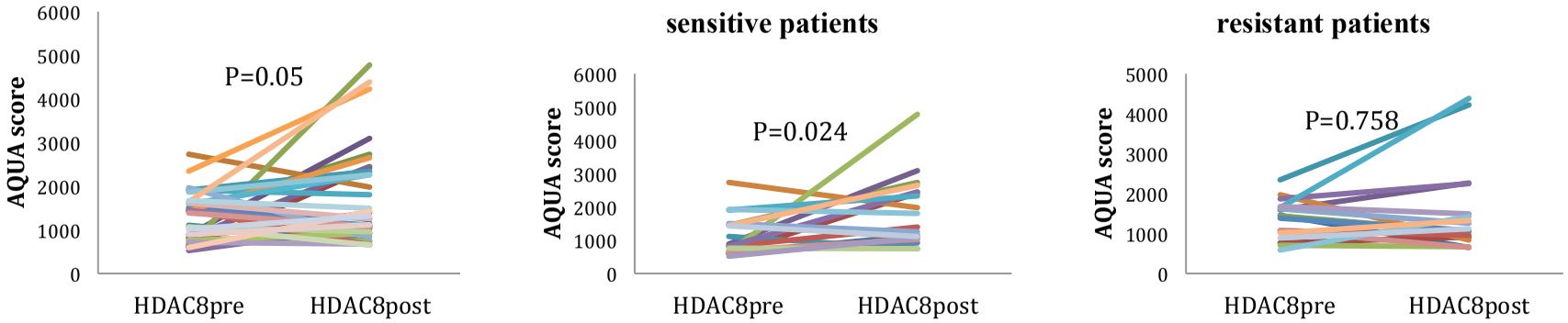

(Continued)

C. HP1γ

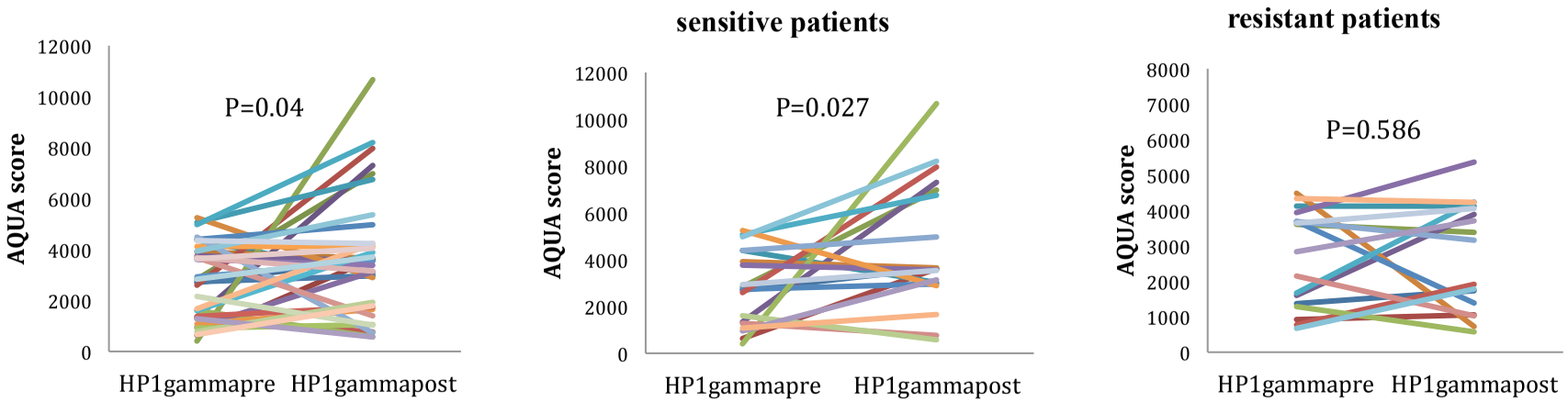

Figure 3.6-1 Variant expression of HDAC members and HP1 isoforms in ovarian cancer tumours from 38 patients before and after chemotherapy. AQUA scores were quantified by the AQUA analysis system and data from proteins with significant differences ($p<0.05$) are illustrated here. Wilcoxon test was performed to compare the matched sample for pre- and post-treatment, and P values are indicated. First panel shows the total data from 38 patients, while the last two panel presents comparison made within sensitive and resistant patients, respectively.

Here we also showed some immunofluorescence images from different patients with significantly enhanced expression of these HDAC and HP1 proteins after chemotherapy in Figure 3.6-2. Remarkably increased expression was observed in some patients, although the enhancement varied between patients. Similar to the results from xenografts, the proteins were located in the nuclear compartment, and were obviously highly expressed in tumours after chemotherapy compared with the expression in control group (red channel in Figure 3.6-2).

A. HDAC4

Pre-treatment

Post-treatment

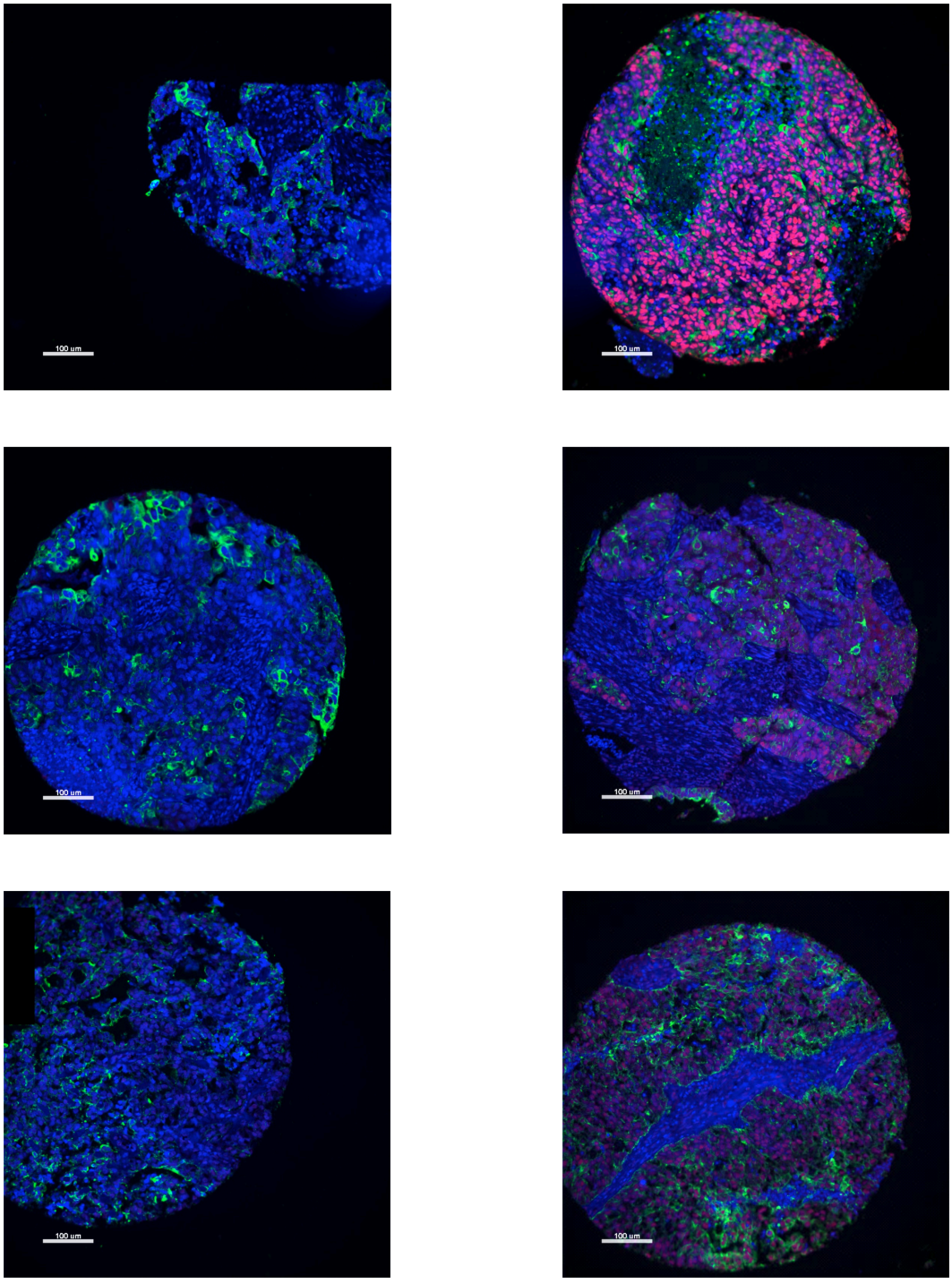

(Contined)

B. HDAC8

Pre-treatment

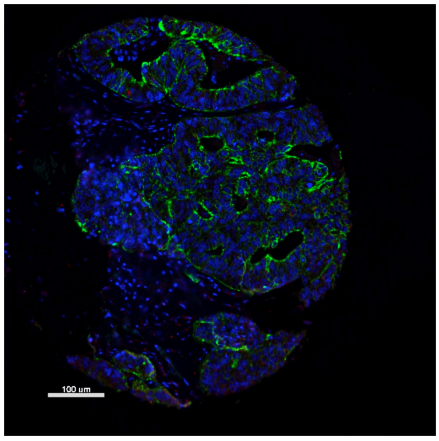

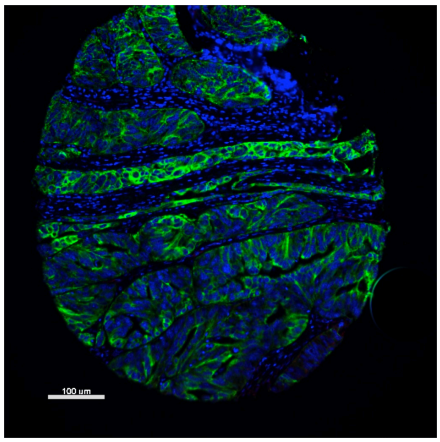

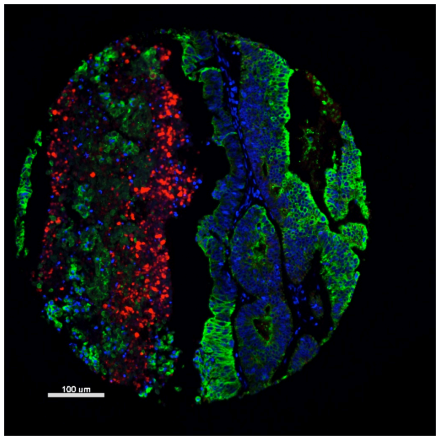

Post-treatment

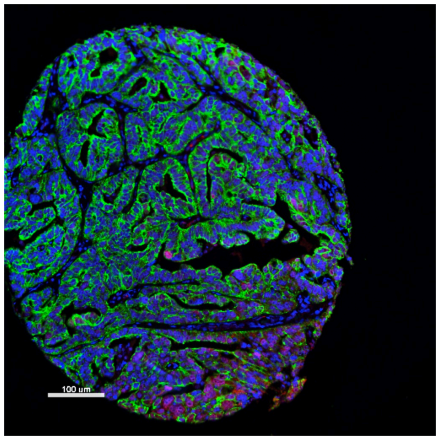

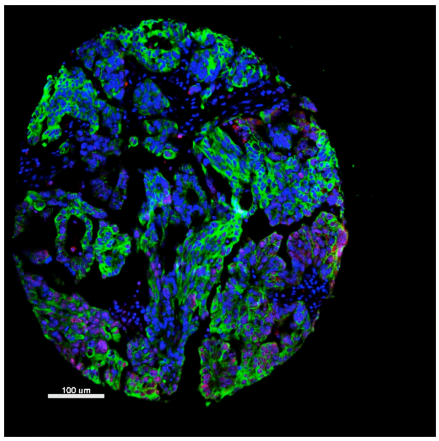

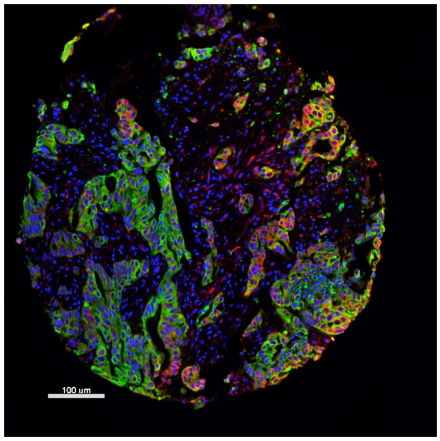

(Continued)

C. HP1γ

Pre-treatment | Post-treatment

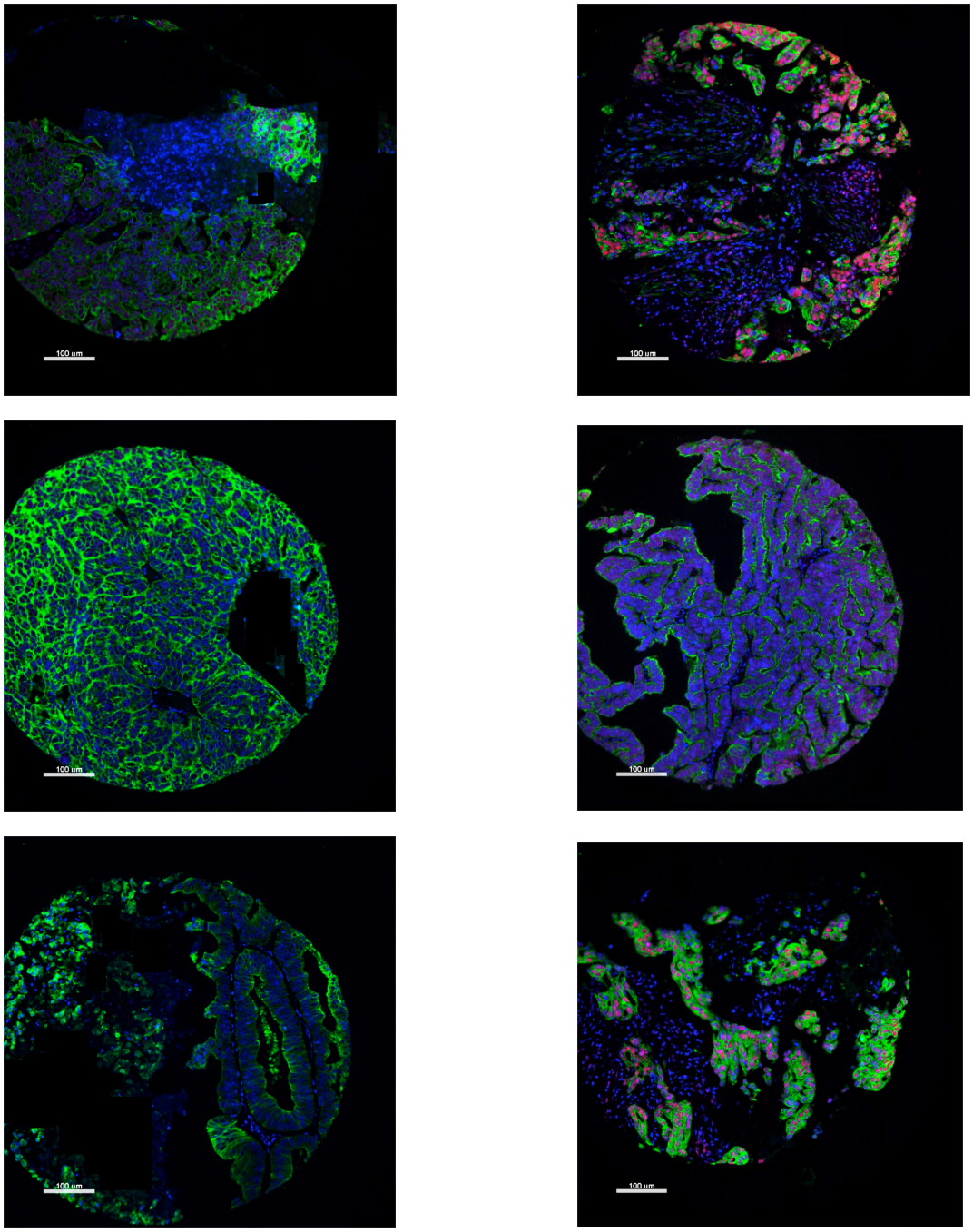

Figure 3.6-2 Selected images for detection of HDAC members and HP1 isoforms in matched clinical ovarian tumours pre- and post-chemotherapy. Sample TMAs were probed using the indicated primary antibodies and immunofluorescence images were visualised by using AQUAsition software at 20x magnification via the DAPI, CY3, and CY5 channels. Blue = DAPI nuclear counterstain, green = cytokeration tumour mask and red = target protein. Images from those proteins with significant change of expression are shown here.

To further investigate the correlation between HP1 and HDAC proteins, Spearman's correlation coefficients were measured for every combination of HDACs and HP1s (Table 3.6-1). In this statistical analysis, HDAC1, HDAC2, HDAC8, and all HP1 proteins showed a correlation with each other ($P<0.05$). Among these compared pairs, HDAC2, HDAC4, HDAC8, and HP1γ showed higher correlation (correlation coefficient>0.5, highlighted in Table3.6-1), indicating the association of HDACs and heterochromatin conformation in some degree.

			HDAC1	HDAC2	HDAC3	HDAC4	HDAC8	HP1α	HP1β	HP1γ
Spearman's rho	HDAC1	Correlation Coefficient		.488**	.327**	.363**	.369**	.351**	.224	.440**
		Sig. (2-tailed)	.	.000	.004	.001	.001	.003	.058	.000
	HDAC2	Correlation Coefficient	.488**		.326**	.554**	.523**	.439**	.464**	.658**
		Sig. (2-tailed)	.000	.	.004	.000	.000	.000	.000	.000
	HDAC3	Correlation Coefficient	.327**	.326**		.061	.045	.065	.155	.116
		Sig. (2-tailed)	.004	.004	.	.602	.706	.587	.192	.328
	HDAC4	Correlation Coefficient	.363**	.554**	.061		.604**	.440**	.462**	.692**
		Sig. (2-tailed)	.001	.000	.602	.	.000	.000	.000	.000
	HDAC8	Correlation Coefficient	.369**	.523**	.045	.604**		.272*	.388**	.665**
		Sig. (2-tailed)	.001	.000	.706	.000	.	.021	.001	.000
	HP1α	Correlation Coefficient	.351**	.439**	.065	.440**	.272*		.629**	.537**
		Sig. (2-tailed)	.003	.000	.587	.000	.021	.	.000	.000
	HP1β	Correlation Coefficient	.224	.464**	.155	.462**	.388**	.629**		.404**
		Sig. (2-tailed)	.058	.000	.192	.000	.001	.000	.	.000
	HP1γ	Correlation Coefficient	.440**	.658**	.116	.692**	.665**	.537**	.404**	
		Sig. (2-tailed)	.000	.000	.328	.000	.000	.000	.000	.

Table 3-7 Spearman's correlation coefficient analysis for HDAC and HP1 expression in paired pre- and post-treatment samples from 38 patients with ovarian cancers treated with chemotherapy. Correlation coefficients and P value (no correlation as null hypothesis) were listed for each pair-wise comparison. Numbers highlighted represents high correlation (>0.5) with p value < 0.05. **Correlation is significant at the 0.01 level (2-tailed). *Correlation is significant at the 0.05 level (2-tailed).

3.6.2 Nuclear texture study in clinical ovarian tumours

To test our hypothesis in clinical tumours, we also evaluated nuclear texture within this group of paired tumours. DAPI staining was performed on TMA slides to visualise nuclei, and parameters representing nuclear texture were analysed using ImageJ as described before. From these images we observed similar morphological changes in the nuclei of several patients, with more heterogeneous structures presented compared with samples from the same patients before chemotherapy (see representative images from on patient in Figure 3.6-3). The observation is consistent with our findings above.

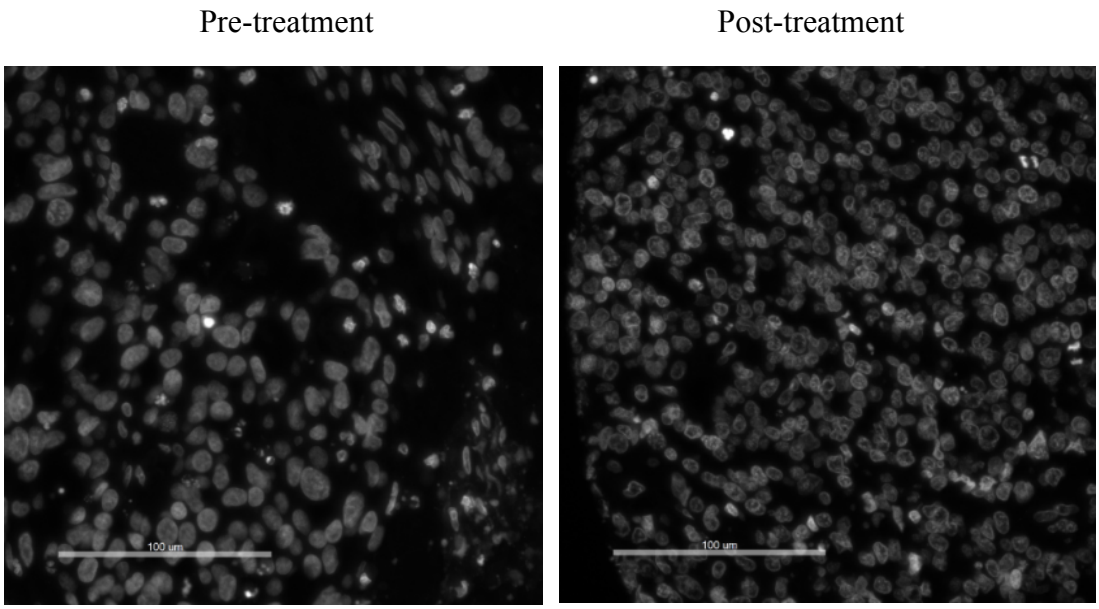

Figure 3.6-3 Representative microscope images taken for nuclear texture analysis in one patient with ovarian cancer pre- and post-chemotherapy.

We also quantified the morphological alterations in terms of nuclear texture, using our established method. Among these nuclear parameters mentioned above,

correlation and inverse difference moment (IDM) showed significant reductions in nuclei from patients after chemotherapy, suggesting increased heterogeneity and contrast of chromatin patterns, respectively (refer to Figure S2 in supplement for full data analysis).

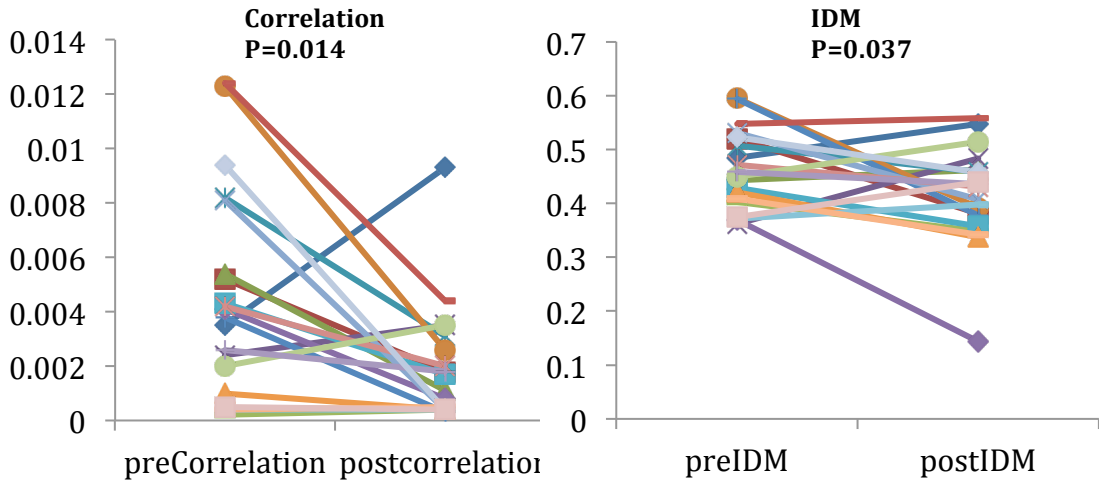

Figure 3.6-4 Comparison of nucelar texture parameters between paired samples from ovarian cancer patients pre- and post-chemotherapy. Tumour samples were spotted onto TMA slides, and nuclei were stained using DAPI. Fluorescent images were analysed using ImageJ, and nuclear texture was measured through several texture-related parameters among which significant changes are presented here. The Wilcoxon test was run for paried sample comparison and P values are indicated.

Here I identified enhanced expression of HDAC and HP1 proteins in cancers after chemotherapy in patients, which also was accompanied by nuclear morphological alteration with increased heterogeneity of chromatin pattern. The result is consistent with our hypothesis and showed the association of HDAC with chromatin conformation change during chemotherapy in clinical tumor samples.

4 Conclusions and discussion

The essential roles of epigenetic regulation for guarding genome integrity have been strongly emphasized in recent years. Along with this, the realisation that epigenetic regulation is also essential during the cellular DNA damage response also has risen, especially in cancer research. The relationship between chromatin status and DDR is far more complicated than we had originally expected. On one hand, the pre-existing condition of the chromatin structure can influence how cells response to extracellular damage. On the other hand, alteration of the chromatin environment on DNA damage is also an important component of the overall orchestration of the DDR pathways. Thus the network of epigenetic modifications of chromatin during DDR is only beginning to be understood, and little is known about the exact roles HDACs play during DDR events. In this study we identified similar alterations in chromatin pattern during DNA damage-based therapies in a variety of tumour settings from clinical patients, cell lines, and xenografts. We linked this phenomenon for the first time to HDAC expression, and suggest that this cellular change represents a response to damage that is mediated by HDACs and associated with DDR pathways in cancer cells. Study methods are illustrated in Figure 4-1.

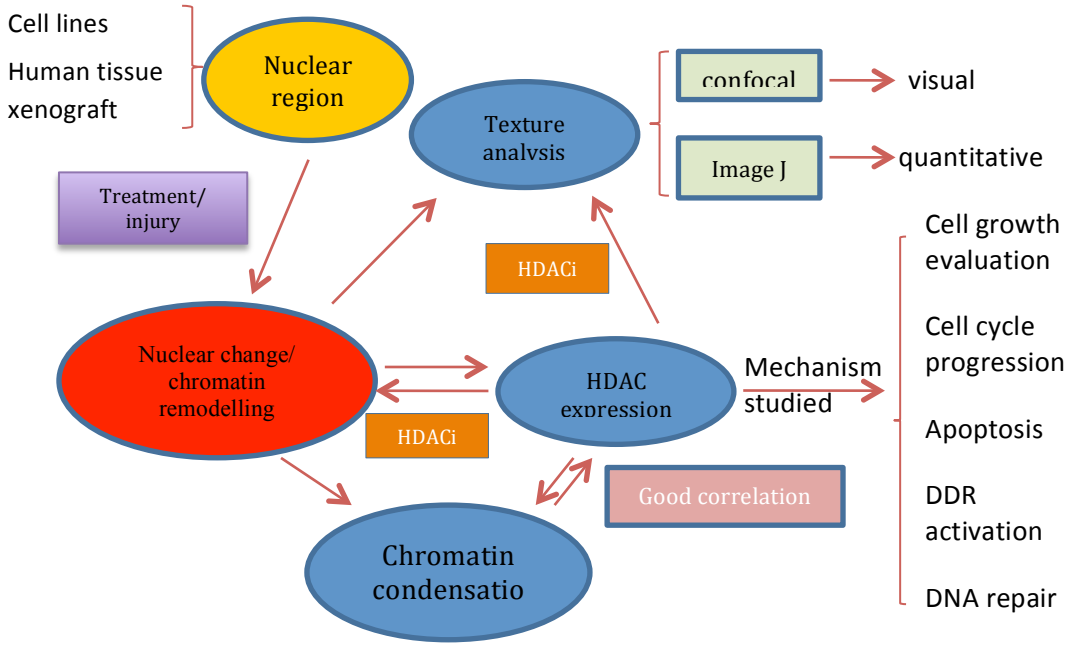

Figure 4- 1 The investigation methodology used in this study to investigate the roles of HDACs in chromatin remodelling and DDR induced by DNA damage-based therapies.

Firstly, quite similar nuclear morphological changes were observed across several tumours after cellualr damage including radiotherapy and chemotherapy, and those nuclear changes were measured in a robust way by measuring nuclear texture. In this way we were able to link the chromatin patterns occurring in cancer cells to the response to chemotherapy. The outcome of increased heterogeneity and decreased homogeneity was consistent with observations seen under the microscope, and provided a quantitative measure of this structural alteration in chromatin during DNA damage. Little is known and has been studied about nuclear morphological changes in response to DNA damage-induced treatment, but there are some data to support our observations. Fragmented nuclei and clumped chromatin in cancer cells have been observed after chemotherapy (Handelsman, Rondon et al. 1998; Marchetti 2005), which also provided evidence to state that this nuclear change is a general phenomenon in cancers during either radiotherapy or chemotherapy. Due to the nature of radiotherapy and chemotherapy as a source of DNA damage, I

hypothesised that this nuclear morphological change was a cellular response to external injuries. At the same time, results from antibody array studies performed in our laboratory showed that histone deacetylation status was able to distinguish cells in terms of exposure or response to platinum treatment. With the knowledge that histone acetylation is important for nuclear peripheralisation induced by DSBs (Peric-Concha and Long 2003), the nuclear morphological changes could mechanistically be connected to HDACs as a mediator of the response to DNA damage in cancer treatment, providing rationale for these studies.

The nuclear change of elevated heterogeneity was assumed to be associated with increased transition from euchromatin and heterochromatin; therefore I tested heterochromatin formation during DNA damage-inducing treatment with platinum both *in vivo and in vitro*. As expected, expression of the heterochromatin marker, HP1 increased after cisplatin treatment *in vitro*, and this was accompanied by enhanced expression of HDAC2 at both mRNA and protein level. Studies *in vivo* and on clinical tumour samples also showed elevated expression of both HDAC and HP1 after chemotherapy in ovarian cancer, especially in those sensitive to treatment. As an essential component of heterochromatin formation, HP1 has been already found to be accumulated or recruited to damaged sites in either UV-lesions or irradiation in a variety of studies (Leese, Hejaz et al. 2005; Bradley, Rathkopf et al. 2009; Di Bussolo and Minutolo 2011; Kim and Bae 2011), which indicates that chromatin reorganization occurs during DNA damage-based treatment. This study showed a similar result, with enhanced heterochromatin formation following chemotherapy both *in vivo* and *in vitro*, and furthermore provided evidence that HDAC is a regulator involved in this response to chemotherapy. HDAC was up-regulated after

24h of treatment with cisplatin *in vitro*, with similar results seen *in vivo* and in ovarian cancer xenografts. With its well-known function as a structural regulator to form condensed chromatin, HDAC potentially explained the observed changes in nuclear texture and was presumed to be a mediator during DDR. This alteration in chromatin pattern might also indicate that transcriptional silencing is occurring after chemotherapy, which might be a form of cellular self-protection upon injury. In fact, there is evidence demonstrating the participation of HDAC-containing complexes including Mi-2/NuRD and/or Sin3/HDAC chromatin-modifying complex (containing HDAC1 and HDAC2) in the reorganisation of nuclear structure for their repressive function during development (Stronach, Alfraidi et al. 2011). Other studies have also shown that Mi-2/NuRD and mSin3/HDAC co-repressor complexes are necessary for the process of pericentric heterochromatin assembly and chromosome segregation (Kartalou and Essigmann 2001; Kim, Kim et al. 2013).

To explore the detailed roles of HDAC during chemotherapy in cells in our study, I next evaluated its effect on cell growth. HDACs are associated with malignancy and poor clinical outcomes in several cancers (Kothandapani, Dangeti et al. 2011), and this suggests a possible function in tumour growth, invasion, and even metastasis in cancer. Moreover, a range of studies have shown the potential effect of HDAC inhibition on cancer cell growth (Podhorecka, Halicka et al. 2009; Atsumi, Inase et al. 2013; Lu, Xiong et al. 2013), which makes HDAC inhibitors exciting drug candidates for cancer treatment. A number of studies have also demonstrated effective combinatorial treatment with both HDAC inhibitors and chemotherapy in cancers. One HDAC inhibitor, Romidepsin (FK228), which is approved in phase I and II trials, enhances the cytotoxic effects of cisplatin by reducing cell growth and

causing more DNA damage-induced cell death when used in combination both *in vitro* and *in vivo* (Lu, Shi et al. 2008). I also demonstrated the inhibitory effect of the HDAC inhibitor TSA on ovarian cancer cells when treating the cells with TSA alone or TSA and cisplatin. Since HDAC2 in particular was associated with the early response to cisplatin in our cell culture studies, cell growth was further evaluated with HDAC2 knockdown using siRNA. The IC50 of cisplatin was significantly reduced by HDAC2 depletion in both PEO1 and PEO4 cells, which means specific knockdown of HDAC2 contributed to the effect of cisplatin treatment; however, this effect is additive and at this point there is a shortage of evidence to elucidate if there is synergistic mechanism for HDAC2 in the cellular response to cisplatin. Follow-on experiments indeed suggested the distinct roles for HDAC2 in regulating the cell cycle distribution and apoptosis induced by cisplatin in sensitive and resistant cell lines. Increased cellular apoptosis in both cell lines could be the reason for cell growth inhibition induced by HDAC2 knockdown during cisplatin treatment, and this induction of apoptosis might result from activation of different pathways. It seems that the repression of cell growth in sensitive PEO1 cells by cisplatin after HDAC2 silencing is caused by induction of apoptosis through accumulated S phase arrest, based on single treatment with cisplatin. In contrast, HDAC2 depletion seemed to resume the cell cycle in PEO4 cells treated with cisplatin, which means apoptosis is induced by cisplatin after HDAC2 knockdown by restoring cell cycle progression. The differences here between PEO1 and PEO4 cells indicated that HDAC2 might function via different pathways to participate in the cellular response to cisplatin treatment, and also in another way implies the distinct characteristics between the cell lines in terms of cisplatin sensitivity. The blockage of cell cycle

progression has been reported to occur as a result of checkpoint activation during DNA damage-based therapy, and one of the representative checkpoint proteins, Chk1, showed up-regulation in the process of intra-S phase accumulation by affecting chromatin formation and interfering with initiation and elongation of DNA replication (Liu, Parry et al. 2008). I therefore suppose that HDAC2 might interact with those checkpoint proteins to prevent DNA replication by forming a condensed structure as a type of self-protection, and also be involved in distinct pathways to trigger apoptosis induced by cisplatin between sensitive and resistant cells. Several mechanisms have been suggested to explain HDAC inhibitor-induced apoptosis, such as altered gene transcription and modified DDR and DNA damage repair proteins (Lu, Zhu et al. 2006; Tanaka, Kurose et al. 2006; Zykova, Zhu et al. 2006).

Early up-regulation (after 24h) of HDAC2 in sensitive cells suggests that HDAC2 is acting as a sensor of DNA damage, while the relative global down-regulation of all the HDACs measured was observed after 48h treatment in a time-dependent manner. This occurred along with up-regulation of DDR proteins, suggesting that DDR is active throughout the observed time course. I assumed that an initial accumulation of HDAC2 was required upon damage to trigger downstream DDR events (such as activation of ATM, ATR, and BRCA1) and chromatin remodelling, followed by histone hyperacetylation to form a less condensed structure to facilitate the recruitment of more DDR mediators to the damaged site. Therefore, more detailed involvement of HDAC was assessed by profiling the expression of proteins known to play key roles in the DDR (pBRCA1, ATM, ATR, γH2AX, and Rad51) during cisplatin treatment after HDAC2 knockdown. The accumulation of DSBs measured by γH2AX expression was demonstrated after 24 hours of cisplatin treatment in

PEO1 cells with HDAC2 depletion, and this cumulative effect from both siHDAC and cisplatin seemed to be gradually lost during incubation until 72h. However, a similar result was not present in PEO4 cells. Moreover, the γH2AX foci assay also confirmed distinct roles for HDAC2 in DSB formation between sensitive and resistant cells. High expression levels of γH2AX have previously been associated with cell viability and apoptosis in ovarian cancer (Lu, Zhu et al. 2006), which was attributed to the cell type tested and observation time after damage. Quite late H2AX activation has also been noted a number of days after treatment with an HDAC inhibitor, which implies increased expression of γH2AX occurs as a consequence to cancer cell death (Huang, Kurose et al. 2006). Suppression of DDR activation (pATM, pATR, pBRCA1, and RAD51) after HDAC2 knockdown strongly suggests involvement of HDAC2 in the cellular response to the DNA damage-based treatment. Distinct results between PEO1 and PEO4 cells in DSB accumulation and time of pathway activation or suppression is consistent with the differences mentioned above in cell cycle progression, and also might be due to the character of the two cell lines in terms of their cisplatin sensitivity. The two major pathways for DSB repair, NHEJ and HR, are suggested to have a compensatory effect with respect to each other (Jeggo, Geuting et al. 2011), and the balance between them might be disrupted by the distinct status of BRCA2 in PEO1 (BRCA2 deficiency) and PEO4 (secondary mutation to restore BRCA2 proficiency) cells, which might influence the dominant mechanism of repair in the two cell lines and cause differences in the observed functional activity of the measured DNA damage response proteins at different stages after cisplatin treatment.

A main challenge in this study was to reverse the observed nuclear changes by knocking down HDAC to show the causative effect of HDAC in mediating the morphological alterations. If the epigenetic modifications were indeed reversible, the chromatin structure should have been altered after HDAC2 depletion. This did occur, at least in part, with the textural parameters tending to indicate more homogeneity after HDAC2 knockdown. However, the result was more complicated than expected, and several possibilities were considered. Firstly, previous studies have shown that the immediate DDR occurs within minutes after damage (Trainor, Butterworth et al. 2012), so it is likely that the ideal observation time point was missed based on the assumption that HDAC2 was an early mediator of the DNA damage response. Furthermore, the compensatory effect of HDAC1 from HDAC2 depletion also needs to be taken into account, which might have reduced or mitigated the effects of HDAC2 knockdown; additionally, HDAC2 knockdown might affect the balance between HDAC and other chromatin structural regulators, with a negative feedback effect causing complex alterations in chromatin patterns. Last, but not least, the toxicity from transfection cannot be completely excluded, which also is considered as an injury to the cells and therefore be assumed to cause chromatin reorganization if our hypothesis is correct. Further studies might be done through more comprehensive profiling, or using a different model such as stable HDAC2 knockdown models.

All these results suggest that chromatin remodelling caused by increased expression of HDACs might be an early cellular event (within 24h) in response to DNA damage treatment, and also indicated the possible involvement of HDACs in the DNA damage response in ovarian cancer. We postulate that in sensitive tumours, the early

alteration in the chromatin pattern induced by chemotherapy mediated by histone deacetylation serves as a form of cellular 'self-defense' to extra injury, which is also a necessary step to slow down transcription, initiate downstream events during chemotherapy-triggered DDR, and promote survival. This is followed by alteration to a less condensed chromatin conformation through histone hyperacetylation, such as via H3k56Ac and H4k16Ac, which is suggested to provide accessibility of downstream proteins into damaged sites to precede DDR (Kurose, Tanaka et al. 2005; Kurose, Tanaka et al. 2006; Tanaka, Kurose et al. 2006). However, resistant tumours behave differently in terms of their response to DNA damage to chemotherapy; this might be due to their initial chromatin environment, or due to other changes in the components of the DDR response pathways that HDACs also participate in (model illustrated in Figure 4-2).

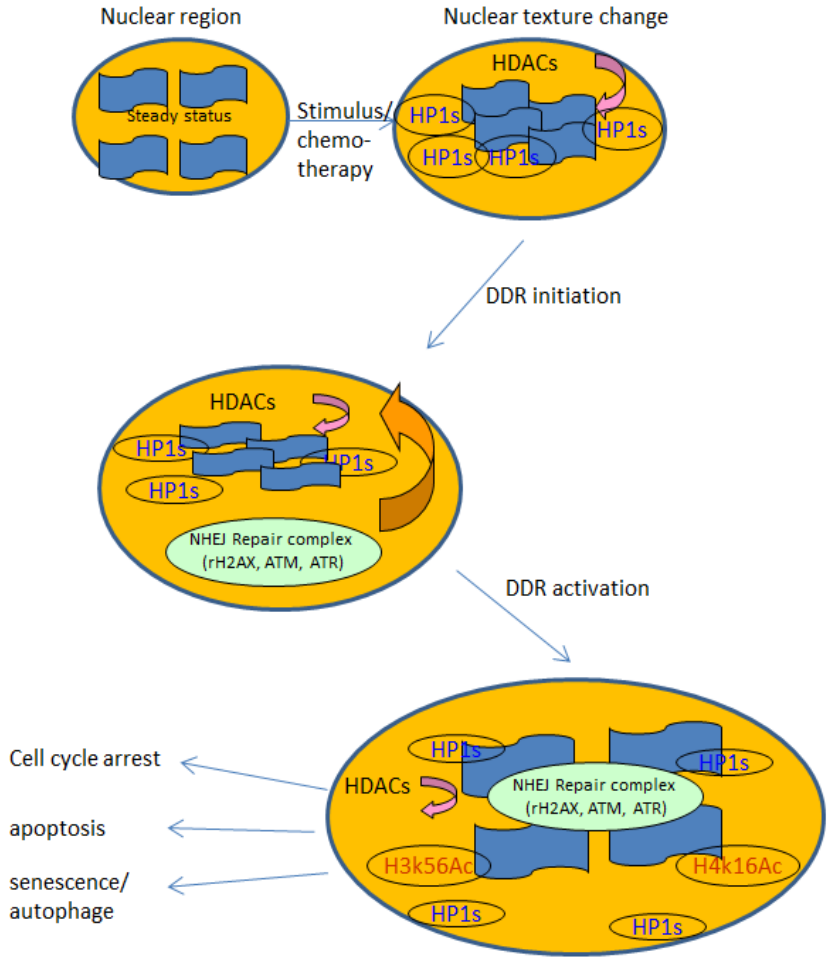

Figure 4- 2 A proposed model of the role of HDACs based on the study.

Interestingly, one important published study supports these assumptions, with HDAC1/2-associated immediate histone hypoacetylation occurring after laser microirradiation in an human osteosarcoma cell line to promote NHEJ, which was followed by hypoacetylation to enhance HR and guard genome integrity (Miller, Tjeertes et al. 2010). These data also provide evidence about the roles of HDACs in cellular DDR in a dynamic way, which makes studies in this field rather complicated.

Several issues are raised based on our studies worthy of future investigation. Different HDAC family members showed the potential to mediate chemotherapy-

induced DDR in this study. Apart from limitations caused by tissue heterogeneity and sample size which could be responsible for differing results, it also highlights the possibility that HDACs function in a tissue or cell type-dependent manner, and raises the importance of investigating their roles in more specific cancer types. or even subtypes, for drug development. Secondly, caution in interpretation of the cell culture studies described here, since different chromatin densities and radiation sensitivities have been observed between two- and three-dimensional cell cultures (Halicka, Huang et al. 2005). This might also be a reason for differing results *in vitro* and *in vivo*; in the future, 3D cultures may be a more accurate model to investigate. Moreover, cytotoxity from siRNA knockdown cannot be completely excluded, although we showed little effect on expression of other HDAC family members and included several controls throughout the experimental design. This may have limited our evaluation of reversal of nuclear texture after HDAC knockdown. Stable knockout of specific HDACs might be useful step to identify their roles in this system, and dual silencing of HDAC1 and HDAC2 should also be included due to their identified compensatory effect to each other (Jurkin, Zupkovitz et al. 2011). Fourthly, besides their epigenetic function in regulating chromatin structure, HDACs possess both nuclear and cytoplasmic functions, and a number of studies have linked their roles during DDR with deacetylation of non-histone proteins (Huang, Traganos et al. 2003; Robert, Vanoli et al. 2011). Therefore, further studies on HDAC cellular localization, and even co-localization with DDR proteins at damaged sites, are essential to solve these questions and showed clear evidence of the participation of HDACs at damaged sites to promote cellular DDR events. Furthermore, with the current opinion about re-modelling factors orchestrating the modification of

chromatin structure (Rogakou, Nieves-Neira et al. 2000), investigation is urgently required about how HDACs function during DDR along with other chromatin modifiers, such as DNA/histone methylation and poly-ADP-ribosylation.

This study for the first time associates the cellular morphological changes seen in real human cancers with possible molecular mechanisms mediating this phenomenon, contributes to current knowledge about epigenetic regulation during chemotherapy-induced DNA damage responses, and also suggests an additive effect of HDACs in terms of the cellular response to chemotherapy. By identifying more detailed roles of HDACs in cellular DNA damage responses in terms of chromatin remodelling, we hope to better understand the molecular processes behind these morphological alterations to identify novel mechanisms of response to chemotherapy in ovarian cancer, and other cancers and diseases. In this way HDACi can be better tailored as a therapeutic option and further developed to provide new targets, or combinatorial strategies, for the treatment of cancer and other diseases.

5 Supplement results and materials

5.1 Supplement results

Table S1: Basic statistics for all five texture parameters for xenograft data

Day	Treatment	No. Of samples	Average number of nuclei per sample	Average Angular Second Moment				Average Contrast			
				Mean	Std. Error of Mean	Std. Deviation	Median	Mean	Std. Error of Mean	Std. Deviation	Median
1	Control	13	71	0.0085	0.0015	0.0055	0.0086	118.82	9.677	34.891	126.73
	Carbo	14	81	0.0084	0.0010	0.0039	0.0084	101.19	7.112	26.610	93.83
2	Control	13	120	0.0077	0.0011	0.0041	0.0086	74.39	6.947	25.049	71.03
	Carbo	18	91	0.0043	0.0008	0.0035	0.0036	118.56	9.159	38.857	118.05
4	Control	17	97	0.0069	0.0012	0.0051	0.0065	100.72	7.209	29.724	101.23
	Carbo	15	89	0.0065	0.0013	0.0053	0.0052	76.32	6.793	26.311	74.36
7	Control	19	130	0.0072	0.0010	0.0045	0.0068	103.36	9.010	39.275	93.76
	Carbo	19	101	0.0071	0.0012	0.0050	0.0066	77.64	7.338	31.984	63.73
14	Control	21	157	0.0052	0.0006	0.0031	0.0048	77.18	5.067	23.221	75.25
	Carbo	18	97	0.0069	0.0011	0.0050	0.0056	114.99	8.481	35.983	113.79

(Continued)

Day	Treatment	Average Inverse Difference Moment				Average Entropy				Average Correlation			
		Mean	Std. Error of Mean	Std. Deviation	Median	Mean	Std. Error of Mean	Std. Deviation	Median	Mean	Std. Error of Mean	Std. Deviation	Median
1	Control	0.203	0.0063	0.0227	0.2021	7.24	0.0836	0.301	7.27	0.000458	0.0000177	0.000064	0.000460
	Carbo	0.219	0.0069	0.0258	0.2189	7.07	0.0494	0.185	7.08	0.000468	0.0000116	0.000043	0.000477
2	Control	0.248	0.0093	0.0334	0.2560	6.91	0.0566	0.204	6.92	0.000411	0.0000207	0.000074	0.000391
	Carbo	0.200	0.0085	0.0359	0.2004	7.19	0.0504	0.214	7.17	0.000473	0.0000176	0.000075	0.000456
4	Control	0.220	0.0125	0.0517	0.2336	7.07	0.0866	0.357	6.93	0.000442	0.0000234	0.000096	0.000453
	Carbo	0.227	0.0110	0.0426	0.2233	7.09	0.0721	0.279	7.12	0.000428	0.0000376	0.000146	0.000422
7	Control	0.229	0.0075	0.0315	0.1257	6.91	0.0610	0.266	6.80	0.000450	0.0000238	0.000104	0.000468
	Carbo	0.241	0.0079	0.0035	0.2529	6.98	0.0079	0.037	6.92	0.00046	0.0000220	0.000096	0.000439
14	Control	0.229	0.0072	0.0329	0.2404	6.91	0.0553	0.254	6.87	0.000470	0.0000226	0.000104	0.000437
	Carbo	0.212	0.0064	0.0270	0.2071	7.03	0.0517	0.219	7.09	0.000479	0.0000156	0.000066	0.000456

Table S2 Tukey HSD Post Hoc test following one-way ANOVA analysis for comparison between groups during theatment in PEO1 and PEO4 cells.

Multiple Comparisons (PEO1)

Tukey HSD

Cell line	Treatment	Treatment	Sig.
PEO1	Control	Cisplatin	.000
		TSA	.000
		TSA+cisplatin	.000
	Cisplatin	Control	.000
		TSA	.000
		TSA+cisplatin	.000
	TSA	Control	.000
		Cisplatin	.000
		TSA+cisplatin	.000
	TSA+cisplatin	Control	.000
		Cisplatin	.000
		TSA	.000

Multiple Comparisons (PEO4)

Cell line	Treatment	Treatment	Sig.
PEO4	Control	Cisplatin	.000
		TSA	.000
		TSA+cisplatin	.000
	Cisplatin	Control	.000
		TSA	.002
		TSA+cisplatin	.000
	TSA	Control	.000
		Cisplatin	.002
		TSA+cisplatin	.000
	TSA+cisplatin	Control	.000
		Cisplatin	.000
		TSA	.000

Table S3 Tukey HSD Post Hoc test following one-way ANOVA analysis for comparison between groups during knockdown of HDAC2 in PEO1 cells.

Time	Treatment	Treatment	*Sig.*
48h	untransfected	mock	*.942*
		negative control	*.840*
		siHDAC2 10pmol	*.094*
		siHDAC2 100pmol	*.001*
	mock	untransfected	*.942*
		negative control	*.998*
		siHDAC2 10pmol	*.276*
		siHDAC2 100pmol	*.002*
	negative control	untransfected	*.840*
		mock	*.998*
		siHDAC2 10pmol	*.396*
		siHDAC2 100pmol	*.003*
	siHDAC2 10pmol	untransfected	*.094*
		mock	*.276*
		negative control	*.396*
		siHDAC2 100pmol	*.052*
	siHDAC2 100pmol	untransfected	*.001*
		mock	*.002*
		negative control	*.003*
		siHDAC2 10pmol	*.052*
72h	untransfected	mock	*.201*
		negative control	*.231*
		siHDAC2 10pmol	*.000*
		siHDAC2 100pmol	*.000*
	mock	untransfected	*.201*
		negative control	*1.000*
		siHDAC2 10pmol	*.000*
		siHDAC2 100pmol	*.000*
	negative control	untransfected	*.231*
		mock	*1.000*
		siHDAC2 10pmol	*.000*
		siHDAC2 100pmol	*.000*
	siHDAC2 10pmol	untransfected	*.000*
		mock	*.000*
		negative control	*.000*
		siHDAC2 100pmol	*.742*
	siHDAC2 100pmol	untransfected	*.000*
		mock	*.000*
		negative control	*.000*
		siHDAC2 10pmol	*.742*
96h	untransfected	mock	*.713*
		negative control	*1.000*
		siHDAC2 10pmol	*.001*
		siHDAC2 100pmol	*.001*
	mock	untransfected	*.713*
		negative control	*.693*
		siHDAC2 10pmol	*.000*
		siHDAC2 100pmol	*.000*
	negative control	untransfected	*1.000*
		mock	*.693*
		siHDAC2 10pmol	*.001*
		siHDAC2 100pmol	*.001*
	siHDAC2 10pmol	untransfected	*.001*
		mock	*.000*
		negative control	*.001*
		siHDAC2 100pmol	*.999*
	siHDAC2 100pmol	untransfected	*.001*
		mock	*.000*
		negative control	*.001*
		siHDAC2 10pmol	*.999*
120h	untransfected	mock	*.030*
		negative control	*.811*
		siHDAC2 10pmol	*.000*
		siHDAC2 100pmol	*.000*
	mock	untransfected	*.030*
		negative control	*.159*
		siHDAC2 10pmol	*.000*
		siHDAC2 100pmol	*.000*
	negative control	untransfected	*.811*
		mock	*.159*
		siHDAC2 10pmol	*.000*
		siHDAC2 100pmol	*.000*
	siHDAC2 10pmol	untransfected	*.000*
		mock	*.000*
		negative control	*.000*
		siHDAC2 100pmol	*.970*
	siHDAC2 100pmol	untransfected	*.000*
		mock	*.000*
		negative control	*.000*
		siHDAC2 10pmol	*.970*

Table S4 Tukey HSD Post Hoc test following one-way ANOVA analysis for comparison between groups during γH2AX foci formation induced by cisplatin in cells with HDAC2 knockdown.

Multiple Comparisons

Cell line	Treatment	Treatment	Sig.
PEO1 foci counting	NC	NC+cis	.000
		siRNA	.004
		siRNA+cis	.000
	NC+cis	NC	.000
		siRNA	.053
		siRNA+cis	.028
	siRNA	NC	.004
		NC+cis	.053
		siRNA+cis	.001
	siRNA+cis	NC	.000
		NC+cis	.028
		siRNA	.001
PEO4 foci counting	NC	NC+cis	.000
		siRNA	.887
		siRNA+cis	.032
	NC+cis	NC	.000
		siRNA	.001
		siRNA+cis	.019
	siRNA	NC	.887
		NC+cis	.001
		siRNA+cis	.088
	siRNA+cis	NC	.032
		NC+cis	.019
		siRNA	.088

Table S5 Games-Howell pot HOC test was performed to compare between groups for cell cycle distribution with cisplatin treatment in PEO1 and PEO4 cells after HDAC2 knockdown.

PEO1								
		Mock	NC	siRNA	Untransfected +Cis	Mock+ Cis	NC+Cis	siRNA+Cis
G1	Untransfected	.996	.240	.994	.000	.000	.000	.000
	Mock		.198	.917	.000	.000	.000	.000
	NC			.297	.001	.000	.000	.000
	siRNA				.000	.000	.000	.000
	Untransfected +Cis					.994	.070	.000
	Mock+Cis						.779	.001
	NC+Cis							.000
S	Untransfected	.220	1.0000	.001	.000	.001	.000	.000
	Mock		.763	.000	.000	.001	.000	.000
	NC			.034	.001	.000	.001	.000
	siRNA				.000	.003	.000	.000
	Untransfected +Cis					.696	.273	.000
	Mock+Cis						.258	.004
	NC+Cis							.000
G2	Untransfected	.131	.998	.000	.001	.001	.000	.000
	Mock		.758	.000	.001	.001	.000	.000
	NC			.006	.007	.001	.001	.001
	siRNA				.934	.317	.785	.137
	Untransfected +Cis					.371	.630	.127
	Mock+Cis						.175	.043
	NC+Cis							.385

(Continued)

PEO4								
		Mock	NC	siRNA	Untransfected +Cis	Mock+ Cis	NC+Cis	siRNA+Cis
G1	Untransfected	.849	.962	.169	.605	.010	.003	.010
	Mock		1.000	.160	.598	.002	.003	.013
	NC			.156	.599	.001	.003	.011
	siRNA				.743	.000	.000	.007
	Untransfected +Cis					.950	.887	.997
	Mock+Cis						.496	.002
	NC+Cis							.001
S	Untransfected	.391	.999	.812	.596	.000	.000	.002
	Mock		.455	.266	.570	.000	.001	.005
	NC			.647	.591	.000	.000	.003
	siRNA				.621	.000	.000	.001
	Untransfected +Cis					.941	.946	.994
	Mock+Cis						1.000	.001
	NC+Cis							.001
G2	Untransfected	.921	.660	.057	.610	.006	.047	.000
	Mock		.899	.173	.757	.005	.039	.003
	NC			.971	.992	.115	.104	.026
	siRNA				1.000	.022	.113	.003
	Untransfected +Cis					.471	.438	.083
	Mock+Cis						1.000	.012
	NC+Cis							.071

Table S6 Tukey HSD pot HOC test was performed to compare between groups for apoptosis with cisplatin treatment in PEO1 and PEO4 cells after HDAC2 knockdown.

PEO1								
		Mock	NC	siRNA	Untransfected +Cis	Mock+ Cis	NC+Cis	siRNA+Cis
Early apoptosis	Untransfected	1.000	.931	.029	.055	.055	.337	.047
	Mock		1.000	.017	.273	.264	.311	.014
	NC			.039	.076	.032	.360	.052
	siRNA				.028	.073	.113	.066
	Untransfected +Cis					.608	.865	.047
	Mock+Cis						.981	.067
	NC+Cis							.019
Late apoptosis	Untransfected	1.000	1.000	.132	.494	.793	1.000	.218
	Mock		1.000	.144	.562	.882	1.000	.234
	NC			.128	.495	.805	1.000	.214
	siRNA				.131	.133	.059	.770
	Untransfected +Cis					.894	.260	.126
	Mock+Cis						0.736	.226
	NC+Cis							.068

PEO4								
		Mock	NC	siRNA	Untransfected +Cis	Mock+ Cis	NC+Cis	siRNA+Cis
Early apoptosis	Untransfected	1.000	.928	.053	.854	.786	.619	.001
	Mock		0.947	.016	.846	.781	.600	.020
	NC			.019	.972	.949	.774	.017
	siRNA				.073	.048	.053	.119
	Untransfected +Cis					1.000	.999	.083
	Mock+Cis						.998	.067
	NC+Cis							.070
Late apoptosis	Untransfected	1.000	.997	.442	.919	.999	1.000	.404
	Mock		1.000	.463	.953	1.000	1.000	.426
	NC			.488	.914	1.000	1.000	.456
	siRNA				.557	.480	.471	1.000
	Untransfected +Cis					.920	.920	.516
	Mock+Cis						1.000	.447
	NC+Cis							.436

Table S7 Proteins included and grouped in accociated pathways in V250 proteomic study

Proteins detected	Associated pathways
Estrogen Receptor-alpha (Phospho-Ser167)	ER
Rac1/cdc42(Phospho-Ser71)	MAPK
Raf1(Phospho-Ser259)	MAPK
MEK1(Phospho-Ser217)	MAPK
MEK1(Phospho-Ser221)	MAPK
MEK1(Phospho-Thr291)	MAPK
MEK-2(Phospho-Thr394)	MAPK
p44/42 MAP Kinase(Phospho-Thr202)	MAPK
p44/42 MAP Kinase(Phospho-Tyr204)	MAPK
Elk-1(Phospho-Ser383)	MAPK
NF kappa B-p100/p52(Phospho-Ser869)	NF kappa B
NF kappa B-p105/p50(Phospho-Ser893)	NF kappa B
NF kappa B-p105/p50(Phospho-Ser907)	NF kappa B
NF kappa B-p105/p50(Phospho-Ser932)	NF kappa B
NF kappa B-p65(Phospho-Ser529)	NF kappa B
NF kappa B-p65(Phospho-Thr254)	NF kappa B
I-kappa-B-alpha(Phospho-Ser32/Phospho-Ser36	NF kappa B
I-kappaB-alpha(Phospho-Tyr42)	NF kappa B
I-kappa-B-beta(Phospho-Ser23)	NF kappa B
I-kappa-B-epsilon(Phospho-Ser22)	NF kappa B
IKK alpha(Phospho-Thr23)	NF kappa B
Rel(Phospho-Ser503)	NF kappa B
JAK1(Phospho-Tyr1022)	JAK/STAT
JAK2(Phospho-Tyr1007)	JAK/STAT
JAK2(Phospho-Tyr221)	JAK/STAT
STAT1(Phospho-Ser727)	JAK/STAT
STAT1(Phospho-Tyr701)	JAK/STAT
STAT3(Phospho-Ser727)	JAK/STAT
STAT3(Phospho-Tyr705)	JAK/STAT
STAT4(Phospho-Tyr693)	JAK/STAT
STAT5A (Phospho-Ser780)	JAK/STAT
STAT5A (Phospho-Tyr694)	JAK/STAT
STAT6(Phospho-Thr645)	JAK/STAT
STAT6(Phospho-Tyr641)	JAK/STAT
TYK2(Phospho-Tyr1054)	JAK/STAT
Beta-Catenin	Beta-Catenin
Beta-Catenin(Phospho-Ser37)	Beta-Catenin
Beta-Catenin(Phospho-Thr41/Phospho-Ser45	Beta-Catenin
BAD(Phospho-Ser112)	Mitochondrial Apoptosis
BAD(Phospho-Ser136)	Mitochondrial Apoptosis
BAD(Phospho-Ser155)	Mitochondrial Apoptosis
BCL-2(Phospho-Ser70)	Mitochondrial Apoptosis
BCL-2(Phospho-Thr56)	Mitochondrial Apoptosis
BCL-XL(Phospho-Ser62)	Mitochondrial Apoptosis
Rb(Phospho-Ser780)	Early cell cycle

Proteins detected	Associated pathways
CDK2(Phospho-Thr160)	Early cell cycle
p21Cip1(Phospho-Thr145)	Early cell cycle
p27Kip1(Phospho-Ser10)	Early cell cycle
p27Kip1(Phospho-Thr187)	Early cell cycle
FKHR(Phospho-Ser256)	Early cell cycle
p53(Phospho-Ser315)	Late cell cycle/DNA damage
p53(Phospho-Ser6)	Late cell cycle/DNA damage
Chk1(Phospho-Ser280)	Late cell cycle/DNA damage
Chk1(Phospho-Ser317)	Late cell cycle/DNA damage
Chk1(Phospho-Ser345)	Late cell cycle/DNA damage
Chk2(Phospho-Ser516)	Late cell cycle/DNA damage
Chk2(Phospho-Thr68)	Late cell cycle/DNA damage
CDC2(Phospho-Tyr15)	Late cell cycle/DNA damage
cdc25A (Phospho-Ser75)	Late cell cycle/DNA damage
cdc25C(Phospho-Ser216)	Late cell cycle/DNA damage
BRCA1(Phospho-Ser1423)	Late cell cycle/DNA damage
BRCA1(Phospho-Ser1524)	Late cell cycle/DNA damage
Histone H2A.X(Phospho-Ser139)	Late cell cycle/DNA damage
Akt(Phospho-Ser473)	AKT/mTOR
Akt(Phospho-Thr308)	AKT/mTOR
Akt2(Phospho-Ser474)	AKT/mTOR
PTEN(Phospho-Ser380/Phospho-Thr382/Phosp-Thr383	AKT/mTOR
mTOR(Phospho-Ser2448)	AKT/mTOR
GSK3-alpha(Phospho-Ser21)	AKT/mTOR
GSK3-beta(Phospho-Ser9)	AKT/mTOR
p70 S6 Kinase (Phospho-Ser424)	AKT/mTOR
4E-BP1(Phospho-Thr36)	AKT/mTOR
PDK1(Phospho-Ser241)	AKT/mTOR
AMPK1(Phospho-Thr174)	AKT/mTOR/AMPK
P38 MAPK(Phospho-Thr180)	P38 MAPK
P38 MAPK(Phospho-Tyr182)	P38 MAPK
MKK3(Phospho-Ser189)	P38 MAPK
SAPK/JNK(Phospho-Thr183)	P38 MAPK
Myc(Phospho-Ser62)	Transcriptional regulation
Myc(Phospho-Thr358)	Transcriptional regulation
Myc(Phospho-Thr58)	Transcriptional regulation
JunB(Phospho-Ser259)	Transcriptional regulation
JunB(Phospho-Ser79)	Transcriptional regulation
JunD(Phospho-Ser255)	Transcriptional regulation
c-Jun (Phospho-Thr239)	Transcriptional regulation
c-Jun(Phospho-Ser243)	Transcriptional regulation
c-Jun(Phospho-Ser73)	Transcriptional regulation
CREB(Phospho-Ser133)	Transcriptional regulation
Trk B(Phospho-Tyr515)	Tyrosine kinase/adapters
c-Kit(Phospho-Tyr721)	Tyrosine kinase/adapters
EGFR(Phospho-Tyr1110)	Tyrosine kinase/adapters

Proteins detected	Associated pathways
FGF Receptor 1(Phospho-Tyr154)	Tyrosine kinase/adapters
IGF-1R (Phospho-Tyr1161)	Tyrosine kinase/adapters
Met(Phospho-Tyr1349)	Tyrosine kinase/adapters
PDGF Receptor beta(Phospho-Tyr751)	Tyrosine kinase/adapters
VEGFR2(Phospho-Tyr951)	Tyrosine kinase/adapters
HER2(Phospho-Tyr877)	Tyrosine kinase/adapters
CrkII(Phospho-Tyr221)	Tyrosine kinase/adapters
FAK(Phospho-Tyr861)	Tyrosine kinase/adapters
FAK(Phospho-Tyr925)	Tyrosine kinase/adapters
Pyk2(Phospho-Tyr402)	Tyrosine kinase/adapters
Src(Phospho-Tyr418)	Tyrosine kinase/adapters
Src(Phospho-Tyr529)	Tyrosine kinase/adapters
Shc(Phospho-Tyr349)	Tyrosine kinase/adapters
SHP-2(Phospho-Tyr580)	Tyrosine kinase/adapters
HSF1(Phospho-Ser303)	Heat-shock
HSP27(Phospho-Ser15)	Heat-shock
HSP27(Phospho-Ser78)	Heat-shock
HSP90B(Phospho-Ser254)	Heat-shock
ICAM-1(Phospho-Tyr512)	Adhesion/cell contact
Integrin beta-3(Phospho-Tyr773)	Adhesion/cell contact
Integrin beta-3(Phospho-Tyr785)	Adhesion/cell contact
Smad3(Phospho-Ser425)	SMAD
eEF2K(Phospho-Ser366)	Calcium
CaMKII (Phospho-Thr286)	Calcium
Caveolin-1(Phospho-Tyr14)	Cholesterol/lipid
eIF2 alpha(Phospho-Ser51)	Transcriptional regulation
eIF4E(Phospho-Ser209)	Transcriptional regulation
HDAC8(Phospho-Ser39)	Deacetylation
Keratin 18(Phospho-Ser33)	Structural
Tau(Phospho-Ser404)	Structural
14-3-3 Zeta(Phospho-Ser58)	Misc

Table S8 Full information of the clinical samples from ovarian cancer patients before and after chemotherapy. (A. Information table, B. Relative definitions)

A.

	Patient No	Date Dx	Date Sx	Date CRx	Regimen	FIGO stage	Grade	Histology	Debulking	Path Year 1	Path Year 2
PRIMARY RESPONSIVE	1	12/01/2001	12/01/2001	06/02/2001	CRB/TXL	3A	3	ENDOMETRIOID	<2cm	2001	2002
	2	01/03/1994	01/03/1994	31/03/1994	CISPLATIN	3C	2	ENDOMETRIOID	2-5cm	1994	1996
	3	06/08/1998	06/08/1998	06/10/1998	CARBOPLATIN	3C	2	ENDOMETRIOID	Unknown	1998	2000
	4	29/06/1995	29/06/1995	10/08/1995	CARBOPLATIN	3C	2	MUCINOUS	<2cm	1995	1998
	5	03/03/1991	03/03/1991	03/05/1991	CARBOPLATIN	3 (pre FIGO)	3	SEROUS PAP	>5cm	1991	1991
	6	29/11/1993	29/11/1993	11/01/1994	CISPLATIN	2C	3	SEROUS PAP	<2cm	1993	1998
	7	18/12/2000	18/12/2000	18/01/2001	CRB/TXL	3C	3	SEROUS PAP	2-5cm	2000	2006
	8	08/08/2002	08/08/2002	12/09/2002	CARBOPLATIN	2A	3	SEROUS PAP	<2cm	2002	2006
	9	26/02/2003	26/02/2003	27/03/2003	CRB/TXL	3C	3	SEROUS PAP	>5cm	2003	2003
	10	05/05/1998	05/05/1998	02/06/1998	CARBOPLATIN	3C	3	MIXED SEROUS/ENDO	2-5cm	1998	2000
	11	23/08/2000	23/08/2000	04/10/2000	CRB/TXL	4	2	SEROUS PAP	>5cm	2000	2001
	12	17/01/1991	17/01/1991	11/02/1991	CISPLATIN	3	U/K	ENDOMETRIOID	<2cm	2991	1992
	13	29/12/2003	30/12/2003	30/01/2004	CARBOPLATIN	4	3	SEROUS PAP	>5cm	2003	2004
	14	24/02/1999	24/02/1999	22/03/1999	CARBOPLATIN	3C	3	SEROUS PAP	<2cm	1999	2000
	15	18/12/1989	18/12/1989	11/01/1990	CISPLATIN	3C	3	ENDOMETRIOID	>5cm	1989	1992
	16	23/12/2002	23/12/2002	13/02/2003	CRB/TXL	3C	2	SEROUS PAP	2-5cm	2002	2003
	17	10/04/2002	23/04/2002	03/07/2002	CRB/TXL	3A	2	MUCINOUS	<2cm	2002	2004
	18	21/11/1995	21/11/1995	19/12/1995	CARBOPLATIN	3 (pre FIGO)	2	SEROUS PAP	Unknown	1995	1998
	19	28/04/1999	28/04/1999	27/05/1999	CARBOPLATIN	NA	3	CLEAR CELL	Unknown	1999	2000
	20	29/11/1994	29/11/1994	20/01/1995	CARBOPLATIN	3 (pre FIGO)	3	ENDOMETRIOID	<2cm	1994	1996
PRIMARY RESISTANT/ REFRACTORY	21	09/09/1999	09/09/1999	26/10/1999	CARBOPLATIN	2A	3	CLEAR CELL	<2cm	1999	2000
	22	19/10/1992	19/10/1992	13/11/1992	CISPLATIN	3 (pre FIGO)	3	ENDOMETRIOID	2-5cm	1992	1993
	23	03/07/1996	03/07/1996	22/07/1996	CSP/TPT	3C	3	ENDOMETRIOID	<2cm	1996	1998
	24	23/11/1999	23/11/1999	22/12/1999	CARBOPLATIN	4	3	MIXED ENDO/CLEAR	>5cm	1999	2000
	25	04/06/1999	04/06/1999	30/06/1999	CARBOPLATIN	4	3	ENDOMETRIOID	Unknown	1999	2000
	26	10/08/1999	10/08/1999	13/09/1999	CRB/TXL	4	3	MIXED ENDO/CLEAR	Unknown	1999	2000
	27	23/10/2002	23/10/2002	21/11/2002	CARBOPLATIN	3C	2	SEROUS PAP	>5cm	2002	2003
	28	01/11/1996	01/11/1996	29/11/1996	CSP/TPT	3 (pre FIGO)	3	UNDIFFERENTIATED CARCINOMA	<2cm	1996	1998
	29	22/08/2001	22/08/2001	24/09/2001	CRB/TXL	2B	3	ENDOMETRIOID	2-5cm	2001	2002
	30	21/10/1996	21/10/1996	22/11/1996	CSP/TPT	3C	3	ENDOMETRIOID	2-5cm	1996	1997
	31	16/12/2003	16/12/2003	30/01/2004	CRB/TXL	3C	3	SEROUS PAP	>5cm	2003	2004
	32	21/10/1996	21/10/1996	12/12/1996	CISPLATIN	3C	2	MUCINOUS	2-5cm	1996	1998
	33	11/11/1997	11/11/1997	08/12/1997	CARBOPLATIN	2C	3	SEROUS PAP	2-5cm	1997	1998
	34	02/05/1985	02/05/1985	30/05/1985	CISPLATIN	4	3	SEROUS PAP	2-5cm	1985	1986
	35	18/07/2000	18/07/2000	24/08/2000	CRB/TXL	2B	3	ENDOMETRIOID	2-5CM	2000	2000
	36	26/05/1995	26/05/1995	06/07/1995	CARBOPLATIN	Inadequate	2	ENDOMETRIOID	<2cm	1995	1996
	37	23/11/1994	23/11/1994	14/12/1994	CARBOPLATIN	3C	3	ENDOMETRIOID	Unknown	1994	1995
	38	30/03/2001	30/03/2001	26/04/2001	CRB/TXL	3C	3	SEROUS PAP	>5cm	2001	2001

B. Definitions referred to Table S8A

Heading	Definition
Date Dx	Date of histological Diagnosis
Date Sx	Date of surgery
Date CRx	Date of first Chemotherapy infusion
Regimen	Chemotherapy Regimen
Stage	FIGO Stage (where no letter is listed, is prior to new staging system - eg 'Stage 3'
Grade	Grade of histological differentiation
Histology	Histological subtype
Debulking	Debulking status :Not debulked = >5cm, Partial debulk = 2-5cm, Debulked = <2cm the largest diameter lesion left post surgery
Path year1 & Path 2	Year when matched pathology specimen acquired

Figure S1 Variant expression of HDAC members and HP1 isoforms in ovarian cancer tumours from 38 patients before and after chemotherapy.

HDAC1

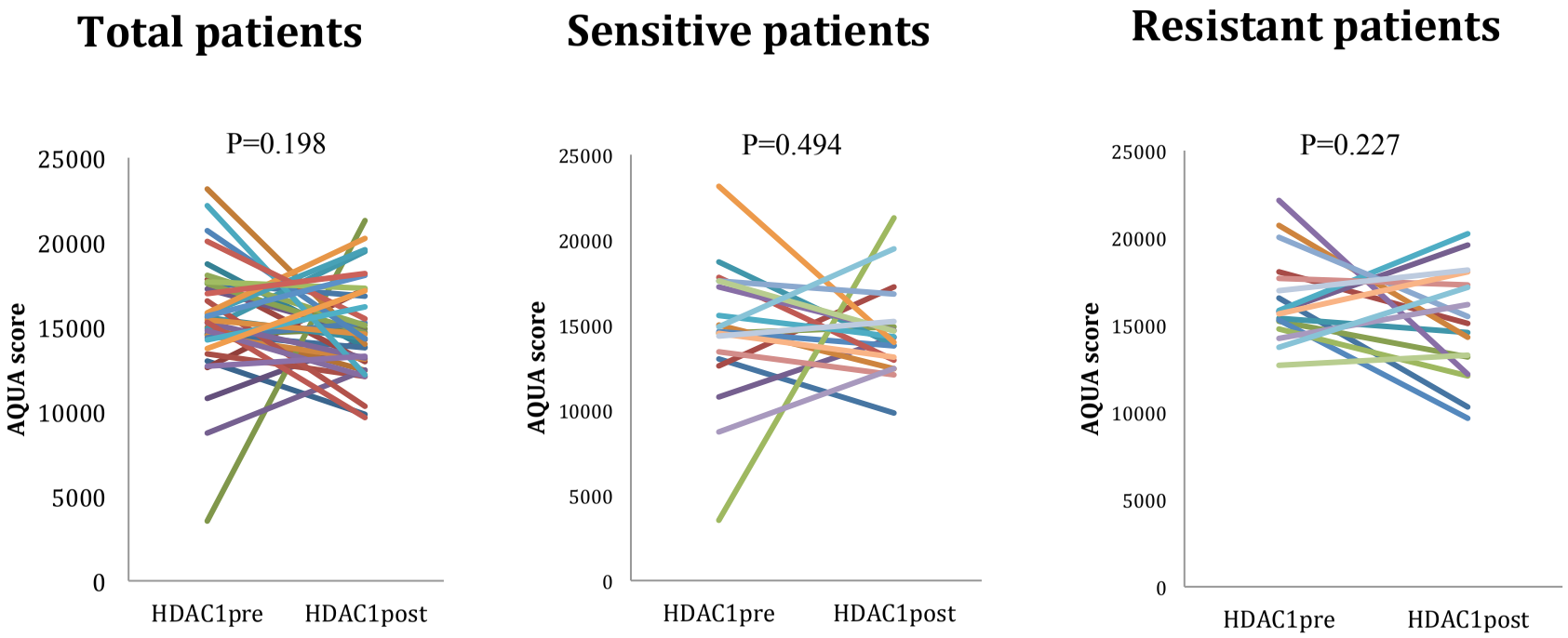

(Continued)

HDAC2

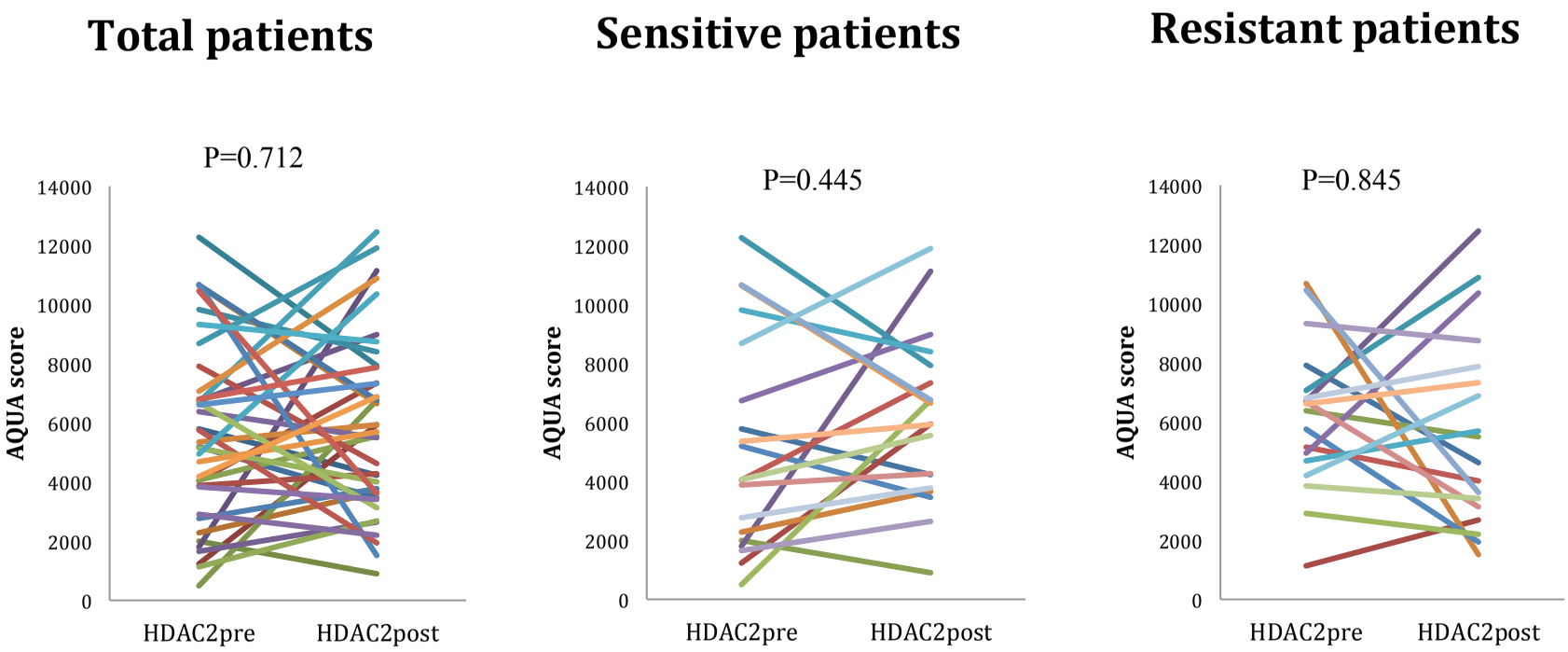

(Continued)

HDAC3

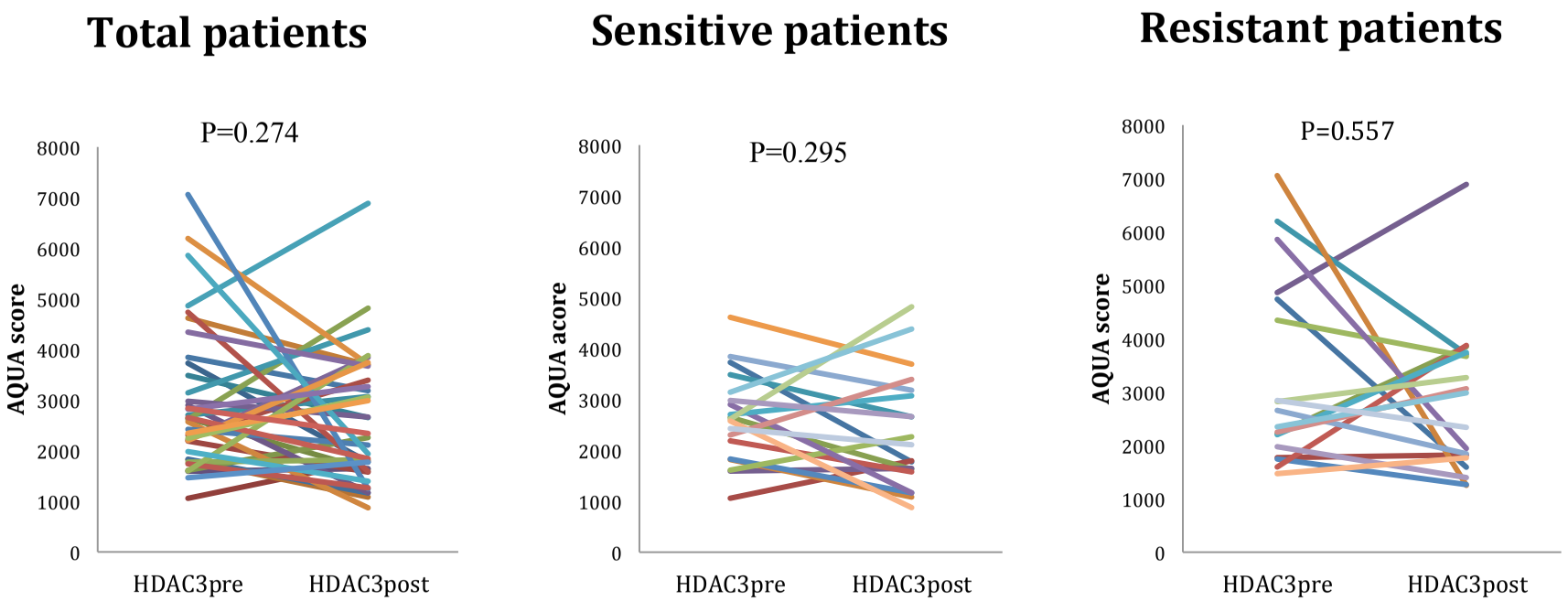

(Continued)

HDAC4

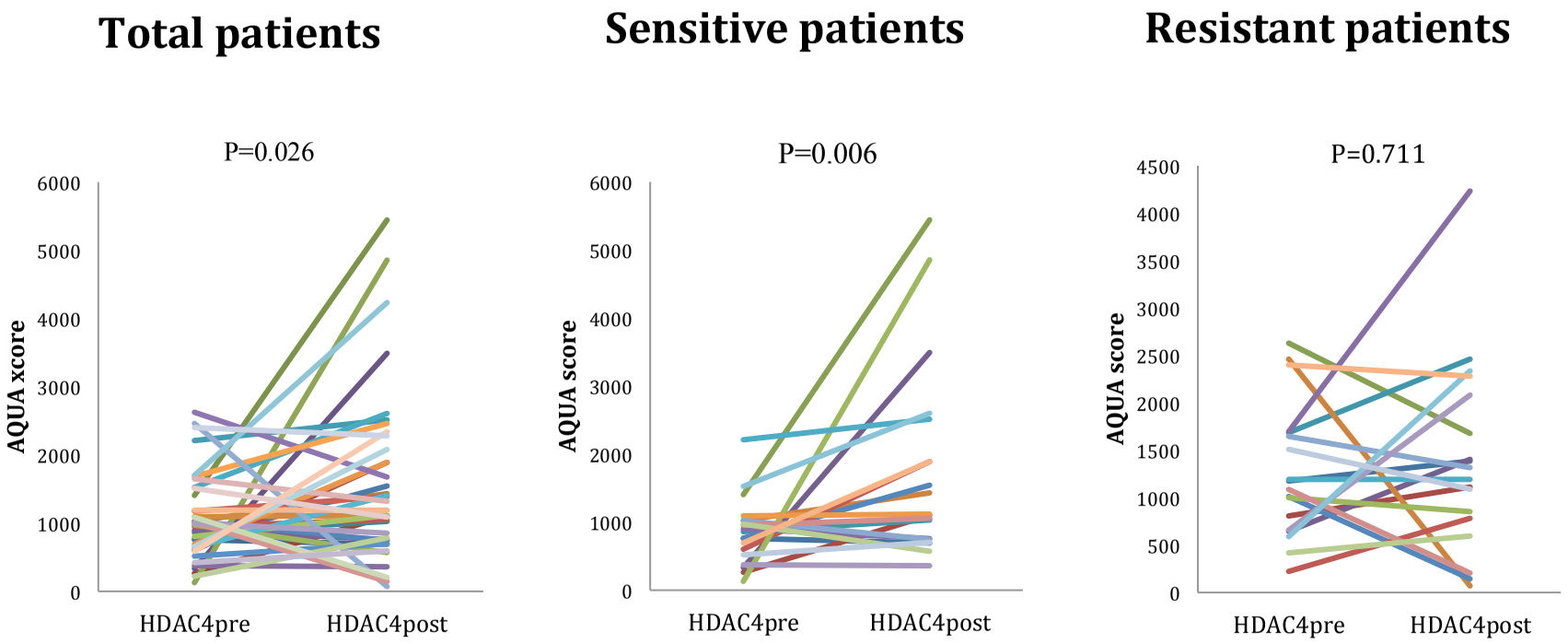

(Continued)

HDAC8

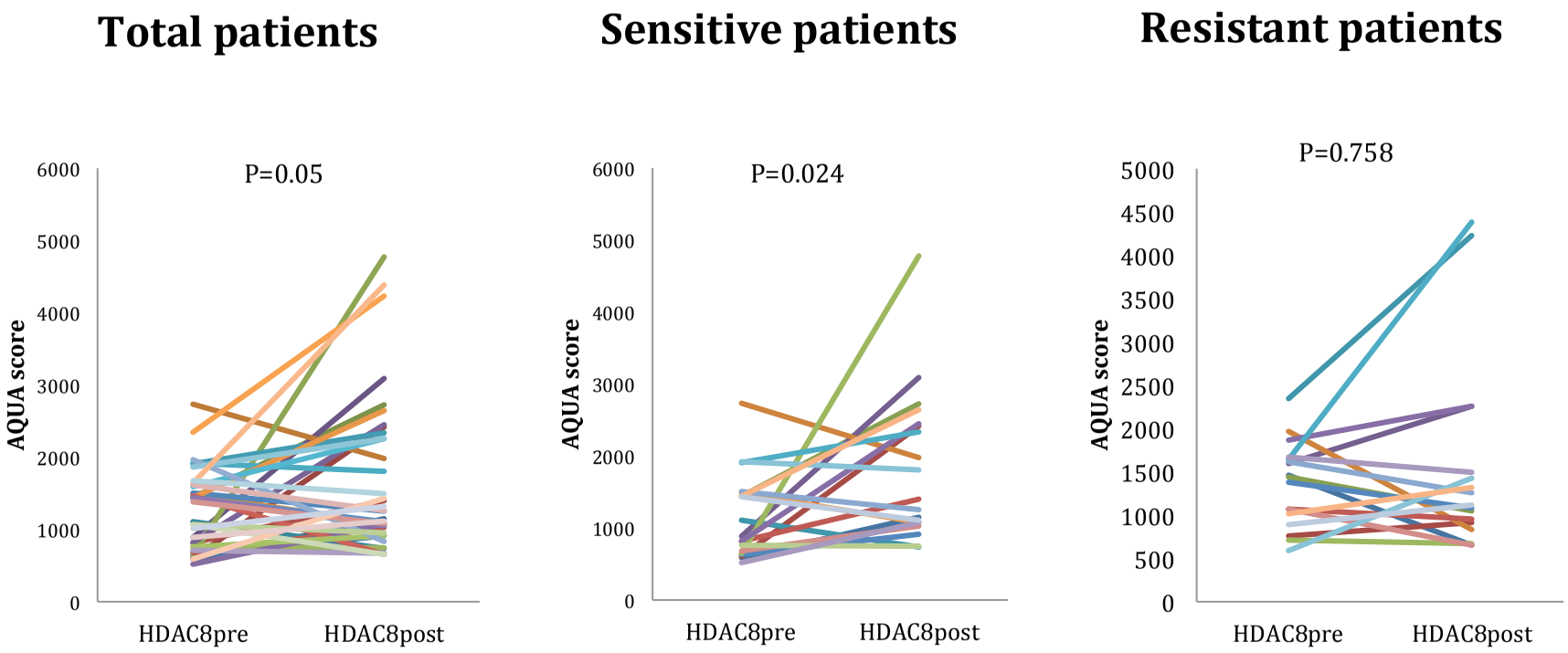

(Continued)

HP1α

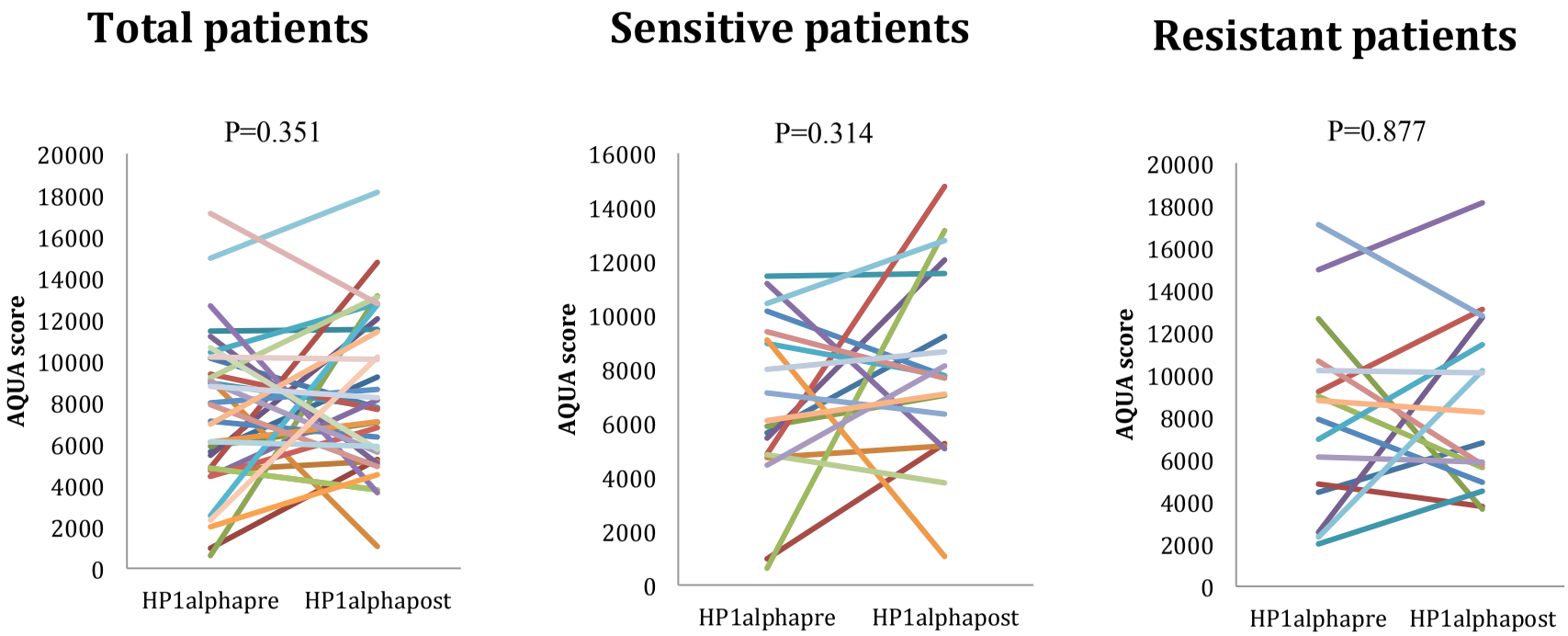

(Continued)

HP1β

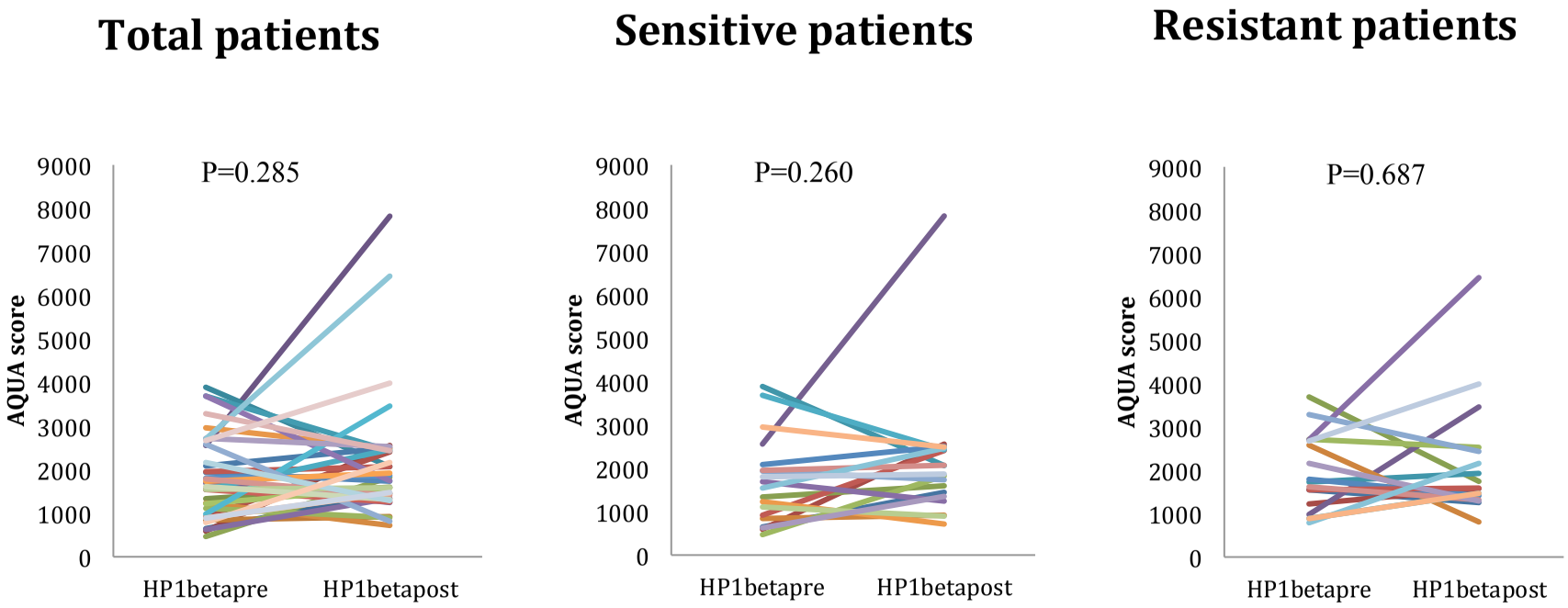

(Continued)

HP1γ

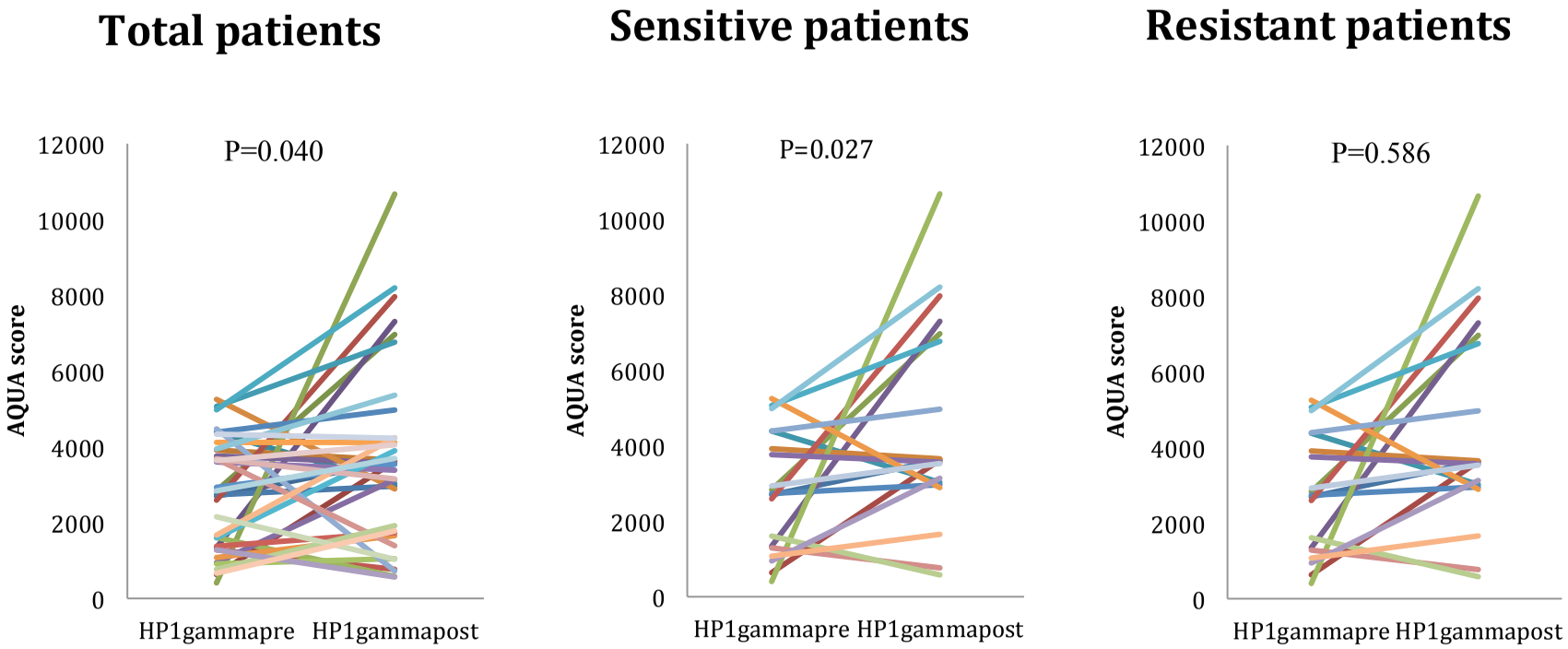
Total patients
P=0.040
12000
10000
8000
6000
4000
2000
0
AQUA score
HP1gammapre
HP1gammapost
Sensitive patients
P=0.027
12000
10000
8000
6000
4000
2000
0
AQUA score
HP1gammapre
HP1gammapost
Resistant patients
P=0.586
12000
10000
8000
6000
4000
2000
0
AQUA score
HP1gammapre
HP1gammapost

Figure S2 Comparison of nucelar texture parameters between paired samples from responsive ovarian cancer patients pre- and post-chemotherapy. (ASM=Angular Second Moment, IDM=Inverse Difference Moment)

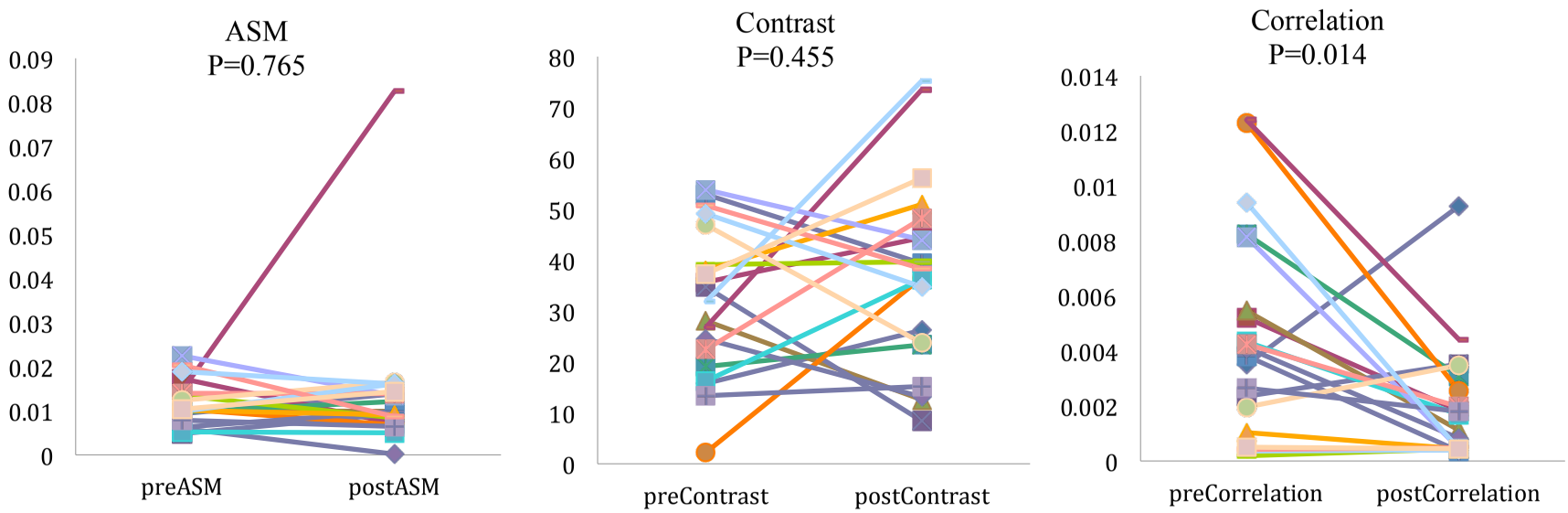

(Continued)

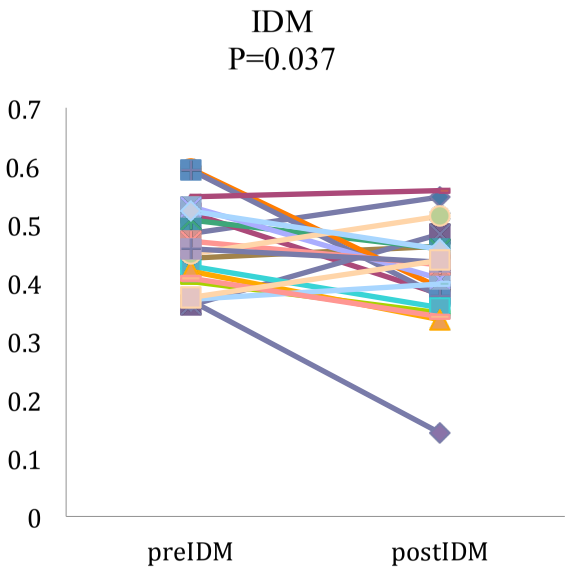
IDM
P=0.037
0.7
0.6
0.5
0.4
0.3
0.2
0.1
0
preIDM
postIDM

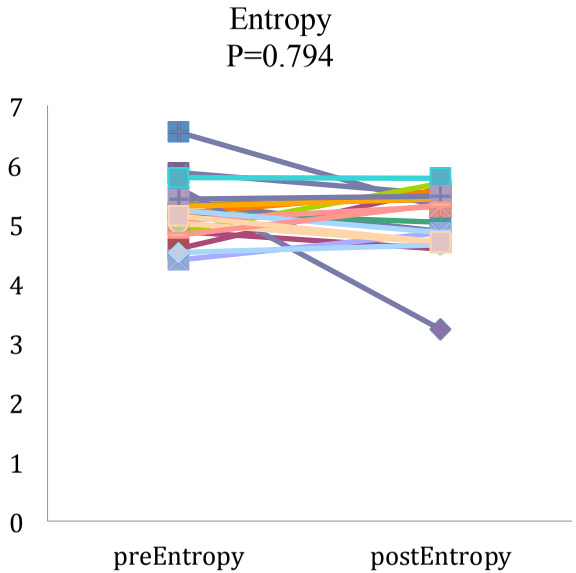
Entropy
P=0.794
7
6
5
4
3
2
1
0
preEntropy
postEntropy

Figure S3 Densitometry of relative protein expression levels after 24h cisplatin treatment in PEO1 and PEO4 cells. Column charts show the relative expression level of protein after cisplatin treatment normalized with untreated group. Data are presented as mean ratios of protein expression level after treatment over that in untreated group, erro bat represents SD from biological duplicate or triplicate samples.

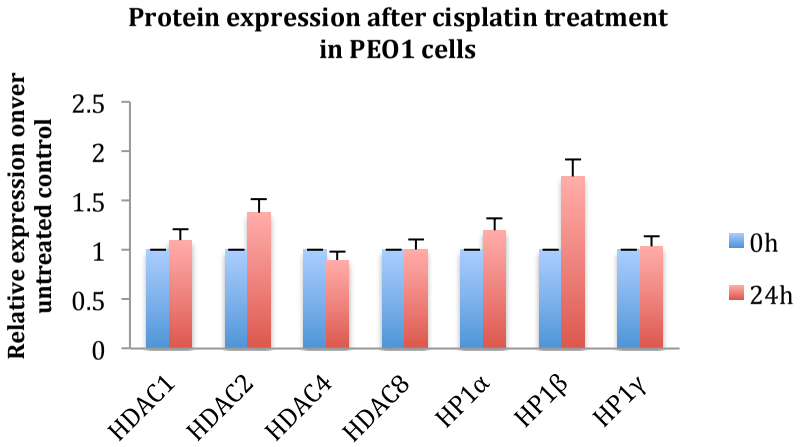

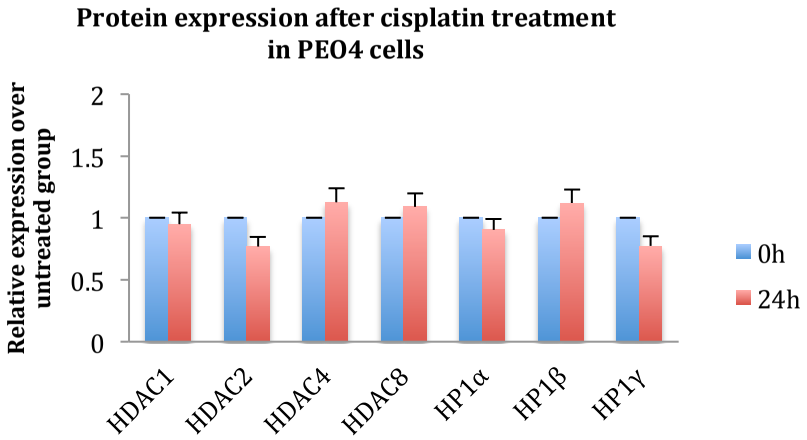

Figure S4 Densitometry of protein expression levels after time course cisplatin treatment in PEO1 cells. Column charts show the relative expression level of protein normalised with tubulin. Data are presented as a mean Integrated Intensity (I.I., correlated with the fluorescence intensity of second antibody) ratio of target protein over tubulin +SD from biological triplicate samples.

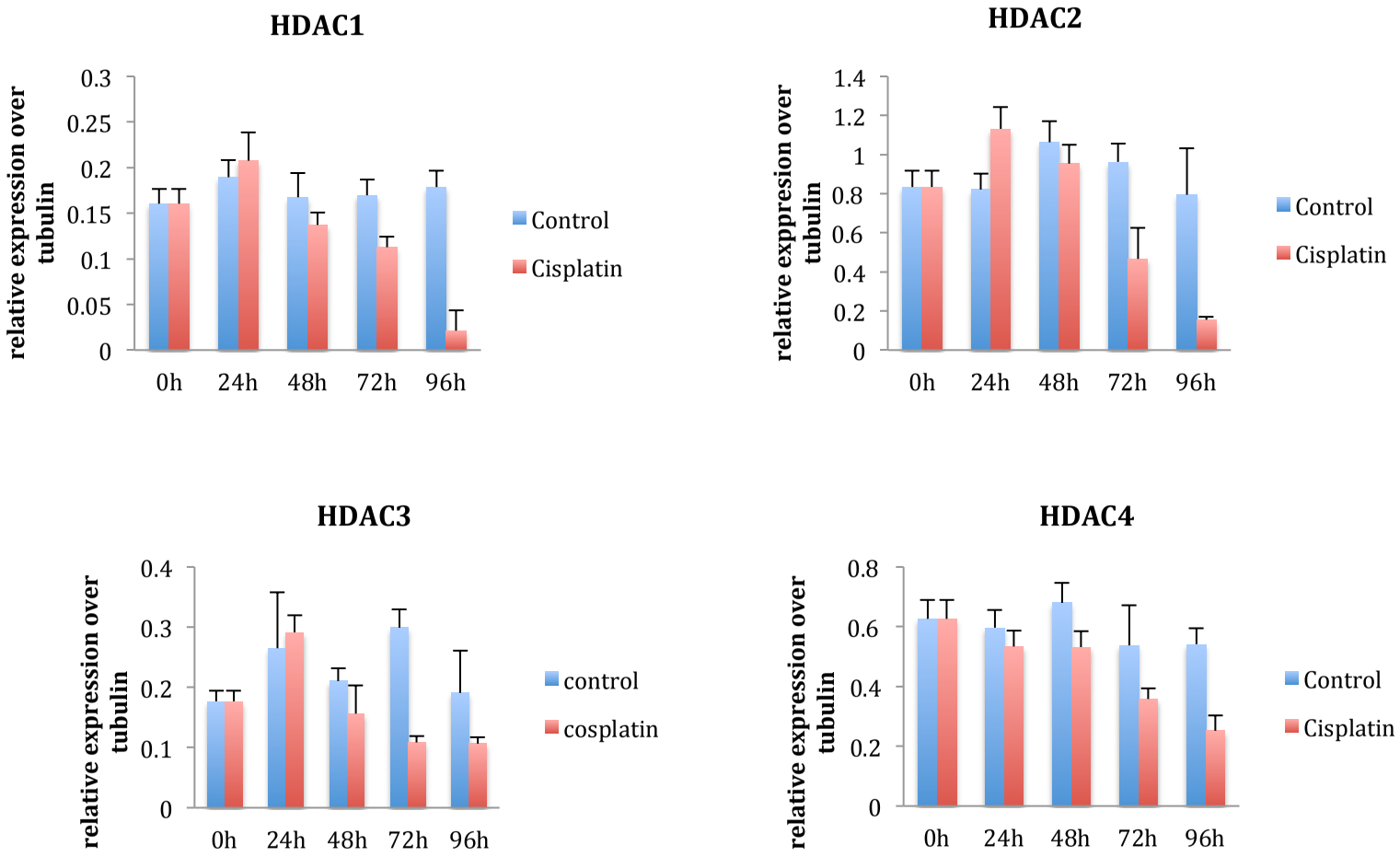

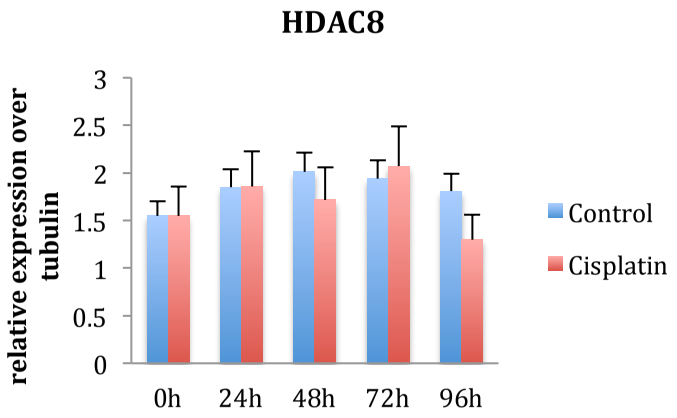
HDAC8
relative expression over tubulin
3
2.5
2
1.5
1
0.5
0
0h
24h
48h
72h
96h
Control
Cisplatin

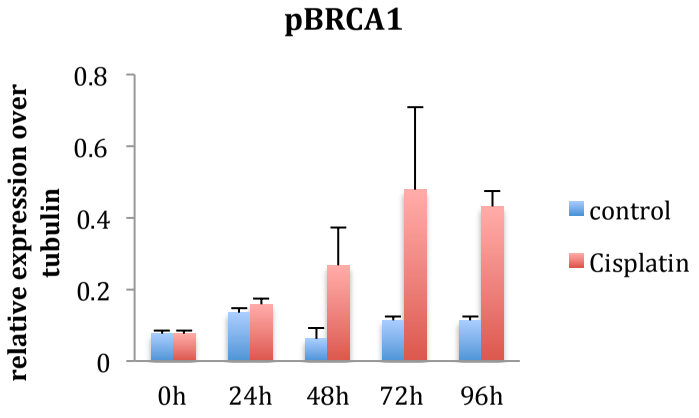
pBRCA1
relative expression over tubulin
0.8
0.6
0.4
0.2
0
0h
24h
48h
72h
96h
control
Cisplatin

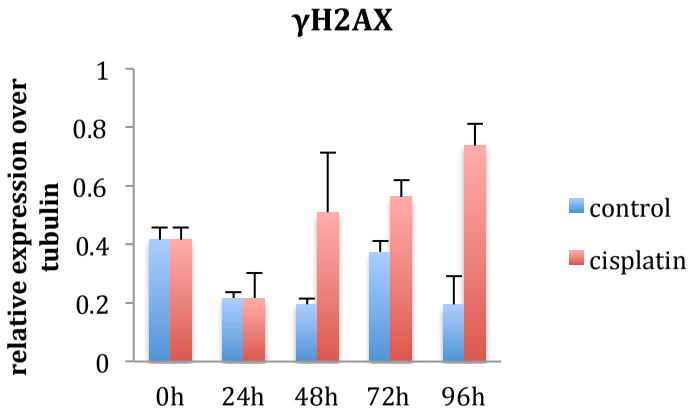
γH2AX
relative expression over tubulin
1
0.8
0.6
0.4
0.2
0
0h
24h
48h
72h
96h
control
cisplatin

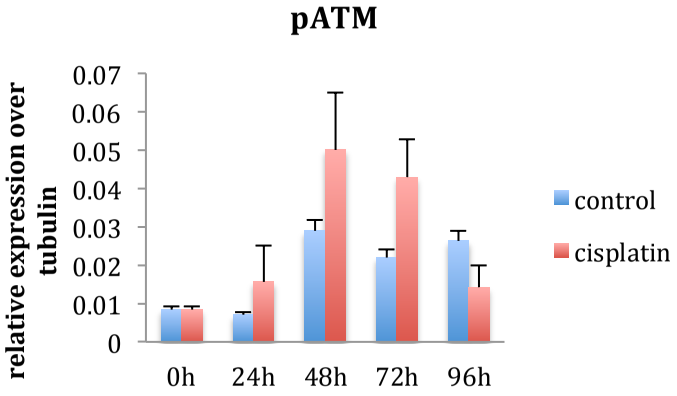
pATM
relative expression over tubulin
0.07
0.06
0.05
0.04
0.03
0.02
0.01
0
0h
24h
48h
72h
96h
control
cisplatin

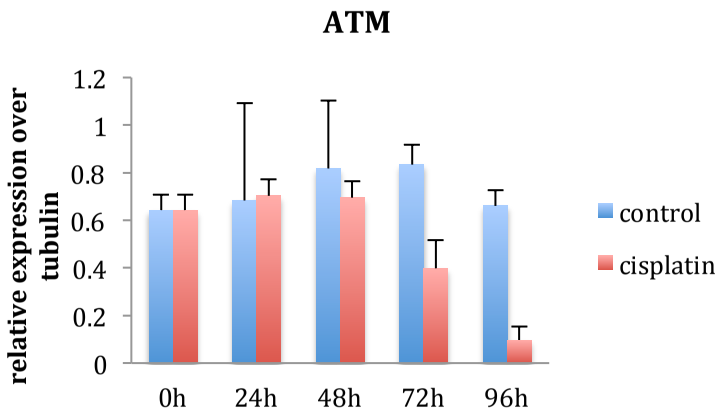
ATM
relative expression over tubulin
1.2
1
0.8
0.6
0.4
0.2
0
0h
24h
48h
72h
96h
control
cisplatin

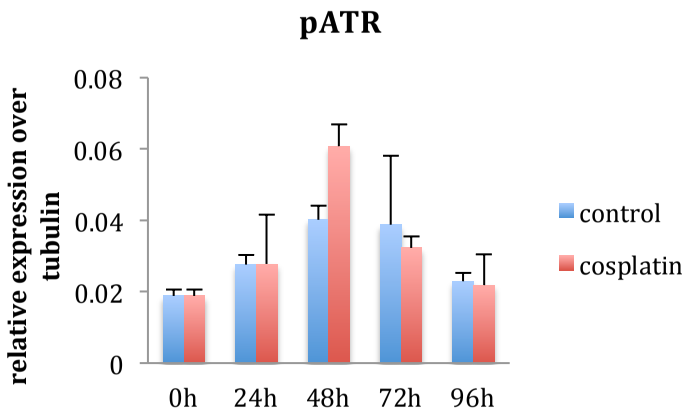
pATR
relative expression over tubulin
0.08
0.06
0.04
0.02
0
0h
24h
48h
72h
96h
control
cosplatin

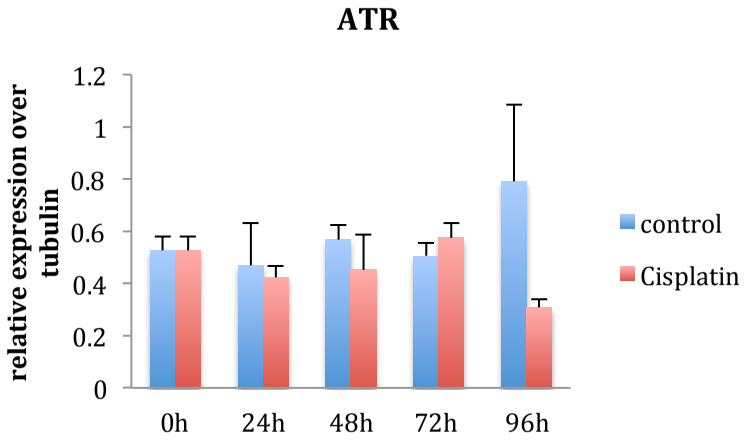
ATR
relative expression over tubulin
1.2
1
0.8
0.6
0.4
0.2
0
0h
24h
48h
72h
96h
control
Cisplatin

Figure S5 Densitometry of protein expression levels after HDAC2 depletion by SiRNA in PEO1 cells at 48h, 72h, 96h, and 120h. Column charts show the relative expression level of protein normalised with tubulin. Data are presented as Integrated Intensity (I.I., correlated with the fluorescence intensity of second antibody) ratio of target protein over tubulin

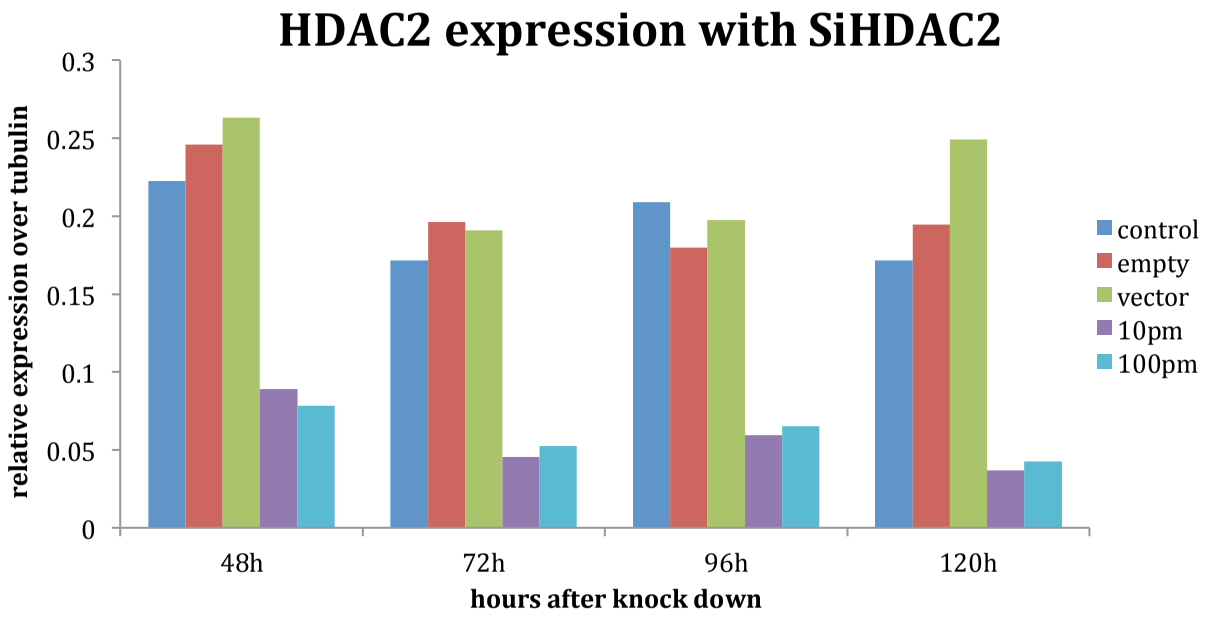

Figure S6 Densitometry of protein expression levels after HDAC2 depletion by SiRNA in PEO1 cells at 72h. Column charts show the relative expression level of protein normalised with tubulin. Data are presented as Integrated Intensity (I.I., correlated with the fluorescence intensity of second antibody) ratio of target protein over tubulin.

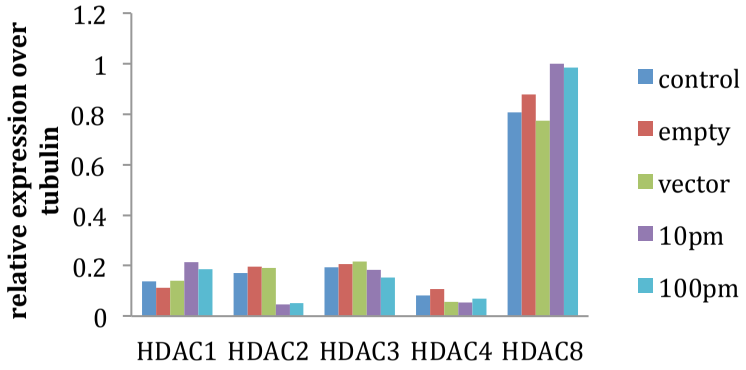

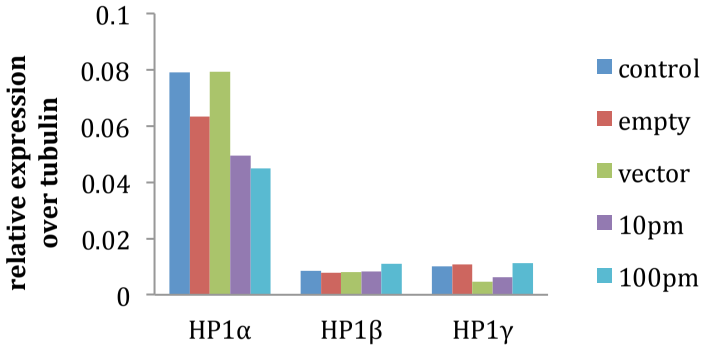

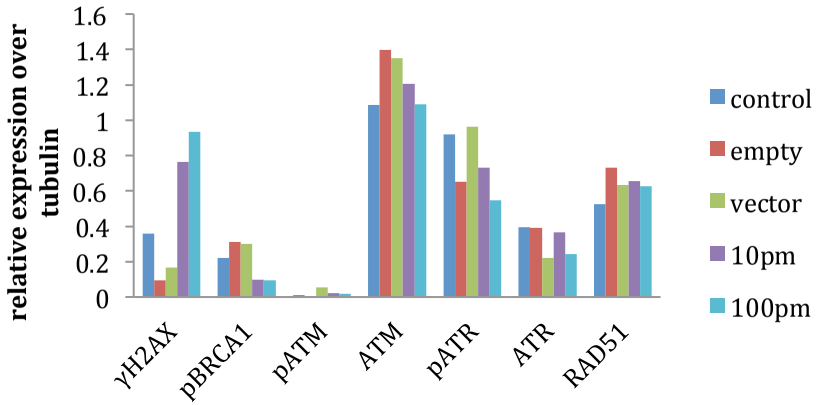

Figure S7 Densitometry of protein expression levels after cisplatin treatment with or without HDAC2 knockdown by siRNA in PEO1 cells at 6h, 24h, 48h, and 72h. Column charts show the relative expression level of protein normalised with tubulin. Data are presented as Integrated Intensity (I.I., correlated with the fluorescence intensity of second antibody) ratio of target protein over tubulin.

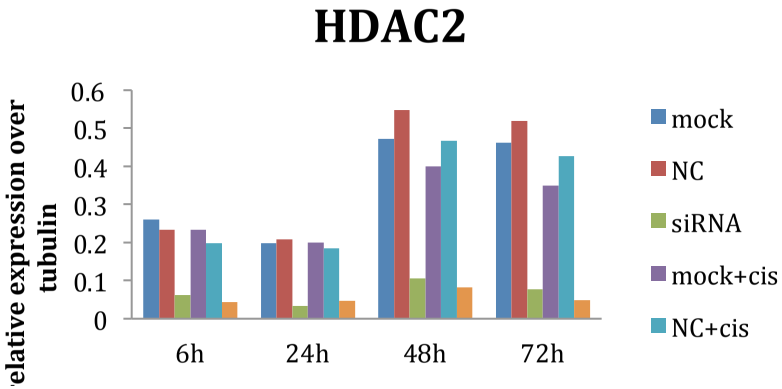

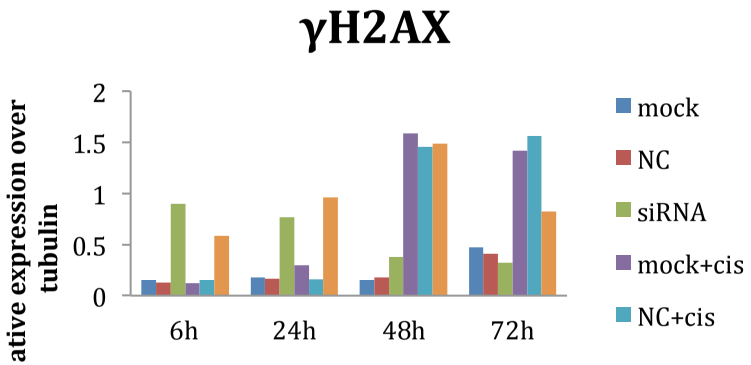

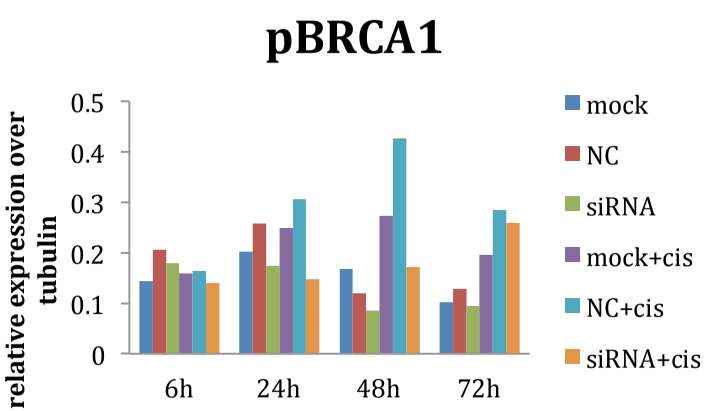

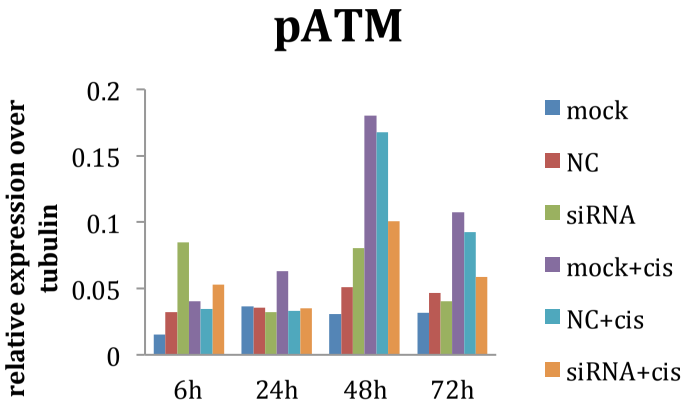

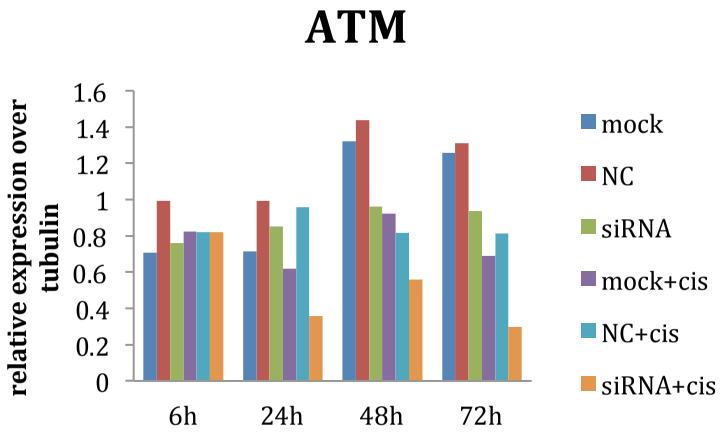
ATM
relative expression over tubulin
1.6
1.4
1.2
1
0.8
0.6
0.4
0.2
0
6h
24h
48h
72h
mock
NC
siRNA
mock+cis
NC+cis
siRNA+cis

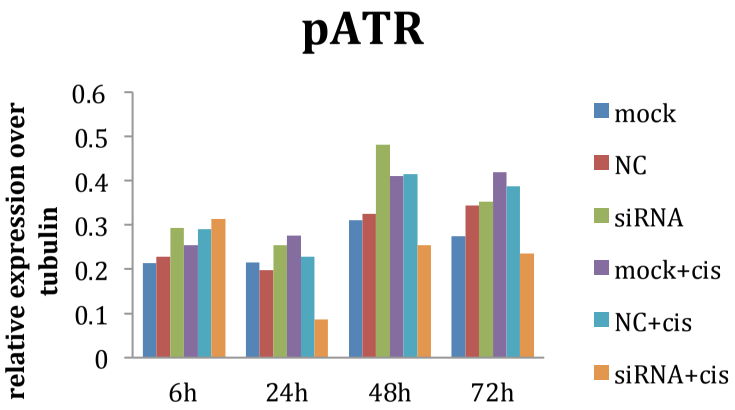
pATR
relative expression over tubulin
0.6
0.5
0.4
0.3
0.2
0.1
0
6h
24h
48h
72h
mock
NC
siRNA
mock+cis
NC+cis
siRNA+cis

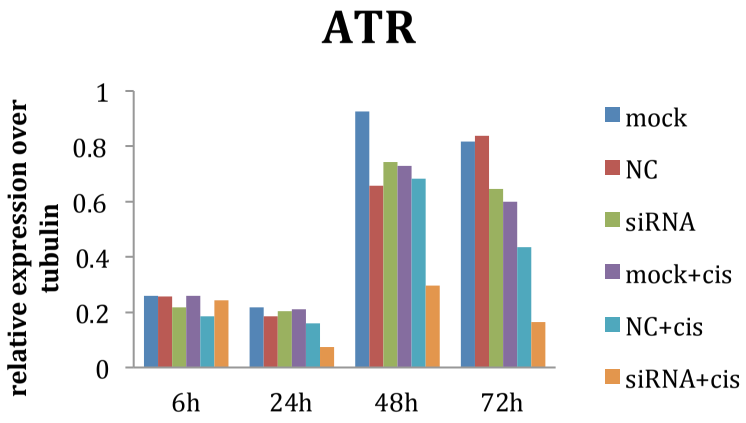
ATR
relative expression over tubulin
1
0.8
0.6
0.4
0.2
0
6h
24h
48h
72h
mock
NC
siRNA
mock+cis
NC+cis
siRNA+cis

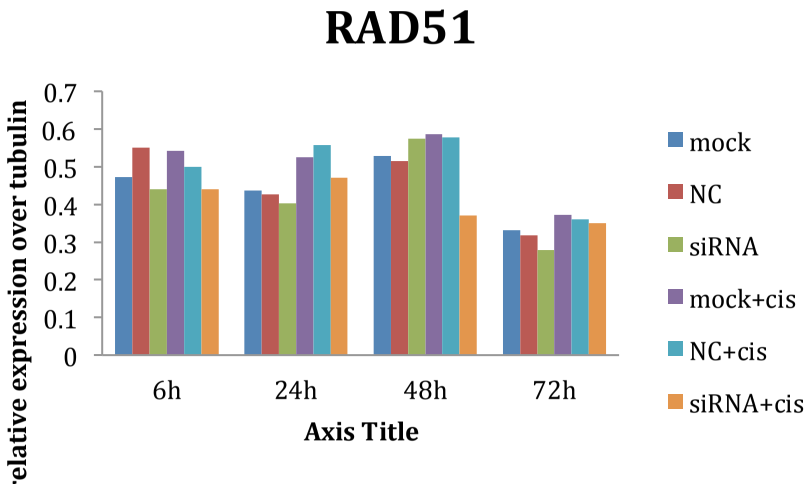
RAD51
relative expression over tubulin
0.7
0.6
0.5
0.4
0.3
0.2
0.1
0
6h
24h
48h
72h
Axis Title
mock
NC
siRNA
mock+cis
NC+cis
siRNA+cis

Figure S8 Densitometry of protein expression levels after cisplatin treatment with or without HDAC2 knockdown by siRNA in PEO4 cells at 6h, 24h, 48h, and 72h. Column charts show the relative expression level of protein normalised with tubulin. Data are presented as Integrated Intensity (I.I., correlated with the fluorescence intensity of second antibody) ratio of target protein over tubulin.

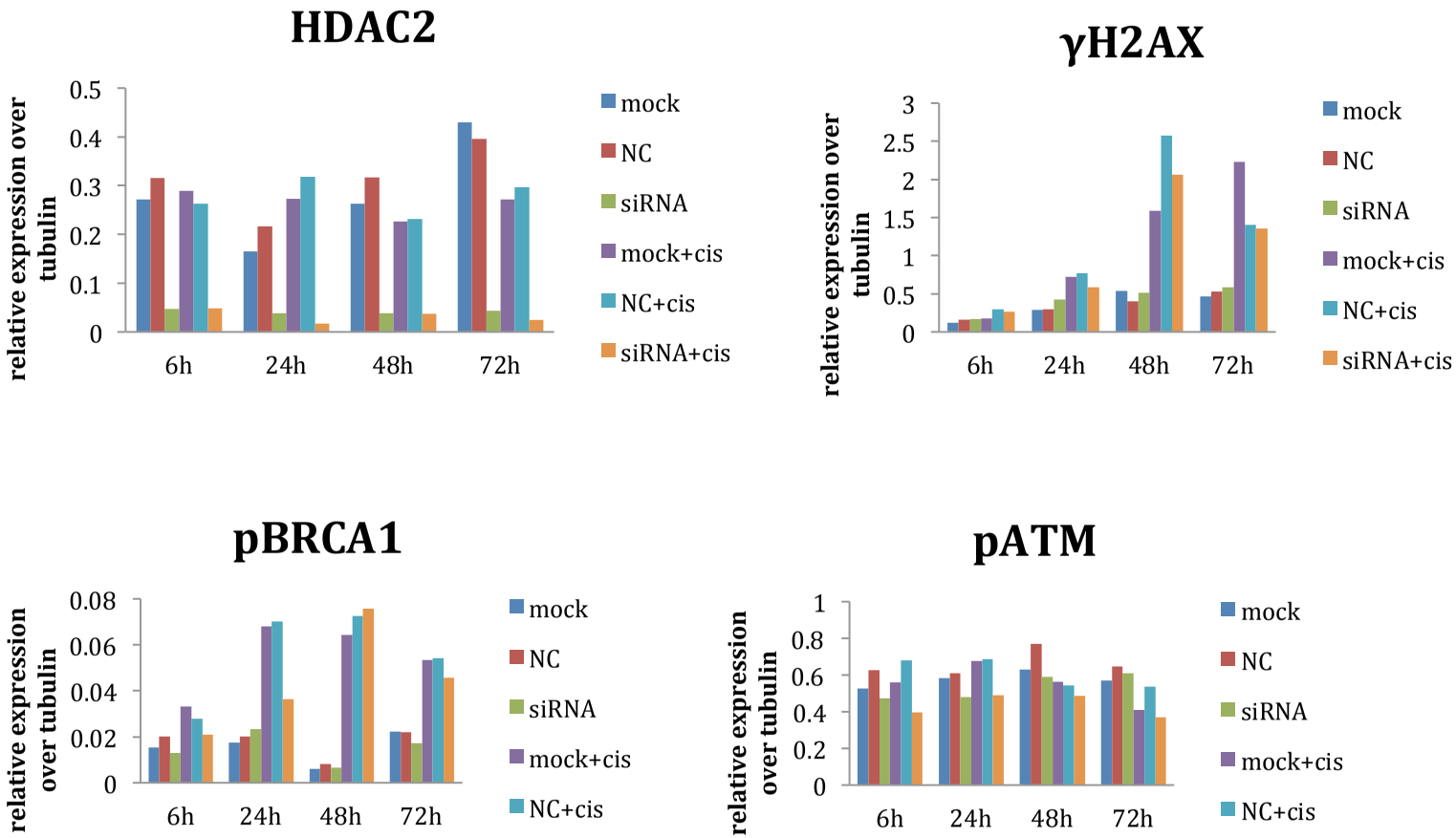

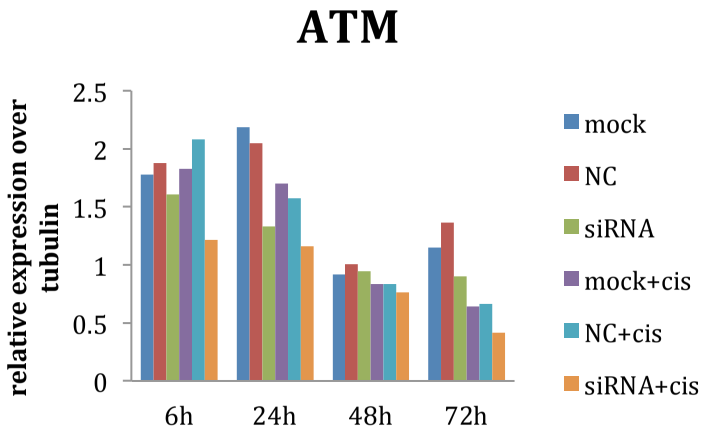
ATM
relative expression over tubulin
2.5
2
1.5
1
0.5
0
6h
24h
48h
72h
mock
NC
siRNA
mock+cis
NC+cis
siRNA+cis

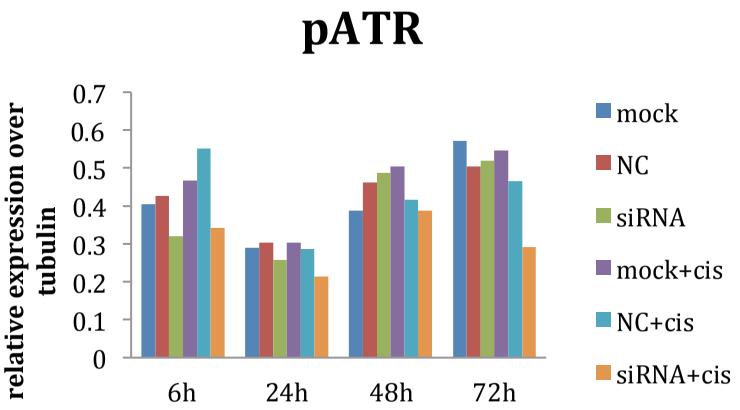
pATR
relative expression over tubulin
0.7
0.6
0.5
0.4
0.3
0.2
0.1
0
6h
24h
48h
72h
mock
NC
siRNA
mock+cis
NC+cis
siRNA+cis

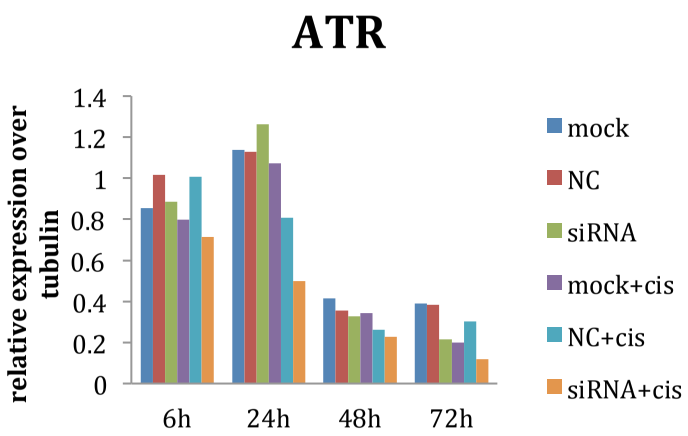
ATR
relative expression over tubulin
1.4
1.2
1
0.8
0.6
0.4
0.2
0
6h
24h
48h
72h
mock
NC
siRNA
mock+cis
NC+cis
siRNA+cis

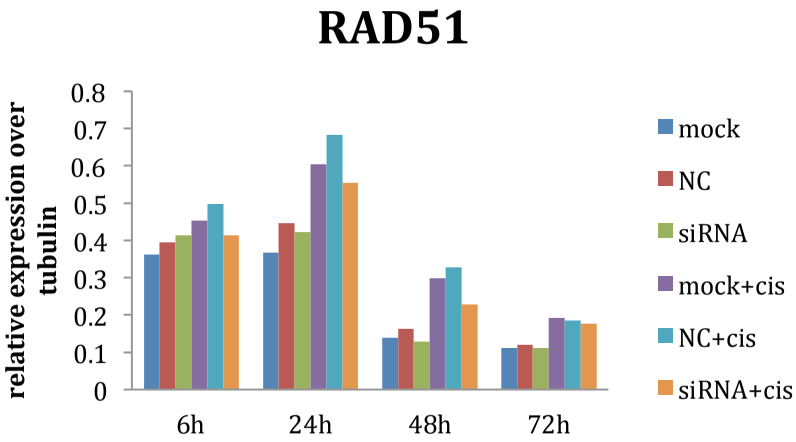
RAD51
relative expression over tubulin
0.8
0.7
0.6
0.5
0.4
0.3
0.2
0.1
0
6h
24h
48h
72h
mock
NC
siRNA
mock+cis
NC+cis
siRNA+cis

5.2 Supplement Materials

5.2.1 Cell culture reagents

Product	*Manufactures or Supplier/Catalogue No.*
Penicillin / Streptomycin	Invitrogen/15140-122
Trypsin-EDTA	Invitrogen/25300
Dulbecco's minimal essential media (DMEM)	Gibco/21875-091
Fetal calf serum	Harlen Sera-Lab LTD/S-0001 AE
PBS tablets	OXOID/BR0014G

5.2.2 Reagents for treatment

Product	*Manufactures/Supplier*
Trichostatin A (TSA)	Calbiochem
Cisplatin	TEVA

5.2.3 Reagents for protein detection in cell lines

Product	*Manufactures or Supplier/catalogue*
Mini complete protease inhibitor cocktail tablets	Sigma Aldrich/A6279
Aprotinin	Sigma Aldrich/P2850
Phosphatase inhibitor cocktail 1	Sigma Aldrich/P5726
Phosphatase inhibitor cocktail 2	Biochain Institute, Inc., CA, USA/K3013010
CNMCS Compartmental Protein Extraction Kit	Severn Biotech Ltd/20-2100-05
30% acrylamide/Bis acrylamide stock solution	BioRad/161-0801
TEMED	BDH Laboratory supplies /102246L
2-Propanol	BDH Laboratory supplies /261296H
Methanol	BioRad/170-6531
PVDF membrane	Millipore/IPVH304F0

Tween-20	Roche Applied Science/11836153001
Odyssey Blocking Buffer	LI-COR Biosciences/927-40000

5.2.4 Reagents for protein detection in tumours

Product	*Manufactures/Supplier*
DAKO Protein Block	
Serum Free	Dako/X0909
DAKO Antibody Diluent	Dako/X0909
Dako Envision+System-	
HRP labelled polymer	Dako/S0809
Anti-rabbit	Dako/ K4003
Dako Envision+System-	
HRP labelled polymer	
Anti-mouse	Dako/ K4001
DAB chromogen	
Mouse anti-cytokeratin	Dako/K5007
(Pan) antibody	Invitrogen/18-0132
Goat anti-mouse Alexa555 antibody	Invitrogen/A21422

Aquantiplex™ assay kit	HistoRX/AQ-EMR1-0001
Prolong Gold anti-fade reagent with DAPI	Invitrogen/P369

Information about other reagents and equipments used is detailed in Materials and Methods.

References:

Acharya, M. R., A. Sparreboom, et al. (2005). "Rational development of histone deacetylase inhibitors as anticancer agents: a review." Mol Pharmacol **68**(4): 917-932.

Adcock, I. M., P. Ford, et al. (2006). "Epigenetics and airways disease." Respiratory research **7**: 21.

Adimoolam, S., M. Sirisawad, et al. (2007). "HDAC inhibitor PCI-24781 decreases RAD51 expression and inhibits homologous recombination." Proceedings of the National Academy of Sciences of the United States of America **104**(49): 19482-19487.

Akahira, J., Y. Sugihashi, et al. (2004). "Decreased expression of 14-3-3 sigma is associated with advanced disease in human epithelial ovarian cancer: its correlation with aberrant DNA methylation." Clinical cancer research : an official journal of the American Association for Cancer Research **10**(8): 2687-2693.

Akhtar, A. and G. Cavalli (2005). "The epigenome network of excellence." PLoS Biol **3**(5): e177.

Alvarenga, A. V., W. C. Pereira, et al. (2007). "Complexity curve and grey level co-occurrence matrix in the texture evaluation of breast tumor on ultrasound images." Medical physics **34**(2): 379-387.

Arafa el, S. A., Q. Zhu, et al. (2009). "Tangeretin sensitizes cisplatin-resistant human ovarian cancer cells through downregulation of phosphoinositide 3-kinase/Akt signaling pathway." Cancer research **69**(23): 8910-8917.

Atsumi, Y., A. Inase, et al. (2013). "The Arf/p53 protein module, which induces apoptosis, down-regulates histone H2AX to allow normal cells to survive in the presence of anti-cancer drugs." The Journal of biological chemistry **288**(19): 13269-13277.

Ayoub, N., A. D. Jeyasekharan, et al. (2008). "HP1-beta mobilization promotes chromatin changes that initiate the DNA damage response." Nature **453**(7195): 682-686.

Bakkenist, C. J. and M. B. Kastan (2003). "DNA damage activates ATM through intermolecular autophosphorylation and dimer dissociation." Nature **421**(6922): 499-506.

Baldeyron, C., G. Soria, et al. (2011). "HP1alpha recruitment to DNA damage by p150CAF-1 promotes homologous recombination repair." The Journal of cell biology **193**(1): 81-95.

Bassa, B. V., D. D. Roh, et al. (1999). "Lysophosphatidylcholine activates mesangial cell PKC and MAP kinase by PLCgamma-1 and tyrosine kinase-Ras pathways." The American journal of physiology **277**(3 Pt 2): F328-337.

Basu, A. and S. Krishnamurthy (2010). "Cellular responses to Cisplatin-induced DNA damage." Journal of nucleic acids **2010**.

Baumann, P. and S. C. West (1998). "Role of the human RAD51 protein in homologous recombination and double-stranded-break repair." Trends in biochemical sciences **23**(7): 247-251.

Blaheta, R. A. and J. Cinatl, Jr. (2002). "Anti-tumor mechanisms of valproate: a novel role for an old drug." Medicinal research reviews **22**(5): 492-511.

Bradley, D., D. Rathkopf, et al. (2009). "Vorinostat in advanced prostate cancer patients progressing on prior chemotherapy (National Cancer Institute Trial 6862): trial results and interleukin-6 analysis: a study by the Department of Defense Prostate Cancer Clinical Trial Consortium and University of Chicago Phase 2 Consortium." Cancer **115**(23): 5541-5549.

Burdak-Rothkamm, S., S. C. Short, et al. (2007). "ATR-dependent radiation-induced gamma H2AX foci in bystander primary human astrocytes and glioma cells." Oncogene **26**(7): 993-1002.

Camp, R. L., G. G. Chung, et al. (2002). "Automated subcellular localization and quantification of protein expression in tissue microarrays." Nat Med **8**(11): 1323-1327.

Chapman, J. R., M. R. Taylor, et al. (2012). "Playing the end game: DNA double-strand break repair pathway choice." Molecular cell **47**(4): 497-510.

Chen, C. C., J. J. Carson, et al. (2008). "Acetylated lysine 56 on histone H3 drives chromatin assembly after repair and signals for the completion of repair." Cell **134**(2): 231-243.

Chen, W. K., Y. Chen, et al. (2004). "[Effect of trichostatin A on histone acetylation level and apoptosis in HL-60 cells]." Zhongguo shi yan xue ye xue za zhi / Zhongguo bing li sheng li xue hui = Journal of experimental hematology / Chinese Association of Pathophysiology **12**(3): 324-328.

Cheutin, T., A. J. McNairn, et al. (2003). "Maintenance of stable heterochromatin domains by dynamic HP1 binding." Science **299**(5607): 721-725.

Chinnaiyan, P., S. Varambally, et al. (2006). "Enhancing the antitumor activity of ErbB blockade with histone deacetylase (HDAC) inhibition." International journal of cancer. Journal international du cancer **118**(4): 1041-1050.

Chiolo, I., A. Minoda, et al. (2011). "Double-strand breaks in heterochromatin move outside of a dynamic HP1a domain to complete recombinational repair." Cell **144**(5): 732-744.

Cieslik, K., C. S. Abrams, et al. (2001). "Up-regulation of endothelial nitric-oxide synthase promoter by the phosphatidylinositol 3-kinase gamma /Janus kinase 2/MEK-1-dependent pathway." The Journal of biological chemistry **276**(2): 1211-1219.

Clingen, P. H., J. Y. Wu, et al. (2008). "Histone H2AX phosphorylation as a molecular pharmacological marker for DNA interstrand crosslink cancer chemotherapy." Biochem Pharmacol **76**(1): 19-27.

Comess, K. M., J. N. Burstyn, et al. (1992). "Replication inhibition and translesion synthesis on templates containing site-specifically placed cis-diamminedichloroplatinum(II) DNA adducts." Biochemistry **31**(16): 3975-3990.

Cooke, S. L., C. K. Ng, et al. (2010). "Genomic analysis of genetic heterogeneity and evolution in high-grade serous ovarian carcinoma." Oncogene **29**(35): 4905-4913.

Corbett, N. P., D. Blimkie, et al. (2010). "Ontogeny of Toll-like receptor mediated cytokine responses of human blood mononuclear cells." PLoS One **5**(11): e15041.

Cowell, I. G., N. J. Sunter, et al. (2007). "gammaH2AX foci form preferentially in euchromatin after ionising-radiation." PLoS One **2**(10): e1057.

Das, B. R. (1993). "Increased ADP-ribosylation of histones in oral cancer." Cancer Lett **73**(1): 29-34.

Davie, J. R. (2003). "Inhibition of histone deacetylase activity by butyrate." J Nutr **133**(7 Suppl): 2485S-2493S.

de Ruijter, A. J., A. H. van Gennip, et al. (2003). "Histone deacetylases (HDACs): characterization of the classical HDAC family." The Biochemical journal **370**(Pt 3): 737-749.

Deans, A. J. and S. C. West (2011). "DNA interstrand crosslink repair and cancer." Nature reviews. Cancer **11**(7): 467-480.

Deng, C. X. (2006). "BRCA1: cell cycle checkpoint, genetic instability, DNA damage response and cancer evolution." Nucleic acids research **34**(5): 1416-1426.

Di Bussolo, V. and F. Minutolo (2011). "Curaxins: a new family of non-genotoxic multitargeted anticancer agents." ChemMedChem **6**(12): 2133-2136.

Di Micco, R., G. Sulli, et al. (2011). "Interplay between oncogene-induced DNA damage response and heterochromatin in senescence and cancer." Nature cell biology **13**(3): 292-302.

Dialynas, G. K., M. W. Vitalini, et al. (2008). "Linking Heterochromatin Protein 1 (HP1) to cancer progression." Mutat Res **647**(1-2): 13-20.

Dinant, C. and M. S. Luijsterburg (2009). "The emerging role of HP1 in the DNA damage response." Molecular and cellular biology **29**(24): 6335-6340.

Duvic, M., R. Talpur, et al. (2007). "Phase 2 trial of oral vorinostat (suberoylanilide hydroxamic acid, SAHA) for refractory cutaneous T-cell lymphoma (CTCL)." Blood **109**(1): 31-39.

Ehrlich, M., M. A. Gama-Sosa, et al. (1982). "Amount and distribution of 5-methylcytosine in human DNA from different types of tissues of cells." Nucleic acids research **10**(8): 2709-2721.

Elia, M. C. and M. O. Bradley (1992). "Influence of chromatin structure on the induction of DNA double strand breaks by ionizing radiation." Cancer research **52**(6): 1580-1586.

Felici, A., J. Verweij, et al. (2002). "Dosing strategies for anticancer drugs: the good, the bad and body-surface area." European journal of cancer **38**(13): 1677-1684.

Fenaux, P., G. J. Mufti, et al. (2009). "Efficacy of azacitidine compared with that of conventional care regimens in the treatment of higher-risk myelodysplastic syndromes: a randomised, open-label, phase III study." The lancet oncology **10**(3): 223-232.

Fernandez-Capetillo, O., A. Celeste, et al. (2003). "Focusing on foci: H2AX and the recruitment of DNA-damage response factors." Cell Cycle **2**(5): 426-427.

Fischle, W., Y. Wang, et al. (2003). "Histone and chromatin cross-talk." Curr Opin Cell Biol **15**(2): 172-183.

Fitzgerald, D. J., C. DeLuca, et al. (2004). "Reaction cycle of the yeast Isw2 chromatin remodeling complex." EMBO J **23**(19): 3836-3843.

Fog, C. K., K. T. Jensen, et al. (2007). "Chromatin-modifying proteins in cancer." APMIS **115**(10): 1060-1089.

Fraga, M. F., E. Ballestar, et al. (2005). "Loss of acetylation at Lys16 and trimethylation at Lys20 of histone H4 is a common hallmark of human cancer." Nature genetics **37**(4): 391-400.

Fuertes, M. A., C. Alonso, et al. (2003). "Biochemical modulation of Cisplatin mechanisms of action: enhancement of antitumor activity and circumvention of drug resistance." Chemical reviews **103**(3): 645-662.

Galluzzi, L., L. Senovilla, et al. (2012). "Molecular mechanisms of cisplatin resistance." Oncogene **31**(15): 1869-1883.

Gibbons, R. J. (2005). "Histone modifying and chromatin remodelling enzymes in cancer and dysplastic syndromes." Hum Mol Genet **14 Spec No 1**: R85-92.

Gius, D., H. Cui, et al. (2004). "Distinct effects on gene expression of chemical and genetic manipulation of the cancer epigenome revealed by a multimodality approach." Cancer cell **6**(4): 361-371.

Gronbaek, K., C. Hother, et al. (2007). "Epigenetic changes in cancer." APMIS **115**(10): 1039-1059.

Groocock, L. M., J. Prudden, et al. (2012). "The RecQ4 orthologue Hrq1 is critical for DNA interstrand cross-link repair and genome stability in fission yeast." Molecular and cellular biology **32**(2): 276-287.

Gui, C. Y., L. Ngo, et al. (2004). "Histone deacetylase (HDAC) inhibitor activation of p21WAF1 involves changes in promoter-associated proteins, including HDAC1." Proc Natl Acad Sci U S A **101**(5): 1241-1246.

Halicka, H. D., X. Huang, et al. (2005). "Histone H2AX phosphorylation after cell irradiation with UV-B: relationship to cell cycle phase and induction of apoptosis." Cell cycle **4**(2): 339-345.

Handelsman, J., M. R. Rondon, et al. (1998). "Molecular biological access to the chemistry of unknown soil microbes: a new frontier for natural products." Chemistry & biology **5**(10): R245-249.

Harms, K. L. and X. Chen (2007). "Histone deacetylase 2 modulates p53 transcriptional activities through regulation of p53-DNA binding activity." Cancer research **67**(7): 3145-3152.

Harper, J. W. and S. J. Elledge (2007). "The DNA damage response: ten years after." Molecular cell **28**(5): 739-745.

Hartlerode, A. J. and R. Scully (2009). "Mechanisms of double-strand break repair in somatic mammalian cells." The Biochemical journal **423**(2): 157-168.

Hassa, P. O. and M. O. Hottiger (2005). "An epigenetic code for DNA damage repair pathways?" Biochem Cell Biol **83**(3): 270-285.

Hayashi, A., A. Horiuchi, et al. (2010). "Type-specific roles of histone deacetylase (HDAC) overexpression in ovarian carcinoma: HDAC1 enhances cell proliferation and HDAC3 stimulates cell migration with downregulation of E-cadherin." International journal of cancer. Journal international du cancer **127**(6): 1332-1346.

Hirning, T., I. Zuna, et al. (1989). "Quantification and classification of echographic findings in the thyroid gland by computerized B-mode texture analysis." European journal of radiology **9**(4): 244-247.

Ho, L. and G. R. Crabtree (2010). "Chromatin remodelling during development." Nature **463**(7280): 474-484.

Hoeijmakers, J. H. (2001). "Genome maintenance mechanisms for preventing cancer." Nature **411**(6835): 366-374.

Huang, B. H., M. Laban, et al. (2005). "Inhibition of histone deacetylase 2 increases apoptosis and p21Cip1/WAF1 expression, independent of histone deacetylase 1." Cell death and differentiation **12**(4): 395-404.

Huang, X., A. Kurose, et al. (2006). "Sequential phosphorylation of Ser-10 on histone H3 and ser-139 on histone H2AX and ATM activation during premature chromosome condensation: relationship to cell-cycle phase and apoptosis." Cytometry. Part A : the journal of the International Society for Analytical Cytology **69**(4): 222-229.

Huang, X., M. Okafuji, et al. (2004). "Assessment of histone H2AX phosphorylation induced by DNA topoisomerase I and II inhibitors topotecan and mitoxantrone and by the DNA cross-linking agent cisplatin." Cytometry A **58**(2): 99-110.

Huang, X., F. Traganos, et al. (2003). "DNA damage induced by DNA topoisomerase I- and topoisomerase II-inhibitors detected by histone H2AX phosphorylation in relation to the cell cycle phase and apoptosis." Cell cycle **2**(6): 614-619.

Iacovoni, J. S., P. Caron, et al. (2010). "High-resolution profiling of gammaH2AX around DNA double strand breaks in the mammalian genome." The EMBO journal **29**(8): 1446-1457.

James, T. C., J. C. Eissenberg, et al. (1989). "Distribution patterns of HP1, a heterochromatin-associated nonhistone chromosomal protein of Drosophila." Eur J Cell Biol **50**(1): 170-180.

Jeggo, P. A., V. Geuting, et al. (2011). "The role of homologous recombination in radiation-induced double-strand break repair." Radiotherapy and oncology : journal of the European Society for Therapeutic Radiology and Oncology **101**(1): 7-12.

Jeppesen, P. (1997). "Histone acetylation: a possible mechanism for the inheritance of cell memory at mitosis." Bioessays **19**(1): 67-74.

Jin, K. L., J. H. Pak, et al. (2008). "Expression profile of histone deacetylases 1, 2 and 3 in ovarian cancer tissues." Journal of gynecologic oncology **19**(3): 185-190.

Johnstone, R. W. and J. D. Licht (2003). "Histone deacetylase inhibitors in cancer therapy: is transcription the primary target?" Cancer Cell **4**(1): 13-18.

Jones, P. A. and S. B. Baylin (2007). "The epigenomics of cancer." Cell **128**(4): 683-692.

Joseph, G. B., T. Baum, et al. (2011). "Texture analysis of cartilage T2 maps: individuals with risk factors for OA have higher and more heterogeneous knee cartilage MR T2 compared to normal controls--data from the osteoarthritis initiative." Arthritis research & therapy **13**(5): R153.

Jurkin, J., G. Zupkovitz, et al. (2011). "Distinct and redundant functions of histone deacetylases HDAC1 and HDAC2 in proliferation and tumorigenesis." Cell cycle **10**(3): 406-412.

Kao, G. D., W. G. McKenna, et al. (2003). "Histone deacetylase 4 interacts with 53BP1 to mediate the DNA damage response." The Journal of cell biology **160**(7): 1017-1027.

Kartalou, M. and J. M. Essigmann (2001). "Mechanisms of resistance to cisplatin." Mutation research **478**(1-2): 23-43.

Kee, Y. and A. D. D'Andrea (2010). "Expanded roles of the Fanconi anemia pathway in preserving genomic stability." Genes & development **24**(16): 1680-1694.

Kelland, L. (2007). "The resurgence of platinum-based cancer chemotherapy." Nature reviews. Cancer **7**(8): 573-584.

Kelly, T. K., D. D. De Carvalho, et al. (2010). "Epigenetic modifications as therapeutic targets." Nature biotechnology **28**(10): 1069-1078.

Kerr, J. F., C. M. Winterford, et al. (1994). "Apoptosis. Its significance in cancer and cancer therapy." Cancer **73**(8): 2013-2026.

Khan, O. and N. B. La Thangue (2012). "HDAC inhibitors in cancer biology: emerging mechanisms and clinical applications." Immunology and cell biology **90**(1): 85-94.

Kim, H. J. and S. C. Bae (2011). "Histone deacetylase inhibitors: molecular mechanisms of action and clinical trials as anti-cancer drugs." American journal of translational research **3**(2): 166-179.

Kim, H. L., S. U. Kim, et al. (2013). "A novel role for Gadd45alpha in base excision repair: modulation of APE1 activity by the direct interaction of Gadd45alpha with PCNA." Biochemical and biophysical research communications **434**(2): 185-190.

Kim, J. A., M. Kruhlak, et al. (2007). "Heterochromatin is refractory to gamma-H2AX modification in yeast and mammals." The Journal of cell biology **178**(2): 209-218.

Kirschmann, D. A., R. A. Lininger, et al. (2000). "Down-regulation of HP1Hsalpha expression is associated with the metastatic phenotype in breast cancer." Cancer Res **60**(13): 3359-3363.

Klenova, E. and R. Ohlsson (2005). "Poly(ADP-ribosyl)ation and epigenetics. Is CTCF PARt of the plot?" Cell cycle **4**(1): 96-101.

Kornberg, R. D. and Y. Lorch (1999). "Twenty-five years of the nucleosome, fundamental particle of the eukaryote chromosome." Cell **98**(3): 285-294.

Kothandapani, A., V. S. Dangeti, et al. (2011). "Novel role of base excision repair in mediating cisplatin cytotoxicity." The Journal of biological chemistry **286**(16): 14564-14574.

Kruhlak, M. J., A. Celeste, et al. (2006). "Changes in chromatin structure and mobility in living cells at sites of DNA double-strand breaks." The Journal of cell biology **172**(6): 823-834.

Kurose, A., T. Tanaka, et al. (2005). "Assessment of ATM phosphorylation on Ser-1981 induced by DNA topoisomerase I and II inhibitors in relation to Ser-139-histone H2AX phosphorylation, cell cycle phase, and apoptosis." Cytometry. Part A : the journal of the International Society for Analytical Cytology **68**(1): 1-9.

Kurose, A., T. Tanaka, et al. (2006). "Effects of hydroxyurea and aphidicolin on phosphorylation of ataxia telangiectasia mutated on Ser 1981 and histone H2AX on Ser 139 in relation to cell cycle phase and induction of apoptosis." Cytometry. Part A : the journal of the International Society for Analytical Cytology **69**(4): 212-221.

Lafon-Hughes, L., M. V. Di Tomaso, et al. (2008). "Chromatin-remodelling mechanisms in cancer." Mutation research **658**(3): 191-214.

Lafon-Hughes, L., M. V. Di Tomaso, et al. (2008). "Chromatin-remodelling mechanisms in cancer." Mutat Res **658**(3): 191-214.

Langdon, S. P., S. S. Lawrie, et al. (1988). "Characterization and properties of nine human ovarian adenocarcinoma cell lines." Cancer research **48**(21): 6166-6172.

Lee, G. E., J. H. Kim, et al. (2010). "DNA methyltransferase 1-associated protein (DMAP1) is a co-repressor that stimulates DNA methylation globally and locally at sites of double strand break repair." The Journal of biological chemistry **285**(48): 37630-37640.

Lee, S. I., M. K. Brown, et al. (1999). "Comparison of the efficacy of 7-hydroxystaurosporine (UCN-01) and other staurosporine analogs to abrogate cisplatin-induced cell cycle arrest in human breast cancer cell lines." Biochemical pharmacology **58**(11): 1713-1721.

Leese, M. P., H. A. Hejaz, et al. (2005). "A-ring-substituted estrogen-3-O-sulfamates: potent multitargeted anticancer agents." Journal of medicinal chemistry **48**(16): 5243-5256.

Liang, B., D. Kong, et al. (2012). "Autophagy inhibition plays the synergetic killing roles with radiation in the multi-drug resistant SKVCR ovarian cancer cells." Radiation oncology **7**: 213.

Lieber, M. R. (2010). "The mechanism of double-strand DNA break repair by the nonhomologous DNA end-joining pathway." Annual review of biochemistry **79**: 181-211.

Lin, R. J., T. Sternsdorf, et al. (2001). "Transcriptional regulation in acute promyelocytic leukemia." Oncogene **20**(49): 7204-7215.

Liu, H., D. Chen, et al. (2011). "Multifunctional gold nanoshells on silica nanorattles: a platform for the combination of photothermal therapy and chemotherapy with low systemic toxicity." Angewandte Chemie **50**(4): 891-895.

Liu, Y., J. A. Parry, et al. (2008). "Soluble histone H2AX is induced by DNA replication stress and sensitizes cells to undergo apoptosis." Molecular cancer **7**: 61.

Lu, C., Y. Shi, et al. (2008). "Serum starvation induces H2AX phosphorylation to regulate apoptosis via p38 MAPK pathway." FEBS letters **582**(18): 2703-2708.

Lu, C., M. Xiong, et al. (2013). "Genome-wide transcriptional analysis of apoptosis-related genes and pathways regulated by H2AX in lung cancer A549 cells." Apoptosis : an international journal on programmed cell death **18**(9): 1039-1047.

Lu, C., F. Zhu, et al. (2006). "Cell apoptosis: requirement of H2AX in DNA ladder formation, but not for the activation of caspase-3." Molecular cell **23**(1): 121-132.

Luijsterburg, M. S., C. Dinant, et al. (2009). "Heterochromatin protein 1 is recruited to various types of DNA damage." The Journal of cell biology **185**(4): 577-586.

Mahlknecht, U. and D. Hoelzer (2000). "Histone acetylation modifiers in the pathogenesis of malignant disease." Mol Med **6**(8): 623-644.

Maloney, A., P. A. Clarke, et al. (2007). "Gene and protein expression profiling of human ovarian cancer cells treated with the heat shock protein 90 inhibitor 17-allylamino-17-demethoxygeldanamycin." Cancer Res **67**(7): 3239-3253.

Marchetti, P. (2005). "Natural medicine: a 'new frontier' in oncology?" Annals of oncology : official journal of the European Society for Medical Oncology / ESMO **16**(3): 339-340.

Margueron, R., P. Trojer, et al. (2005). "The key to development: interpreting the histone code?" Curr Opin Genet Dev **15**(2): 163-176.

Martin, N. M. (2001). "DNA repair inhibition and cancer therapy." Journal of photochemistry and photobiology. B, Biology **63**(1-3): 162-170.

Masumoto, H., D. Hawke, et al. (2005). "A role for cell-cycle-regulated histone H3 lysine 56 acetylation in the DNA damage response." Nature **436**(7048): 294-298.

McCluggage, W. G., R. W. Lyness, et al. (2002). "Morphological effects of chemotherapy on ovarian carcinoma." Journal of clinical pathology **55**(1): 27-31.

McHugh, P. J., V. J. Spanswick, et al. (2001). "Repair of DNA interstrand crosslinks: molecular mechanisms and clinical relevance." The lancet oncology **2**(8): 483-490.

McKinsey, T. A. and E. N. Olson (2005). "Toward transcriptional therapies for the failing heart: chemical screens to modulate genes." The Journal of clinical investigation **115**(3): 538-546.

McWhir, J., J. Selfridge, et al. (1993). "Mice with DNA repair gene (ERCC-1) deficiency have elevated levels of p53, liver nuclear abnormalities and die before weaning." Nature genetics **5**(3): 217-224.

Medina, P. P., O. A. Romero, et al. (2008). "Frequent BRG1/SMARCA4-inactivating mutations in human lung cancer cell lines." Human mutation **29**(5): 617-622.

Meissner, A. (2010). "Epigenetic modifications in pluripotent and differentiated cells." Nature biotechnology **28**(10): 1079-1088.

Miller, K. M., J. V. Tjeertes, et al. (2010). "Human HDAC1 and HDAC2 function in the DNA-damage response to promote DNA nonhomologous end-joining." Nature structural & molecular biology **17**(9): 1144-1151.

Minc, E., Y. Allory, et al. (2001). "Immunolocalization of HP1 proteins in metaphasic mammalian chromosomes." Methods Cell Sci **23**(1-3): 171-174.

Mine-Hattab, J. and R. Rothstein (2012). "Increased chromosome mobility facilitates homology search during recombination." Nature cell biology **14**(5): 510-517.

Miyake, K., T. Yoshizumi, et al. (2008). "Expression of hypoxia-inducible factor-1alpha, histone deacetylase 1, and metastasis-associated protein 1 in pancreatic carcinoma: correlation with poor prognosis with possible regulation." Pancreas **36**(3): e1-9.

Munster, P. N., T. Troso-Sandoval, et al. (2001). "The histone deacetylase inhibitor suberoylanilide hydroxamic acid induces differentiation of human breast cancer cells." Cancer research **61**(23): 8492-8497.

Murata, S., K. Mochizuki, et al. (2002). "Detection of underlying characteristics of nuclear chromatin patterns of thyroid tumor cells using texture and factor analyses." Cytometry **49**(3): 91-95.

Murray, J. M., T. Stiff, et al. (2012). "DNA double-strand break repair within heterochromatic regions." Biochemical Society transactions **40**(1): 173-178.

Ng, C. K., S. L. Cooke, et al. (2012). "The role of tandem duplicator phenotype in tumour evolution in high-grade serous ovarian cancer." The Journal of pathology **226**(5): 703-712.

O'Brien, V. and R. Brown (2006). "Signalling cell cycle arrest and cell death through the MMR System." Carcinogenesis **27**(4): 682-692.

O'Hagan, H. M., H. P. Mohammad, et al. (2008). "Double strand breaks can initiate gene silencing and SIRT1-dependent onset of DNA methylation in an exogenous promoter CpG island." PLoS genetics **4**(8): e1000155.

Ocker, M. and R. Schneider-Stock (2007). "Histone deacetylase inhibitors: signalling towards p21cip1/waf1." The international journal of biochemistry & cell biology **39**(7-8): 1367-1374.

Olsen, E. A., Y. H. Kim, et al. (2007). "Phase IIb multicenter trial of vorinostat in patients with persistent, progressive, or treatment refractory cutaneous T-cell lymphoma." Journal of clinical oncology : official journal of the American Society of Clinical Oncology **25**(21): 3109-3115.

Oza, P., S. L. Jaspersen, et al. (2009). "Mechanisms that regulate localization of a DNA double-strand break to the nuclear periphery." Genes Dev **23**(8): 912-927.

Ozaki, K., F. Kishikawa, et al. (2008). "Histone deacetylase inhibitors enhance the chemosensitivity of tumor cells with cross-resistance to a wide range of DNA-damaging drugs." Cancer science **99**(2): 376-384.

Peixoto, P., V. Castronovo, et al. (2012). "HDAC5 is required for maintenance of pericentric heterochromatin, and controls cell-cycle progression and survival of human cancer cells." Cell death and differentiation **19**(7): 1239-1252.

Peric-Concha, N. and P. F. Long (2003). "Mining the microbial metabolome: a new frontier for natural product lead discovery." Drug discovery today **8**(23): 1078-1084.

Petru, E., B. U. Sevin, et al. (1997). "Radiosensitivity patterns of four human ovarian cancer cell lines in vitro." Gynecologic oncology **64**(3): 490-492.

Piacentini, L., L. Fanti, et al. (2003). "Heterochromatin protein 1 (HP1) is associated with induced gene expression in Drosophila euchromatin." The Journal of cell biology **161**(4): 707-714.

Podhorecka, M. (2009). "[gamma H2AX in the recognition of DNA double-strand breaks]." Postepy higieny i medycyny doswiadczalnej **63**: 92-98.

Podhorecka, M., H. D. Halicka, et al. (2009). "Thalidomide induces phosphorylation of histone H2AX and increases rate of apoptosis caused by fludarabine in malignant lymphocytes of chronic lymphocytic leukemia in short-term cell cultures." Leukemia research **33**(7): 997-1000.

Popova, E. Y., D. F. Claxton, et al. (2006). "Epigenetic heterochromatin markers distinguish terminally differentiated leukocytes from incompletely differentiated leukemia cells in human blood." Exp Hematol **34**(4): 453-462.

Portela, A. and M. Esteller (2010). "Epigenetic modifications and human disease." Nature biotechnology **28**(10): 1057-1068.

Probst, A. V., E. Dunleavy, et al. (2009). "Epigenetic inheritance during the cell cycle." Nat Rev Mol Cell Biol **10**(3): 192-206.

Qiu, L., A. Burgess, et al. (2000). "Histone deacetylase inhibitors trigger a G2 checkpoint in normal cells that is defective in tumor cells." Molecular biology of the cell **11**(6): 2069-2083.

Ratnam, K. and J. A. Low (2007). "Current development of clinical inhibitors of poly(ADP-ribose) polymerase in oncology." Clin Cancer Res **13**(5): 1383-1388.

Richon, V. M., T. W. Sandhoff, et al. (2000). "Histone deacetylase inhibitor selectively induces p21WAF1 expression and gene-associated histone acetylation." Proceedings of the National Academy of Sciences of the United States of America **97**(18): 10014-10019.

Robert, T., F. Vanoli, et al. (2011). "HDACs link the DNA damage response, processing of double-strand breaks and autophagy." Nature **471**(7336): 74-79.

Robertson, K. D. (2005). "DNA methylation and human disease." Nature reviews. Genetics **6**(8): 597-610.

Robertson, K. D. and P. A. Jones (2000). "DNA methylation: past, present and future directions." Carcinogenesis **21**(3): 461-467.

Rogakou, E. P., W. Nieves-Neira, et al. (2000). "Initiation of DNA fragmentation during apoptosis induces phosphorylation of H2AX histone at serine 139." The Journal of biological chemistry **275**(13): 9390-9395.

Rogakou, E. P., D. R. Pilch, et al. (1998). "DNA double-stranded breaks induce histone H2AX phosphorylation on serine 139." J Biol Chem **273**(10): 5858-5868.

Ruginis, T., L. Taglia, et al. (2006). "Consequence of gastrin-releasing peptide receptor activation in a human colon cancer cell line: a proteomic approach." J Proteome Res **5**(6): 1460-1468.

Sacile, R., E. Montaldo, et al. (2003). "A decision support system to detect morphologic changes of chromatin arrangement in normal-appearing cells." IEEE transactions on nanobioscience **2**(2): 118-123.

Saha, A., J. Wittmeyer, et al. (2005). "Chromatin remodeling through directional DNA translocation from an internal nucleosomal site." Nat Struct Mol Biol **12**(9): 747-755.

Sakai, W., E. M. Swisher, et al. (2009). "Functional restoration of BRCA2 protein by secondary BRCA2 mutations in BRCA2-mutated ovarian carcinoma." Cancer research **69**(16): 6381-6386.

San Filippo, J., P. Sung, et al. (2008). "Mechanism of eukaryotic homologous recombination." Annual review of biochemistry **77**: 229-257.

Sandor, V., A. Senderowicz, et al. (2000). "P21-dependent g(1)arrest with downregulation of cyclin D1 and upregulation of cyclin E by the histone deacetylase inhibitor FR901228." British journal of cancer **83**(6): 817-825.

Santos-Rosa, H. and C. Caldas (2005). "Chromatin modifier enzymes, the histone code and cancer." Eur J Cancer **41**(16): 2381-2402.

Santra, M. K., N. Wajapeyee, et al. (2009). "F-box protein FBXO31 mediates cyclin D1 degradation to induce G1 arrest after DNA damage." Nature **459**(7247): 722-725.

Schmidt, D. R. and S. L. Schreiber (1999). "Molecular association between ATR and two components of the nucleosome remodeling and deacetylating complex, HDAC2 and CHD4." Biochemistry **38**(44): 14711-14717.

Senese, S., K. Zaragoza, et al. (2007). "Role for histone deacetylase 1 in human tumor cell proliferation." Mol Cell Biol **27**(13): 4784-4795.

Shanbhag, N. M., I. U. Rafalska-Metcalf, et al. (2010). "ATM-dependent chromatin changes silence transcription in cis to DNA double-strand breaks." Cell **141**(6): 970-981.

Sharma, S., T. K. Kelly, et al. (2010). "Epigenetics in cancer." Carcinogenesis **31**(1): 27-36.

Shimizu, S., F. Nomura, et al. (2004). "Expression of poly(ADP-ribose) polymerase in human hepatocellular carcinoma and analysis of biopsy specimens obtained under sonographic guidance." Oncol Rep **12**(4): 821-825.

Siddik, Z. H. (2003). "Cisplatin: mode of cytotoxic action and molecular basis of resistance." Oncogene **22**(47): 7265-7279.

Solomon, J. M., R. Pasupuleti, et al. (2006). "Inhibition of SIRT1 catalytic activity increases p53 acetylation but does not alter cell survival following DNA damage." Molecular and cellular biology **26**(1): 28-38.

Sorenson, C. M., M. A. Barry, et al. (1990). "Analysis of events associated with cell cycle arrest at G2 phase and cell death induced by cisplatin." Journal of the National Cancer Institute **82**(9): 749-755.

Stiborova, M., T. Eckschlager, et al. (2012). "The synergistic effects of DNA-targeted chemotherapeutics and histone deacetylase inhibitors as therapeutic strategies for cancer treatment." Current medicinal chemistry **19**(25): 4218-4238.

Storch, K., I. Eke, et al. "Three-dimensional cell growth confers radioresistance by chromatin density modification." Cancer Res **70**(10): 3925-3934.

Stronach, E. A., A. Alfraidi, et al. (2011). "HDAC4-regulated STAT1 activation mediates platinum resistance in ovarian cancer." Cancer research **71**(13): 4412-4422.

Sulli, G., R. Di Micco, et al. (2012). "Crosstalk between chromatin state and DNA damage response in cellular senescence and cancer." Nature reviews. Cancer **12**(10): 709-720.

Taberlay, P. C. and P. A. Jones (2011). "DNA methylation and cancer." Progress in drug research. Fortschritte der Arzneimittelforschung. Progres des recherches pharmaceutiques **67**: 1-23.

Tanaka, T., A. Kurose, et al. (2006). "Nitrogen oxide-releasing aspirin induces histone H2AX phosphorylation, ATM activation and apoptosis preferentially in S-phase cells: involvement of reactive oxygen species." Cell cycle **5**(15): 1669-1674.

Tanaka, T., A. Kurose, et al. (2006). "ATM activation and histone H2AX phosphorylation as indicators of DNA damage by DNA topoisomerase I inhibitor topotecan and during apoptosis." Cell proliferation **39**(1): 49-60.

Ting, A. H., K. M. McGarvey, et al. (2006). "The cancer epigenome--components and functional correlates." Genes Dev **20**(23): 3215-3231.

Tishler, R. B., P. B. Schiff, et al. (1992). "Taxol: a novel radiation sensitizer." International journal of radiation oncology, biology, physics **22**(3): 613-617.

Tjeertes, J. V., K. M. Miller, et al. (2009). "Screen for DNA-damage-responsive histone modifications identifies H3K9Ac and H3K56Ac in human cells." The EMBO journal **28**(13): 1878-1889.

Trainor, C., K. T. Butterworth, et al. (2012). "DNA damage responses following exposure to modulated radiation fields." PLoS One **7**(8): e43326.

Vakoc, C. R., S. A. Mandat, et al. (2005). "Histone H3 lysine 9 methylation and HP1gamma are associated with transcription elongation through mammalian chromatin." Molecular cell **19**(3): 381-391.

Vannini, A., C. Volpari, et al. (2004). "Crystal structure of a eukaryotic zinc-dependent histone deacetylase, human HDAC8, complexed with a hydroxamic acid inhibitor." Proc Natl Acad Sci U S A **101**(42): 15064-15069.

Verdone, L., E. Agricola, et al. (2006). "Histone acetylation in gene regulation." Brief Funct Genomic Proteomic **5**(3): 209-221.

Ververis, K., A. Hiong, et al. (2013). "Histone deacetylase inhibitors (HDACIs): multitargeted anticancer agents." Biologics : targets & therapy **7**: 47-60.

Vries, R. G., V. Bezrookove, et al. (2005). "Cancer-associated mutations in chromatin remodeler hSNF5 promote chromosomal instability by compromising the mitotic checkpoint." Genes Dev **19**(6): 665-670.

Ward, I. M., K. Minn, et al. (2003). "Accumulation of checkpoint protein 53BP1 at DNA breaks involves its binding to phosphorylated histone H2AX." J Biol Chem **278**(22): 19579-19582.

Weichert, W., A. Roske, et al. (2008). "Histone deacetylases 1, 2 and 3 are highly expressed in prostate cancer and HDAC2 expression is associated with shorter PSA relapse time after radical prostatectomy." British journal of cancer **98**(3): 604-610.

Weichert, W., A. Roske, et al. (2008). "Class I histone deacetylase expression has independent prognostic impact in human colorectal cancer: specific role of class I histone deacetylases in vitro and in vivo." Clinical cancer research : an official journal of the American Association for Cancer Research **14**(6): 1669-1677.

Williams, R. R., V. Azuara, et al. (2006). "Neural induction promotes large-scale chromatin reorganisation of the Mash1 locus." J Cell Sci **119**(Pt 1): 132-140.

Wilting, R. H., E. Yanover, et al. (2010). "Overlapping functions of Hdac1 and Hdac2 in cell cycle regulation and haematopoiesis." The EMBO journal **29**(15): 2586-2597.

Witt, O., H. E. Deubzer, et al. (2009). "HDAC family: What are the cancer relevant targets?" Cancer letters **277**(1): 8-21.

Wu, X., W. Fan, et al. (2003). "Sensitization to the cytotoxicity of cisplatin by transfection with nucleotide excision repair gene xeroderma pigmentosun group A antisense RNA in human lung adenocarcinoma cells." Clinical cancer research : an official journal of the American Association for Cancer Research **9**(16 Pt 1): 5874-5879.

Yamaguchi, T., F. Cubizolles, et al. (2010). "Histone deacetylases 1 and 2 act in concert to promote the G1-to-S progression." Genes & development **24**(5): 455-469.

Yang, X. J. (2004). "The diverse superfamily of lysine acetyltransferases and their roles in leukemia and other diseases." Nucleic Acids Res **32**(3): 959-976.

Yatouji, S., V. El-Khoury, et al. (2007). "Differential modulation of nuclear texture, histone acetylation, and MDR1 gene expression in human drug-sensitive and -resistant OV1 cell lines." International journal of oncology **30**(4): 1003-1009.

Yeung, F., J. E. Hoberg, et al. (2004). "Modulation of NF-kappaB-dependent transcription and cell survival by the SIRT1 deacetylase." The EMBO journal **23**(12): 2369-2380.

Yoshida, M., M. Kijima, et al. (1990). "Potent and specific inhibition of mammalian histone deacetylase both in vivo and in vitro by trichostatin A." The Journal of biological chemistry **265**(28): 17174-17179.

Zarebski, M., E. Wiernasz, et al. (2009). "Recruitment of heterochromatin protein 1 to DNA repair sites." Cytometry. Part A : the journal of the International Society for Analytical Cytology **75**(7): 619-625.

Zhang, J., H. Willers, et al. (2004). "Chk2 phosphorylation of BRCA1 regulates DNA double-strand break repair." Mol Cell Biol **24**(2): 708-718.

Zhu, Q., G. M. Pao, et al. "BRCA1 tumour suppression occurs via heterochromatin-mediated silencing." Nature **477**(7363): 179-184.

Zofall, M. and S. I. Grewal (2006). "Swi6/HP1 recruits a JmjC domain protein to facilitate transcription of heterochromatic repeats." Molecular cell **22**(5): 681-692.

Zykova, T. A., F. Zhu, et al. (2006). "Lymphokine-activated killer T-cell-originated protein kinase phosphorylation of histone H2AX prevents arsenite-induced apoptosis in RPMI7951 melanoma cells." Clinical cancer research : an official journal of the American Association for Cancer Research **12**(23): 6884-6893.